

**Nanoparticle Based Apigenin Delivery  
Intended to Control Hepatocellular  
Carcinoma**

Thesis Submitted

By

**SANCHARI BHATTACHARYA**

**Doctor of Philosophy (Pharmacy)**

**Department of Pharmaceutical Technology  
Faculty Council of Engineering and Technology  
Jadavpur University  
Kolkata, India**

**2018**

**JADAVPUR UNIVERSITY  
KOLKATA-700 032, INDIA**

**INDEX NO: 161/13/Ph.**

**1. Title of the thesis:**

“Nanoparticle Based Apigenin Delivery Intended to Control Hepatocellular Carcinoma”

**2. Name, Designation and Institution of the Supervisor/s:**

Dr. Biswajit Mukherjee

Professor,

Department of Pharmaceutical Technology

Jadavpur University,

Kolkata-700 032, India

**3. List of Publications:**

- i. Sanchari Bhattacharya**, Laboni Mondal, Biswajit Mukherjee, Lopamudra Dutta, Iman Ehsan, Mita C. Debnath, Raghuvir H. Gaonkar, Murari M. Pal, Subrata Majumdar. Apigenin loaded nanoparticle delayed development of hepatocellular carcinoma in rats. **Nanomedicine: Nanotechnology, Biology, and Medicine**, 2018; 14: 1905–1917. **(Impact Factor 6.5)**.
- ii.** Lopamudra Dutta, Biswajit Mukherjee, Tapash Chakraborty, Malay Kumar Das, Laboni Mondal, **Sanchari Bhattacharya**, Raghuvir H. Gaonkar, Mita Chatterjee Debnath. **Drug Delivery**. 2018; 25 (1): 504–516. **(Impact Factor 6.402)**.
- iii.** Laboni Mondal, Biswajit Mukherjee, Shreyasi Chakraborty, **Sanchari Bhattacharya**, Iman Ehsan, Soma Sengupta, Murari P Pal. **Novel Approaches in Drug designing and Development**. 2018; 3(5): 1-8.

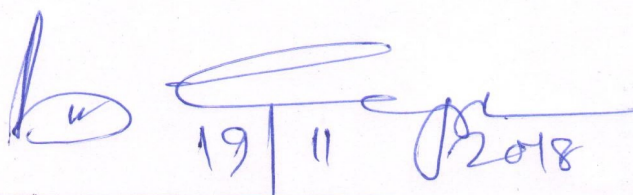
**4. List of Patents:** NIL

**5. List of Presentations in National/International/Conferences/Workshops:**

- i. Participated and presented a poster in the **National Seminar** on “*Novel Pharmaceutical Technologies: Challenges and Opportunities*”, held on 15<sup>th</sup> November, 2015 in Manipal College of Pharmaceutical Sciences, Manipal University, Manipal.
- ii. Participated and presented a poster in the **JU IAPST National Seminar** on “*Drug and Diseases: Role of Pharmacists and Doctors*”, held on 16<sup>th</sup> January, 2016 in Department of Pharmaceutical Technology, Jadavpur University, Kolkata.
- iii. Participated and presented a poster in the 2<sup>nd</sup> Pharm. Tech. **IAPST International Conference** on “*New Insights into Diseases and Recent Therapeutic Approaches*”, held on 17<sup>th</sup> -19<sup>th</sup> January, 2014 in Department of Pharmaceutical Technology, Jadavpur University, Kolkata.
- iv. Participated and presented a poster in the **International Conference** on “*Molecular Biology and Its Application*”, held on 14<sup>th</sup> -15<sup>th</sup> February, 2014 in Department of Life Science and Biotechnology, Jadavpur University, Kolkata.
- v. Participated and presented a poster in the 4<sup>th</sup> **International conference** on “*Nanomedicine and Tissue Engineering*” held on 12<sup>th</sup> – 14<sup>th</sup> August, 2016 in Mahatma Gandhi University, Kottayam, Kerala, India. (Received the third best poster award).

### CERTIFICATE FROM THE SUPERVISOR

*This is to certify that the thesis entitled "Nanoparticle Based Apigenin Delivery Intended to Control Hepatocellular Carcinoma" submitted by Smt Sanchari Bhattacharya, who got her name registered on 7<sup>th</sup> January, 2013, for the award of Ph.D. (Pharmacy) degree of Jadavpur University is absolutely based upon her own work under the supervision of Prof. Biswajit Mukherjee, Department of Pharmaceutical Technology, Jadavpur University, Kolkata 700 032, India and that neither her thesis nor any part of the thesis has been submitted for any degree/diploma or any other academic award anywhere before.*



**Signature of the Supervisor  
and date with Office Seal**

Professor (Dr.) Biswajit Mukherjee  
Department of Pharmaceutical Technology  
Jadavpur University  
Kolkata - 700032, India

***Dedicated To My Family***

### *Acknowledgements*

I would like to express my sincere gratitude to my supervisor **Prof. (Dr.) Biswajit Mukherjee**, Department of Pharmaceutical Technology, Jadavpur University, Kolkata-32, India, for his patience, motivation, and immense knowledge. His guidance helped me throughout my Ph.D. tenure and encouraged me as to grow as a researcher. I could not have imagined having a better advisor and mentor for my Ph.D. course. His advice on both research as well as on my career have been invaluable.

I would like to express my gratitude towards INSPIRE Fellowship Grant, Department of Science and Technology (**DST**), Government of India, New Delhi, for the financial support to carry out my work related to this thesis.

My sincere thanks also goes to Professor Subrata Majumder, Division of Molecular Medicine, Bose Institute, Kolkata, West Bengal, India, who provided me an access to his laboratory and research facilities which helped me a lot to gather a part of my research related data.

I would like to acknowledge the contributions of Central Instrumentation Facility of Bose Institute, Kolkata, India, Indian Association for the cultivation of Science (IACS) Kolkata, India, and Indian Institute of Chemical Biology (IICB) Kolkata, India, for extending cooperation and allowing me to use the laboratories/instruments during my Ph.D. tenure.

I would like to thank all the seniors from my lab, my current lab mates and my juniors for all the supports, encouragements and fun filled days which I enjoyed for the last six years. My special thanks goes to Laboni Mondal, Department of Pharmaceutical Technology, Jadavpur University, Kolkata as without her constant support it would not be easy for me to go through this journey.

I also thank my fellow lab mates from other labs of the Department of Pharmaceutical Technology, Jadavpur University, Kolkata, for their valuable inputs in my professional life, as well as helping me to use institutional instrumentation facilities.

Last but not the least; I would like to express my love for my family and friends without whom I may not be able to fulfill my dreams. I sincerely thank my husband Swarnab, for holding my hands strongly throughout all the ups and downs during this research tenure. Words can't express how much grateful I am to my mother, father, mother-in-law, father-in-law, my brother and my brother-in law who constantly supported, motivated and helped me a lot to complete this research successfully.

Date: 19.11.2018  
Place: Kolkata

Sanchari Bhattacharya  
Sanchari Bhattacharya

## Abbreviations

---

### List of abbreviations

<b>g</b>	gram	<b>FTIR</b>	Fourier Transform Infrared Spectroscopy
<b>mg</b>	milligram	<b>GST</b>	Glutathione S Transferase
<b>µg</b>	microgram	<b>HAF</b>	Hepatic Altered Foci
<b>ng</b>	nanogram	<b>HCC</b>	Hepatocellular Carcinoma
<b>2-AAF</b>	2-Acetylaminofluorene	<b>HN</b>	Hyperplasic Nodule
<b>AEC</b>	Animal Ethics Committee	<b>HSA</b>	Human Serum Albumin
<b>AFM</b>	Atomic Force Microscopy	<b>i.v</b>	Intravenous
<b>API</b>	Apigenin	<b>LC/MS-MS</b>	Liquid Chromatography and Mass Spectroscopy
<b>AUC</b>	Area Under The Curve	<b>MRT</b>	Mean Residence Time
<b>CL</b>	Clearance	<b>MTT</b>	3-(4,5-Dimethylthiazol-2-Yl)-2,5-Diphenyltetrazolium Bromide
<b>Cyt P-450</b>	Cytochrome P-450	<b>PBS</b>	Phosphate Buffer Saline
<b>DCM</b>	Dichloromethane	<b>PDI</b>	Poly Dispersity Index
<b>DDW</b>	Double Distilled Water	<b>PLGA</b>	Poly Lactic Co-Glycolic Acid
<b>DENA</b>	Diethylnitrosamine	<b>PNPs</b>	Polymeric Nanoparticles
<b>DMEM</b>	Dulbecco's Modified Eagle Medium	<b>PVA</b>	Poly (Vinyl Alcohol)
<b>DMSO</b>	Dimethyl Sulfoxide	<b>RFA</b>	Radiofrequency Ablation
<b>DNA</b>	Deoxyribonucleic Acid	<b>RH</b>	Relative Humidity
<b>DPX</b>	Dibutylphthalate Polystyrene Xylene	<b>TEM</b>	Transmission Electron Microscopy
<b>FACS</b>	Fluorescence Activated Cell Sorter	<b>Tc</b>	Technetium Chloride
<b>FBS</b>	Fetal Bovine Serum	<b>UDPGT</b>	UDP- Glucuronyl Transferase
<b>FESEM</b>	Field Emission Scanning Electron Microscope	<b>US-FDA</b>	United States Food and Drug Administration
<b>FITC</b>	Fluorescein Isothiocyanate	<b>V<sub>ss</sub></b>	Steady State Volume Distribution

Contents

<b>Chapter</b>	<b>Title</b>	<b>Page no</b>
<b>1.</b>	<b>Introduction</b>	<b>1-7</b>
1.1	Hepatocellular Carcinoma (HCC)	1
1.1.1	HCC etiology and classification	1
1.1.2	HCC treatment	2
1.2	Dietary flavonoids against HCC	4
1.3	Apigenin as therapeutic agent	5
1.3.1	Mechanism of action of Apigenin	5
1.3.2	Apigenin solubility and bioavailability	6
1.4	Nanoparticle based drug delivery	6
<b>2.</b>	<b>Literature Review</b>	<b>8-25</b>
2.1	Nanotechnology	8
2.2	Nanomedicine	8
2.3	Nanoparticles	12
2.3.1	Tumor targeting by nanoparticles	12
2.3.2	Preparation of polymeric nanoparticles (PNPs)	13
2.3.3	Polymeric nanoparticles for targeted therapy in hepatocellular carcinoma	15
2.3.4	PLGA nanoparticles against HCC	16
2.4	Excipients specific review	17
2.4.1	PLGA	18
2.4.2	PVA	21
2.5	Drug specific review: Apigenin	22
<b>3.</b>	<b>Objectives and plan of study</b>	<b>26-28</b>
3.1	Objectives	26
3.2	Plan of Study	27



<b>4</b>	<b>Materials and Methods</b>	<b>29-44</b>
4.1	<b>Materials</b>	29-32
4.1.1	Chemicals	29
4.1.2	Instruments	30
4.2.	<b>Experimental Methods</b>	<b>32-44</b>
4.2.1	Preformulation Studies	32
4.2.1.1	Preparation of different buffers used in the study	32
4.2.1.1	UV-VIS absorption maxima of apigenin	33
4.2.1.3	Calibration Curve of Apigenin by UV spectroscopy	33
4.2.2	Preparation of Nanoparticles	33
4.2.3	Fourier Transform Infrared Spectroscopy	34
4.2.4	Morphology of nanoparticles	35
4.2.5	Particle size assessment	35
4.2.6	Drug loading and loading efficiency	36
4.2.7	Stability studies	36
4.2.8	<i>In-vitro</i> drug release	37
4.2.9	<i>In-vitro</i> studies using human HCC cells	38
4.2.9.1	<i>In-vitro</i> cytotoxicity by MTT assay	38
4.2.9.2	Cellular uptake studies	38
4.2.10	<i>In-vivo</i> studies	39
4.2.10.1	Radiolabeling and gamma scintigraphy study	39
4.2.10.2	Pharmacokinetics study and biodistribution of apigenin by LC-MS/MS	41
4.2.10.3	Experimental protocol for development of chemical induced hepatocellular carcinoma in rats	42
4.2.10.4	Macroscopic and histopathological studies	42
4.2.10.5	Activities various marker enzymes/iso-enzyme	43
4.2.11	Statistical analysis	44

<b>5.</b>	<b>Results</b>	<b>45-80</b>
5.1	Preformulation Studies	45
5.2	Preparations of polymeric nanoparticles of apigenin	47
5.3	Fourier Transform Infrared Spectroscopy (FTIR)	48
5.4	Determination of surface morphology	49
5.5	Particle size and Poly dispersity Index (PDI)	51
5.6	Surface charge determination by zeta potential	52
5.7	Stability Study	53
5.8	<i>In-vitro</i> drug release and kinetics study	55
5.9	<i>In-Vitro</i> cytotoxicity and cellular uptake study	57-67
5.9.1	Cytotoxicity measurement by MTT assay	57
5.9.2	Cellular uptake by confocal microscopy	60
5.9.3	Quantification of cellular uptake by FACS	65
5.10	<i>In-Vivo</i> studies	67-80
5.10.1	Radiolabeling and Gamma Scintigraphy	67
5.10.2	LC-MS/MS study	70
5.10.3	Experiments on animals with chemically induced hepatocellular carcinoma	72-80
<b>6.</b>	<b>Discussion</b>	<b>81-88</b>
<b>7.</b>	<b>Summary</b>	<b>89-91</b>
<b>8.</b>	<b>Conclusion</b>	<b>92</b>
	<b>References</b>	<b>93-110</b>
	<b>Appendix (s) - Reprints</b>	<b>--</b>

## *List of Tables and Figures*

## *List of Tables and Figures*

---

### **List of Tables:**

<b>Table No</b>	<b>Description</b>	<b>Page no</b>
2.1	Few commonly used nanomedicines with US-FDA approved marketed products	9
2.2	List of PLGA molecular weights versus polymeric ratios	19
2.3	PLGA nanoparticles developed against different types of diseases	20
4.1.1	Name and sources of the chemicals and other important materials	29
4.1.2	Name and sources of the major instruments used	30
5.1	Composition of different nanoparticles and their drug loading	47
5.2	Different release kinetics models of apigenin release from ApNp3	57
5.3	Organ/tissue wise biodistribution of apigenin in mice received i.v injection (1mg drug/ml) of equivalent $^{99m}\text{Tc}$ -ApNp3/ $^{99m}\text{Tc}$ -API	70
5.4	Plasma and hepatic pharmacokinetic parameters of apigenin from API and ApNp3 after intravenous bolus administration of API and ApNp3 with an equivalent amount of drug in balb/c mice.	72
5.5	A quantitative data on the effect of API/ApNp3 treatment of hepatic tumor incidences, number and total area of hepatic altered foci (HAF)	73

---

## *List of Tables and Figures*

---

### List of Figures:

Figure No	Description	Page No
1.1	Progression towards hepatocellular carcinoma	3
2.1	Applications of nanotechnology	8
2.2	A schematic diagram illustrating the tumor site specific delivery of polymeric nanoparticles.	13
2.3	Synthesis and structure of PLGA	18
2.4	Common sources of apigenin in nature	23
2.5	Different molecular pathways regulated by apigenin <i>in-vitro</i> and <i>in-vivo</i>	25
3.1	A simple schematic diagram explaining the objectives of the study	26
4.1	Schematic diagram representing different steps used for the preparation of nanoparticles in multiple emulsion and solvent evaporation method	34
4.2	Schematic presentation of carcinogen treatment along with the treatment of apigenin loaded nanoparticles and free drug	43
5.1	Absorbance maxima of Apigenin	45
5.2 (A & B)	Calibration curve of apigenin in DDW and PBS (pH 7.4)	46
5.3	FTIR spectra of drug, excipients and formulations	48
5.4	Surface morphology of apigenin loaded nanoparticles by FESEM	50
5.5	Transmission electron scanning microscopic images of ApNp3	50

---

## *List of Tables and Figures*

---

5.6	Three dimensional surface morphology of ApNp3 by AFM	51
5.7	Particle size distributions of ApNp3 (A) and ApNp5 (B) respectively	51
5.8	Zeta potential values of ApNp3 (A) and ApNp5 (B) respectively	53
5.9	Hydrolytic stability study of ApNp3 in different pH buffers.	54
5.10	Accelerated stability study of ApNp3 at different temperature conditions	55
5.11	<i>In vitro</i> drug release profile of ApNp3 in different pH buffers.	56
5.12	<i>In-vitro</i> cytotoxicity of ApNp3 and API in HepG2 and Huh-7 cells along with determination of IC <sub>50</sub> values.	58-59
5.13	Time dependent cellular uptake of ApNp3 in HepG2 and Huh-7 cells by confocal microscopy	61-64
5.14	Quantification of cellular uptake by FACS	65-67
5.15	Radiolabeling and Gamma Scintigraphy studies	68-69
5.16	Pharmacokinetics and biodistribution of the drug determined by LC/MS-MS	71
5.17	Different marker enzyme and iso-enzyme activities	74-75
5.18	Macroscopic images of livers of normal rats (A), carcinogen control rats (B) and carcinogenic rats treated with ApNp3 (C).	76
5.19 (A-F)	Microscopic histopathology study of treated and untreated rat liver sections	78-80

---

# Chapter 1

## *Introduction*

## 1. Introduction

### 1.1 *Hepatocellular Carcinoma*

Hepatocellular Carcinoma (HCC) is one of the most common malignant solid tumors with a very poor prognosis [Li *et al*, 2015] and survival rate [Weledji *et al*, 2014] in humans. HCC-related death has been reported as the second highest in men [Torre *et al*, 2015, McGlynn *et al*, 2015] accounting for 9.1% of all cancer related deaths worldwide [Wong *et al*, 2017, Ferlay *et al*, 2013]. Gender and racial dispersity on prevalence of HCC is noticeable among multi-ethnic populations in almost all countries. According to the global cancer statistics 2012, number of liver cancer incident estimation was 782,500, and the death related to HCC was 745,500 (521,000 in men and 224, 500 in women) worldwide [Colombo and Maisonneuve 2017, Torre *et al*, 2015]. Generally, the reason for two to three times higher rate of HCC in males than females include excessive alcohol abuse, obesity and cirrhosis of liver [Yuan *et al*, 2004; Alcorn T 2011; Saunders *et al*, 2010]. Half of the total deaths were accounted in China, and the main reason behind high HCC rates in parts of Asia and Africa reflect the chronic hepatitis B and C (HBV and HCV respectively) prevalence in these parts. On the other hand, obesity, type-2 diabetes, alcohol abuse, non-alcoholic fatty liver disease (NAFLD), non-alcoholic steatohepatitis (NASH) and smoking are the major reasons for prevalence of this disease in western countries. Beside this, consumption of peanuts, soybeans, grains and corn that have been stored in warm, moist conditions for a long time and contaminated with a poison called aflatoxin, is another risk factor for HCC [Shin *et al*, 2010; Mittal *et al*, 2013; Altekruse *et al*, 2009; Torre *et al*, 2015]. A genetic disorder called hemochromatosis is (excessive iron storage in hepatic cells) also associated with increased risk to HCC [Kew MS, 2014]. These statistics are based on GLOBOCAN estimates of cancer incidence and mortality produced by the International Agency for Research on Cancer (IARC) for 2012 [Ferlay *et al* 2015 and Torre *et al*, 2015].

#### 1.1.1 *HCC etiology and classification*

HCC is a multistage disease which unlike any other neoplastic disease, generally occurs in a previously damaged liver. However, the occurrence rate of HCC in non-fibrotic or



minimum portal fibrotic liver is 15-20% [Anzola M, 2004; Fattovich *et al*, 2004; Bralet *et al*, 2000]. There are few precursor lesions to this disease such as hepatocellular adenoma (HCA), dysplastic foci and dysplastic nodules. HCA is a type of metabolic syndrome which is associated with mutation of beta-catenin and leads to HCC in 4-8% patients. Tumor histopathology of HCA and HCC in non-cirrhotic liver is almost similar and could be hard to differentiate [Evason *et al*, 2013; Fattovich *et al* 1994]. Small focal hepatic altered dysplastic cells are called dysplastic foci. The characteristic of dysplastic foci are increased nuclear/cytoplasm ratio and uniform lesions of less than 1 mm in size, hence criteria for malignancy is not fulfilled. Due to their lower rate of apoptosis and high proliferation rate than the surrounding liver tissues, dysplastic nodules are generally considered as a pre-malignant precursor to HCC [WP International, 1995; Schlagater *et al* 2014]. Dysplastic nodules are usually found in liver cirrhosis. They are bigger in size (larger than 1 mm) and can be divided into two sub-types of high-grade and low-grade lesions. Minimum abnormality is observed in low grade nodules, whereas high grade nodules show irregular nuclear border, larger cell plates, basophilic cytoplasm and occasional unpaired arteries. Multiple nodules are characteristic feature of hepatocellular carcinoma. [Roncalli M, 2004; Schlagater *et al*, 2014]. HCC is classified by WHO and International consensus group as: A) Early HCC: well differentiated form with less than 2 cm size and margins and nodules are not well defined and B) Progressed HCC: moderately differentiated with more than 2 cm in size and nodules are distinct. Further progressed HCC can be divided into three sub-types, nodular (single/multiple nodule), massive (large irregular tumor) and diffused (many small nodules in one lobe or whole organ) [The International Consensus Group for Hepatocellular Neoplasia, 2009; IARC WHO Classification of Tumours, 2010].

### **1.1.2 HCC treatment**

The appropriate therapy of HCC depends on the underlying status of the liver and the stage of the disease depending on the factors such as size of tumor growth, tumor location etc and can be divided into surgical and non-surgical approaches. The surgical treatment includes ablation therapy, liver resection and liver transplantation [Jarnagin *et al*, 2010]. Non resectional ablation therapy can be divided into radiofrequency ablation (RFA) and

transarterial chemoembolization (TAE). Both of these are effective against tumor necrosis and small size tumors (<3cm) [Livraghi *et al*, 2008; Lu *et al*, 2005]. Hepatic resection can be divided into two subtypes such as open liver resection and laparoscopic resection. Hepatic resection is applicable in patients with solitary tumors without major vascular invasion (HCC patients without cirrhosis). Survival rate is higher in liver resection but recurrence of the disease is frequent [Bryant *et al*, 2008; Vigano *et al*, 2009]. Orthotopic liver transplantation (OLT) is done in patients having liver cirrhosis along with large HCC tumor. Organ donation and organ sharing is a key factor for this type of surgery [Cha *et al*, 2003; Marsh *et al*, 2003]. According to Milan criteria the early stage of HCC that is patient with a single tumor (< 5cm) or 1-3 tumors (<3 cm of each) should undergo OLT. Survival rate and improved quality of life is generally acquired after successful surgery procedure of OLT. [Mazzaferro *et al*, 1996; Jarnagin *et al*, 2010].

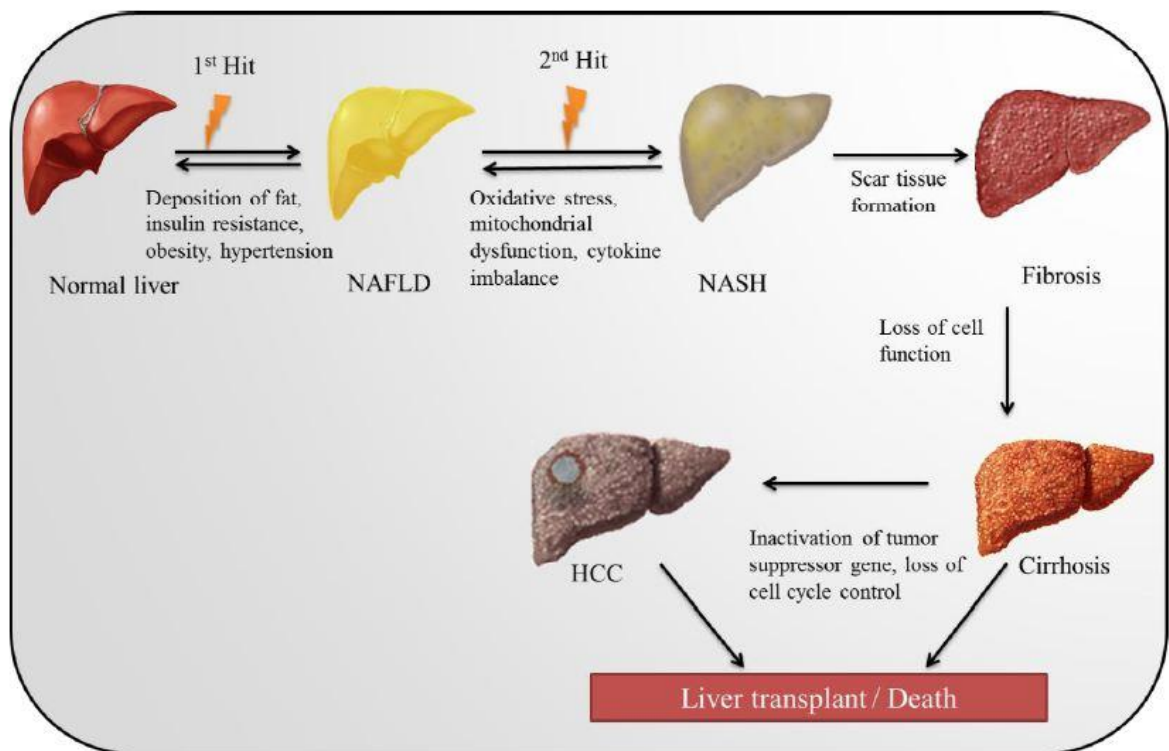


**Figure 1.1: Progression towards hepatocellular carcinoma [Anjana *et al*, 2018]**

Non-surgical treatment of HCC mainly focuses on systemic chemotherapy and cytotoxic chemotherapy. Other than that, radiotherapy, immunotherapy, hormone therapy and oncolytic virotherapy are also types of approaches to treat hepatic carcinoma which are

currently being investigated in various phases of clinical trials. The first line drug of choice for standard online systemic chemotherapy is sorafenib, a multikinase inhibitor which is the first targeted therapy approved for the treatment of advanced HCC in patients with relatively preserved liver function. Mostly, combination of sorafenib along with TAE is used for treating advanced stage of HCC. However, as per report, in average, sorafenib is useful against only 30% of HCC patients, and drug resistance is developed within six months of treatment. Doxorubicin and cisplatin are used as cytotoxic chemotherapeutic agents, but they have very high toxicity in normal hepatic cells. As liver is the main organ for metabolism, non-cirrhotic HCC patients those who have adequate hepatic function, are preferably treated with cytotoxic chemotherapeutic agents. [Zhou *et al*, 2016; Sanoff *et al*, 2016; Liu *et al*, 2015; Sanyal *et al*, 2010; Hootegem *et al*, 2016 Dhanasekaran *et al*, 2012].

## **1.2 Dietary flavonoids against HCC**

Problems associated with the treatment of hepatocellular carcinoma, such as, recurrence of the disease, drug resistance, drug induced hepatotoxicity and other adverse effects made researchers to find out alternative treatment for HCC which includes use of dietary supplements as tumor suppressive or therapeutic agents. Plenty of earlier researches showed that a regular intake of high fiber rich diet along with green vegetables and fruits, have decreased the risk, prevalence and progress of many types of cancer including HCC and increased a general well being in patients [Zhou *et al*, 2016; Smith RJ, 2012, Lippman *et al*, 2002; Wang *et al*, 2014]. Many dietary plant flavonoids act as a chemo-preventive or tumor-suppressive or anti-proliferative or chemopreservative agent at the promotional or proliferative stage of liver cancer by protecting against carcinogens, inhibiting the tumor cell growth and reducing metastasis. They can act as immunomodulating agents or may enhance the effect of other chemoprotective drugs when used as an adjuvant therapy against HCC. Flavonoids are a group of dietary products which have proven their selective anti-proliferative and cytotoxic activities against various types of cancer cells which are very important criteria against compromised hepatic environment, as normal hepatocytes are generally not affected by using those flavonoids or dietary supplements [Chatterjee and Mitra, 2015; Thoppil *et al*, 2012; Zhou *et al*, 2016].

### 1.3 *Apigenin as therapeutic agent*

Apigenin (API) is a bioactive dietary flavonoid found in various common vegetables and fruits. It has effective chemo-preservative and/or tumor-suppressive activity against many kinds of common malignancies including prostate, oral, skin, colon, breast, lungs, pancreatic, colo-rectal and hepatic cancer [Yan *et al*, 2017; Das *et al*, 2013; Valdameri *et al*, 2011, Cai *et al*, 2011]. API exerts its anticancer potential by different kinds of pathways. The main three mechanism of action of API includes cell cycle arrest (anti-proliferative effect), induction of autophagy and apoptotic pathway in tumor cells (anti-oxidant effect) and maintenance of intracellular level of p<sup>53</sup> genes (tumor-suppressive effect) [Maggioni *et al*, 2013; Lee *et al* 2014; Chen *et al*, 2016, Sung *et al*, 2016]. An unique criteria of apigenin is that it possesses much lower cytotoxicity in normal cellular environment and has been proven to have negligible side effects when consumed in a much higher dose [Xu *et al*, 2011]. The preferential cytotoxicity of API against cancerous growth has made it a very popular therapeutic strategy in anti-cancer research.

#### 1.3.1 *Mechanism of action of Apigenin*

In maximum cases, the anti-oxidant and anti-inflammatory activities of API are closely related to its anti-cancer effects [Ali *et al*, 2017]. API promotes metal chelating and scavenges free radicals which are produced due to oxidative stress inside carcinogenic cells during progression of the disease. API also induces the activities of phase II metabolic enzymes in liver, which are involved in detoxification of cytotoxic materials [Middleton *et al*, 2000] and also take part in down-regulation of lympholytic DNA damage by carcinogen(s) [Kim *et al*, 2003]. Pro-apoptotic activities of API involve regulation of many genes which include down-regulation of plasminogen activator inhibitor-2 by suppression of protein kinase B (PKB) phosphorylation, maintaining the ratio of bax/bcl-2 genes, release of cytochrome-c protein and induction of apoptotic protease activating factor 1 (Apaf-1) towards up-regulation of caspase (3, 8 and 9) pathways resulting in cleavage of poly ADP ribose polymerase (PARP) enzyme [Zeng *et al*, 2015; Valdameri G; Wang *et al*, 1999; ]. API significantly induces G<sub>0</sub>/M and G<sub>1</sub>/G<sub>2</sub> cell cycle arrest in cancerous cells by inhibiting p<sup>34</sup>cdc<sup>2</sup> gene [Wang *et al*, 2000]. API increases the stability of p<sup>53</sup> and p<sup>21</sup> genes and down-regulates expression of cyclin-dependent kinase 4 (CDK4) which in turn leads to

tumor-suppressive and anti-proliferative effect of this chemical [Chiang *et al*, 2006, Shukla and Gupta, 2010]. Further, API has proved to reduce cell viability and induce apoptotic cell death by ROS generation through NADPH oxidative pathway in different types of HCC cells [Choi *et al*, 2009]. Very few *in-vivo* reports have also indicated that at a higher dose, API has protective effects against oxidative stress and DNA damage by external carcinogen in experimental rats [Jeybal *et al*, 2005].

### 1.3.2 *Apigenin solubility and bioavailability*

However, the therapeutic efficacy of API is severely limited by two unwanted drawbacks with this chemical. Firstly, API has a major solubility problem in water and secondly it has a very low bioavailability when administered orally [Ding *et al*, 2014]. API gets cleaved in gastrointestinal (GI) track after oral ingestion and gets absorbed and distributed inside the GI lumen. This leads to a lower bioavailability of API in other organs of the body when given orally [Lefort and Blay, 2013]. Besides, API has a very strong affinity for human serum albumin (HSA), that is, 10,000 times more than the other flavonoids of same group which may also lead to the low bioavailability of it [Cao *et al*, 2011]. Further, API is a class II drug with high intestinal membrane permeation, poor solubility and very long half life of 91.8 h when administered orally [Gradolatto *et al*, 2004]. The average solubilities of API in hydrophobic and hydrophilic media are 0.001-1.63mg/ml and 2.16µg/ml respectively [Zhang *et al*, 2012; Ding *et al*, 2014]. This is also a severe disadvantage to clinical feature of API.

### 1.4 *Nanoparticle based drug delivery*

All these things cumulatively triggered the scientists to develop new technologies which can deliver hydrophobic moieties in a sustained manner to the target area to have a much higher bioavailability of API in cancerous tissue. There are few published works which have indicated that polymeric solid lipid nanoparticles loaded with API may solve all these problems and have a beneficial effect against different types of cancers [Ding *et al*, 2014; Das *et al*, 2013; Zhai *et al*, 2013, Jeetah *et al*, 2014] including HCC [Wu *et al*, 2017] *in-vitro*. Polymeric nanoparticles are excellent drug delivery systems (DDS) for optimum delivery of hydrophobic/hydrophilic drug moieties, flavonoids, vaccines, genes, protein *etc*.

to the target site of delivery in a sustained drug release pattern [Masood F, 2016]. Poly lactic co-glycolic acid (PLGA) based polymeric nanoparticles gained most popularity in this field due to their non-toxic and biodegradable nature and PLGA has been approved by the United States Food and Drug Administration (US FDA) for using in intravenous drug delivery for humans [Gentile *et al*, 2014].

Here we have developed and characterized PLGA nanoparticles loaded with API (ApNp) and modified the required parameters for a successful parenteral delivery of apigenin to treat hepatocellular carcinoma *in-vitro* and *in-vivo*. Particle size was optimized according to the need for delivery in hepatic tissues. Surface morphology were also engineered to increase the bioavailability of apigenin and to ensure the sustained drug release in the target site for a prolonged period of time. The cytotoxic effects of ApNp as well as raw API were tested against two human hepatocellular cancer cell lines, HepG2 and Huh-7. Cellular uptakes of nanoparticles were also checked by confocal microscopy and fluorescence activated cell sorting. Biodistribution and bioavailability of API as well as ApNp were measured by bio imaging and pharmacokinetic studies *in-vivo*. Further, to observe the tumor suppressive and anti-proliferative effect of API and ApNp, an HCC animal model was prepared and treated with API/ApNp and compared all the data with normal and untreated group of animals. Marker enzyme assays, macroscopic observation and histopathology investigation were done to establish the outcome of this work.

## Chapter 2

### *Literature Review*

## 2. Literature Review

### 2.1 Nanotechnology

Nanotechnology, as the term indicates, is the field of science which deals with the nanosized materials (less than 1000 nm) or specifically engineered molecules to have a sub-micron size range to reach a scientific goal towards betterment of life. The term ‘nanotechnology’ was first tossed in early 70’s (in the last century) by N Taniguchi but popularized by K. E. Drexler in 1986 [Taniguchi N, 1974; Drexler KE, 1986]. In last few decades, nanotechnology was extensively studied and used in novel applications. Few major applications of nanotechnology are depicted in **Figure 2.1**.

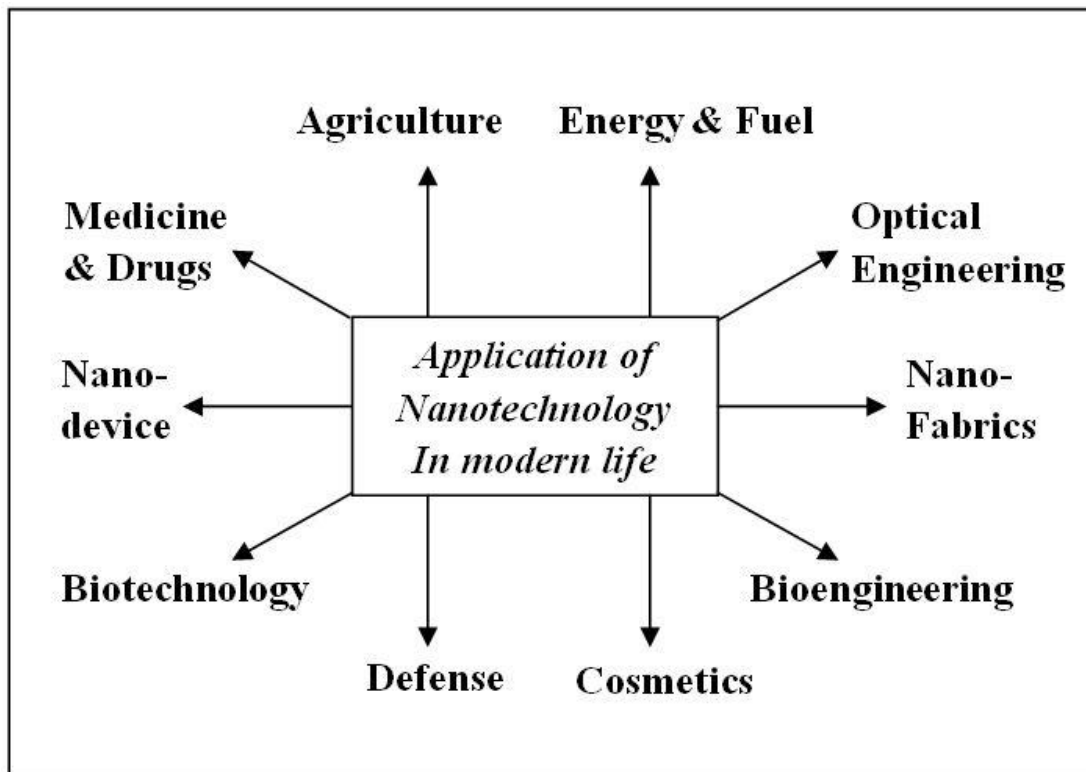


**Figure: 2.1** Applications of nanotechnology

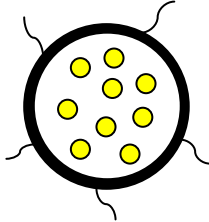
### 2.2 Nanomedicine

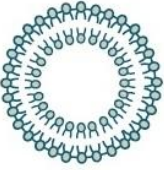
Nanomedicine or nanotherapeutics is the use of nanotechnology in the field of healthcare and medicine. Basically, any type of nanomaterials or nanosized biological devices or nanosensors which are used in biomedical research and application are termed as nanomedicines. Drug delivery to a specific target site, or nanomaterials specially engineered with required characters with the help of biotechnology or bioengineering have

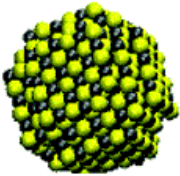


opened up a new window in medical science [Prasad M *et al*, 2018; Bharali and Mousa, 2010]. Nanotechnology is extensively used to improve the bioavailability of a drug in a specific environment [Gunasekaran *et al*, 2010] or to modify the pharmacokinetic parameters or biodistribution of a drug as required [Hamidi *et al*, 2013] or as a bioimaging tool for diagnosis purposes [Jyothi *et al*, 2013]. Types of commonly used nanomedicines with some of the US-FDA approved products with current status are listed in **Table 2.1**.

**Table 2.1: Few commonly used nanomedicines with US-FDA approved marketed products**

Type of Nanomedicine	Product Name (Active Compound)	Current Status	Indication(s)
<b>Polymeric Nanoparticles</b> 	Adagen® (adenosine deaminase enzyme)	Marketed (1990)	Severe combined immunodeficiency disease (SCID)
	Oncaspar® (L-aspargase)	Marketed (1994)	Acute lymphoblastic leukemia
	Copaxone® (Random copolymer of amino acids)	Marketed (1996)	Multiple Sclerosis (MS)
	Cimzia® (certolizumab)	Marketed (2008, 2009, 2013)	Crohn's disease, Rheumatoid arthritis, Psoriatic Arthritis, Ankylosing Spondylitis
	Eligard® (Leuprolide acetate and polymer)	Marketed (2002)	Prostate Cancer
	Mircera® (erythropoiesis-stimulating agent. ESA)	Marketed (2007)	Anemia associated with chronic kidney disease
	Neulasta® (GCSF protein)	Marketed (2002)	Chemotherapy induced neutropenia,
	Pegasys® (IFN alpha-2a protein)	Marketed (2002)	Hepatitis B and Hepatitis C
	Renagel® (Poly(allylamine hydrochloride))	Marketed (2000)	Chronic kidney disease
	PegIntron® (IFN alpha-2b protein)	Marketed (2001)	Hepatitis C
Somavert® (HGH receptor antagonist )	Marketed (2003)	Acromegaly	

	Plegridy® (PEGylated IFN-β-1a)	Marketed (2014)	Multiple Sclerosis
<b>Liposome</b>  	DaunoXome® (Daunorubicin)	Marketed (1996)	Karposi's Sarcoma
	DepoCyt© (Cytarabine)	Marketed (1996)	Lymphomatous meningitis
	Doxil® (Doxorubicin)	Marketed (1995, 2005, 2008)	Karposi's Sarcoma; Ovarian cancer; multiple myeloma
	Abelcet® (Amphotericin B)	Marketed (1995)	Fungal infection
	Curosurf® (Liposome-proteins SP-B and SP-C)	Marketed (1999)	Respiratory Distress Syndrome
	AmBisome® (Amphotericin B)	Marketed (1997)	Protozoa/fungal infection
	Visudyne® (Verteporfin)	Marketed (2000)	Macular degeneration, myopia, ocular histoplasmosis
	DepoDur® (Morphine Sulfate)	Marketed (2004)	Post-operative analgesia
	Marqibo® (Vincristine)	Marketed (2012)	Acute Lymphoblastic Leukemia
	Onivyde® (Irinotecan)	Marketed (2015)	Pancreatic cancer
MM-398(Irinotecan)	Phase III clinical trial	Small cell lung cancer, metastatic pancreatic adenocarcinoma, pediatric solid tumors	
LiPlacis (Cisplatin)	Phase II clinical trial	Advanced or refractory solid tumors, metastatic breast	
<b>Inorganic and metallic nanoparticles</b>	Nanotherm® (MagForce)	Marketed (2010)	Glioblastoma
	Feraheme™/ferumoxytol (AMAG pharmaceuticals)	Marketed (2009)	Deficiency anemia iron deficiency in chronic kidney disease (CKD)
	Venofer® (Luitpold Pharmaceuticals)	Marketed (2000)	Iron deficiency in chronic kidney disease (CKD)
	Feridex®/Endorem® (AMAG pharmaceuticals)	Marketed (1996)	Imaging agent
	DexIron®/Dexferrum® (Sanofi Avertis)	Marketed (1957)	Iron deficiency in chronic kidney disease (CKD)

	Emend® (Aprepitant)	Marketed (2003)	Antiemetic
	Tricor® (Fenofibrate)	Marketed (2004)	Hyperlipidemia
	Rapamune® (Sirolimus)	Marketed (2000)	Immunosuppressant
	Megace ES® (Megestrol acetate)	Marketed (2001)	Anti-anorexic
	Avinza® (Morphine sulfate)	Marketed (2002, 2015)	Psychostimulant
	Focalin XR® (Dexamethyl-phenidate HCl)	Marketed (2005)	Psychostimulant
	Ritalin LA® (Methylphenidate HCl)	Marketed (2002)	Psychostimulant
	Zanaflex® (Tizanidine HCl)	Marketed (2002)	Muscle relaxant
	Vitoss® (Calcium phosphate)	Marketed (2003)	Bone substitute
	Ostim® (Hydroxyapatite)	Marketed (2004)	Bone substitute
Invega® Sustenna® (Paliperidone Palmitate)	Marketed (2009, 2014)	Schizophrenia	
Ryanodex® (Eagle Pharmaceuticals)	Marketed (2014)	Malignant hypothermia	
<b>Protein nanoparticles combined with drugs or biologics</b>	Abraxane® (albumin-paclitaxel)	Marketed (2005 2012, 2013)	Breast cancer, pancreatic cancer
	Ontak® (Eisai Inc)	Marketed (1997)	Cutaneous T-Cell Lymphoma
<b>Micellar nanoparticles combined with drugs</b>	Estrasorb™ (Novavax)	Marketed (2003)	Menopausal therapy

[Bobo *et al*, 2016; Piktel *et al*, 2016; Tran *et al*, 2017]

Beside these, there are few other nanocarriers such as dendrimers, micelles, antibody drug conjugates, polymeric nanoshells, quantum dots, nanospheres etc. which are being extensively studied for their therapeutic use against different types of diseases [Tran *et al*, 2017].

### 2.3 Nanoparticles

In recent past, nanoparticles (NP) has gained very strong attention in nanomedicine field for their controlled drug delivery strategies [Rizvi and Saleh, 2018; Bhattacharyya and Singh, 2009; Zhang, J., Saltzman, M., 2013]. They are solid-colloidal drug delivery systems which are used against various types of life threatening diseases including different malignancies as a chemotherapeutic agent [Prabhu *et al*, 2015]. Cleverly engineered NPs can ensure prolonged drug residence time, greater biodistribution, higher safety and biocompatibility, specific delivery to target site, less cytotoxicity to normal cells and reduced overall cost for chemotherapy in patients [Phillips *et al*, 2010]. Many types of NPs are studied for their drug delivery purposes and among them solid-lipid polymeric nanoparticles (PNPs) are very popular in clinical medicine and research for their unique characteristics. PNP can incorporate a wide range of anticancer drugs of both hydrophobic and hydrophilic nature to their core [Mukherjee *et al*, 2009]. Delivery of such drugs can be achieved by either passive delivery or ligand based active targeting (**Figure 2.2**). [Danhier *et al*, 2010]

#### 2.3.1 Tumor targeting by nanoparticles

Passive targeting of polymeric nanoparticles uses the physiological conditions of tumor site, leaky vasculature (enhanced permeability and retention effect), surface characteristics, temperature and pH of tumor environment etc. for specific drug delivery. Ligand based targeted delivery involves conjugation of a ligand to the surface of NPs such as antibody (proteins), aptamar (nucleic acids) or any other type of ligand (peptides or vitamins or carbohydrates) and targeted delivery is ensured depending upon the appropriate receptors which are overexpressed by particular tumor cells to be treated [Gu *et al*, 2007; Maeda *et al*, 2001; Yatvin *et al*, 1980; James *et al*, 1956; Kirpotin *et al*, 2006].

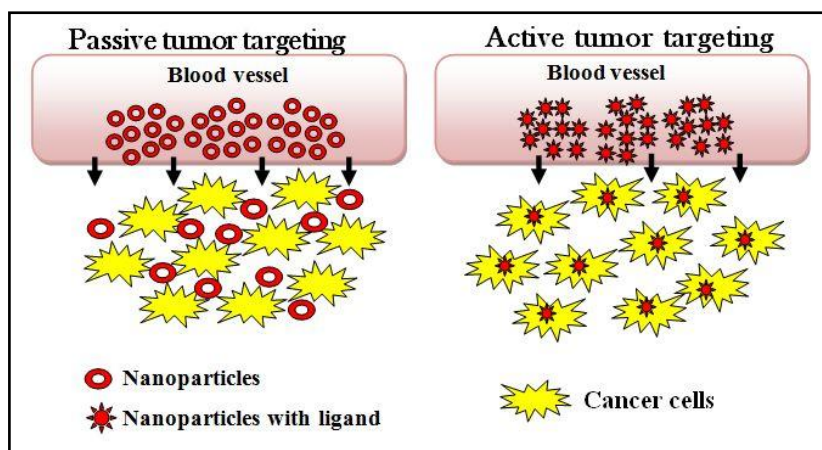


**Figure 2.2** A schematic diagram illustrating the tumor site specific delivery of polymeric nanoparticles.

### 2.3.2 Preparation of polymeric nanoparticles (PNPs)

The preparation of PNP involves the use of therapeutic agents which are generally dissolved, absorbed, entrapped or encapsulated inside the biocompatible and biodegradable polymeric matrix of solid lipid nanoparticles. Several techniques have been developed for preparation of polymeric nanoparticles which are classified depending upon the process of particle formation that is by dispersion or polymerization or ionic gelation of monomers [Yadav *et al*, 2012].

*The common methods for preparation of PNPs by dispersion of preformed polymer:*

- a) **Solvent evaporation:** Here polymeric solutions are dissolved in a volatile substance such as dichloromethane or chloroform or ethyl acetate and a single emulsion (o/w) or double emulsion (w/o/w) is formed with the help of a high speed homogenizer. After that, the organic solvent is evaporated, PNPs are sedimented by centrifugation and dry product is collected after lyophilization [Reis *et al*, 2006].
- b) **Nanoprecipitation:** This method is also known as solvent displacement technique. Here the preformed polymer is precipitated in an organic solvent and the organic solvent is diffused in an aqueous medium in presence or absence of a surfactant which leads to formation of colloidal suspension instantly [Barichello *et al*, 1999].
- c) **Emulsification/solvent diffusion (ESD):** It is a modified form of solvent evaporation technique. Here the polymer is dissolved in a semi water soluble

solvent and saturated with water. Then the polymers are precipitated and PNPs are prepared by emulsification of polymer-water saturated solvent phase in an aqueous medium according to oil to polymer ratio [Quintanar-Guerrero *et al* 1998].

- d) **Dialysis:** In this method, polymer is dissolved in organic solvent and kept inside a dialysis bag. Dialysis is performed against a non-solvent miscible with organic solvent. Displacement of the solvent inside the dialysis bag leads to polymer aggregation and formation of homogeneous nanoparticles [Niwa *et al*, 1993].
- e) **Salting out:** This technique is used to separate a water miscible liquid from aqueous solvent by salting out effect. Polymer and drug is dissolved in an organic solvent followed by emulsification to aqueous gel containing a stabilizer and salting out agent and this results in formation of nanoparticles when diluted with aqueous phase [Fessi *et al*, 1989].
- f) **Supercritical fluid technology:** By this method, environment friendly PNPs can be prepared which are of high purity and without any trace of organic solvents. Generally two types of techniques are used here: (i) rapid expansion of supercritical solution (RESS) and rapid expansion of supercritical solution into liquid solvent (RESOLV) [York *et al*, 1999].

#### ***Preparation of PNPs by polymerization of a monomer***

- a) **Emulsion polymerization:** This is a rapid method to produce emulsions. Here an aqueous continuous phase is used where the monomer is dissolved. After that polymerization process is initiated. Phase separation and formation of solid nanoparticles take place before and after the termination of polymerization reaction [Ekman *et al*, 1978].
- b) **Interfacial polymerization:** Interfacial polymerization is a newly developed method. Stepwise polymerization takes place between two monomers which have been dissolved in two different phases (i.e., continuous and dispersed phase) and the reaction takes place in the interface of two liquids [Crespy *et al*, 2007].
- c) **Controlled/living radical polymerization (C/LRP):** C/LRP is done by (i) nitroxide-mediated polymerization, (ii) atom transfer radical polymerization, (iii) reversible addition and fragmentation transfer chain polymerization etc [Zetterlund *et al*, 2008].

***Preparation of PNPs by ionic gelation/coacervation of hydrophilic polymers***

a) **Ionic gelation:** This process is used to develop nanoparticles from biodegradable hydrophilic polymers such as chitosan, sodium alginate and gelatin. Positively charged hydrophilic polymers react with negatively charged polyanion compound to form ion gels with a size range of nanoparticles. Here, electrostatic interactions take place between the two aqueous phases [Calvo *et al*, 1997].

**2.3.3 *Polymeric nanoparticles for targeted therapy in hepatocellular carcinoma:***

HCC is a type of primary liver cancer which accounts for the third highest cancer related deaths worldwide. There are several risk factors associated with HCC such as hepatitis B and C, liver cirrhosis, alcohol consumption, various metabolic disorders etc. which may lead to HCC in patients. Treatment strategy for HCC includes surgical (liver transplantation or resection) and non-surgical (chemotherapy and radiotherapy) techniques. No such drug or surgical method is yet to discover that could provide curative treatment of HCC. Further, the underlying cause of this disease is not fully understood till date. The main reasons for an unsuccessful chemotherapy in HCC patients include drug resistance, reduced bioavailability of the drug at tumor site after oral and parenteral delivery, side effects of drugs in normal hepatic tissue etc [Reddy and Couvreur, 2011; Fattal *et al*, 1989]. Scientists have shown that these difficulties can be overcome by using polymer based nanoparticles to deliver drugs of both hydrophilic and hydrophobic nature in the HCC tumor site at a much higher concentration in a sustained drug release pattern. Some of the drug loaded nanoparticles which have achieved clinical and pre-clinical success against HCC has been discussed below.

a) Doxorubicin loaded poly (isohexylcyanoacrylate) nanoparticles (also known as doxorubicin transdrug or DT) have successfully controlled HCC incidences in-vivo animal model and currently undergoing clinical trials for liver tumors. DT is active against a multidrug resistant protein which is overexpressed in HCC patients. After the safety and toxicological studies, a dose of 35 mg/m<sup>2</sup> was considered to be safe for usage in human. Recently, a phase II trial was conducted on efficacy of DT that indicated that after 18 months of study on patients, 88.9% survival rate were

achieved when a repeated dose of 30 mg/m<sup>2</sup> were given [Barraud *et al*, 2005; Merle *et al*, 2006].

- b) Another phase II clinical trial was conducted on treatment of HCC with mitoxantrone-loaded polybutylacrylate nanoparticles intravenous formulation. A slight improvement in efficacy with a 2.2 fold higher survival time was achieved with this treatment [Zhou *et al*, 2009].
- c) Carboplatin encapsulated chitosan coated magnetic nanoparticles combined with magnetic fluid hyperthermia technique were applied on HCC tumor in preclinical mice model with reasonable success. These nanoparticles were intra-arterially injected to the animals and then animals were subjected to hyperthermia. A prolonged survival rate and 93% tumor inhibition was achieved by this treatment [Li *et al*, 2009].
- d) Galactosylated polymeric nanoparticles were tested against asialoglycoprotein receptors overexpressed on hepatic cells in HCC [Jain *et al*, 2010].
- e) Sorafenib loaded polymeric nanoparticles showed much higher stability and release of sorafenib in liver cancer cells in-vitro. Sorafenib loaded polymeric nanoparticles tagged with an antibody had a great tumor inhibitory effect on HCC xenograft nude mice model, without the obvious side effects of sorafenib as a free drug [Tang *et al*, 2018].
- f) Super magnetic iron oxide nanoparticles (SPION) are used as a liver imaging tool for detecting the stage of liver cancer. It acts by measuring the accumulation of SPION in different types of hepatic environment. Two different SPION such as ferumoxide (dextran-coated SPION, Endorem, Ferridex) and ferucarbotran (carboxydextran-coated SPION, Resovist) are clinically approved for hepatic cancer imaging [Digumarthy *et al*, 2005; Tanimoto *et al*, 2006].

#### **2.3.4 PLGA nanoparticles against HCC**

Some investigations involving poly (lactic-co-glycolic) acid nanoparticles (PLGA-nanoparticles) drug delivery system against HCC are listed below.



- a) Kumar *et al*, (2017) showed that umbelliferone  $\beta$ -D-galactopyranoside (UFG) loaded PLGA nanoparticles have a potential anti-cancer activity against HCC both in-vitro and in-vivo.
- b) Arginine-glycineaspartic acid (RGD) modified lipid coated PLGA nanoparticles were developed for targeted delivery of two different drugs such as sorafenib and quercetin and their combinations against HCC in-vitro and in-vivo. Studies showed that the combination drug loaded nanoparticles showed a significant inhibition of HCC tumors resulting in elevated therapeutic efficacy on this disease [Wang *et al*, 2016].
- c) Devulapally *et al* (2016) reported that antisense miRNA-21 and gemcitabine co-encapsulated in pegylated PLGA nanoparticles increased efficacy of the drugs when treated against HCC cells.
- d) PLGA nanoparticles loaded with betulinic acid showed a better therapeutic response against HCC both in-vitro and in-vivo and could serve as future candidate molecule for HCC treatment [Kumar P *et al*, 2018].
- e) Pandey and co-workers showed that rutin loaded PLGA loaded nanoparticles reduced incidences of hepatic nodules, necrosis formation, infiltration of inflammatory cells, blood vessel inflammation etc. along with down-regulation of various pro-inflammatory cytokines in HCC animal model [Pandey *et al*, 2018].

#### 2.4 *Excipients specific review*

Several polymers such as poly (lactide-co-glycolide) (PLGA), polylactide (PLA), polyglycolide, polycaprolactone (PCL), poly (d,l-lactide), chitosan, and PLGA–polyethylene glycol (PEG) have been developed for passive and ligand-targeted delivery of therapeutic moieties to the target site [Nair *et al*, 2011; Cheng *et al*, 2012; Park *et al*, 2009; Prabhu *et al*, 2015]. Among them PLGA have been studied and used extensively as the carrier matrix for nanoparticles and we used PLGA 85:15 grade in our formulations. Beside this, in our study, two different concentrations of polyvinyl alcohol (PVA) were used as the water phase of the double emulsion.

### 2.4.1 PLGA

It is a synthetic co-polymer of lactic acid and glycolic acid. Lactic acid is an intermediate metabolite or end product of carbohydrate metabolism cycle, hence abundantly found in the natural sources. On the other hand, glycolic acid is also found in nature but in a much lesser extent than lactic acid. PLGA is a biodegradable polymer. It degrades in lactate and glycolate (salt forms of lactic acid and glycolic acid respectively). Ligands can be easily added and manipulated on the surface of PLGA for targeted drug delivery [Avgoustakis K, 2005; Gentile *et al*, 2014].

#### Synthesis

PLGA is mainly synthesized by ring opening co-polymerization reaction of two different monomers of glycolic acid and lactic acid [Erbetta *et al*, 2012]. Different forms of PLGA (e.g. 50:50, 75:25, 85:15 etc.) are synthesized depending upon the lactides/glycolides ratio which indicates the percentages of lactic acid and glycolic acid in that particular form of PLGA [Hyon *et al*, 1997].

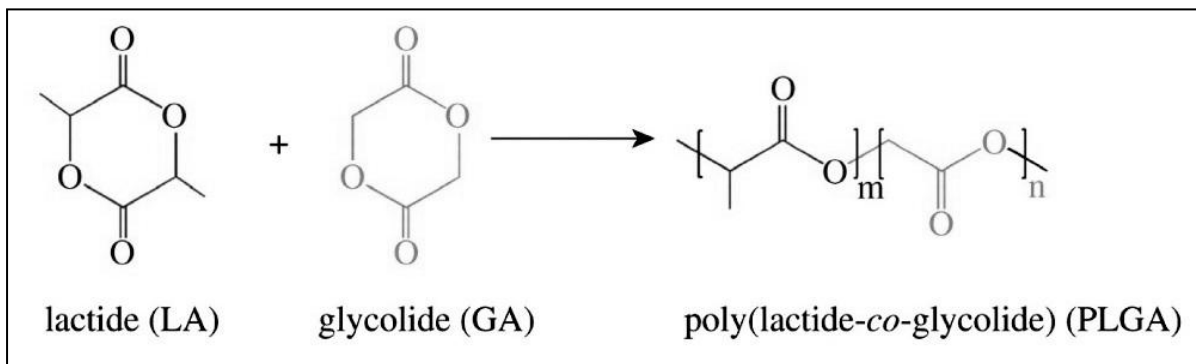


**Figure: 2.3 Synthesis and structure of PLGA, where *m* and *n* are the number of units of lactides and glycolides respectively. [Pan et al, 2012]**

#### Solubility

The solubility of PLGA depends on the ratio of lactide and glycolide. When the amount of glycolide is less than 50%, PLGA is soluble in wide range of organic solvents (such as dichloromethane etc). But when the percentage of glycolic acid is more that 50% in the polymer, it is insoluble in most organic solvents. Only few unusual solvent like propanolol can dissolve that form of PLGA [Avgoustakis K, 2005].

**Molecular weight:**

PLGA polymers have variety of molecular weights depending upon different ratios of lactide and glycolide tabulated in **Table 2.2**.

**Table 2.2 List of PLGA molecular weights versus polymeric ratios**

<b>Ratio of Lactide: Glycolide</b>	<b>Molecular weight of that form</b>
50:50	30,000-60,000
50:50 (ester terminated)	100,000
65:35	40,000-75000
75:25	66,000-107,000
80:20	200,000
85:15	190,000-240,000

**Crystallinity**

The glycol content in PLGA consisting 0-75% of total amount results in an amorphous form of the polymer. Depending on crystallinity, the thermal stability and melting point of PLGA differs [Gilding and Reed, 1979].

**Thermal stability and storage**

In absence of moisture, various forms of PLGA are generally thermostable. Prolonged heating of PLGA over 200 °C in nitrogen vacuum results in degradation of the polymer. PLGA should be stored at a cool and dry place in an air tight container [Silva *et al*, 2015; Gilding and Reed, 1979; Lu *et al*, 1999].

**Degradation**

PLGA undergoes hydrolytic degradation via breaking of ester bonds by hydrolysis. In normal condition, the average degradation time taken for PLGA 50/50, 75/25 and 85/15 are 1-2 months, 4-5 months and 5-6 months respectively [Park *et al*, 1995; Pitt and Gu, 1987; Tracy *et al*, 1999].

**Elimination**

The lactate residue converts into CO<sub>2</sub> and pyruvate. The pyruvate residue then enters in Krebs's cycle. Glycolic acid is generally excreted via urine [Anderson and Shive, 1997; Drury and Wick, 1956].

### Biomedical applications of PLGA

PLGA is nontoxic, biocompatible and biodegradable compound and it is approved by US-FDA for internal usage in human [Gentile *et al*, 2014; Hans and Lowman, 2002]. PLGA is being used since 1974 (product name was Vicryl) in biomedical field and currently being extensively used by numbers of commercial manufacturers [Ulery *et al*, 2011; Conn *et al*, 1974]. PLGA have great cell adhesion properties, making it an excellent drug carrier for variety of molecules such as chemotherapeutics, genes, proteins, enzymes, antibodies, aptamers etc. for application in drug delivery field. Most often PLGA is used to prepare nanoparticles, microspheres, microcapsules, nanospheres or nanofibers to facilitate controlled drug delivery [Ulery *et al*, 2011]. Few types of drug loaded PLGA nanoparticles as chemotherapeutic drug delivery system are listed in **Table 2.3** [Prabhu *et al*, 2015].

**Table: 2.3** PLGA nanoparticles developed against different types of diseases

Polymer Name	Drug Name	Passive/Active targeting	Indication
PLGA	Paclitaxel	Passive	Human cervical cancer
	Cisplatin	Passive	Colon adenocarcinoma
	5-Flurouracil	Passive	Glioma, breast carcinoma
	Doxorubicin	Passive	Breast cancer, cervical cancer
PLGA-mPEG	Tamoxifen	Passive	Breast cancer
	Cisplatin	Passive	Prostate cancer, ovarian cancer
PLGA-mPEG-CMC-GCS	5-Flurouracil	Passive	HCC
PLGA-HSA-PLC	Doxorubicin, Tamoxifen	Passive	HCC, glioblastoma, breast cancer, cervical cancer
PLGA	Gemicitabine	Active (EGFR antibody)	Epithelial growth factor disease
PLGA-b-PEG	Peptide	Active (Aptamer)	Prostate cancer
PLGA-PEG	Peptide	Active (EGFR antibody)	Epithelial growth factor disease

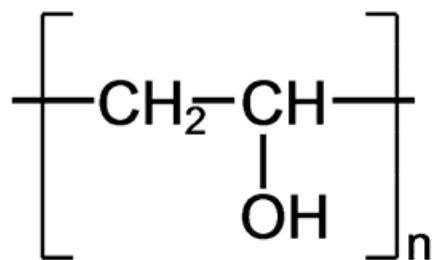
**Abbreviations:** PLGA, poly(lactide-co-glycolide); mPEG, methoxy-polyethylene glycol; CMC, carboxymethyl cellulose; GCS, glycosylated chitosan; HSA, human serum albumin; PLC, poly(d,l-lactide-co-caprolactone); EGFR, epithelial growth factor receptor

### 2.4.2 PVA

Poly (vinyl alcohol) or PVA is a water soluble synthetic polymer. It is biodegradable and biocompatible in nature and hence it is used extensively as emulsion polymerization and is suitable for drug delivery system along with other polymers [Brough *et al*, 2016, Part I and II].

**Synthesis:** PVA is synthesized in two steps, polymerization of vinyl acetate leads to poly (vinyl acetate) and this is further converted to PVA [Brough *et al*, 2016, Part I].

**Chemical structure:**



**Molecular weight:** 20,000-200,000 Da

**CAS-No.** 9002-89-5

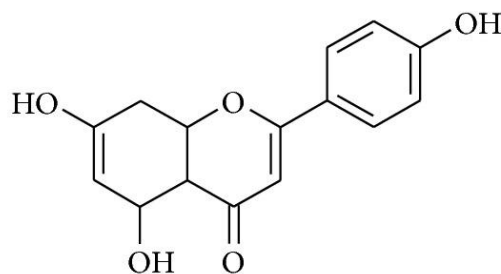
**Physical and chemical properties:** It is a crystalline substance having melting points of 230 °C (fully hydrolyzed PVA) to 180-190 °C (partially hydrolyzed PVA). At high temperature, it undergoes pyrolysis. PVA is soluble in water, sparingly soluble in 95% ethanol and insoluble in organic solvents.

**Storage:** PVA should be stored at a cool and dry place in an air tight container.

**Biomedical uses:** PVA is currently being used in a variety of pharmaceutical applications. It is used as a stabilizing agent for emulsions in topical pharmaceutical and in ophthalmic formulations. It is used in artificial tears and integrated into contact lenses for lubrication purposes. Polyvinyl alcohol can be made into microspheres and is used as an emulsifier in creating PLGA nanoparticles. It has also been used in sustained-release formulations for oral administration and transdermal patches [Winterton *et al*, 2007; Thanoo *et al*, 1993; Sahoo *et al*, 2002; Mu *et al*, 2003; Riis *et al*, 2007; Davaran *et al*, 2005].

**Safety and toxicity:**

PVA is a non-toxic synthetic polymer. It is nonirritant to skin and eye hence used in ophthalmic formulations and cosmetics. The LD<sub>50</sub> of PVA is 14,700 mg/kg in mouse. It is an acceptable non-medical ingredient and included in FDA inactive ingredients database [<https://www.spectrumchemical.com/MSDS/P2152-AGHS.pdf>].

**2.5 Drug specific review****APIGENIN****Chemical Structure:**

**Identifications:** CAS Number 520-36-5; Drug Bank DB07352; PubChem 5280443

**IUPAC Name:** 5, 7-Dihydroxy-2-(4-hydroxyphenyl)-4H-chromen-4-one

**Molecular formula :** C<sub>15</sub>H<sub>10</sub>O<sub>5</sub>

**Molecular weight:** 270.24 g/mol

**Physical properties**

- **Description:** Apigenin is a yellow crystalline solid
- **Solubility:** It is a hydrophobic chemical and insoluble in water. It is soluble in dimethylsulfoxide (DMSO) and potassium hydroxide (KOH).

- **Melting point:** 345 to 350 °C (653 to 662 °F)
- **UV-vis ( $\lambda_{\text{max}}$ ):** 267, 336 nm in methanol
- **Storage:** Apigenin should be stored in an air tight container and to be kept at a cool and dry place

**Source:**

Apigenin is a bioflavonoid, naturally found in many fruits and vegetables, including apples, grape fruits, oranges, onions and celery. A high amount of apigenin can be isolated from several popular spices, including chamomile, basil, oregano, tarragon, cilantro, and parsley [McKay and Blumberg, 2006; Birt *et al*, 2001; Patel *et al*, 2007; Bevilacqua *et al*, 2004, Shukla and Gupta, 2010].



**Figure 2.4: Common sources of apigenin in nature**

**Pharmacokinetics properties:**

- **Absorption and distribution:** Apigenin, when consumed orally, is well absorbed in gastric lumen. It is highly bound to plasma protein (10,000 times more than other flavonoids) [Cao *et al*, 2011; Xiao *et al*, 2009]. The half life of apigenin is 91.8 h

and it appears in the blood 24 hours after initial ingestion [Gradolatto *et al*, 2005]. For this reason, bioavailability of apigenin is much low.

- **Metabolism and excretion:** It is rapidly metabolized via UDP glucuronosyltransferase and released into serum as glucoside and sulfate conjugates. It is mostly excreted via the urine in the form of glucosides and sulfate conjugates, but there is some fecal excretion as well due to enterohepatic ejection [Griffiths *et al*, 1972].

### **Safety and toxicity:**

No apparent toxicity is recorded for apigenin overdose in normal cells. However, it has a preferential cytotoxic effect on a variety of cancer cells. [Ross *et al*, 2002; Hollman *et al*, 1999].

### **Biological effects:**

Apigenin possesses variety of biological functions such as anti-tumor, anti-diabetic, anti-oxidant, anti-viral, anti-inflammatory, anti-bacterial, immuno-suppressive, antigenotoxic, antiangiogenic, anxiolytic and sedative effects. Researchers have shown that, there are numbers of diseases such as cardiovascular diseases, hepatotoxicity, nephrotoxicity, lung fibrosis, ischemia, auto immune diseases, homeostasis, muscle regeneration, Alzheimer's disease, parkinsonism, HIV, multiple sclerosis, arthritis etc. where apigenin showed strong beneficial effects. The chemotherapeutic potential of apigenin is also very high and it showed a strong anti-proliferative and tumor-suppressive effect against different types of malignancies including hepatocellular carcinoma [Yan *et al*, 2017; Shukla and Gupta, 2010; Balez *et al*, 2016]

### **Mechanism of action:**

Apigenin possess its biological functions by regulating different cellular pathways in different diseases. A schematic diagram of major pathways by which apigenin exerts its pharmacological effects is given in **Figure 2.5**.



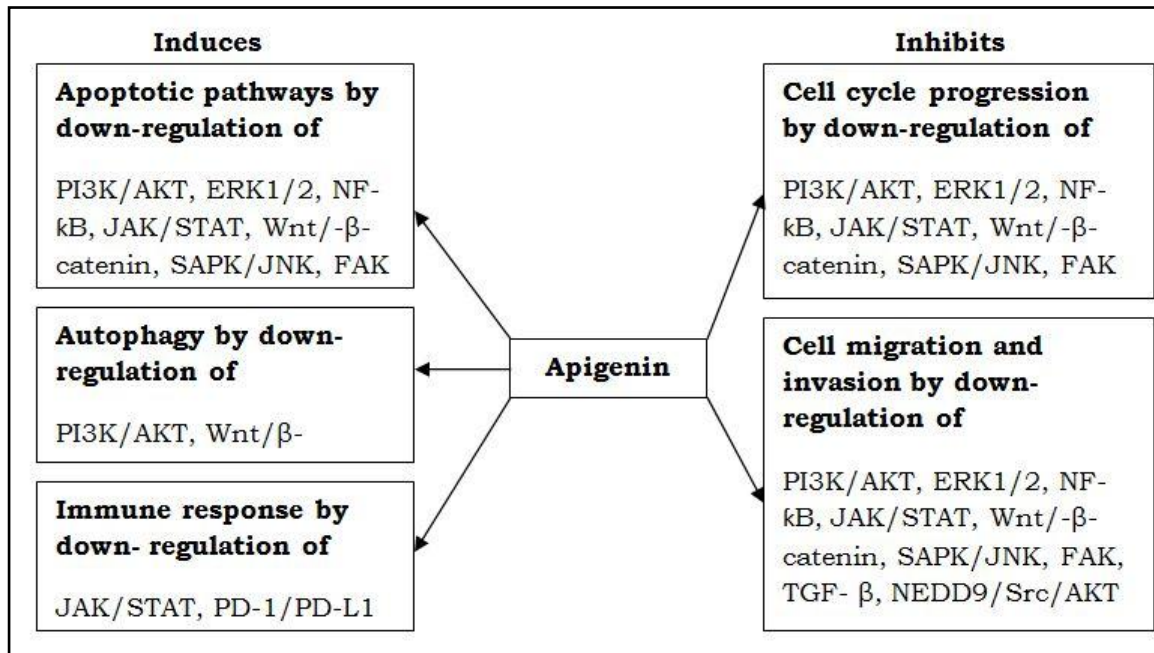


**Figure: 2.5** Different molecular pathways regulated by apigenin *in-vitro* and *in-vivo*. [Yan *et al*, 2017]

## Chapter 3

### *Objectives & Plan of Study*

### 3. Objectives and plan of study

#### 3.1 Objectives

The objective of this research work was to develop and optimize apigenin (API) loaded PLGA nanoparticles to enhance the bioavailability of apigenin and to investigate them as a targeted therapy against hepatocellular carcinoma *in-vitro* and *in vivo*.

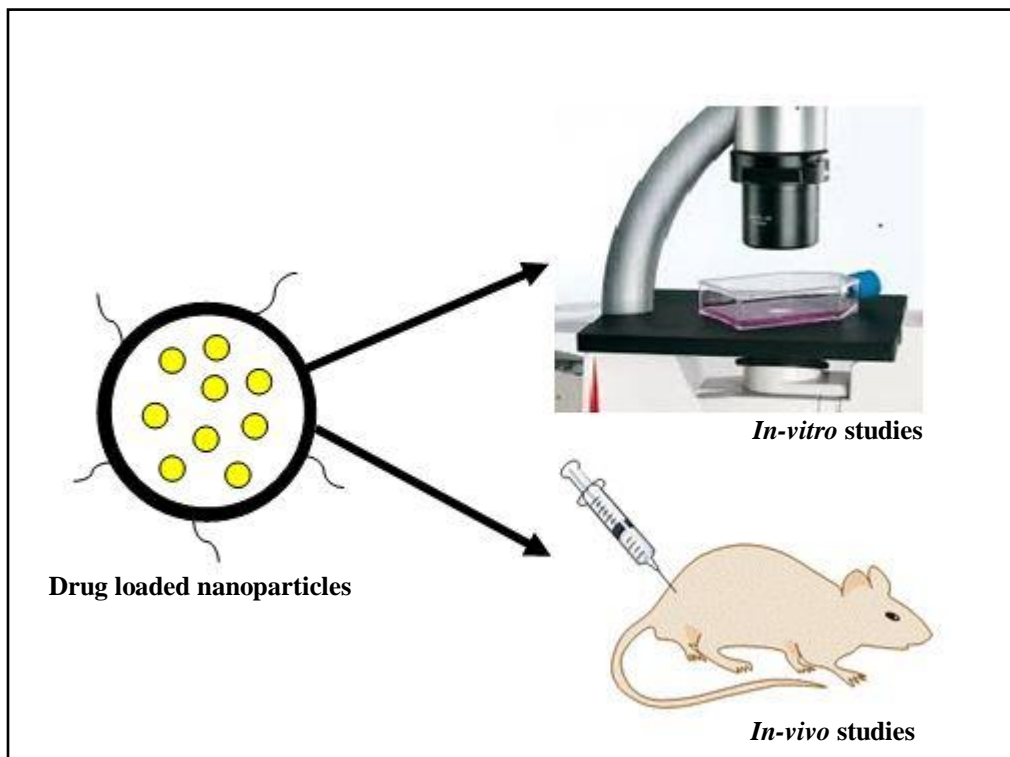


**Figure 3.1** A simple schematic diagram explaining the objectives of the study

### 3.2 *Plan of study*

The study was planned as given below

#### *Preformulation studies of apigenin*

- Preparation of different buffers used in the study
- Analytical method development of API by UV-Visible spectroscopy
- Development of Calibration Curve of apigenin by UV spectroscopy

#### *Formulations of polymeric nanoparticles of API*

- Preparation of apigenin loaded polymeric nanoparticles (ApNp) by multiple emulsion and solvent evaporation technique.
- Optimization of particle size and surface characteristics to ensure optimum targeted delivery of ApNp to hepatic environment.
- Investigation of presence of any physical or chemical interactions between drug and excipient by Fourier transform infra red (FTIR) spectroscopy
- Evaluation of surface morphology of the prepared nanoparticles using field emission scanning electron microscopy (FESEM), transmission electron microscopy (TEM) and atomic force microscopy (AFM).
- Assessment of stability of prepared ApNp by accelerated stability study and hydrolytic stability study.

#### *In-vitro drug release studies*

- *In-vitro* drug release ApNp was performed in PBS (pH 7.4), citric acid buffer (pH 3) and acetic acid buffer (pH 5) using cumulative drug release method.
- Assessment of various drug release kinetics and regression coefficients of the prepared formulation in different buffers.

***In-vitro experiments on human HCC cell lines***

- Evaluation of cytotoxicity of ApNp and API on HepG2 and Huh-7 cells and determination of respective IC<sub>50</sub> values.
- Visualization of cellular uptake of ApNp in both HCC cells by confocal microscopy
- Quantification of cellular uptake of ApNp by FACS

***In-vivo experiments***

- Development of chemical induced HCC rat model and the treatment of the animals with ApNp and API to determine the efficacy of the formulation against the control groups of rats.
- Pharmacokinetic studies and biodistribution of optimized nanoparticles and API in balb/c mice and evaluation of pharmacokinetic parameters
- Time dependent bio-imaging and assessment of organ specific biodistribution of radiolabeled nanoparticles (<sup>99m</sup>Tc-ApNp) and radiolabeled free drug (<sup>99m</sup>Tc-API) in untreated and HCC bearing experimental animals.
- Assessment of variation in contents/activities of hepatocellular carcinoma-specific marker isoenzymes/enzymes (cyt P-450, GST, UDPGT and SOD) in different experimental groups of rats.
- Macroscopic and microscopic investigations of livers dissected from different groups of experimental rats.

***Statistical Analysis***

- Statistical analysis of the data by one way ANOVA and Student's t-test wherever applicable.

## Chapter 4

### *Materials and Methods*

## 4.1 Materials

### 4.1.1 Chemicals

- Name and sources of the chemicals and other import materials used

Serial No	Name	Source
1.	2-Acetylaminofluorene	Sigma-Aldrich Co, St Louis, MO, USA.
2.	Acetone	Merck Life Science Pvt. Ltd, Bengaluru, India
3.	Acetonitrile	Merck Life Science Pvt. Ltd, Bengaluru, India
4.	Ammonium formate	Sigma-Aldrich Co, St Louis, MO, USA.
5.	Apigenin	Sigma-Aldrich Co, St Louis, MO, USA.
6.	Chloroform	Merck Life Science Pvt. Ltd, Bengaluru, India
7.	Citric acid	Merck Life Science Pvt. Ltd, Bengaluru, India
8.	Cytochrome P-450 assay kit	Thermo Fisher Scientific, Mumbai, India
9.	4',6-diamidino-2-phenylindole	Sigma-Aldrich Co, St Louis, MO, USA.
10.	Dichloromethane	Merck Life Science Pvt. Ltd, Bengaluru, India
11.	Diethylnitrosamine	Sigma-Aldrich Co, St Louis, MO, USA.
12.	Disodium hydrogen phosphate	Merck Life Science Pvt. Ltd, Bengaluru, India
13.	Dulbecco's Modified Eagle Medium	HiMedia Laboratories, Mumbai, India.
14.	Dimethyl Sulfoxide	Merck Life Science Pvt. Ltd, Bengaluru, India
15.	Dibutylphthalate Polystyrene Xylene	Merck Life Science Pvt. Ltd, Bengaluru, India
16.	ethylenediaminetetraacetate	Merck Life Science Pvt. Ltd, Bengaluru, India
17.	Ethyl acetate	Merck Life Science Pvt. Ltd, Bengaluru, India
18.	Fetal Bovine Serum	HiMedia Laboratories, Mumbai, India
19.	Fluorescein Isothiocyanate	HiMedia Laboratories, Mumbai, India
20.	Glacial acetic acid	Merck Life Science Pvt. Ltd, Bengaluru, India
21.	Glutathione S Transferase assay kit	Sigma-Aldrich Co, St Louis, MO, USA
22.	Hematoxyline and eosine	Sigma-Aldrich Co, St Louis, MO, USA.
23.	Methanol	Merck Life Science Pvt. Ltd, Bengaluru, India

24.	3-(4,5-Dimethylthiazol-2-Yl)-2,5 Diphenyltetrazolium Bromide	HiMedia Laboratories, Mumbai, India
25.	Naringenin	Sigma-Aldrich Co, St Louis, MO, USA.
26.	Penicillin-Streptomycin	HiMedia Laboratories, Mumbai, India
27.	Poly Lactic Co-Glycolic Acid	Sigma-Aldrich Co, St Louis, MO, USA.
28.	Pottasium dihydrogen phosphate	Merck Life Science Pvt. Ltd, Bengaluru, India
29.	Poly (Vinyl Alcohol)	S D Fine-Chemicals limited, Mumbai, India
30.	Sodium acetate	Merck Life Science Pvt. Ltd, Bengaluru, India
31.	Sodium bicarbonate	Merck Life Science Pvt. Ltd, Bengaluru, India
32.	Sodium carbonate	Merck Life Science Pvt. Ltd, Bengaluru, India
33.	Sodium citrate	Merck Life Science Pvt. Ltd, Bengaluru, India
34.	Sodium hydroxide	Merck Life Science Pvt. Ltd, Bengaluru, India
35.	Technetium chloride	Sigma-Aldrich Co, St Louis, MO, USA.
36.	Trypsine	HiMedia Laboratories, Mumbai, India

#### 4.1.2 Instruments

- Name and sources of the major instruments used

Serial No	Name	Source
1.	0.22 membrane filter	Merck Life Science Pvt. Ltd, Mumbai, India
2.	-80° C Freezer (Model no U410-86)	New Brunswick Scientific, Eppendorf House, Arlington Business Park, Stevenage, UK
3.	Atomic force microscope	Dimension icon, Bruker, Billerica, MA, USA
4.	Automatic plate reader	Thermo Scientific Multiskan EX, Thermo Fisher Scientific, Waltham, MA, USA
5.	Bath sonicator	Trans-O-Sonic, Mumbai, India
6.	BD-FACS Verse T <sub>m</sub>	BD biosciences, San Jose, USA
7.	CO <sub>2</sub> incubator	Thermo Fisher Scientific, Waltham, MA, USA



8.	Cold centrifuge	HERMLE Labortechnik GmbH, Wehingen, Germany
9.	Confocal microscope	TCS-SP8 confocal microscope, Leica, Germany
10.	Digital camera	Canon Power Shot SX50 HS, Tokyo, Japan
11.	Digital pH meter (EUTECH)	Thermo Fisher Scientific India Pvt. Ltd., Hiranandani Business Park, Mumbai India
12.	Digital weigh machine	Sartorius Corporate Administration, Otto-Brenner- Straße 20, Goettingen, Germany
13.	Disposable syringe (Dispo Van)	Hindustan Syringes and Medical Devices Limited, Ballabgarh, Faridabad, Haryana, India
14.	FTIR instrument	Magna-IR 750, Series II, Nicolet Instruments Inc, Madison, Wisconsin, USA
15.	Gamma camera	GE Infinia Gamma Camera with Xeleris Work station, GE, Cleveland, OH, USA
16.	Gamma counter	Electronic Corporation of India, model LV4755, Hyderabad, India
17.	High speed homogenizer	IKA Laboratory Equipment, Model T10B Ultras- Turrax, Staufen, Germany
18.	Incubator shaker	BOD-INC-1S, Incon, India
19.	Laminar airflow bio- safety hood	Thermo Fisher Scientific, Waltham, MA USA
20.	LC-MS/MS	LC: Shimadzu Model 20AC, MS: AB-SCIEX, Model: API4000. GenTech Scientific, Inc, Arcade, NY, USA
21.	Light microscope	Carl Zeiss: Axiostar plus, Jena, Germany
22.	Laboratory freeze dryer (lyophilizer)	Instrumentation India, Kolkata, India
23.	Magnetic stirrer	Remi Sales & Engineering Ltd, Ganesh Chandra Avenue, Bando House, Dharmatala, Kolkata, India
24.	Normal Freezer	LG double door, Yeouido-dong, Seoul, South Korea
25.	Particle size and zetasizer	Zetasizer nano ZS 90, Malvern Zetasizer Limited, Malvern, UK
26.	Transmission	JEOL JEM-2010 TEM, JEOL, Japan

	electron microscope	
27.	UV-VIS spectrophotometer	LI-295 UV VIS Single Beam, Lasany International, Haryana, India
28.	Vortex mixture	Remi Sales & Engineering Ltd, Ganesh Chandra Avenue, Bando House, Dharmatala, Kolkata, India
29.	YMC Trait C-18 Column	30X2.1 mm, 5 $\mu$ , YMC CO., LTD., Koyto, Japan

## 4.2. Experimental Methods

### 4.2.1 *Preformulation Studies*

#### 4.2.1.1 *Preparation of different buffers used in the study*

##### **Phosphate buffer saline (PBS, pH 7.4): 100 ml**

PBS was prepared according to the formula mentioned in Indian pharmacopoeia (volume 1). At first, for 100 ml of PBS buffer, 0.8 g of Sodium chloride, 0.238 g di Sodium hydrogen phosphate and 0.019 g of potassium dihydrogen phosphate were taken in a 100 ml volumetric flask and dissolved in 90 ml of double distilled water (DDW). The pH of the solution was adjusted to 7.4 with continuous shaking. Finally, the volume was made up to 100 ml with DDW.

##### **Citrate buffer (pH 3): 100 ml**

For 100 ml of citrate buffer, we took 1.204 g Sodium citrate dehydrate and 1.134 g citric acid in a volumetric flask and dissolved the mixture in 80 ml of DDW. The pH of the buffer was adjusted to 3.0 with 0.1N HCL and final volume was made up to 100 ml with DDW.

##### **Acetate buffer (pH 5): 100 ml**

0.55 g of Sodium acetate and 0.177 g of acetic acid was mixed and dissolved in 80 ml of DDW at a continuous stirring. The pH of the solution was adjusted to 5.0 with 10N HCL and the final volume was made up to 100 ml with DDW.

#### 4.2.1.2 UV-VIS absorption maxima of apigenin

To determine the exact absorption maximum of apigenin, we had scanned a dilute apigenin solution (DDW/PBS, pH 7.4) from 200-600 nm. A small amount of API was dissolved in DMSO and this solution was dissolved in DDW/PBS. Base line for the study was created using the software (LI-295 UV VIS Single Beam Spectrophotometer). The absorbance spectrum was set at zero taking blank solution (with DMSO) at wavelength range of 200-600 nm.  $\lambda_{\max}$  value of the drug was determined at 340 nm.

#### 4.2.1.3 Development of Calibration Curve of Apigenin by UV Spectroscopy

Absorbance of apigenin in solutions was determined at  $\lambda_{\max}$  value of 340 nm in DDW/PBS using spectrophotometer. At first, stock solution (1 mg/ml) of apigenin was prepared in DDW and PBS (pH 7.4) respectively. Concentrations ranging from 1-10  $\mu\text{g/ml}$  were prepared from both the stock solutions and the absorbance was measured (LI-295 UV VIS Single Beam Spectrophotometer) against the respective blank solutions (DDW without drug and PBS without drug). The absorbances versus concentration curves were prepared and the slope and regression of coefficient were measured.

#### 4.2.2 Preparation of Nanoparticles:

Apigenin loaded PLGA nanoparticles were prepared by multiple emulsion solvent evaporation method [Maji et al, 2014]. The predetermined amounts of apigenin were dissolved in 0.2ml dimethylsulfoxide (DMSO). PLGA was dissolved in 2.3 ml of dichloromethane (DCM, Merck Life Science Pvt. Ltd, India) and kept on a magnetic stirrer and apigenin- DMSO solution was gradually added to it. The aqueous phase consisted of 2.5% (w/v) and 1.5% (w/v) of polyvinyl alcohol (PVA, MW 125,000) respectively. Initially 2.5% of PVA was added drop wise in the organic phase with a continuous homogenization at an optimized speed (22,500 rpm) using a high-speed homogenizer (IKA Laboratory Equipment, Model T10B Ultras-Turrax, Staufen, Germany) and hence, the primary emulsion (w/o) was prepared. This primary emulsion was then added slowly to 1.5% PVA solution at continuous homogenization speed of 22,500 rpm and secondary (w/o/w) emulsion was prepared. This secondary emulsion was then sonicated for half an hour in a bath sonicator (Trans-O-Sonic, Mumbai, India) and kept overnight on a magnetic stirrer for solidification of particles and complete evaporation of the organic phase,

followed by centrifugation of the emulsion in two different rotation speeds as given below (Hermle Labortechnik GmbH, Wehingen, Germany). Larger particles were separated out in a centrifugation speed of 5000 rpm and the nano-sized particles were then precipitated at a speed of 16000 rpm. The precipitated particles were washed three times with Milli-Q (Millipore Corp., Billerica, MA, USA) water and lyophilized for 8-10 h (Laboratory Freeze Drier, Instrumentation India Ltd, Kolkata, India) to obtain the dry and solid product. The process is shown in **Figure 4.1**.

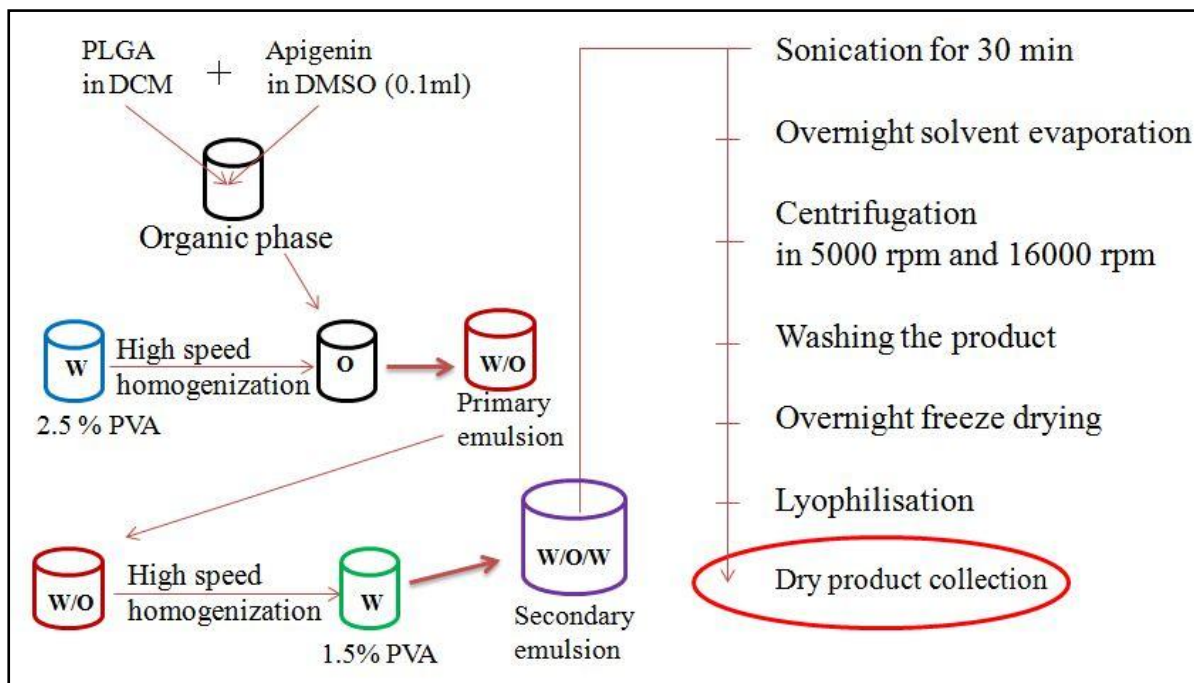


**Figure 4.1** Schematic diagram representing different steps used for the preparation of nanoparticles in multiple emulsion and solvent evaporation method

#### 4.2.3 Fourier Transform Infrared spectroscopy:

Fourier transform infrared (FTIR) spectroscopy was used to investigate any physical or chemical interactions between apigenin, and the excipients selected for the formulations. Pure apigenin/the excipients used/the physical mixture of drug (apigenin) and the excipients, formulations with and without drug (each on a separate basis)/formulation stored for stability study was mixed with IR grade potassium bromide (1:100 ratio) and compressed in a hydraulic press to form pellets. Pellets were scanned over a wave number

range of 4000-400  $\text{cm}^{-1}$  in FTIR instrument (Magna-IR 750, Series II, Nicolet Instruments Inc, Madison, Wisconsin, USA).

#### 4.2.4 *Morphology of nanoparticles:*

##### **FESEM:**

The lyophilized formulation was mounted on the stubs using double-sided adhesive tapes. The stubs were then coated with platinum in vacuum using JEOL JFC 1600 autofine coater at an acceleration voltage of 5 kV and examined under the field emission scanning electron microscope (FESEM, JEOL JSM 6700 F, JEOL, Tokyo, Japan).

##### **TEM:**

The drug distribution in the particles and internal morphology were further investigated by transmission electron microscope (TEM) (JEOL JEM-2010, JEOL, USA). Apigenin loaded nanoparticles (ApNp) were suspended in Milli-Q water and a drop of the ApNp suspension was given on standard carbon coated copper grid and air dried for overnight. TEM images were taken on the next day.

##### **AFM:**

Atomic Force Microscopy (AFM) (Dimension icon, Bruker, Billerica, Massachusetts, United States) of ApNp was performed in a tapping mode to obtain topographic images, using antimony doped silicon tip. Micro-fabricated silicon cantilever (225  $\mu\text{m}$  length and 35  $\mu\text{m}$  width) was used in this study. The cantilever oscillation frequency was 75 kHz and nominal spring force constant of 3 N/m were used. A small amount of each sample was suspended in 2 ml Milli-Q water. A small drop of that suspension was added to a freshly cleaned slide and a smear was prepared followed by vacuum drying for 24 h at 25°C for AFM viewing.

#### 4.2.5 *Particle size assessment:*

A small amount of lyophilized ApNp was taken in 2 ml of Milli-Q water and sonicated for 15 min followed by vortex for few min. Size distribution, average particle size, polydispersity index (PDI) and zeta potential of the different formulations were determined by Zetasizer nano ZS 90 and analyzed by the instrument Data Transfer Assistance (DTA) software (Malvern Zetasizer Limited, Malvern, UK) by a dynamic light scattering method at 25°C.

#### 4.2.6 Drug loading and loading efficiency:

One milligram of blank nanoparticles and drug loaded nanoparticles (ApNp) was weighed and dissolved in 1 ml DMSO and was sonicated for 30 min. After that, centrifugation (16000 rpm, for 10 min) was done and the supernatant was taken and absorbance was read. Absorbance of ApNp sample was taken against blank nanoparticles at 340 nm ( $\lambda_{\text{max}}$  of Apigenin) in UV-VIS spectrophotometer (LI-295 UV VIS Single Beam, Lasany International, India). The percentage of drug loading and drug loading efficiency were calculated [Maji et al, 2014] using following equations

**Actual drug loading (weight %)** = (Amount of drug present in nanoparticles/Total weight of nanoparticles sample analyzed) X 100 (%)

**Drug loading efficiency (%)** = (Actual drug loading/Theoretical drug loading) X 100 (%)

#### 4.2.7 Stability studies

##### Hydrolytic stability study:

Required amounts (10 mg) of ApNp were taken separately in 2 ml buffer of different pH (3.0, 5.0, 7.4 and 9.0) to measure the hydrolytic degradation of nanoparticles as compared with pure drug. Buffers used were citrate buffer pH 3, acetate buffer pH 5 and phosphate buffered saline pH 7.4. The solutions were kept in an incubator at  $37 \pm 2$  °C with mild shaking. After the scheduled time intervals that is, 7th day, 14th day, 21st day and 28th day, the samples were removed from incubator, centrifuged and washed with double distilled water and dried in speed vacuum for 30 min and then mass of nanoparticles was measured. The incubation medium was completely replaced with fresh medium. For determination of mass loss, the weight of each sample was carefully measured before the hydrolytic degradation measurement. After drying, the weight of the samples was taken to evaluate the change of weight [Mandal et al, 2018]. The weight change was calculated according to the following formula

$$\text{Weight change (\%)} = (W_0 - W_t) / W_0 \times 100,$$

where,  $W_0$  and  $W_t$  represent as the initial weight and weight at time t, respectively.

**Accelerated stability study:**

An accelerated stability study was performed to understand the effect of temperature and relative humidity (RH) on apigenin loaded nanoparticles. Fixed amounts of ApNp3 were weighed and kept in zone III at 4-8°C (in refrigerator), 30°C, 75% RH and 40°C, 75% RH for 30, 60 and 90 days as per the International Conference on Harmonization (ICH) guidelines (ICH, 2003) [Manasadeepa *et al*, 2013]. Samples were withdrawn and FTIR-spectra, FESEM photograph and drug loading were checked for those samples at 30, 60 and 90 days.

**4.2.8 In-vitro drug release:**

Drug release experiment was carried for 60 days in a cumulative drug release method [Abouelmagd *et al*, 2015]. Precisely, 2 mg nanoparticle was suspended in 2 ml of different buffers (citrate buffer pH 3, acetate buffer pH 5 and phosphate buffer saline pH 7.4) and kept at 37°C in an incubator shaker (BOD-INC-1S, Incon, India) with a continuous shaking at 60 rpm. At pre-determined time intervals, the suspensions were centrifuged at 16000 rpm (Hermile Labortechnik GmbH, Wehingen, Germany) at 4°C to separate the supernatant from nanoparticle pellets for 15 min. Supernatant (1 ml) was collected and replaced with the same volume of fresh buffers. Pellets were resuspended and incubated for further sampling. Sample supernatants were immediately analyzed by spectrophotometer (LI-295 UV VIS single Beam, Lasany, International, Haryana, India) at 340 nm against the respected blank buffer (without drug).

All the drug release data were assessed by different drug release kinetics models [Singhvi and Sing, 2011] with their equations as listed below:

**Zero-Order:**  $Q_t = Q_0 + K_0 t$  (% CDR vs. time)

**First-Order:**  $\text{Log } Q_t = \text{Log } Q_0 - Kt / 2.303$  (log % ADR vs. time)

**Higuchi model:**  $Q_t = k_H (t)^{0.5}$  (% CDR vs. root of time)

**Hixson-Crowell model:**  $Q_0^{1/3} - Q_t^{1/3} = K_{HC} t$  (Cube root of % ADR vs. time)

**Korsmeyer-peppas model:**  $M_t/M_\infty = Kt^n$  (log % CDR vs. log t)

Where, CDR is cumulative drug release, ADR is amount of drug to be released,  $Q_t$  is amount of drug release in time  $t$ ,  $Q_0$  is initial amount of drug,  $K$  is release rate constant,  $k_H$  is the release rate constant for the Higuchi model,  $K_{HC}$  is the rate constant for Hixson-Crowell rate equation,  $M_t/M_\infty$  is fraction of drug released at time  $t$ , and  $n$  is the release exponent in Korsmeyer-Peppas model.

#### **4.2.9 *In-vitro studies using human hepatocellular carcinoma cells:***

Two different human hepatocellular carcinoma cell lines (HepG2 and Huh-7) were purchased from National Centre for Cell Science (NCCS), Pune, India. Cell lines were maintained in Dulbecco's Modified Eagle's Medium (DMEM) supplemented with 10% fetal bovine serum (FBS, Sigma-Aldrich Co), 100 U/ml penicillin, 100 U/ml streptomycin and kept in 5% CO<sub>2</sub> incubator (MCO-15AC; Sanyo, Tokyo, Japan) at 37°C, and were used further.

##### **4.2.9.1 *In-vitro cytotoxicity by MTT assay:***

HepG2 and Huh7 cells were seeded in a density of  $8 \times 10^3$  cells/well in 96-well plates for 12 h following the treatment with 100  $\mu$ l of various equivalent apigenin doses of ApNp3/free apigenin (ApNp3/apigenin was suspended in DMEM medium) and incubated for two different time points (24 h and 48 h). Following the incubation, MTT dye was added in each well at a final concentration of 0.5 mg/ml and the plates were incubated for 4 h at 37° C. After that, a volume of 100  $\mu$ l of DMSO was added in each well for dissolving the formazan crystal and kept for 15 min. Absorbance of individual well was recorded using a automatic plate reader (Thermo Scientific Multiskan EX, Thermo Scientific, Waltham, MA USA) at 570 nm [Shaw et al, 2017]. Untreated cells were kept as positive control for all test samples and effect of blank nanoparticles were studied as negative control for ApNp3.

##### **4.2.9.2 *Cellular uptake studies:***

HepG2 and Huh-7 cells were seeded in DMEM medium on cover slip inside 6-well culture plates for 48 h. Further, FITC-labeled ApNp3 (ApNp5) was suspended in DMEM medium



and the cells were incubated with the suspension for 1 h and 4 h. Following the incubation, media were discarded and cover slips were washed with sterile PBS (pH 7.4) thrice and mounted on sterile slides using DPX (dibutylphthalate polystyrene xylene). Cover slips were viewed under confocal microscope (TCS-SP8 confocal microscope, Leica, Germany) for localization of ApNp5 inside cells. Quantification of amount of ApNp5 was determined by flow cytometry using fluorescence activated cell sorter (FACS). Both types of cells were seeded ( $3 \times 10^4$ ) in 6-well culture plates in DMEM medium. After 48 h, the media was replaced with the fresh DMEM media, suspension of ApNp5 was added and incubated for 0.5 to 6 h respectively. A set of cells were incubated with the fresh media without any formulation and was serving as untreated control. Following each of the incubation, cells were scrapped using trypsin, centrifuged at 4000 rpm for 5 min and washed in sterile PBS (pH 7.4) and fixed in chilled ethanol for overnight at  $-20^\circ\text{C}$ . Next day, cells were centrifuged and washed with sterile PBS (pH 7.4) and subjected to flow cytometric analysis by BD-FACS Verse™ machine (BD biosciences, San Jose, USA) [Wang et al, 2012, Shaw et al, 2017].

#### 4.2.10 *In-vivo studies*

##### **Animals:**

Balb/c mice (25-30 gm body weight in average) and Sprague-Dawley rats (150-200 gm body weight in average) of either sex were procured from National Institute of Nutrition, Hyderabad, India. All animals were kept in polypropylene cages and housed in the university animal house at  $25 \pm 1^\circ\text{C}$  and 55% relative humidity environment with normal day and night photoperiod. Animals were fed standard basal diet and drinking water *ad libitum*. They were acclimatized to the animal house environment for 2 weeks prior to any treatment. The animal experiments were designed and conducted upon approval of the Animal Ethics Committee (AEC), Jadavpur University, Kolkata, India (Ref: AEC/PHARM/1410/2014, Dated: 18.12.2014)

##### 4.2.10.1 *Radiolabeling and gamma scintigraphy study*

##### **Radiolabeling of ApNp3 and free apigenin:**

At first, 5 mg of apigenin (API) was dissolved in 0.5 ml ethanol and ApNp3 containing equivalent amount of apigenin was suspended in nitrogen purged water. A volume of 200

$\mu\text{l}$  aqueous solution of  $^{99\text{m}}\text{Tc}$ -pertechnetate ( $^{99\text{m}}\text{TcO}_4^-$ ) 185-300 MBq was added to 200  $\mu\text{l}$  drug solutions and followed by addition of 30  $\mu\text{l}$  freshly prepared stannous chloride dihydrate (20 mg in 10 ml nitrogen purged water containing 100  $\mu\text{l}$  of 6 N HCl) solution to API and 25  $\mu\text{l}$  in case of nanoparticles. Mixtures were incubated for 10-15 min at room temperature and stored in sealed vials for further studies. Instant thin layer chromatography (ITLC) was performed using acetone as mobile phase and silica gel coated aluminum sheets (Merck, Darmstadt, Germany) as stationary phase to determine radiolabeling efficiency. After a while, spots were developed and the sheets were dried. Five strips of 1 cm each were cut from the sheet and quantitative counting was recorded in a well type gamma counter at 140 keV (Electronic Corporation of India, model LV4755, Hyderabad, India).

#### **Biodistribution and gamma scintigraphy study:**

Biodistribution studies of radiolabeled apigenin (API)/apigenin loaded nanoparticles (ApNp3) were performed in balb/c mice weighing 25-30 g. Animals were kept hydrated for one hour by intra-peritoneal administration of 2 ml 0.9% normal saline. After that, a volume of 50  $\mu\text{l}$  of  $^{99\text{m}}\text{Tc}$  labeled apigenin ( $^{99\text{m}}\text{Tc}$ -Ap)/  $^{99\text{m}}\text{Tc}$  labeled ApNp3 ( $^{99\text{m}}\text{Tc}$ -ApNp3) was injected in tail vein. Animals were sacrificed at 2 h and 6 h after injection. The various organs or tissues were excised, washed with normal saline and weighed. Blood samples were collected by cardiac puncture technique [Gaonkar et al, 2016; Satapathy et al, 2016]. The radioactivity of all the samples was measured using a well-type gamma scintillation counter along with an injection standard. The results were expressed as percent injected dose per g of tissue or organ.

#### **Gamma scintigraphy:**

Gamma scintigraphy study was performed to have direct information about localization of apigenin/ApNp3 in experimental animals. For this study both HCC induced and untreated male Sprague-Dawley rats (weighing 200-250 g) and untreated male balb/c mice (weighing 25-30 g) were used. Animals were divided in two groups each containing 5 animals (rats/mice). The rats received 30  $\mu\text{l}$  of  $^{99\text{m}}\text{Tc}$ -Ap/  $^{99\text{m}}\text{Tc}$ -ApNp3. Similarly, mice received 20  $\mu\text{l}$  of  $^{99\text{m}}\text{Tc}$ -Ap/  $^{99\text{m}}\text{Tc}$ - ApNp3 respectively. Animals were anesthetized by intra-muscular injection of ketamine hydrochloride (1 ml) and fixed on a board in the

posterior position for live imaging. Images were taken at two different time points (1 h and 4 h) using a planar gamma camera (GE Infinia Gamma Camera equipped with Xeleris Work station, GE, Cleveland, OH, USA).

#### **4.2.10.2 Pharmacokinetics study and biodistribution of apigenin by LC-MS/MS**

For determination of apigenin quantity in plasma and hepatic tissue, LC-MS/MS method was developed and reported for the first time in this paper. At first, the animals were divided into two groups each containing 36 animals (male: female, 1:1). Group I animals received i.v bolus injection of apigenin suspended in water for injection (API) at dose of 1 mg/kg body weight and group II animals received i.v bolus injection of ApNp3 containing equivalent amount of apigenin (1 mg/kg). Animals (3 animals from each group at every time point) were sacrificed in a predetermined time points (at 0.5, 1, 2, 4, 6, 8, 10, 12, 24, 48 and 72 h, after injection). Blood samples were collected by heart puncture technique, pooled (from each group at a time point), centrifuged and stored with liver samples (washed twice) at -80°C freezer till further use.

Plasma sample (100 µl) was mixed with 10 µl of 500 ng/ml naringenin (internal standard) and 100 µl 10 mM ammonium formate buffer. Then 1 ml ethyl acetate was added, vortexed for 5 min, centrifuged for 10 min at 4°C at 10000 rpm. Supernatant (800 µl) was separated and evaporated to dryness. Content in a tube was resuspended with 1:1 methanol and 10 mM ammonium formate buffer and loaded to LC-MS/MS (LC: Shimadzu Model 20AC, MS: AB-SCIEX, Model: API4000, Software: Analyst 1.6). Analyte was eluted using YMC Triat C18 column (30X2.1 mm, 5 µ, YMC Corp-Japan) and gradient elution technique of two mobile phases (mobile phase A: 10 mM ammonium formate in water and mobile phase B: 50:40:10 methanol/acetonitrile/10 mM ammonium formate in water), with injection volume 20 µl, flow rate 0.8 ml/min and total run time 3.0 min was conducted. Liver samples were weighed, homogenized with water (four times the weight/volume) and processed following the liquid-liquid extraction technique. Here instead of plasma, liver homogenate was used. Both plasma and hepatic drug concentrations were plotted against time and PK parameters were determined by WinNonlin software (Certara, London, UK).

#### 4.2.10.3 *Experimental protocol for development of chemical induced HCC in rats:*

Hepatocellular carcinoma was generated in Sprague-Dawley rats by carcinogen induced method as described [Ghosh et al, 2014]. Animals were divided in six groups each containing six animals (male: female, 1:1).

In group A, rats received normal diet ad libitum, Group B, rats received a single i.p dose (200 mg/kg bodyweight) of diethylnitrosamine (DENa), (Sigma-Aldrich Co, St Louis, MO, USA) at the beginning of the study and this was followed by oral administration of 0.5% w/w 2- acetylaminofluorene (2-AAF), (Sigma-Aldrich Co, St Louis, MO, USA) bi-weekly for 16 weeks with basal diet and water (carcinogen control group); Group C, carcinogen treated animals treated with ApNp3 suspended in water for injection (single i.v dose of 20 mg/kg body weight per week) [Hu et al, 2015] from 22nd to 34th weeks, Group D, normal rats treated with blank nanoparticles suspended in water for injection (single i.v dose of 20 mg/kg body weight per week) from 22nd to 34th weeks, Group E, normal rats treated with API (single i.v dose of 20 mg/kg bodyweight per week) from 22nd to 34th weeks and Group F, carcinogenic rats treated with apigenin suspended in water for injection (API) at a single i.v dose of 20 mg/kg body weight per week from 22nd to 34th weeks. Animals were sacrificed at the 36th week and liver samples from various groups were collected and stored at -80°C for further macroscopic/ histopathological and enzyme activity studies. A schematic diagram illustrating the animal model generation is given in **Figure 4.2.**

#### 4.2.10.4 *Macroscopic and histopathological studies*

Macroscopic images of livers of all the animals from various groups were captured by camera (Canon Power Shot SX50 HS, Japan). Further, a portion of liver samples were processed and embedded into paraffin wax and cut by microtome at a thickness of 5 µm. Those sections were mounted on glass slides and stained with hematoxyline and eosine (H&E) and examined under Carl Zeiss light microscope (Axiostar plus, Jena, Germany).

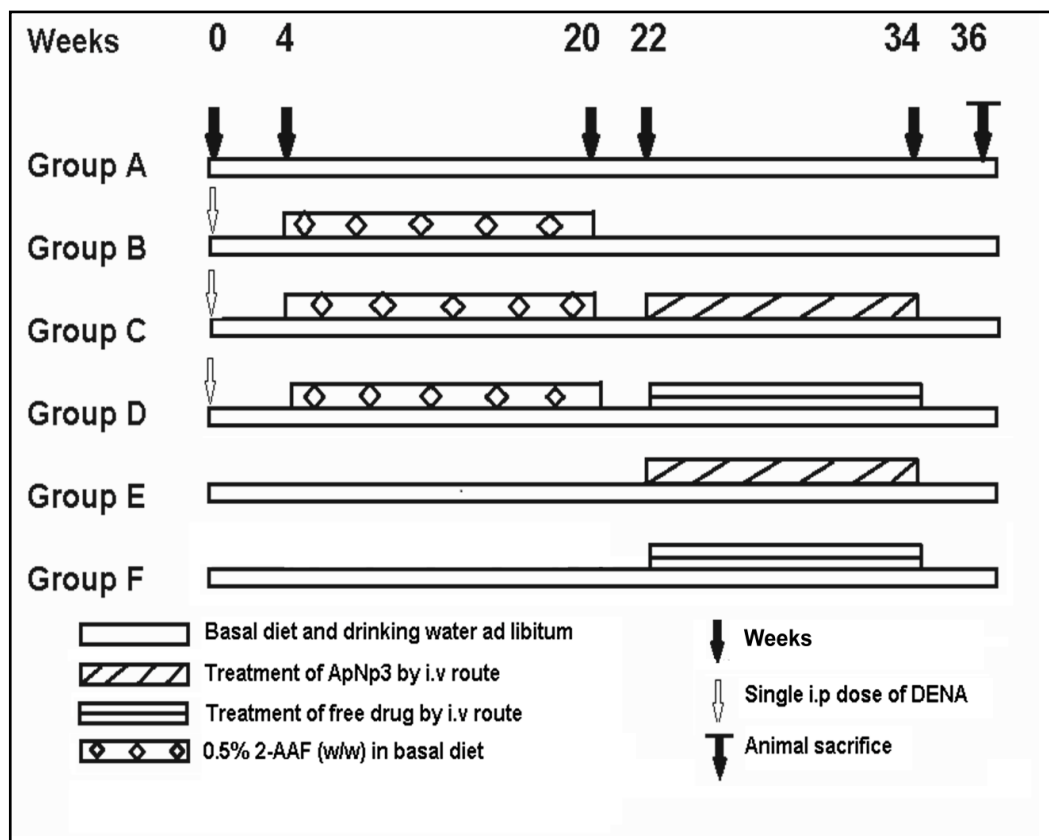


**Figure 4.2** Schematic presentation of carcinogen treatment along with the treatment of apigenin loaded nanoparticles (ApNp3) and free drug (API). The rats were divided in six groups (A) normal control group, (B) rats treated with carcinogen (carcinogen control group), (C) carcinogen treated rats received ApNp3 (20 mg/kg body weight), (D) carcinogen treated rats received API (20 mg/kg body weight). (E) normal rats received ApNp3 (20 mg/kg body weight) and (F) normal rats received API (20 mg/kg body weight).

#### 4.2.10.5 *Activities and content of various marker enzymes/iso-enzyme:*

The frozen liver tissue, obtained from various experimental groups was thawed, blotted with blotting paper briefly, weighed and homogenized in cold 0.1 N potassium chlorides (KCl solution, pH 7.4) with a pre-cooled Teflon coated homogenizer. Further, the obtained homogenate was centrifuged for 15 min at 8,000x g. An aliquot of the supernatant of the liver homogenate was used as cytosolic fraction to study the glutathione S- transferase (GST) activity, and microsomal fraction was further obtained by ultra-centrifugation of a portion of cytosolic fraction at 10,6000X g for 1h at 4°C. The activity of UDP- glucuronyl

transferase (UDPGT), superoxide dismutase (SOD) and cytochrome P-450 content were measured by using the respective assay kits.

### ***Principles of different enzyme assays***

#### **Cytochrome P-450 (CYP):**

The contents of CYP from various groups of hepatic tissues were measured by Thermo Fisher assay kit. The substrates were reduced by a specific cyt P450 enzyme to products of highly fluorescent product in aqueous solution. The fluorescent metabolites were measured at 540 nm.

#### **GST**

Chlorodinitrobenzene (CDNB) was used as the substrate. The thiol group of GST reacted with CDNB and the absorbance of the reaction was recorded at 340 nm. Absorbance recorded at unit time was proportional to the measurement of the GST activity.

#### **UDPGT**

UDPGT activity was measured using competitive enzyme immunoassay technique. Assay samples were incubated with buffer and UDPGT-HRP (monoclonal antibody conjugate) and substrate for HRP were added to it. This enzyme-substrate reaction gave blue color which after adding the stop solution turned into yellow color. This yellow color was measured at 450 nm and the intensity was inversely proportional to UDPGT activity of sample.

#### **SOD**

The rate of the reduction with a superoxide anion is linearly related to the xanthine oxidase (XO) activity, and is inhibited by SOD. The inhibition activity of SOD was determined by a colorimetric method at 450 nm following the guideline of manufacturer of the assay kit.

#### **4.2.11 Statistical analysis**

Minimum of three sets for each experiments were performed *in-vitro* and *in-vivo* to check reproducibility and all data were represented as mean  $\pm$  standard deviation. Student's t-test and one way ANOVA were used for statistical calculations and differences were considered statistically significant when p value (probability) was  $<0.05$  at 95% confidence level.

# Chapter 5

## *Results*

## 5. Results

### 5.1 Preformulation Studies

Initially the absorption maximum ( $\lambda_{\max}$ ) of apigenin was determined and the value was 340 nm in both DDW and PBS solution (**Figure 5.1**). Apigenin showed two peaks, at 268 nm and 340 nm. However, at 340 nm, it gave maximum absorbance. Hence, it was chosen.

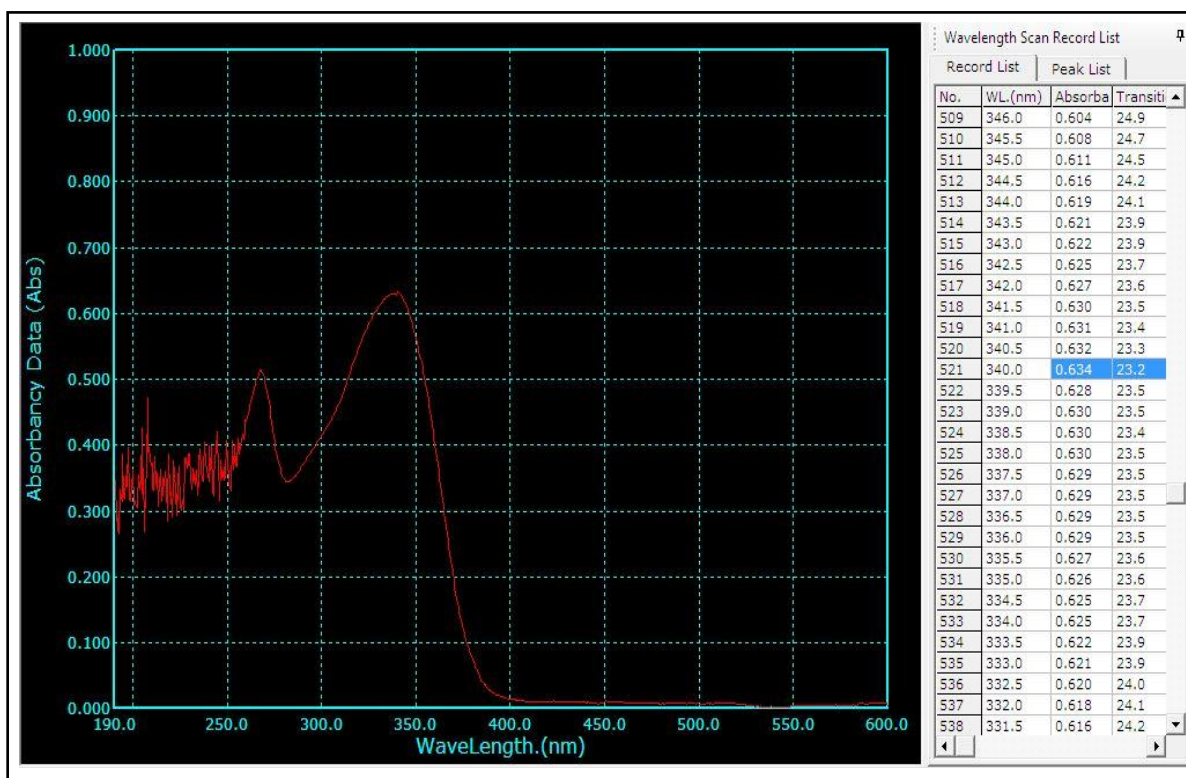


**Figure 5.1 Absorbance maxima of Apigenin**

Respective absorbance of the various solutions of drug with variable drug concentrations were determined in both the solutions (DDW/PBS) and the respective calibration curves (in DDW and PBS) were developed (**Figure 5.2 A and B**). High regression values ( $R^2 > 0.99$ ) in both the solutions (DDW/PBS) showed the accuracy of the calibration curves.



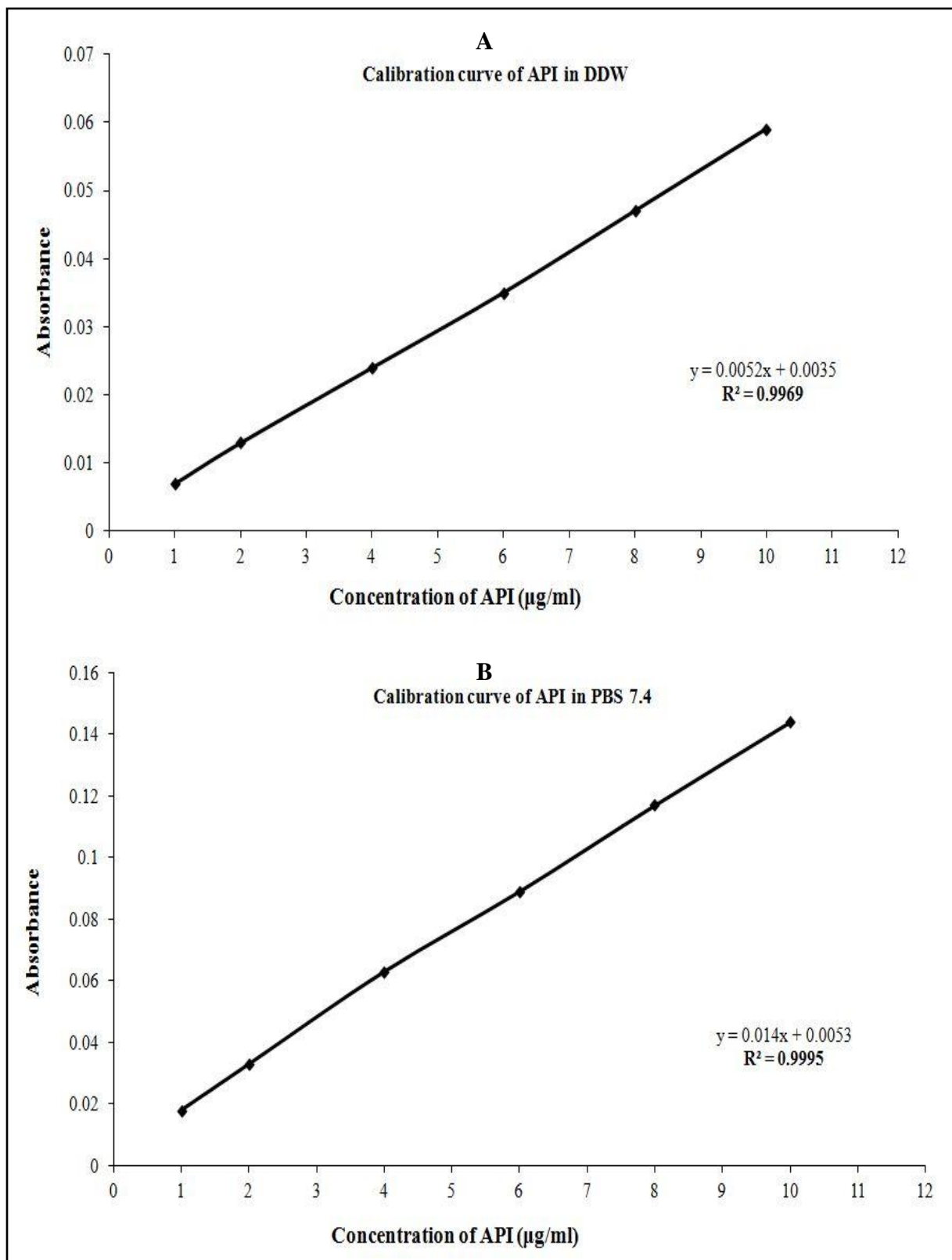


Figure 5.2 A and B Calibration curve of apigenin in DDW and PBS (pH 7.4)

## 5.2 Preparations of polymeric nanoparticles of apigenin

### ➤ Drug loading and Drug loading efficiency

Apigenin loaded PLGA nanoparticles (ApNp) were prepared in multiple emulsion solvent- evaporation technique in various amounts of drug: polymer ratio. Each formulation was prepared in triplicate and best formulation was chosen for further studies depending on their surface morphology, drug loading and other necessary characteristics. Composition of different nanoparticles and their drug loading is listed below in **Table 5.1**. In this study, percentage of drug loading increased with an increasing amount of apigenin incorporated in nanoparticles. It varied from ApNp1 (drug loading, 2.098%) to ApNp3 (drug loading, 19.14%) as shown. Further, ApNp4 showed a nearly similar drug loading (19.09%) to ApNp3 despite an increase in amount of drug incorporated in the formulation. Drug loading efficiency was also more for ApNp3 than ApNp4. Hence we have chosen ApNp3 for further investigation.

**Table 5.1** Composition of different nanoparticles and their drug loading

Sl No	Formulation Code	Ratio of Drug and Polymer† by weight	Concentration of FITC‡ (mg/ml)	Theoretical drug loading (%)	Actual drug loading (%)*	Drug Loading Efficiency (%)
1	ApNp1	1:10	--	9.09	2.098±0.13	23.08
2	ApNp2	1:5	--	16.66	13.97±0.12	83.85
3	ApNp3	1:3.3	--	23.07	19.14±0.16	82.96
4	ApNp4	1:2.5	--	28.57	19.02±0.3	66.57
5	ApNp5	1:3.3	0.4	23.07	18.98±0.14	82.27

\*Data show mean ±SD, (n=3). †Amount of polymer for each formulation was fixed (50 mg). ‡FITC, Fluorescein isothiocyanate

## 5.3 Fourier Transform Infrared Spectroscopy (FTIR)

The FTIR spectra of apigenin, apigenin loaded nanoparticles and the excipients are depicted in **Figure 5.3**.

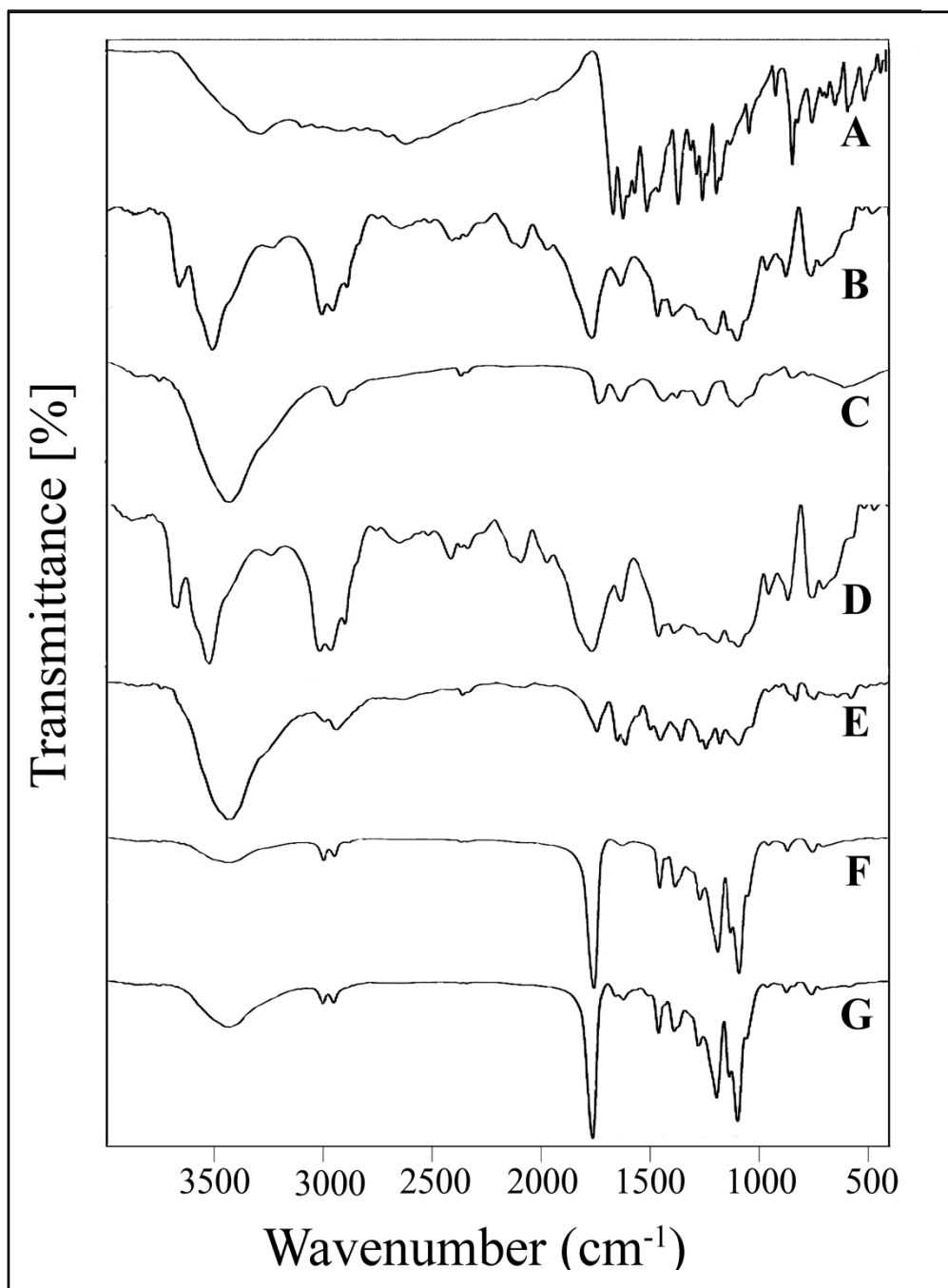


**Figure 5.3** FTIR Spectra of (A) apigenin, (B) PLGA, (C) PVA, (D) physical mixture of excipients, (E) physical mixture of drug and excipients, (F) blank nanoparticles, (G) apigenin loaded nanoparticles (ApNp3)

When the spectra of the drug was compared with the various excipients, with their respective individual spectra, and the spectra of physical mixture of drug and the excipients

and the lyophilized formulations with or without drug, we have observed no chemical interaction existed between the drugs and the excipients. The individual characteristic peak of apigenin [at wave number  $1243\text{ cm}^{-1}$ , responsible for C-C (O) – C stretching] was present in the physical mixture. However, the absence of the peak in the formulation with or without drug indicates that the drug was entirely encapsulated in the formulation. Further, the characteristic peak of PLGA (at wave number  $2948\text{ cm}^{-1}$ , responsible for –OH stretching) and the characteristic peak of PVA (at wave number  $3426\text{ cm}^{-1}$ , responsible for –OH stretching) were present. Thus these data suggests no chemical interaction takes place between the drug and excipients.

#### 5.4 Determination of surface morphology

##### FESEM

Field emission scanning electron microscopy is a high resolution technique used for determination of the surface morphology of polymeric nanoparticles. Here, four different FESEM photographs (in different resolution) of ApNp3 (**Figure 5.4**) showed that prepared particles were in nanosize range, homogeneously and thickley distributed and had smooth outer surface.

##### TEM

TEM images of apigenin loaded nanoparticles (ApNp3) showed that the drug was incorporated in PLGA core. The drug particles were distributed more predominantly along the surface and peripheral region of the particles (**Figure 5.5**). Spotted particles support the presence of a drug in particulate form rather than its distribution in molecular form [Maji et al, 2014].

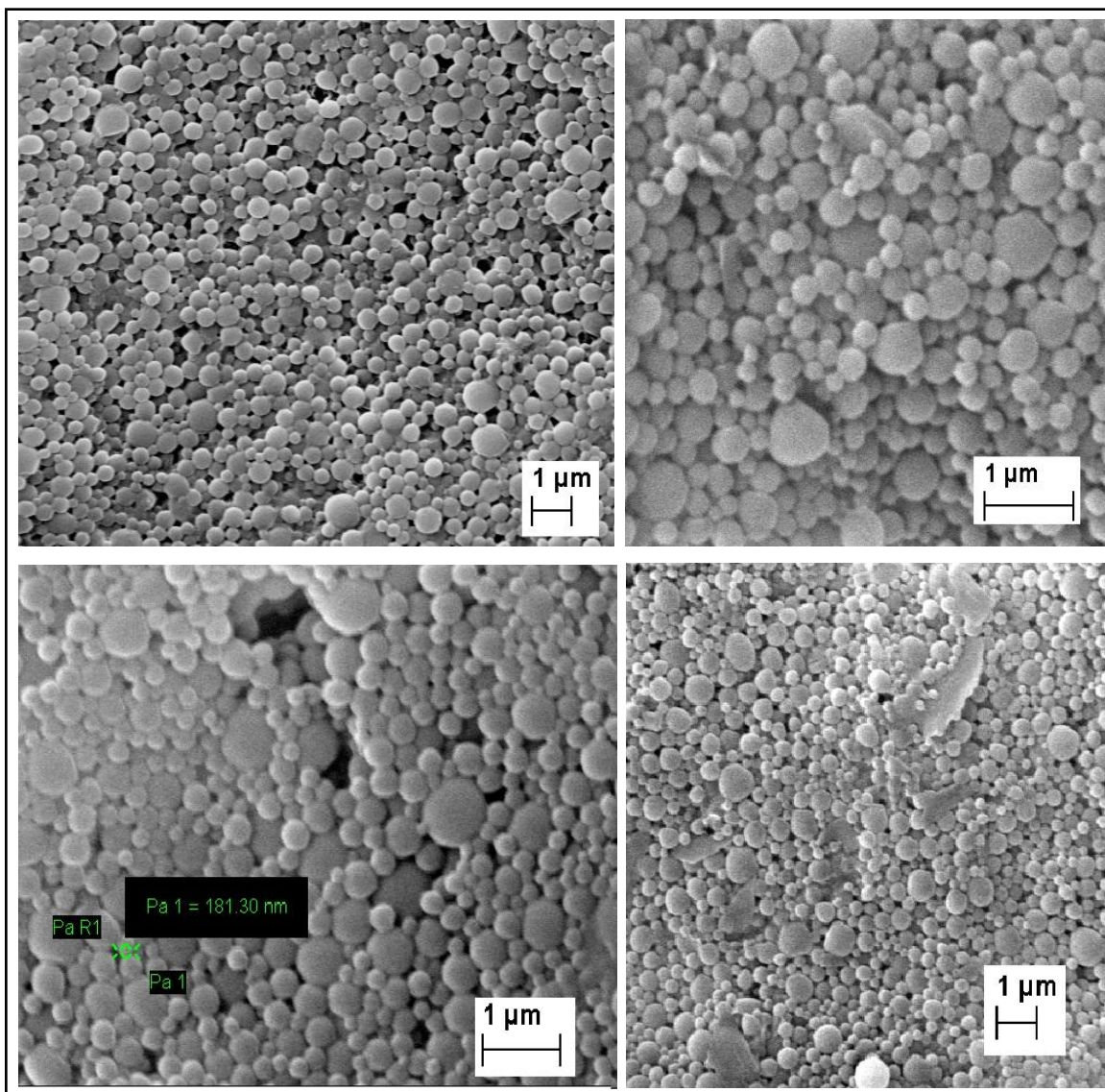


Figure 5.4 Surface morphology of apigenin loaded nanoparticles by FESEM

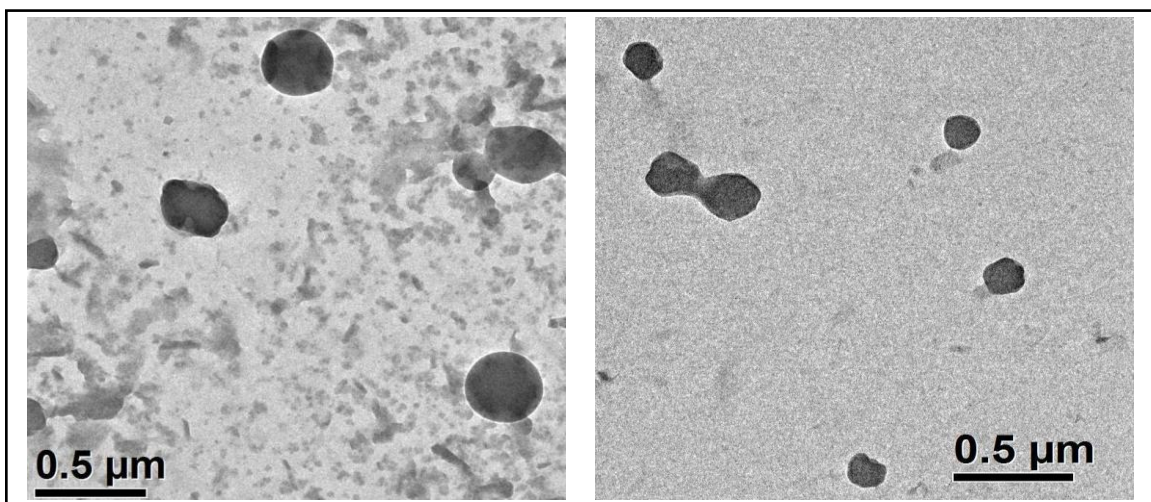
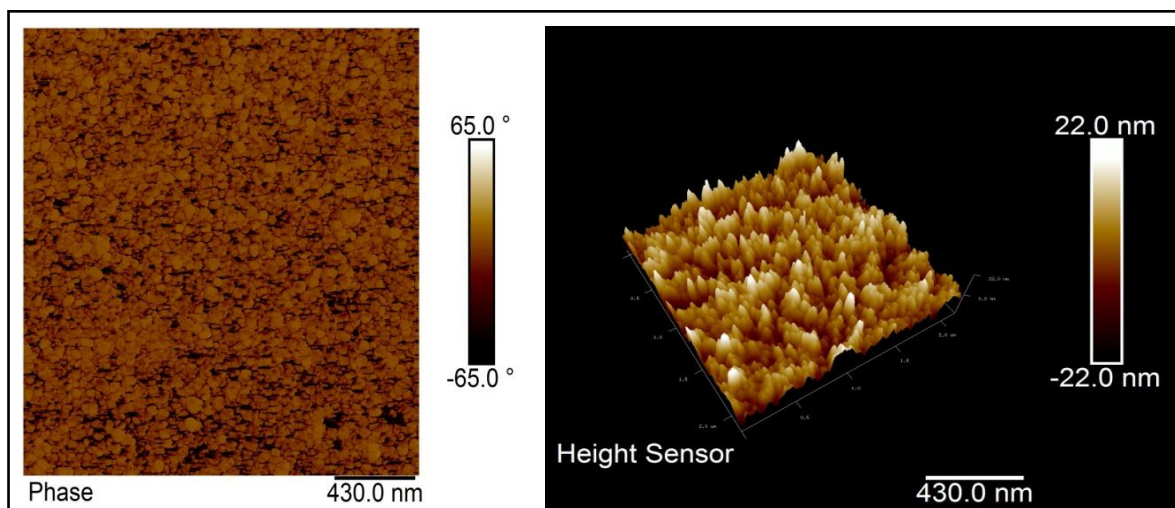


Figure 5.5 Transmission electron scanning microscopic images of ApNp3

**AFM**

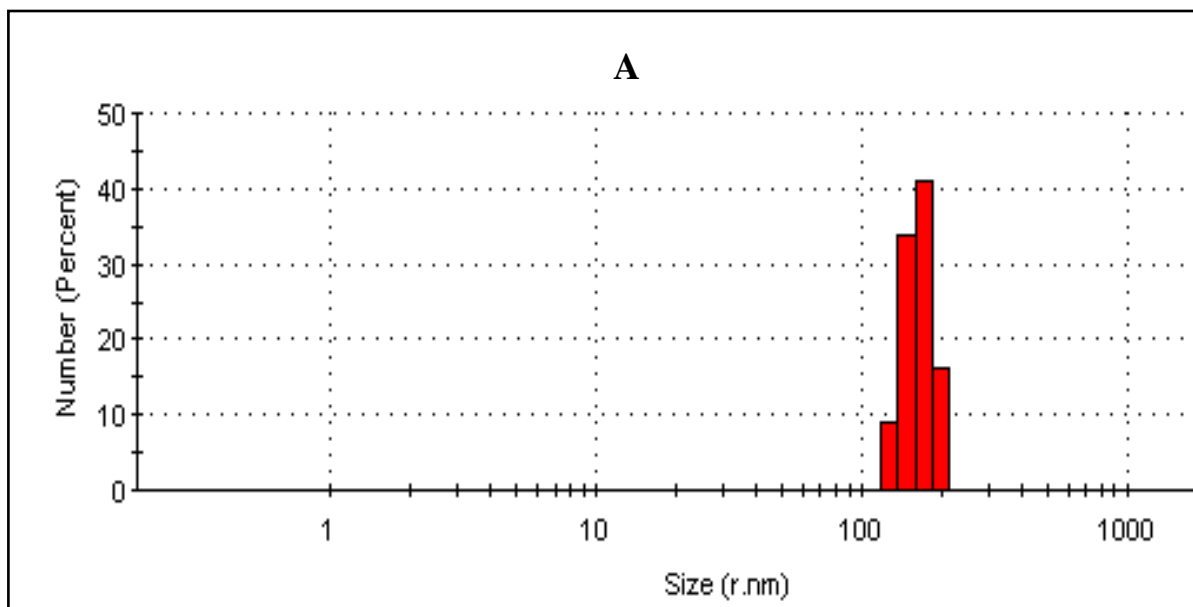
The flattened topography and three dimensional surface morphology of apigenin loaded nanoparticle (ApNp3) were further investigated by 3D AFM images (**Figure 5.6**) where it showed that height of the particles varied between 10-14 nm.



**Figure 5.6** Three dimensional surface morphology of ApNp3 by AFM

**5.5 Particle size and Poly dispersity Index (PDI)**

The average particle sizes of ApNp3 and ApNp5 were 270 nm (**Figure 5.7A**) and 325 nm (**Figure 5.7B**) respectively and PDI values for those formulations were 0.260 and 0.409 respectively. Poly dispersity index indicates the distribution uniformity of the nanoparticles [Danaei et al, 2018].



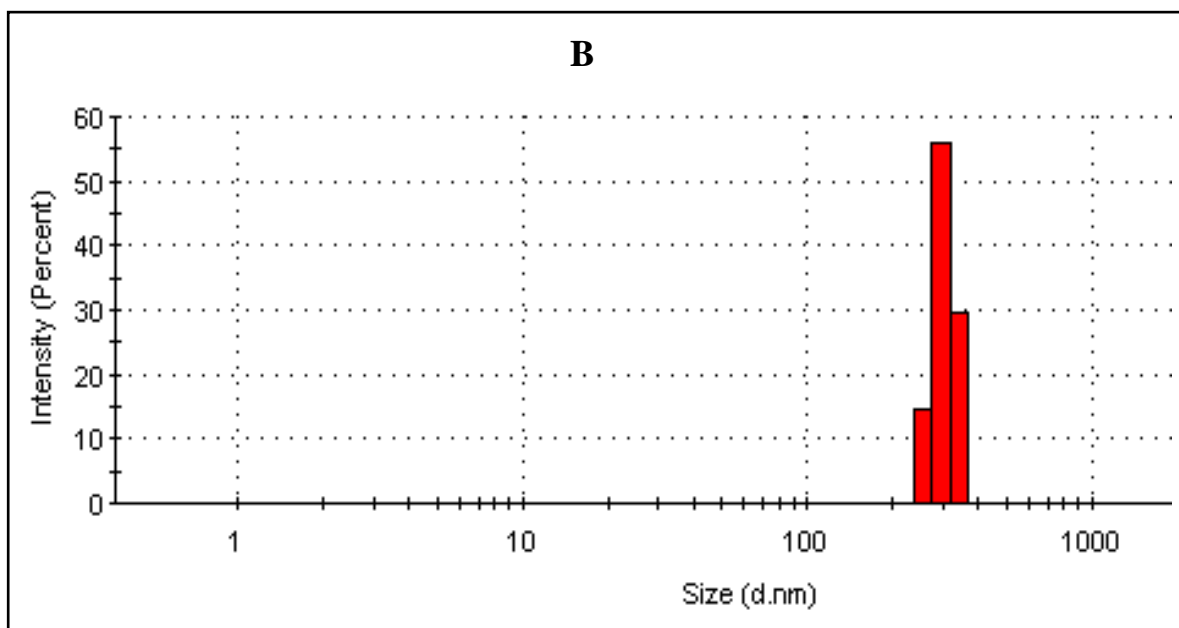


**Figure 5.7** Particle size distributions of ApNp3 (A) and ApNp5 (B) respectively

### 5.6 Surface charge determination by zeta potential

Surface charge plays a crucial role in drug absorption, which in turn affects pharmacokinetics and biodistribution of nanoparticles. Positively charged nanoparticles are rapidly cleared from circulation, to a greater extent, than negatively charged nanoparticles. In contrast, neutral nanoparticles, as well as those with a slight negative charge, show significantly prolonged circulating half-lives [Arvizo et al, 2011; Yao C, 2014]. Zeta potential, the electric potential at the plane of shear, is a crucial parameter for determination of the surface charge of polymeric nanoparticle formulations. The zeta potential values were -4.84 mV (**Figure 5.8 A**) and -4.1mV (**Figure 5.8 B**) for ApNp3 and ApNp5 respectively.

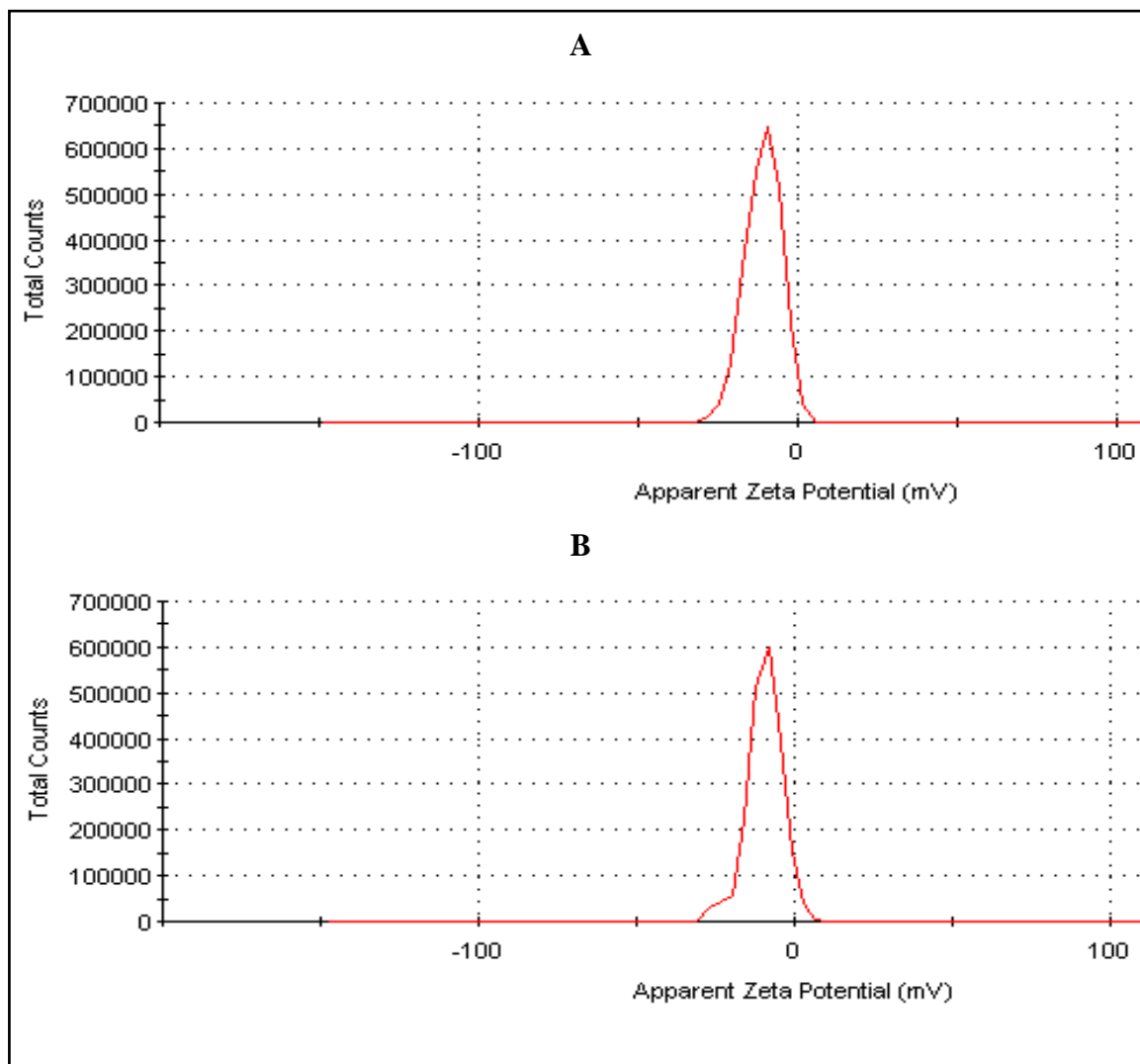


**Figure 5.8** Zeta potential values of ApNp3 (A) and ApNp5 (B) respectively

### 5.7 Stability Study

#### ➤ Hydrolytic stability study

The stabilities of nanoparticles were investigated in three different buffers with altered pH values. Weight loss of particles at different time points was calculated and found to increase with the decrease pH of medium (**Figure 5.9**). After 4 weeks study, the mass loss of ApNp3 at pH 7.4, pH 5 and pH 3 were  $33.87 \pm 0.93\%$ ,  $37.45 \pm 1.13$  and  $52.01 \pm 1.97$  respectively. Nanoparticles showed a higher hydrolytic stability at higher pH values as indicated by this study.



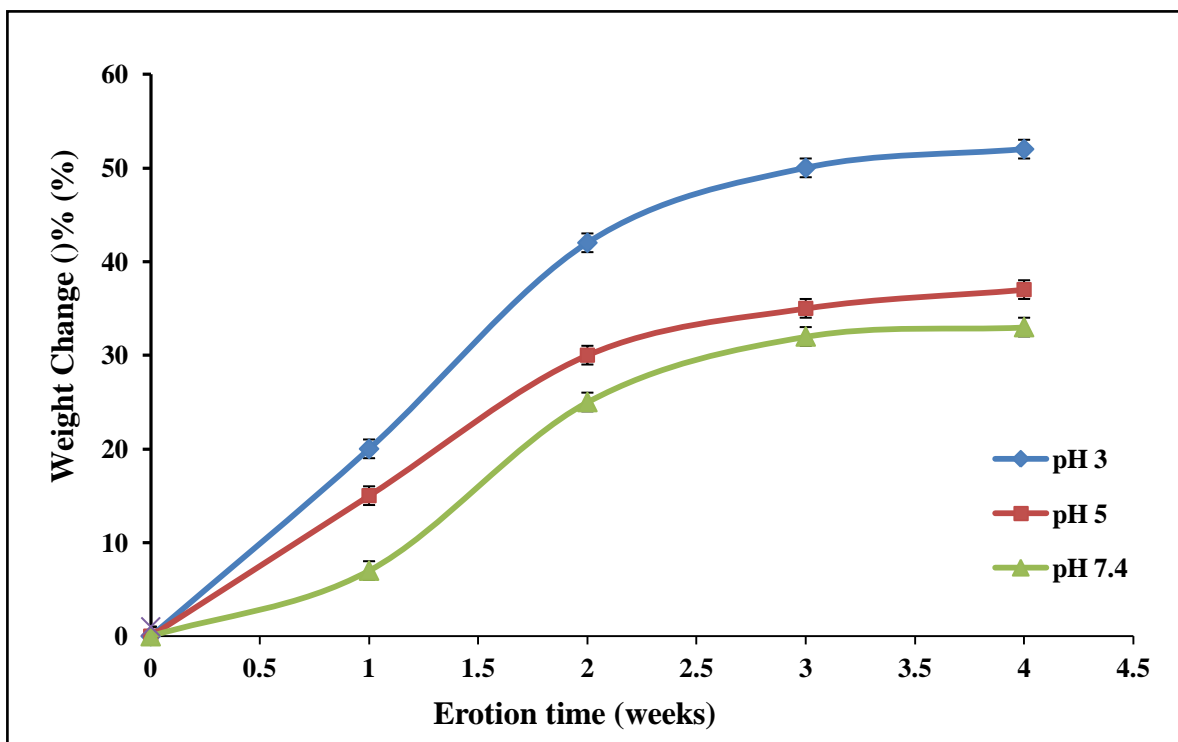


**Figure 5.9** Hydrolytic stability study of ApNp3 in different pH buffers. Data show mean  $\pm$  standard deviation (n=3).

➤ **Accelerated stability study**

Accelerated stability of ApNp3 stored at 4–8°C (in refrigerator), and at 30°C, 75% RH and 40°C, 75% RH in stability chamber for 30, 60 and 90 days were evaluated following ICH guidelines (2003). Samples were kept in appropriate stability chambers and tested for their thermal and moisture stability. At the predetermined time intervals, samples were collected and surface morphology of those particles were investigated. It was seen that over the time, the structure of nanoparticles got soften at the elevated temperature conditions (30°C and 40°C), but those samples which were kept at 4°C were shown to maintain their structures throughout the stability study period. FESEM images of samples kept at each time point with the temperature condition are depicted in **Figure 5.10**.

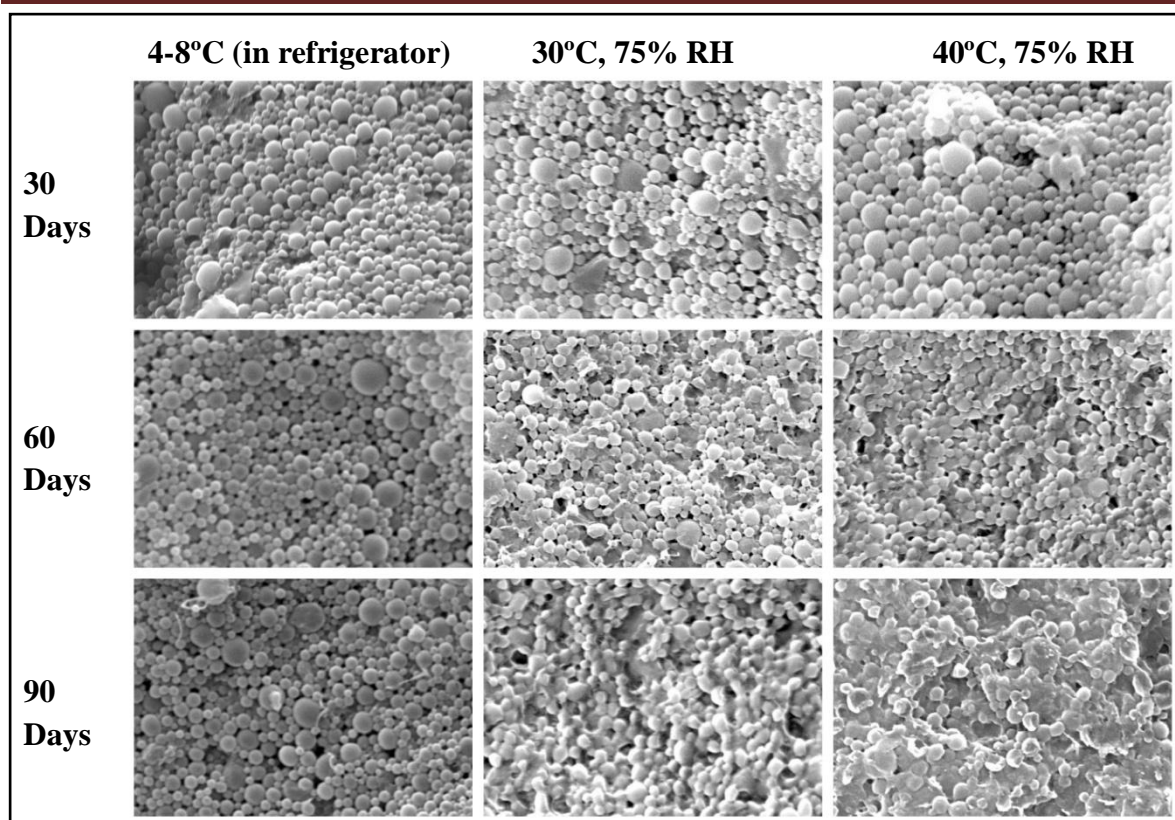


**Figure 5.10** Accelerated stability study of ApNp3 at different temperature conditions

### 5.8 *In-vitro* drug release and kinetics study

#### ➤ *In-vitro* drug release in different mediums

*In vitro*-drug release studies are routinely performed to examine the ability of new nanocarrier formulations to modulate drug release in different pH mediums. A variable *in-vitro* drug release pattern in different buffers was observed in our study (**Figure 5.11**). After 60 days (duration of the study), in PBS (pH 7.4) average percentage cumulative drug release was noted as 52.43% from ApNp3. Drug release was more in lower pH media. The cumulative drug release was reported as 79.06 % and 88.54% at pH 5 and pH 3 respectively, which indicates a faster drug release in acidic pH than in PBS pH 7.4, where the prepared nanoformulations followed a sustained drug release pattern.

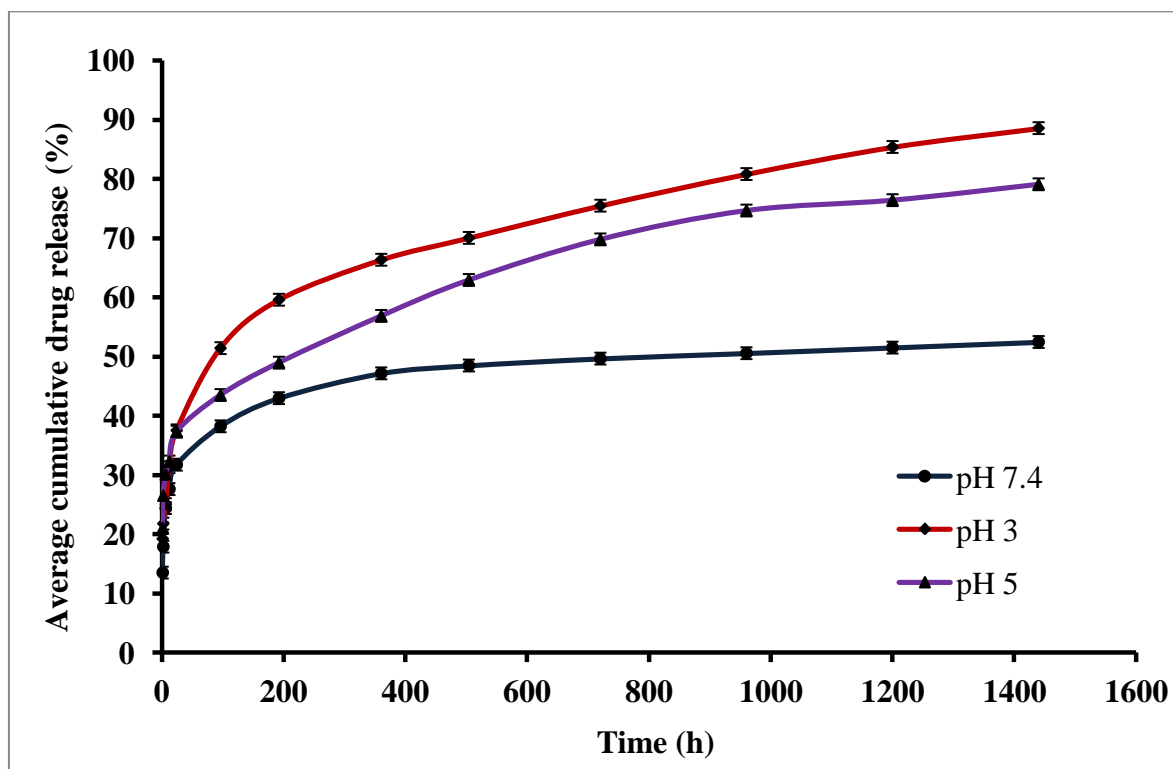


**Figure 5.11:** *In vitro* drug release profile of ApNp3 in different pH buffers. Data show mean  $\pm$  standard deviation (n=3).

#### ➤ Drug release kinetics evaluation

To evaluate the drug-release kinetic pattern in different pH conditions, drug release data were assessed using zero order (blood levels of drugs would remain constant throughout the delivery period), first order (drug release depends on concentration gradient), Hixson-Crowell (release from a system where there is a change in surface area and diameter of particles), Korsmeyer–Peppas (drug release from a polymeric system provides diffusion and erosion), and Higuchi (release of a drug from an insoluble matrix) kinetic models [Singhvi and Sing, 2011]. Various regression co-efficient ( $R^2$ ) values for the kinetics were tabulated (**Table 5.2**). The corresponding plot (log cumulative percent drug release versus log time) of ApNp3 in PBS pH 7.4 followed Korsmeyer-Peppas equation with a good linearity ( $R^2$ , 0.9634). The release exponent (n) value for our formulation was 0.17 which suggests apigenin release followed anomalous diffusion pattern in PBS.

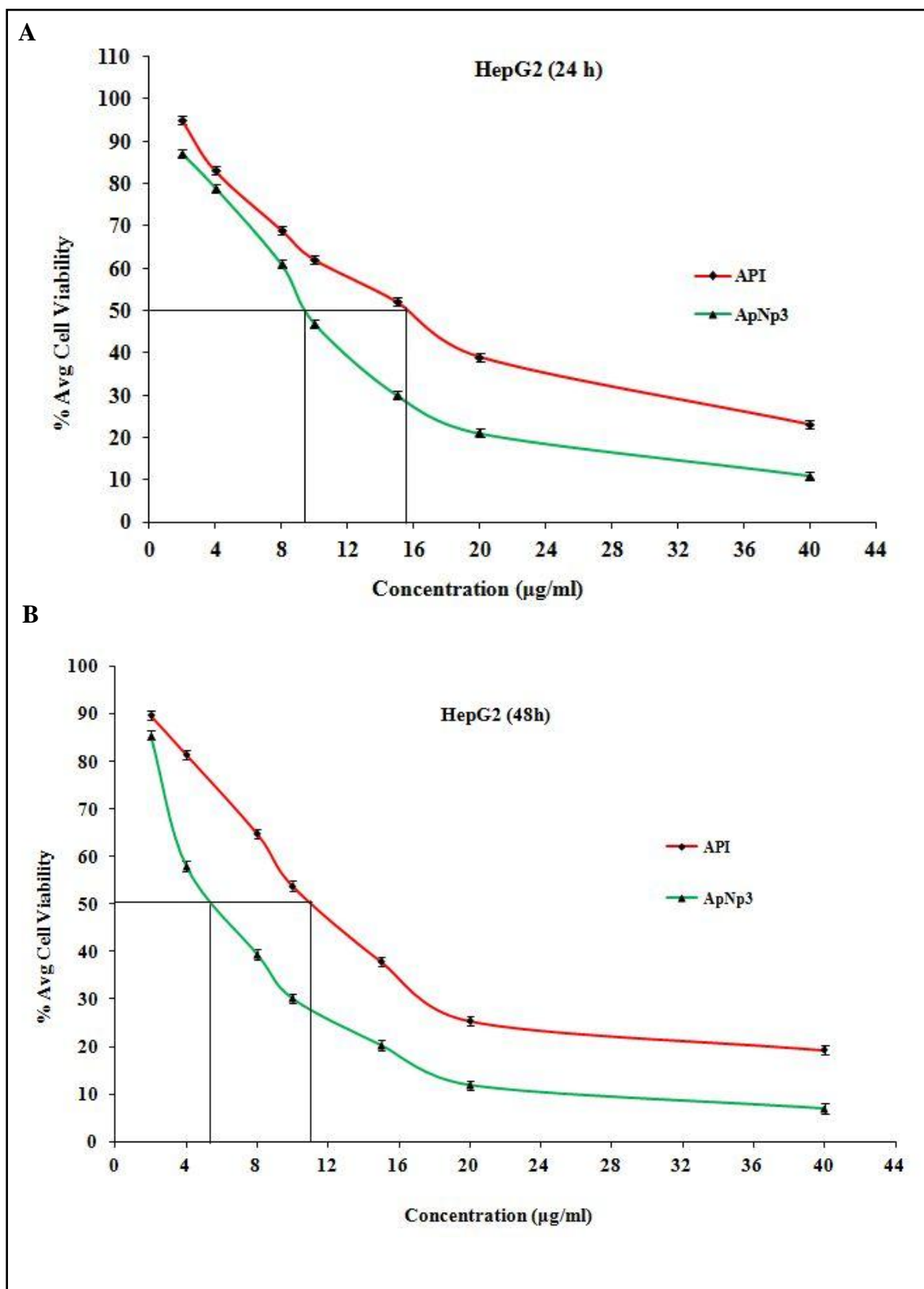
Table 5.2 Different release kinetics models of apigenin release from ApNp3

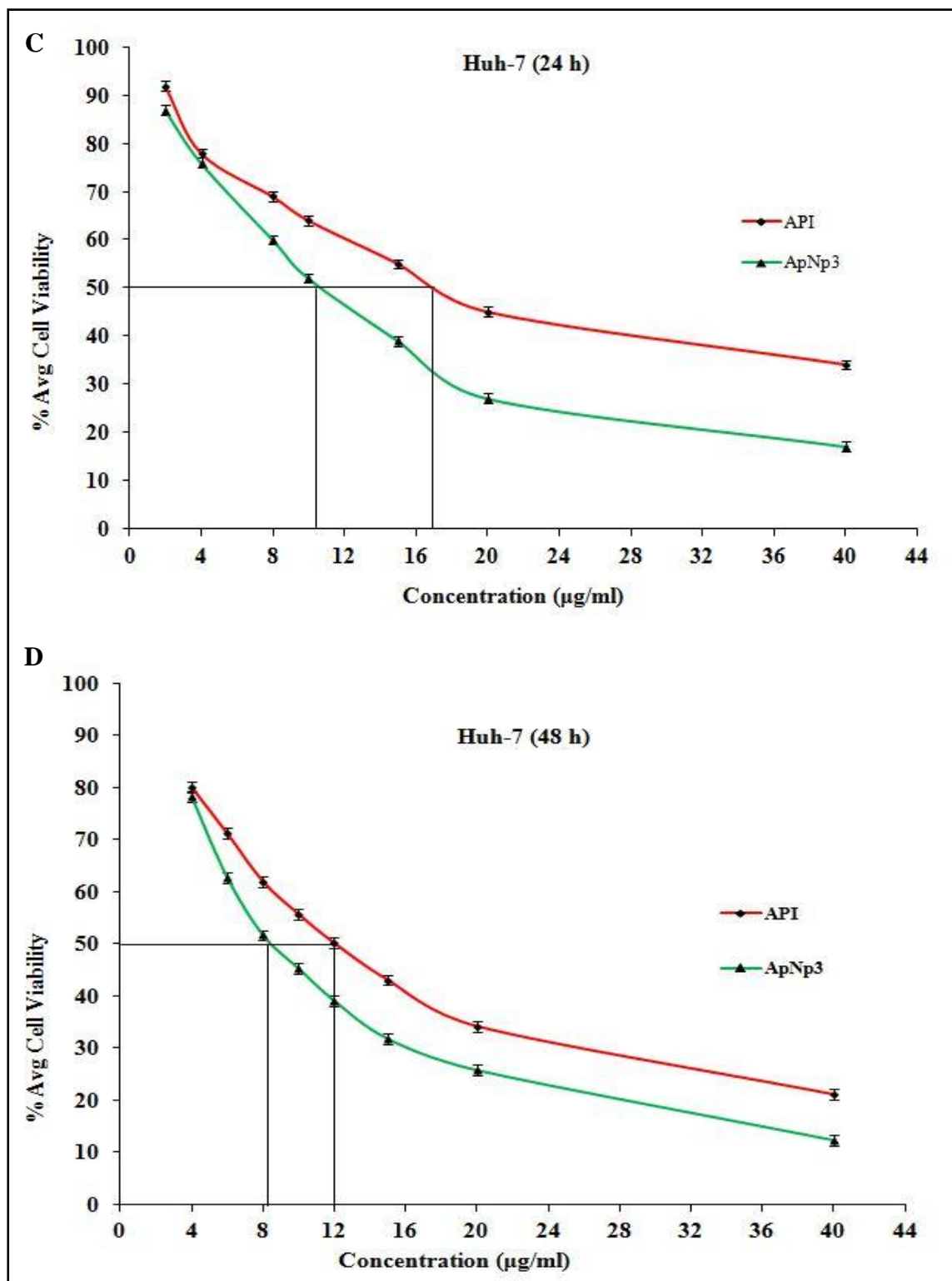
<i>In-vitro</i> kinetic models on which drug release data were assessed	Corresponding Kinetic equation with R <sup>2</sup> value in different buffers		
	Citrate Buffer (pH 3)	Acetate Buffer (pH 5)	Phosphate buffer saline (pH 7.4)
<b>Zero Order</b>	y = 0.0449x + 35.749 <b>R<sup>2</sup> = 0.7994</b>	y = 0.0378x + 34.67 <b>R<sup>2</sup> = 0.8589</b>	y = 0.0267x + 28.64, <b>R<sup>2</sup> = 0.6361</b>
<b>First Order</b>	y = -0.0006x + 1.8141 <b>R<sup>2</sup> = 0.9503</b>	y = -0.0004x + 1.8189 <b>R<sup>2</sup> = 0.9473</b>	y = 0.0002x + 1.85, <b>R<sup>2</sup> = 0.6915</b>
<b>Higuchi</b>	y = 1.8333x + 25.36 <b>R<sup>2</sup> = 0.9499</b>	y = 1.5094x + 26.467 <b>R<sup>2</sup> = 0.9765</b>	y = 1.0288x + 22.79, <b>R<sup>2</sup> = 0.8452</b>
<b>Hixson–Crowell</b>	y = -0.0014x + 4.0088 <b>R<sup>2</sup> = 0.908</b>	y = -0.001x + 4.0324 <b>R<sup>2</sup> = 0.9219</b>	y = 0.0006x + 4.140, <b>R<sup>2</sup> = 0.6733</b>
<b>Korsmeyer–Peppas</b>	y = 0.2152x + 1.269 <b>R<sup>2</sup> = 0.9967</b>	y = 0.1736x + 1.3322 <b>R<sup>2</sup> = 0.9853</b>	y = 0.1732x + 1.217, <b>R<sup>2</sup> = 0.9648</b>

## 5.9 *In-Vitro* cytotoxicity and cellular uptake study

### 5.9.1 Cytotoxicity measurement by MTT assay:

*In-vitro* cytotoxicity and IC<sub>50</sub> of apigenin suspension (API) and ApNp3 in hepatocellular carcinoma cells were determined by MTT assay. Earlier reports suggested that apigenin successfully reduced cell viability and proliferation of HepG2 and Huh-7 cells [Kim et al, 2011; Kim et al, 2013]. In this study, we found ApNp3 had an IC<sub>50</sub> value much lower than that of API in both the cell types at two different time points. After 24 h, in HepG2 cells, IC<sub>50</sub> value of ApNp3 was 9µg/ml, whereas, the IC<sub>50</sub> value of API was calculated as 15µg/ml. However, after 48 h, the IC<sub>50</sub> of API and ApNp3 were 11µg/ml and 5.5µg/ml respectively. In huh-7 cells, the results were quite similar. Apigenin as a suspension had higher IC<sub>50</sub> values at both time points than the apigenin loaded nanoparticles. At 24 h study, IC<sub>50</sub> values of API and ApNp3 were 17µg/ml and 10.5µg/ml respectively whereas, after 48 h, these values were 12µg/ml and 8.5µg/ml respectively. The MTT assay results are depicted in **Figure 5.12**.

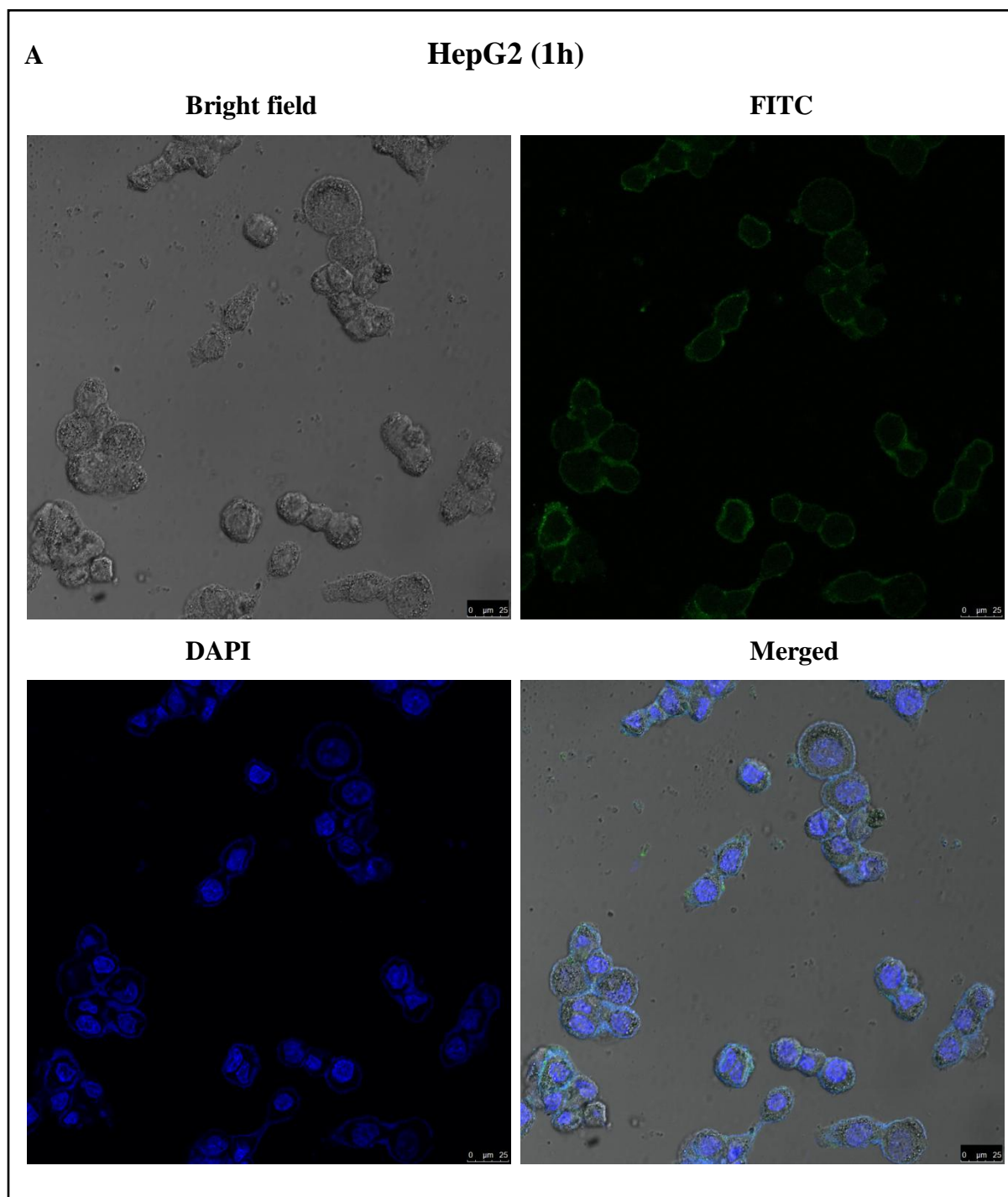




**Figure 5.12** *In-vitro* cytotoxicity of ApNp3 and API was determined in HepG2 and Huh-7 cells in different time points. IC<sub>50</sub> of free drug and nanoparticles in HepG2 cells at 24 h and 48 h are depicted (A and B respectively). IC<sub>50</sub> of free drug and nanoparticles in Huh-7 cells at 24 h and 48 h are depicted (C and D respectively). Data show mean  $\pm$  standard deviation (n=3).

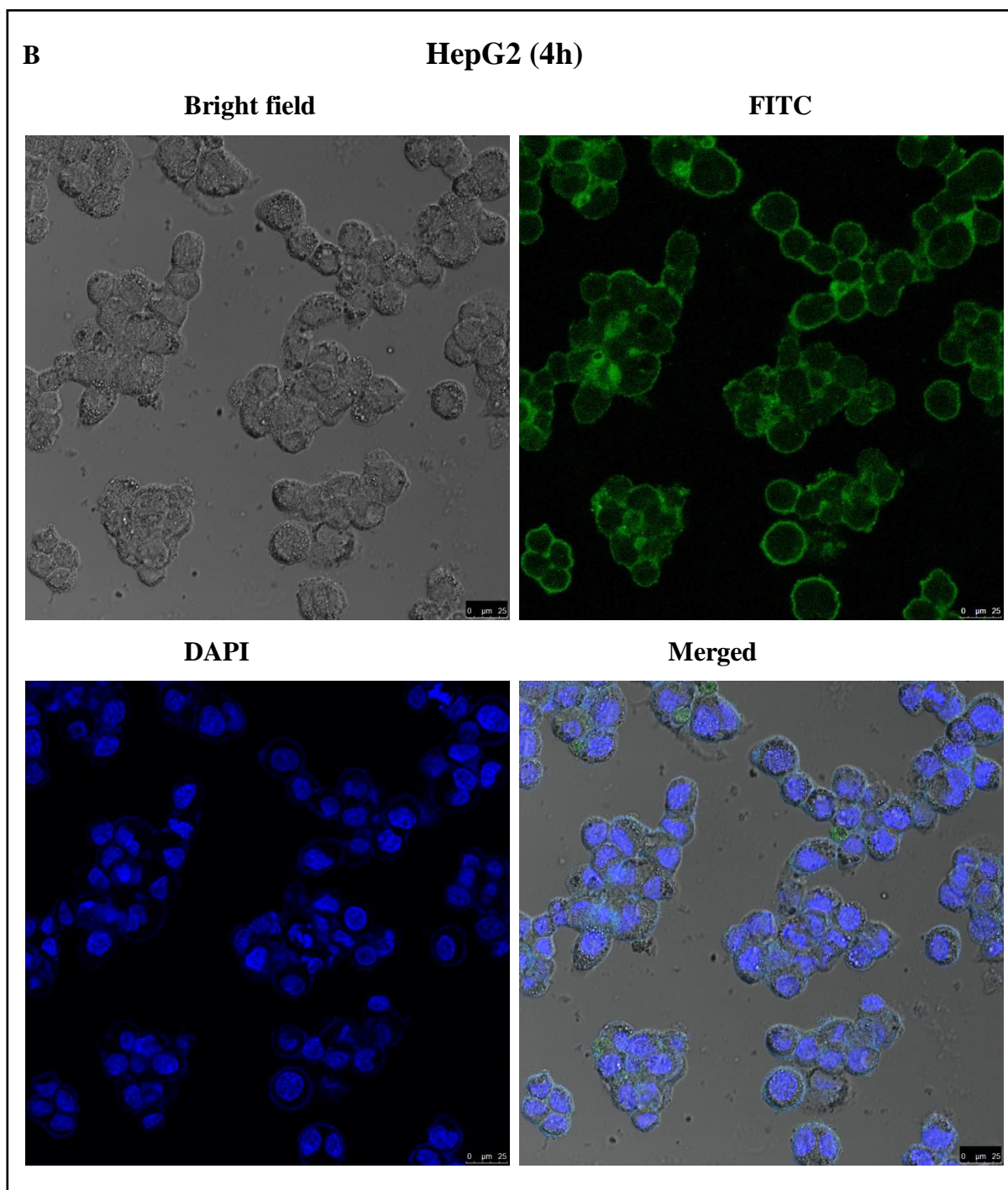
### 5.9.2 Cellular uptake by confocal microscopy:

Confocal microscopy was done to determine the presence and uptake of apigenin loaded nanoparticles inside the human hepatocellular carcinoma cells. A successful cellular uptake of FITC labeled nanoparticles (ApNp5) suggests for a targeted drug delivery and correct optimization of the size of the nanoparticles. Here after incubating the cells with the formulation at different time points, it is clearly observed that a higher cellular uptake took place in both types of cells in a time dependent manner. Images are taken in four different filters such as, brightfield (for cell structures), FITC, DAPI and merged for better visualization of cytoplasm and nucleus. Images are depicted in **Figure 5.13**. Here intensity of FITC is directly proportional to the extent of internalization of nanoparticles in cellular matrix. Blue filter (DAPI) showed the nucleus of the cells, whereas, green field (FITC) showed cytoplasm.

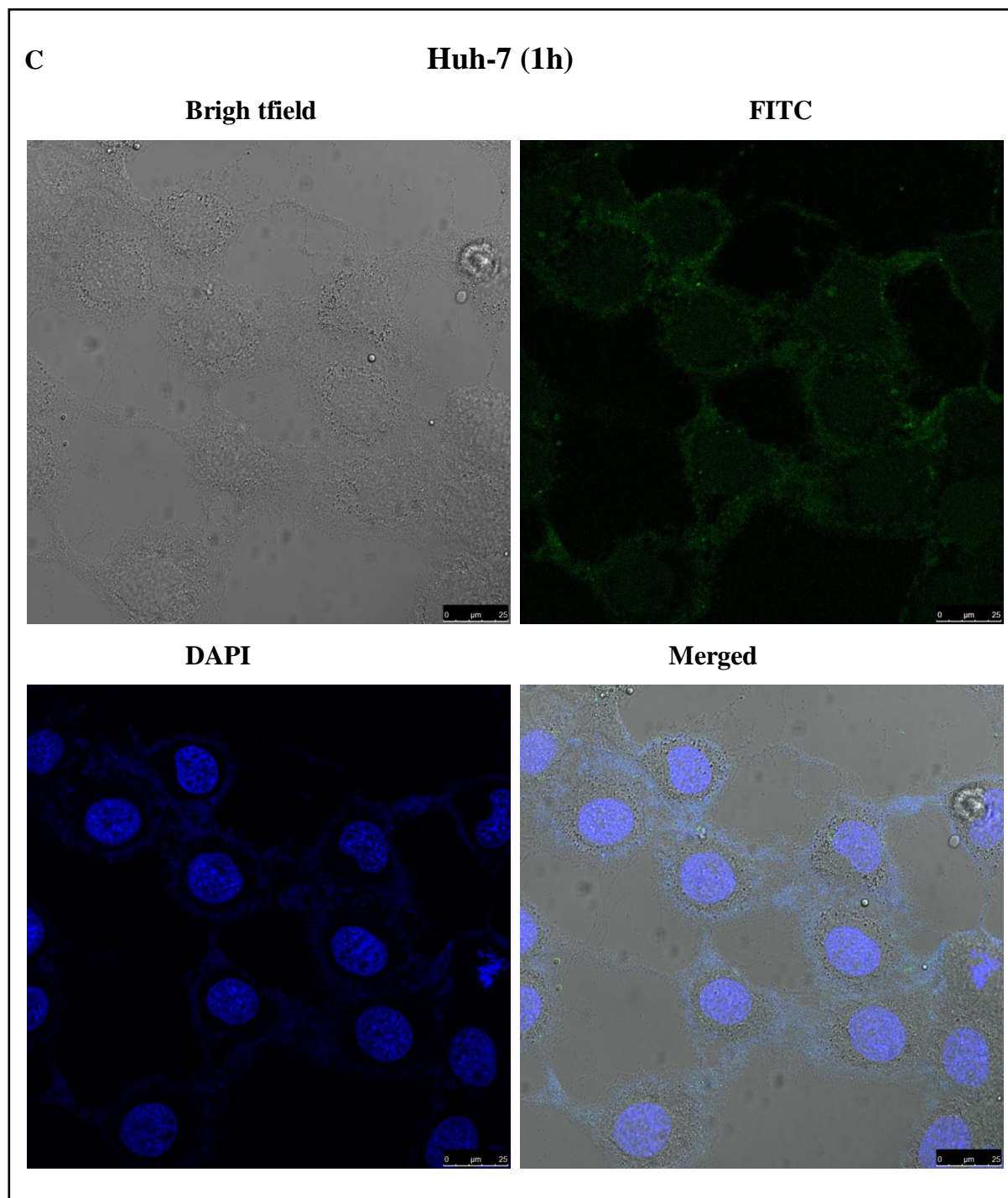


**Figure 5.13 A** At the first hour of study, the color intensity in FITC filter area was less in HepG2 cells. Nanoparticles also penetrated to nucleus shown in DAPI filter area.

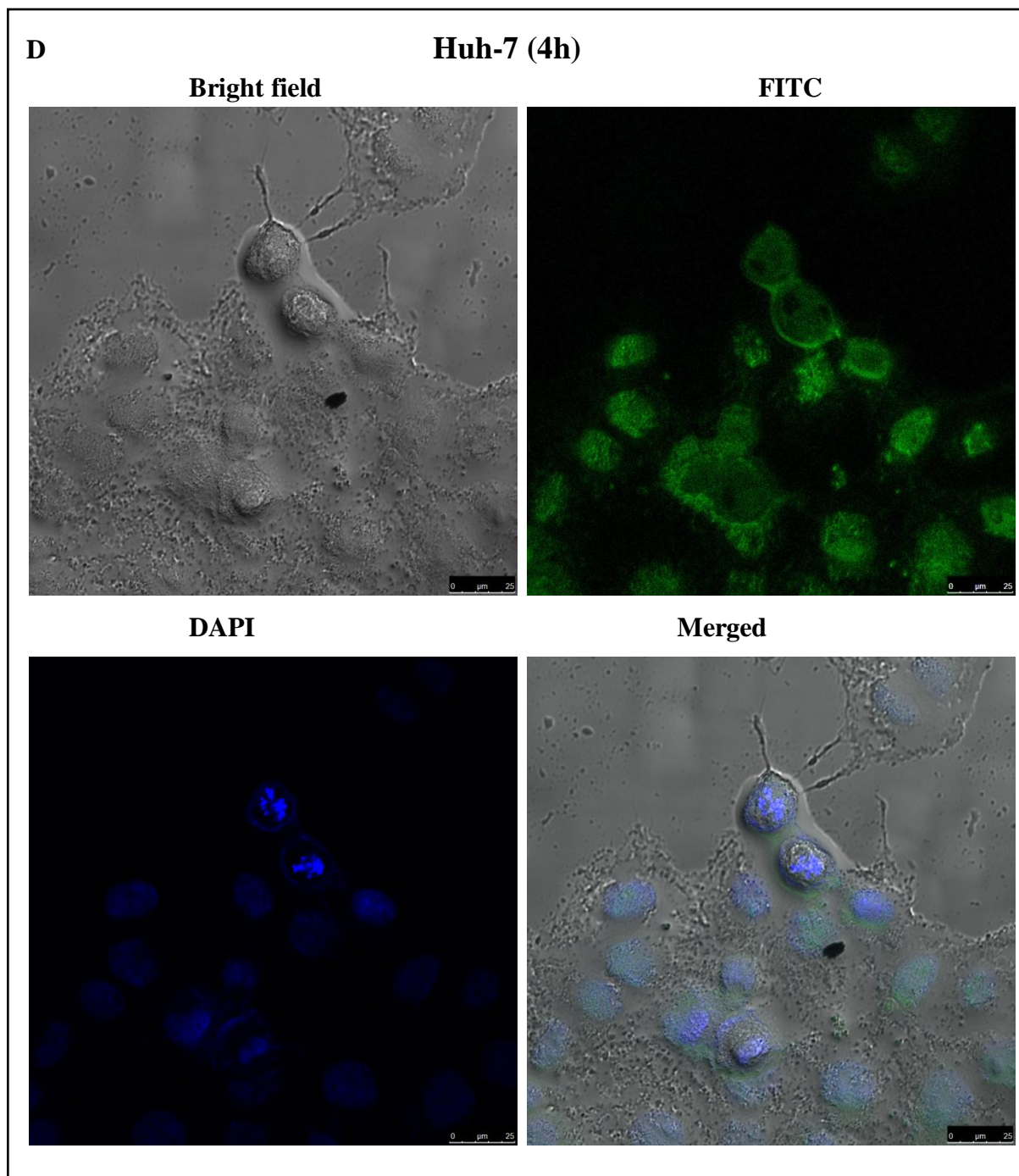




**Figure 5.13B** A time dependent cellular uptake of nanoparticles was observed at 4 h of study in HepG2 cells showed by a much higher intensity in both DAPI and FITC filter areas.



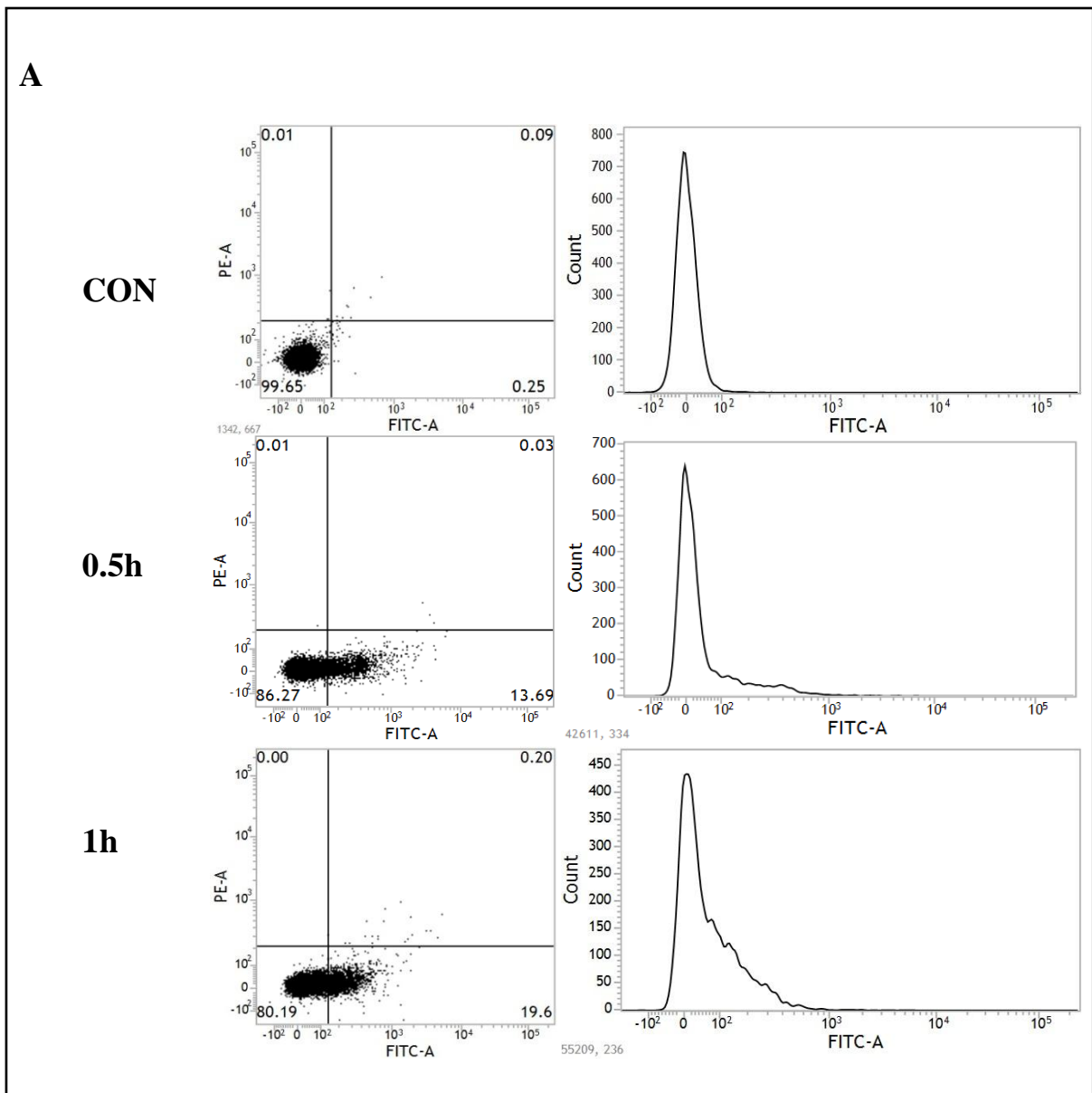
**Figure 5.13 C** At the first hour of study, the color intensity in FITC filter area was less in Huh-7 cells. However, nucleus was seen clearly.

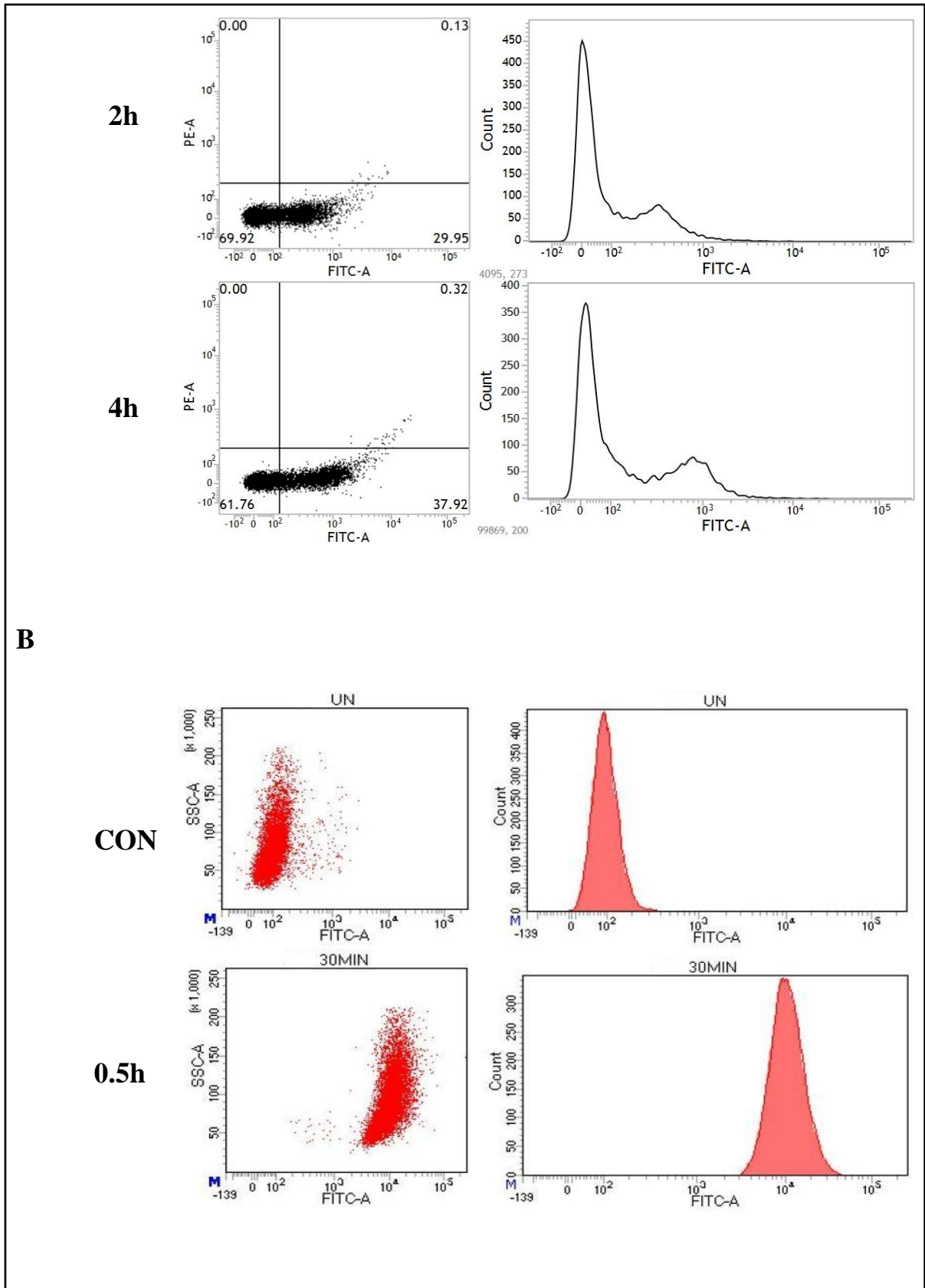


**Figure 5.13 D** Time dependent uptake of nanoparticles inside cytoplasm as well as nucleus was clearly seen at 4h study in Huh-7 cells. In DAPI filter, it was also observed that nanoparticles were destroying the nucleic acid structures by DNA damage.

## 5.9.3 Quantification of cellular uptake by FACS

A quantitative measurement by FACS analysis showed that FITC signals were proportionally increased with the amount of drug incorporated in HepG2 and Huh-7 cells incubated with ApNp5 at different time points (0.5h, 1h, 2h and 4h), as compared to untreated (control) cells (**Figure 5.14**). The FACS analysis data for HepG2 and Huh-7 cells are depicted in panel A and B respectively. The quantifications are indicated by the shifting/counting of cells inside the FITC filter area.





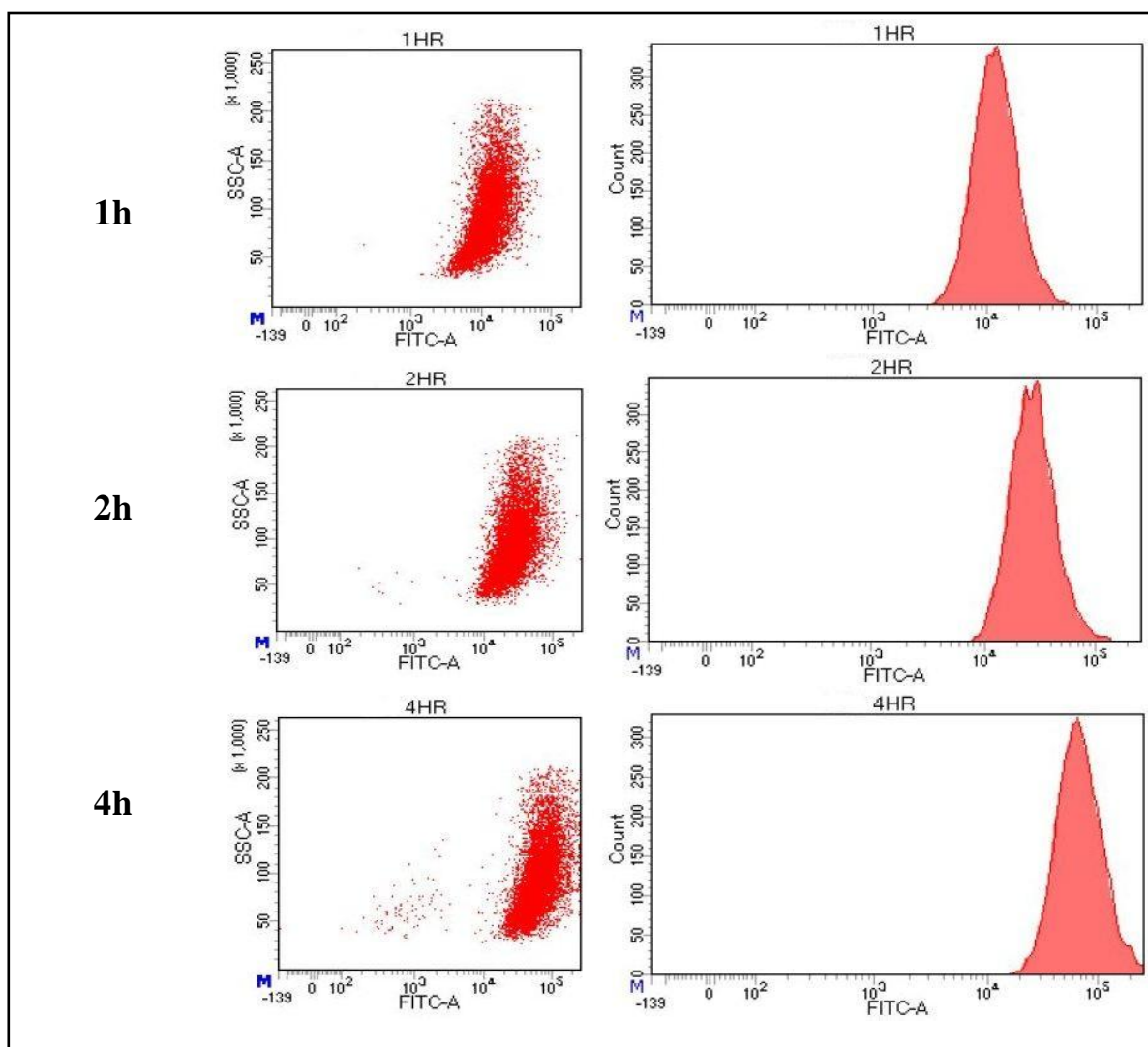


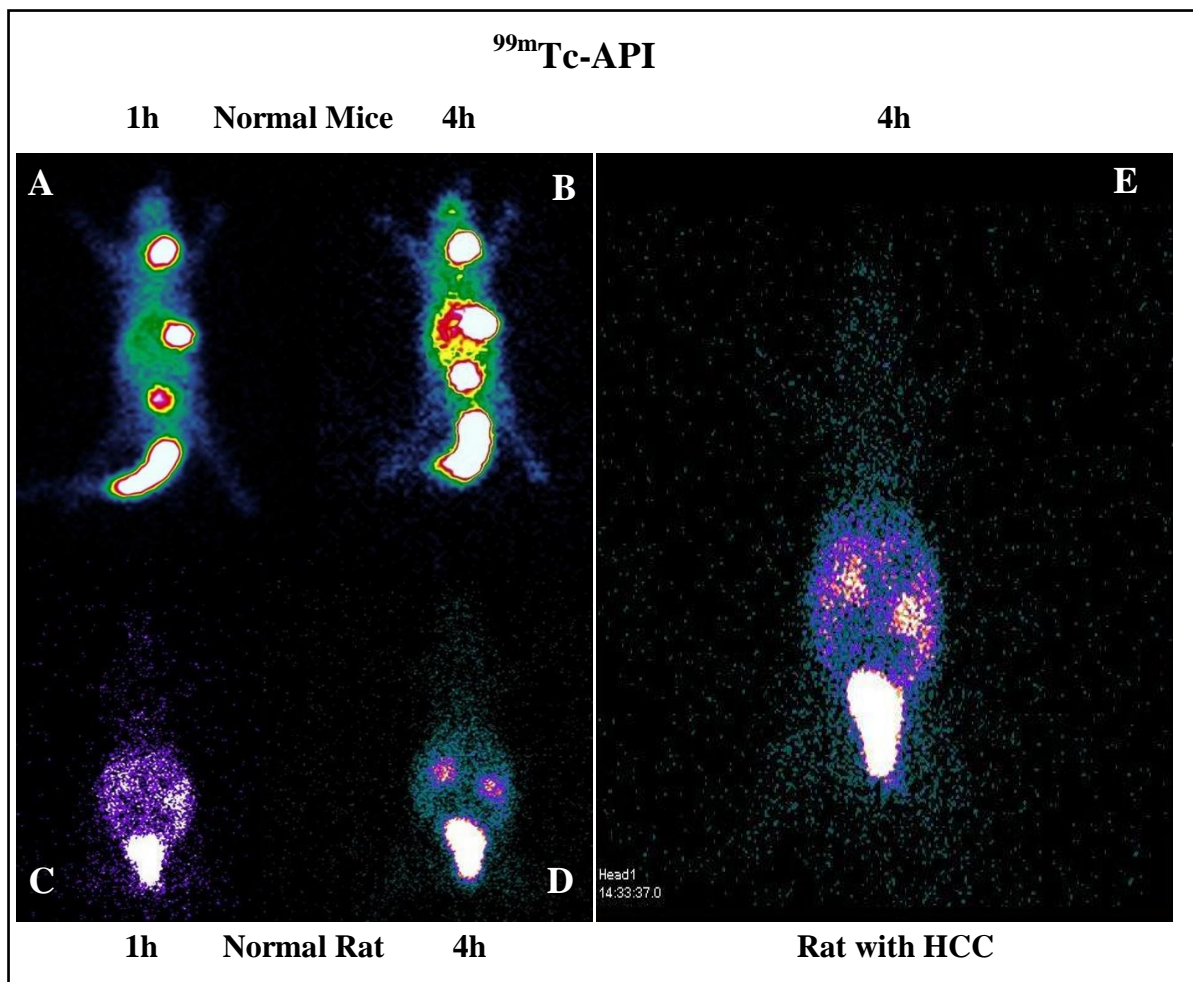
**Figure 5.14** Time dependent cellular uptake and quantification of the nanoparticles were observed into HepG2 (Panel-A) and Huh-7 (Panel-B) cells. A predominant uptake was measured over time in both the types of cells.

## 5.10 *In-Vivo* studies

### 5.10.1 *Radiolabeling and Gamma Scintigraphy*

$^{99m}\text{Tc}$ -API/ $^{99m}\text{Tc}$ -ApNp3 was visualized by gamma scintigraphy in different animals (mice/rats) (**Figure 5.15**) and the investigation showed that labeled ApNp3 accumulated predominantly in liver than  $^{99m}\text{Tc}$ -API. In both the animals, distribution of  $^{99m}\text{Tc}$ -API from the tail vein appeared to be very slow and it was detected in the tail vein at 4h after its administration. Further, predominant time-dependent accumulations were detected in

intestine, thymus gland, stomach and urinary bladder (**Figure 5.15**, A and B) of mice. However, in case of  $^{99m}\text{Tc}$ -ApNp3 administration, prominent time-dependent accumulations in mice liver, urinary bladder as well as in intestinal region were noticed (**Figure 5.15**, F and G). When radiolabeled  $^{99m}\text{Tc}$ -API /  $^{99m}\text{Tc}$ -ApNp3 was administered in normal rats through tail vein, a quick and time-dependent distribution of labeled ApNp3 was observed in liver and the clearance of labeled nanoparticles through urinary bladder was very less (**Figure 5.15**, H and I) as compared to that of  $^{99m}\text{Tc}$ -API in mice. Administration of  $^{99m}\text{Tc}$ -API in rats showed distribution in kidneys, and elimination through urinary track *via* urinary bladder (**Figure 5.15**, C and D). When rats with HCC were treated with  $^{99m}\text{Tc}$ -ApNp3/  $^{99m}\text{Tc}$ -API, predominant localization of  $^{99m}\text{Tc}$ -ApNp3 was seen inside the enlarged (most likely due to inflammation) liver and its surrounding organs (at 4h) and its clearance through urinary bladder was remarkably low (**Figure 5.15**, E and J).



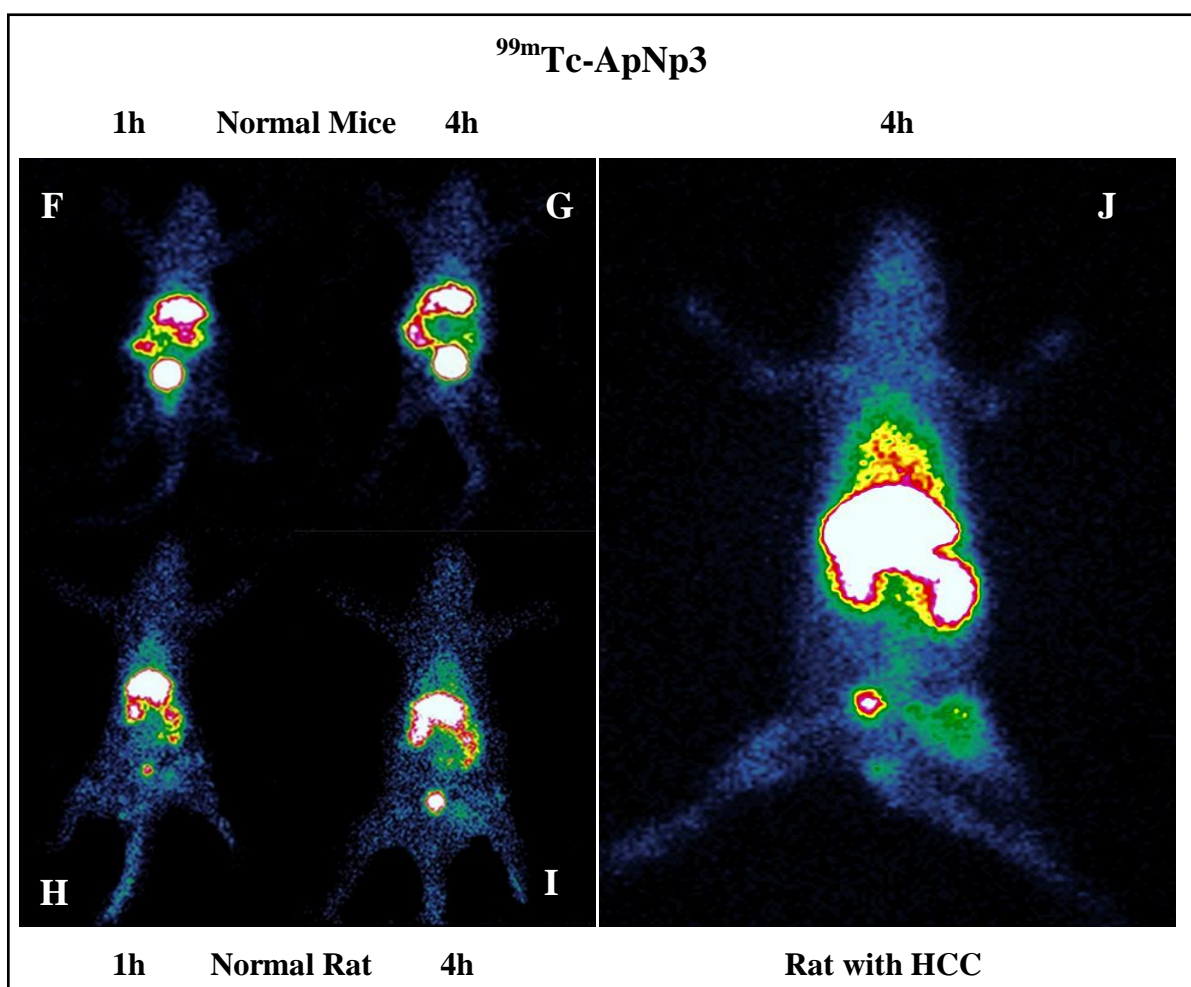


**Figure 5.15** Gamma scintigraphic images of radiolabeled ApNp3/API and apigenin biodistribution *in vivo*. Time dependent biodistribution and accumulation of  $^{99m}\text{Tc}$ -API in mice at 1 h (A) and at 4 h (B); in rats at 1 h (C) and at 4 h (D); in rats with HCC at 4 h (E) along with the accumulation of  $^{99m}\text{Tc}$ - ApNp3 in mice at 1 h (F) and at 4 h (G); in rats at 1 h (H) and at 4 h (I); rats with HCC at 4 h (J) are shown.

### ➤ Biodistribution of API/ApNp3

Biodistribution of  $^{99m}\text{Tc}$ -API and  $^{99m}\text{Tc}$ - ApNp3 was examined in various organs of balb/c mice. Substantial uptake of  $^{99m}\text{Tc}$ - ApNp3 was observed in hepatic region compared to  $^{99m}\text{Tc}$ -API. At both the time points (2 h and 6 h), radiolabeled nanoparticles had much higher residence time in blood and lower distribution in kidney than  $^{99m}\text{Tc}$ -API (**Table 5.3**).



**Table 5.3: Organ/tissue wise biodistribution of apigenin in mice received i.v\* injection (1mg drug/ml) of equivalent  $^{99m}\text{Tc}$ -ApNp3/  $^{99m}\text{Tc}$ -API †**

Organ/ Tissue	$^{99m}\text{Tc}$ -ApNp3		$^{99m}\text{Tc}$ -API	
	2 h	6 h	2 h	6 h
Heart	0.597 ± 0.058 <sup>‡</sup>	0.421 ± 0.049	0.315 ± 0.051	0.284 ± 0.056
Blood	2.230 ± 0.095	1.806 ± 0.087	0.829 ± 0.099	0.631 ± 0.087
Liver	42.15 ± 1.213	54.151 ± 1.191	22.456 ± 1.311	20.561 ± 1.197
Lung	0.747 ± 0.213	1.285 ± 0.222	1.215 ± 0.192	0.997 ± 0.213
Spleen	0.378 ± 0.054	0.721 ± 0.034	1.531 ± 0.049	1.745 ± 0.057
Kidney	2.912 ± 0.211	2.451 ± 0.189	3.990 ± 0.212	4.785 ± 0.191
Intestine	6.160 ± 1.431	8.751 ± 1.212	21.556 ± 1.198	25.612 ± 1.199
Muscle	0.125 ± 0.003	0.156 ± 0.002	0.287 ± 0.007	0.215 ± 0.002

\*i.v, intra-venous, <sup>†</sup> $^{99m}\text{Tc}$ -ApNp3, radiolabeled apigenin loaded nanoparticle;  $^{99m}\text{Tc}$ -API, radiolabeled apigenin; <sup>‡</sup>Data show mean ± SD (n = 4). Results were expressed as % injected dose/g of tissue/organ.

### 5.10.2 LC-MS/MS study:

Graphical representations of the plasma profile and the hepatic accumulation of apigenin upon ApNp3/API administrations were given in **Figure 5.16A** and **Figure 5.16B**, respectively. In case of plasma, ApNp3 was found to maintain a steady blood level of predominantly more amount of drug even up to 72 h (period of the study). In case of hepatic concentration of apigenin, apigenin (from suspension) was detected up to 12h, but the concentration could not be detected in liver at 24 h. In case of ApNp3, the hepatic concentration of drug was detectable up to 72 h (time period of the investigation) which showed maintenance of a steady level of hepatic concentration of apigenin by ApNp3. Hepatic  $t_{\text{max}}$  (time to reach maximum concentration) values were very close for ApNp3 and API (about 1-2 h) suggesting rapid uptake of API and the nanoparticles by liver. The plasma and liver pharmacokinetic data of apigenin from ApNp3 and from API (**Table 4**) showed that administration of ApNp3 by i.v route enhanced plasma half-life of drug by 75% and hepatic half-life of it by 6.6 times in the experimental animals. Values of maximum concentration of drug ( $C_{\text{max}}$ ) in plasma and in liver were more or less similar for

API and ApNp3. Plasma as well as hepatic AUC values markedly increased upon ApNp3 administration from 1.5 to 3 times respectively as compared to those for API. Further, the values of the mean residence time of apigenin (from ApNp3) in plasma and in liver were found to increase by 1.68 and 3.03 times respectively, compared to API.

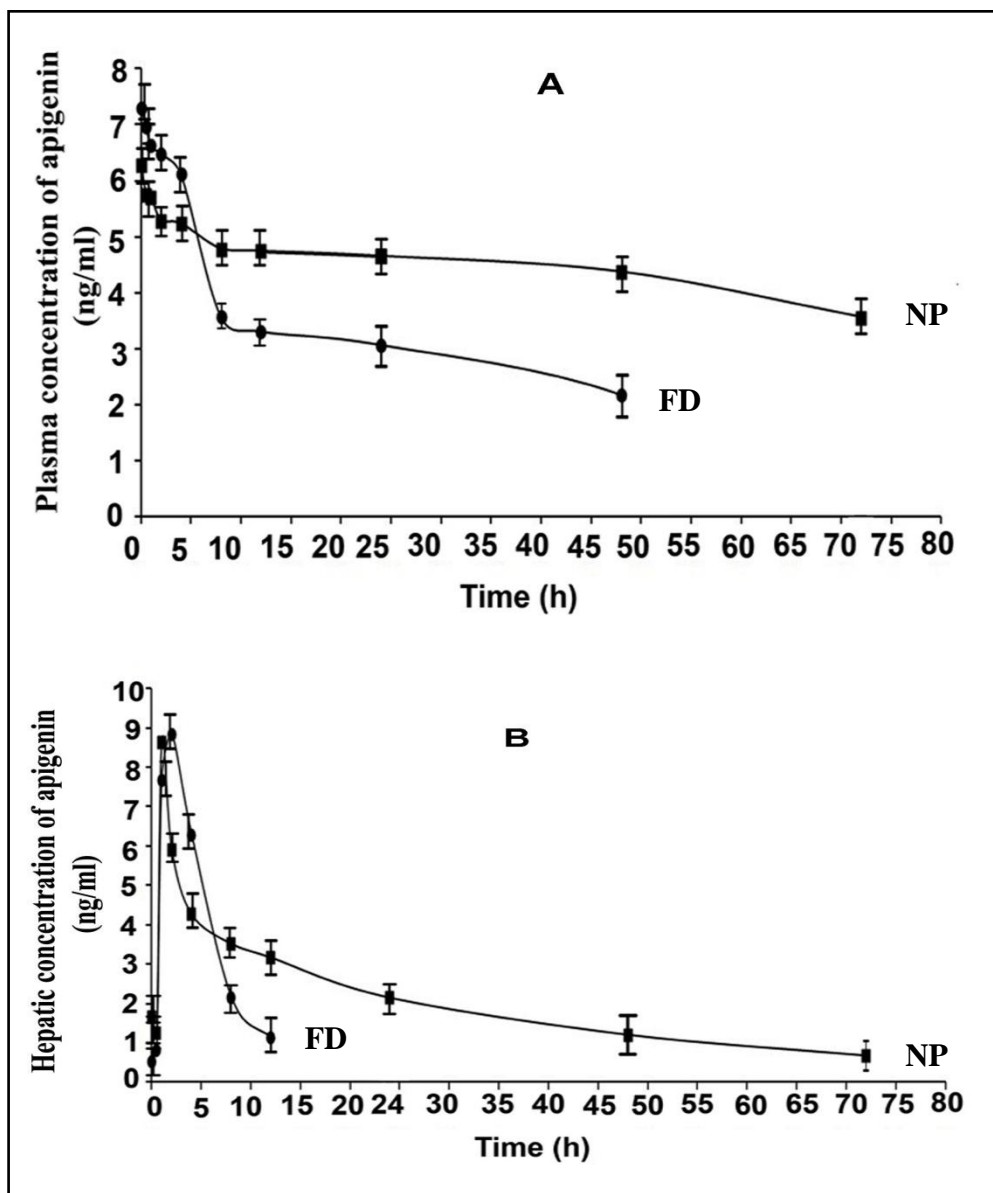


**Figure 5.16** Plasma (A) and hepatic (B) concentration of apigenin upon i.v bolus injection (at a dose of 1mg/kg body weight) of free drug API (FD) and ApNp3 (NP) (equivalent dose) were shown. Data show mean  $\pm$ SD (n = 4).

**Table 5.4:** Plasma and hepatic pharmacokinetic parameters of apigenin from API<sup>†</sup> and ApNp3<sup>\*</sup> after intravenous bolus administration of API and ApNp3 with an equivalent amount of drug in balb/c mice.

Parameters	Plasma values of drug upon API administration <sup>‡</sup>	Plasma values of drug upon ApNp3 administration	Hepatic values of drug upon API administration	Hepatic values of drug upon ApNp3 administration
Half life; t <sub>1/2</sub> (h)	39.8±2.1	70.7±4.3	3.8±0.9	25.1±1.
C <sub>max</sub> (ng/ml)	7.31±1.3	6.29±2.5	8.48±2.78	8.66±1.99
<sup>§</sup> AUC <sub>0-t</sub>	164.6±12.2	338.6±31.67	47.87±4.9	124.13±2.24
AUC <sub>0-inf</sub>	289.9±23.5	701.7±55.31	55.9±4.7	168.2±14
CL (L/h/kg)	3.45±0.75	1.43±0.43	17.9±1.54	5.9±0.88
MRT <sub>last</sub> (h)	20±3.7	33.7±2.24	4.8±1.02	18±2.01
V <sub>ss</sub> (L/kg)	196.5±17.6	151.5±11	113.9±13.6	209.9±17.8

\*ApNp3, apigenin loaded nanoparticles; †API, suspension of apigenin. ‡ Data show mean ±SD (n = 4). §Units of AUC in plasma is h-ng/ml, and in hepatic tissue h-ng/g respectively.

### 5.10.3 Experiments on animals with chemically induced hepatocellular carcinoma

#### ➤ Effect of ApNp3 and API on normal and HCC rat livers:

Animals were divided in six groups each containing of six animals. Each group of animals received different treatments (discussed in material and methods chapter). Animals were sacrificed and livers from different groups were collected. After macroscopic and microscopic observation of the hepatic tissues, the effect of ApNp3 and free apigenin on HAF lesions and total area of the lesions were visualized. In group B, C and D animals, in livers, hepatic altered foci were counted/unit area (cm<sup>2</sup>). Maximum HAF were observed in group B (carcinogen control rats) followed by group D (carcinogenic animals treated with API). However, group C animals (carcinogenic rats treated with ApNp3) showed significantly reduced number and incidences of HAF and total area of lesions. No HAF or lesions were recorded in group A, E and F animals which had normal (untreated/treated) rats. The data are tabulated in **Table 5**.

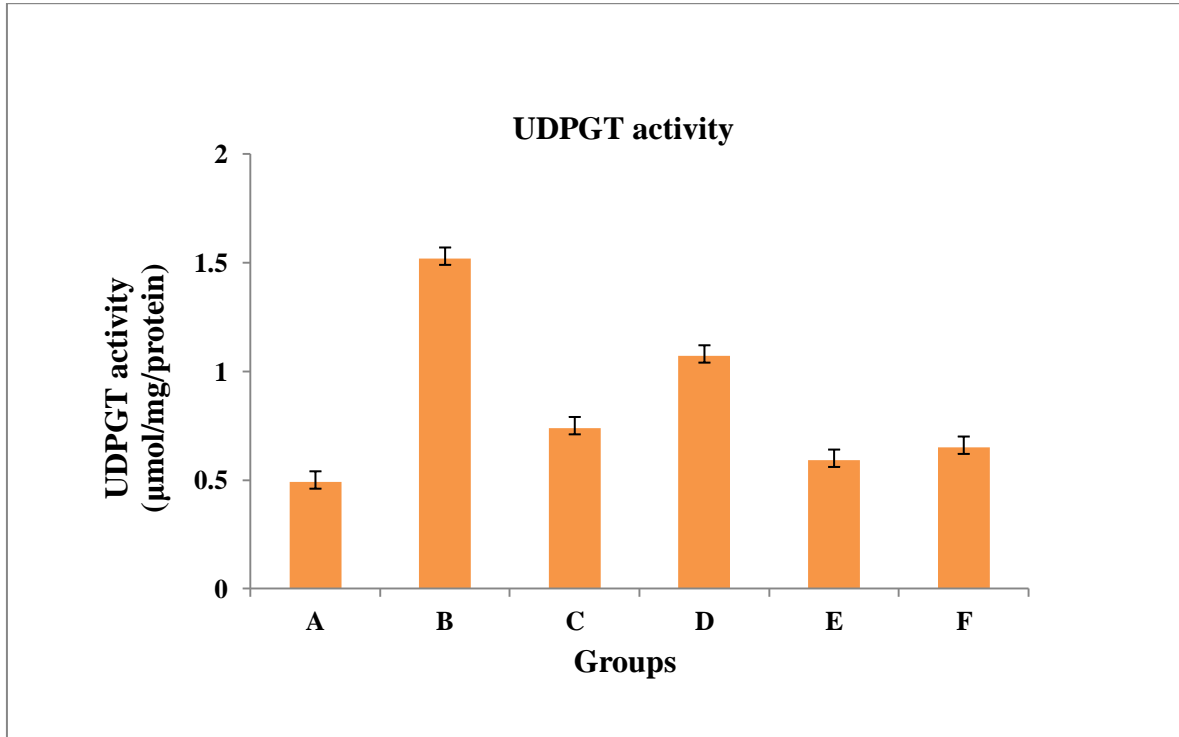
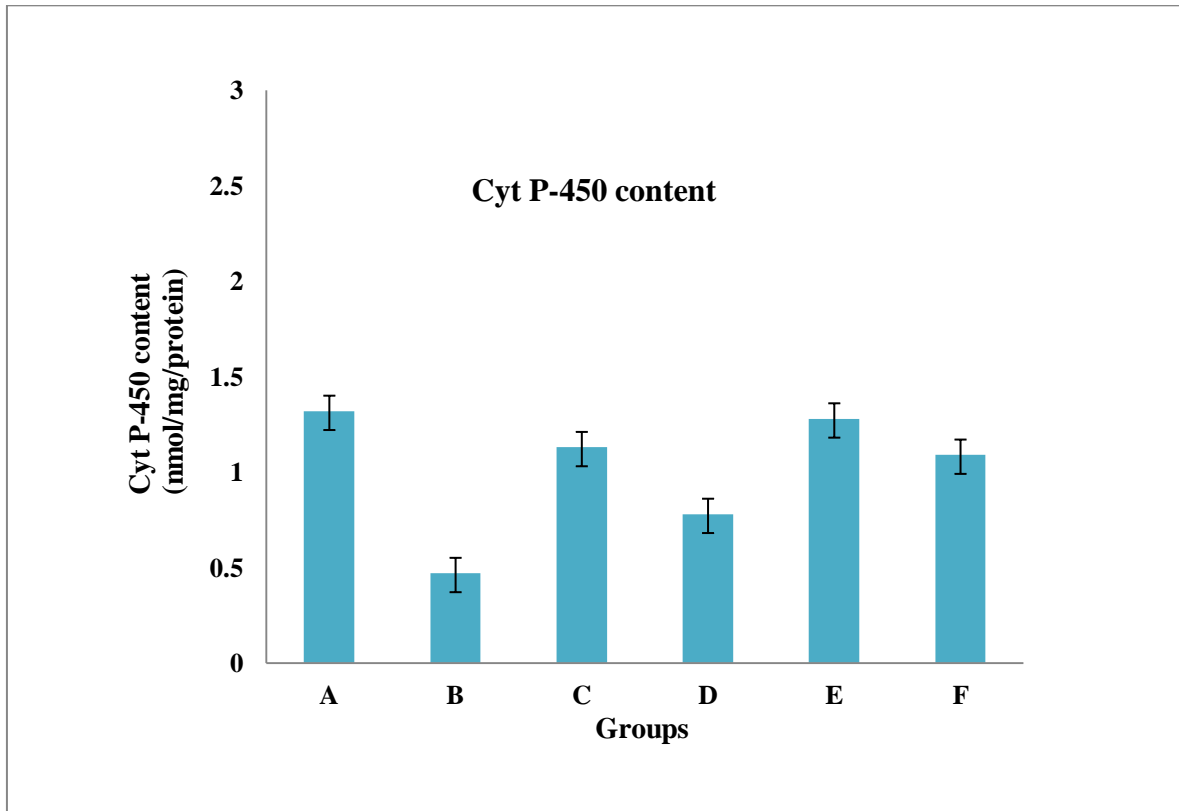
**Table 5.5** A quantitative data on the effect of API/ApNp3 treatment of hepatic tumor incidences, number and total area of hepatic altered foci (HAF)

Groups	Number of rats developed HCC per total number of experimental rats per group	Tumor incidences (%)	Number of HAF <sup>†</sup> /cm <sup>2</sup> of hepatic tissue <sup>†</sup>	Total area of lesion (%)
A	0/6	-	-	-
B	6/6	100	79.57±6.08 <sup>†</sup>	57.76±1.45
C	2/6	66	21.98±3.34 <sup>‡</sup>	12.38±0.98 <sup>‡</sup>
D	-	-	-	-
E	-	-	-	-
F	5/6	83	56.43±5.8 <sup>‡</sup>	36.73±4.65 <sup>‡</sup>

\*HAF: hepatic altered foci; <sup>†</sup>Values represent mean ±SD (n=6 for each group). <sup>‡</sup>p<0.05 when compared against Group B rats.

#### ➤ Marker enzyme Assays

Cytochrome P-450 (cyt p-450) content, glutathione-S-transferase (GST) activity in cytosolic fraction, UDP-glucoronyl transferase (UDPGT) and SOD activity in microsomal hepatic fraction of the experimental animals were shown in **Figure 5.17**. In our study, cyt P-450 content was found to reduce in group B (HCC control) animals both in tumor tissues as well as in tumor surrounding tissue in comparison with the normal rats (group A). ApNp3 treated HCC animals (group C) markedly increased cyt P-450 content in the tumor area when compared with group B (HCC) animals. On the other hand, GST and UDPGT activities were found to increase predominantly in tumor areas of group B rats in comparison with the normal rats. Activities of the two enzymes significantly decreased in tumor area after ApNp-treatment in group C rats indicating the effect of apigenin nanoparticles in repairing or delaying the progress of HCC in rats. SOD activity has a direct relation with ROS generation in hepatocytes. Here, we found that carcinogenic control animals showed a reduced SOD activity when compared to normal control rats. After the treatment with ApNp3, carcinogenic animals showed an elevated SOD activity. API treated carcinogenic rats (group D) also showed an increase in SOD activity but not to the extent of group C animals. Normal animals treated with ApNp3/API moderately altered levels/activities of the marker enzymes/isoenzyme when compared to normal control group of animals.



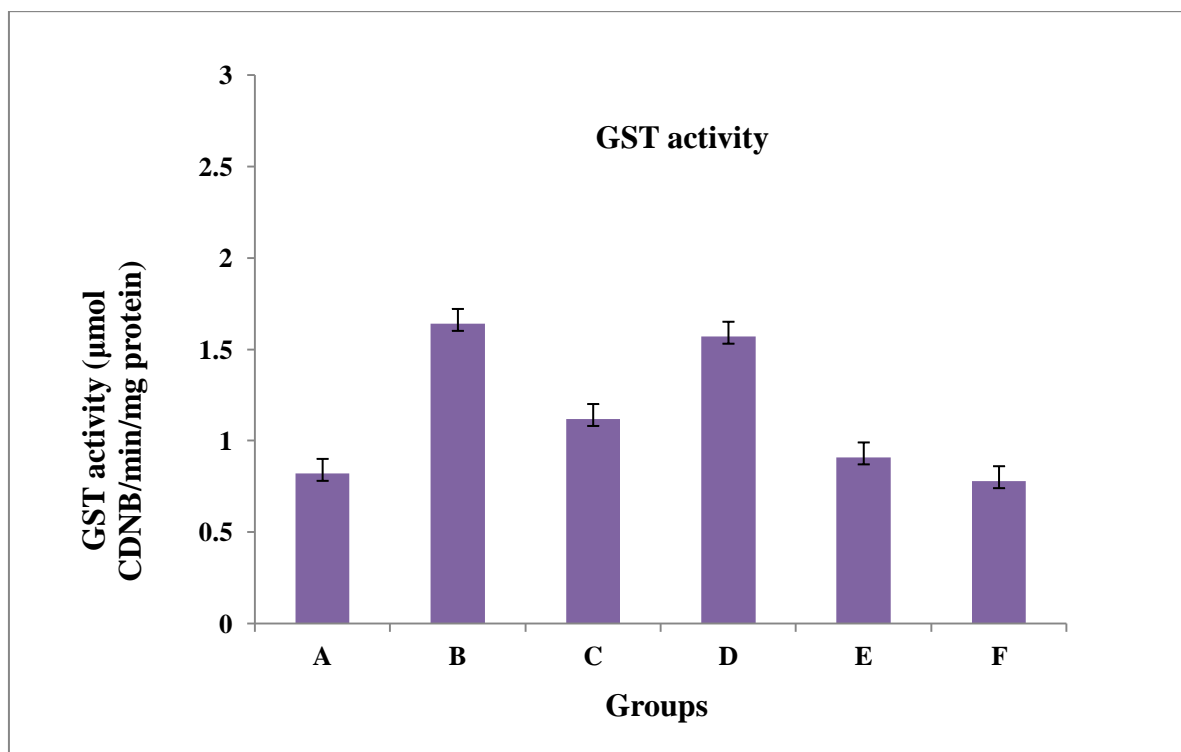
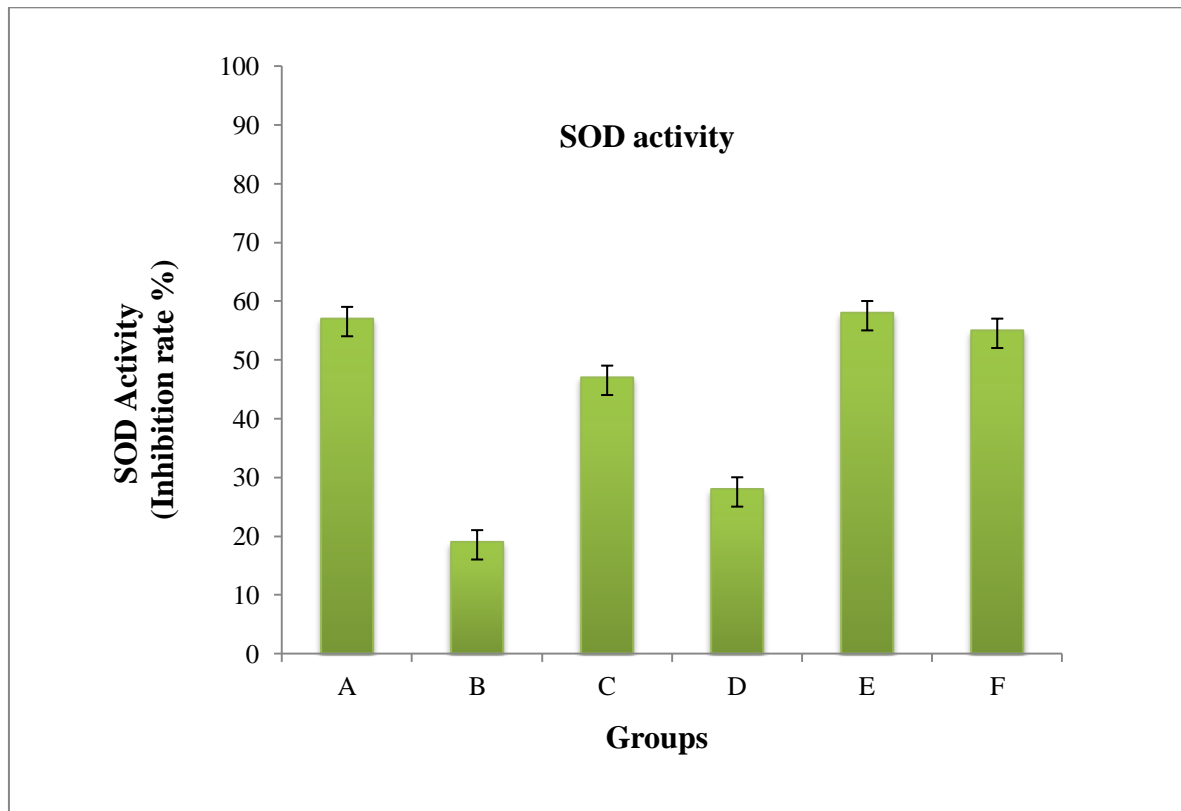


**Figure 5.17** Different marker enzyme and iso-enzyme activities are shown. Data show mean  $\pm$ SD (n = 3).

➤ **Macroscopic Study:**

After sacrificing the animals from various groups, livers were dissected out and some of the samples were kept frozen in a deep freezer (-80 ° C) in 10% formaldehyde and processed for histopathological investigations. Macroscopic images of livers were taken with a help of a camera. A significant alteration of gross hepatic structure was observed among group A, B and C animal livers.

Livers from normal control group (group A) showed no architectural disturbance in hepatic tissues (Figure 5.19A), whereas hyperplastic nodules (HN) and preneoplastic and neoplastic hepatic altered foci (HAF) were clearly visible in HCC control rats (group B) along with a major disturbance in gross liver architecture. However, treatment with apigenin nanoparticles (20 mg apigenin/kg single i.v dose/week) [Hu *et al*, 2015] for 12 weeks (group C) successfully controlled the tumor development in carcinogen treated rats (Figure 5.18C) and upon intravenous treatment with ApNp3, the sizes of the nodules and numbers of lesions were markedly reduced. Macroscopic images are depicted in **Figure 5.18**.

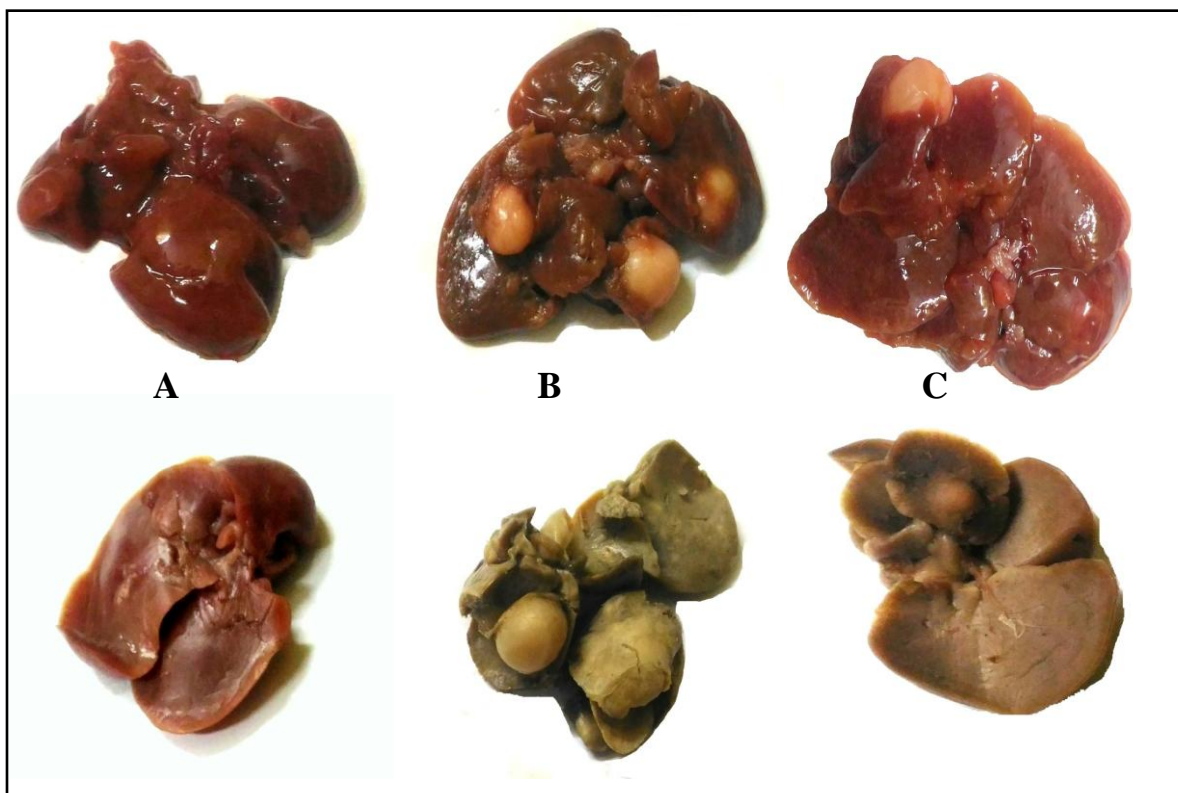


**Figure 5.18** Macroscopic images of livers of normal rats (A), carcinogen control rats (B) and carcinogenic rats treated with ApNp3 (C).

➤ **Hematoxylin and eosin staining and histopathology study**

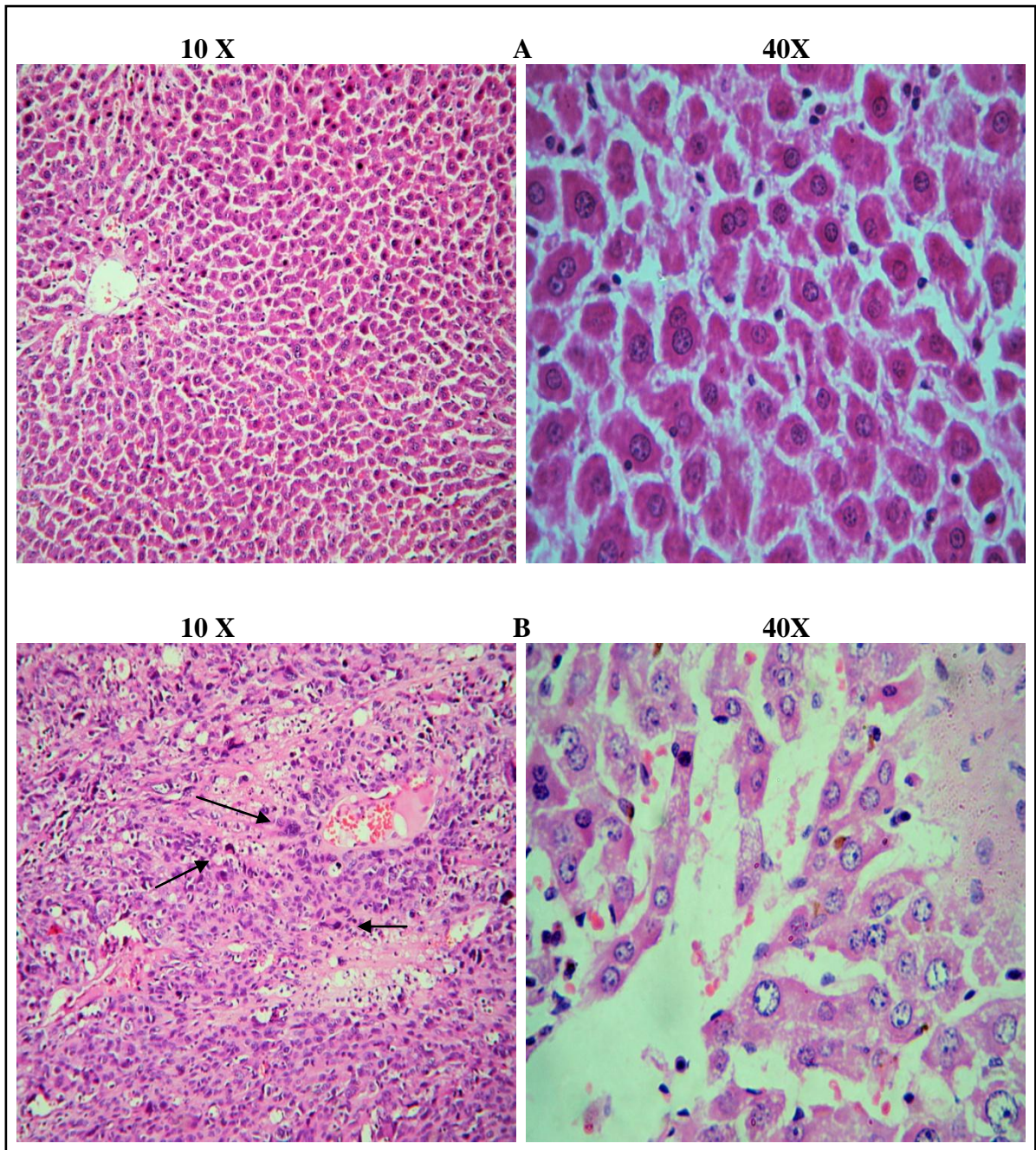
Hematoxylin and eosin staining is a very common staining procedure used in biological science to stain cytoplasm (basic in nature) by eosin stain (light violet or pinkish color) and nucleus (acidic nature) by hematoxylin which are shown by dark violet/blue colors [Fischer et al, 2008]. Here, two different magnifications (lower, 10X and higher, 40X) were used to visualize the tissue sections from each group under microscope. The overall architecture was seen in lower magnification and a closer view of the hepatic tissue was observed in higher magnification.

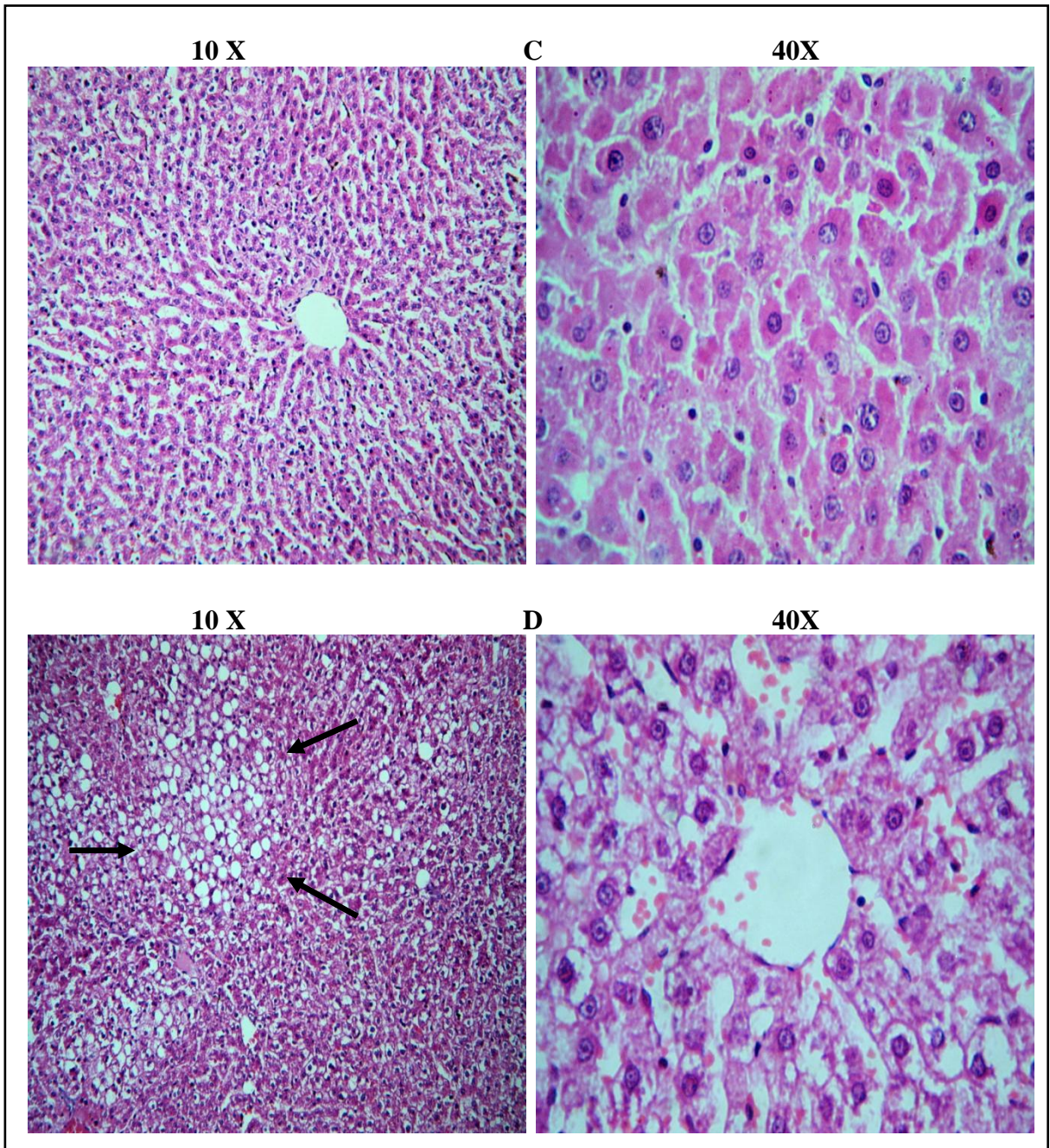
A closer view of histopathological observation indicated that in the carcinogen control animals (**Figure 15.19 B**), focal lesions, tumor formation and scattered lesions with cells of ground glass appearance were visible in the liver and normal hepatic architecture was altered. Cellular death and cells with picnotic nucleus (shown by black arrow) were also observed as compared to the normal liver architecture (**Figure 15.19 A**).

Treatment of apigenin nanoparticles (ApNp3) in carcinogenic animals (**Figure 15.19 C**) was found to hold the hepatocellular architecture predominantly towards normal as compared to the carcinogenic animals treated with free drug (**Figure 15.19 D**). Scattered ground glass appearances (white hollow portion in cells, are shown by black arrow) were present in hepatic sections of free drug treated HCC animals whereas the presence of ground glass appearance was much less in ApNp3 treated HCC animals.

There was no distinguishable change in hepatocellular architecture in normal animals treated with blank nanoparticle (data not shown), ApNp3 (**Figure 15.19 E**) and free drug (**Figure 15.19 F**). Hexagonal hepatic cells can be seen in both of these groups which indicate that there was no toxic effect of PLGA nanoparticles as well as apigenin upon normal hepatic environment.







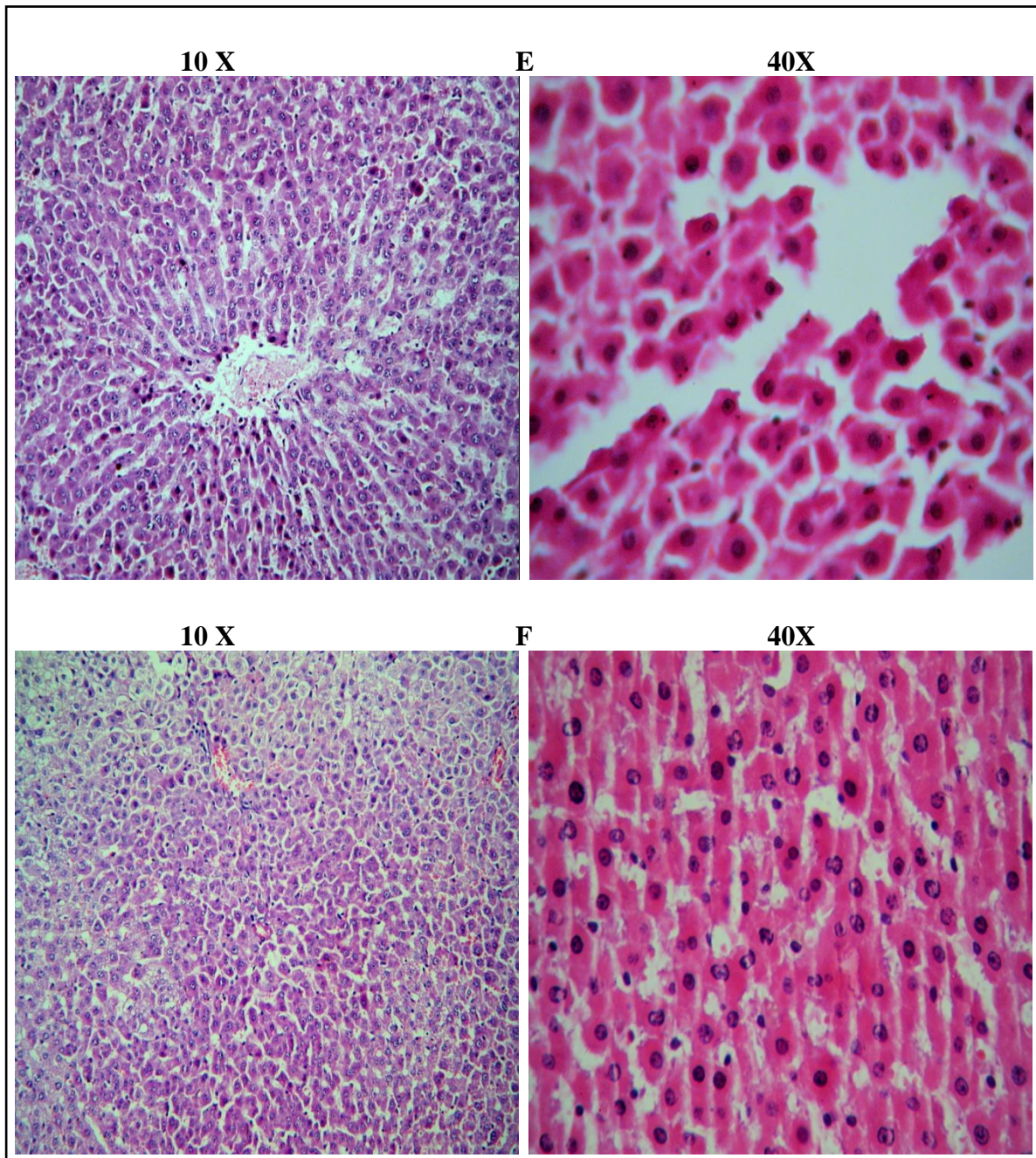


**Figure 5.19** Microscopic images of liver section of normal rats (A), carcinogen treated rats (B), carcinogen treated animals treated with ApNp3 (C), carcinogen treated animals treated with APIs (D), normal animals treated with ApNp3 (E), and normal animals treated with API (F).

# Chapter 6

## *Discussion*

## 6. Discussion

In recent times apigenin has gained much popularity as a naturally occurring flavonoid which has much lower intrinsic toxicity on normal cells compared to cancer cells while used as a tumor-suppressive agent [Sak, 2014]. There are few reports published till date, which showed tumor suppressive effect of apigenin against HCC *in-vitro* [Li et al, 2017; Wu et al, 2017]. All these studies indicated a much higher dosing of apigenin required to acquire the therapeutic activity. To the best of our knowledge, this is the first report showing that apigenin nanoparticles successfully delayed the progress of HCC both *in-vitro* and *in-vivo*. Another uniqueness of our study was that the investigation showed *in-vivo* localization of apigenin-loaded nanoparticle as well as their tissue distribution by gamma scintigraphy. The investigations further support the hypothesis that site (liver) specific delivery of ApNp may ensure a successful treatment to control the progress of HCC.

At first, we checked the absorbance maxima of apigenin by spectrophotometric method. An object absorbs energy from the light when the light passes through that object. This absorption of energy triggers excitement of electrons in that object. This energy absorption by the object reaches at maximum point when a specific wavelength of light passes through it. This wavelength is recorded as maximum wavelength or  $\lambda_{\max}$ . Our study recorded two prominent  $\lambda_{\max}$  of API at 268 nm and 340 nm. We performed rest of our experiments using 340 nm as  $\lambda_{\max}$  as it was the most intense peak of API. Performing this study also ensured us about the purity of the substance as the wavelength was similar to the reported ones [Li et al, 1997].

Calibration curves of apigenin in PBS (pH 7.4) and DDS were prepared and the equations of these graphs were used further while determining the amount of drug loading and drug release in our study. In both the cases graphs were observed with regression coefficients over 0.995 indicating straight and liner data [Schneider et al, 2010], and good accuracy of the experiment.

Drug loading and drug loading efficiency increased proportionally with the increasing amount of drug incorporated inside PLGA core up to a drug polymer ratio of 1:2.5 (ApNp4) with a highest drug loading of formulation ApNp3. But when drug polymer ratio

reached 1:1, it was observed (by FESEM) that the prepared nanoparticles formed colloidal structure, and the cross linking of polymers did not take place properly (data not shown) hence those nanoparticle formation was not proper.

FTIR spectrum of the drug (apigenin) was compared with the various excipients with their respective individual spectrum, and the spectra of physical mixture of drug and the excipients and the lyophilized formulations with or without drug. We have observed no major shifting of peaks indicating no chemical interaction existed between the drugs and the excipients (electrovalent or covalent type reactions) and rather suggested for physical interactions that might be involved in the formation of structure of the nanoparticles [Dutta et al, 2018]. Interestingly, the individual characteristic peak of apigenin [at wave number  $1243\text{ cm}^{-1}$ ] was present in the physical mixture but was absent in the apigenin loaded formulation (ApNp3) which indicates that the drug was entirely encapsulated in the formulation.

Observing the surface morphologies of nanoparticles it can be said that prepared nanoparticles were of spherical shape, had smooth outer surface indicated a particle size range of 150-300 nm (with a PDI range of 0.260-0.409) and the drug was homogeneously distributed inside particles which fulfills the primary requirements (as size increases beyond 150 nm, more and more nanoparticles are entrapped within the liver and spleen) for efficient drug delivery to the target site [Longmire et al, 2008]. Considering the type and site of drug delivery, nanoparticles can be engineered according to their size, polydispersity index (PDI) and surface charge [Bahari et al 2016]. *In-vivo* applications of the nanoparticles depend on the cellular uptake or internalization of those particles [Hoshyar et al, 2016]. Endocytosis (phagocytosis and pinocytosis) is the main process for transporting and engulfing different size particles actively inside the cellular matrix [Sadat et al, 2016]. Particle size and polydispersity index (PDI) are the main physicochemical factors which influence the endocytosis process as tumor vasculature is very different than the normal vasculature and is leakier in nature [Mozafari et al, 2009; Aw-Yong et al, 2018; Danaei et al, 2018]. This leaky environment of tumor site allows high molecular weight and larger particles to accumulate in tumor site. This phenomenon is known as enhanced permeability and retention (EPR) effect [Maeda et al, 2015]. We have prepared particles with a size

range of 150-300 nm, keeping the fact in mind that more and more nanoparticles in the range of 150–200 nm have been shown to enter through vascular architecture of tumors (the EPR effect), entrapped within tumor part and escape filtration by liver [Blanco et al, 2015]. PDI is the term used to define size distribution of nanoparticles. The degree of uniformity/non-uniformity is measured by PDI of that formulation and the ranges can be from 0.0 (perfectly uniform) to 1.0 (highly polydispersed) [Masarudin et al, 2015]. PDI values more than 0.7 indicates that formulation has a broad particle size range. The optimum PDI values from 0.05 to 0.7 are generally used for site specific drug delivery whereas PDI values less than 0.3 are considered acceptable indicator for nanocarriers [Clarke, 2013; Badran, 2014; Chen et al, 2011; Danaei et al, 2018].

Surface charge (measured by zeta potential) of nanoparticles represents another feature that can be tailored to prolong circulation lifetimes and selectively enhance accumulation at specific sites of interest. Nanoparticles with neutral and negative surface charges have been shown to have a much longer circulation half-life. Thus, for effective nanoparticle delivery to tumors, one would desire a neutral or slightly negative nanoparticle surface charge upon intravenous administration [Blanco et al, 2015; Yuan et al, 2012; Alexis et al, 2008]. On the other hand, nanoparticles with zeta potential ranging from -30 mV to +30 mV, have a tendency to settle down quickly as compared to those having zeta potential range  $> +30$  mV or  $< -30$  mV which generally form colloidal dispersion [Meißner et al, 2009; Basu et al, 2012]. But the particles with zeta potential values ranging from -30 mV to +30 mV never settle down so quickly that they would not be administered intravenously. They should be stored in a powder form (at 4-8°C) and suspended in saline solution or water for injection and shaken well before administration. Here the optimized apigenin loaded nanoparticles had zeta potential values ranging from -4 mV to -5 mV which indicated a stable formulation having a preferable surface charge for delivery in hepatic tumor sites.

Polymer composition has a critical role in stability of biodegradable PLGA nanoparticles in different pH media. PLGA degrades via ester bond breakage in the polymeric matrix by hydrolytic attack of water molecules [Keles et al, 2015; Houchin and Topp, 2008; Kenley et al, 1987]. A variable hydrolytic degradation of nanoparticles was observed in different pH buffers. Nanoparticles were found to be more stable in PBS (pH 7.4) in comparison

with acetate (pH 5) and citrate (pH 3) buffers. It indicates that the formulation is not suitable for oral delivery as gastric juice have highly acidic environment. It was reported earlier that PLGA undergoes biodegradation/hydrolysis more in acidic medium as compared to slightly alkaline or neutral environment [Makadia et al, 2011; Zolnik et al, 2007]. Thermal degradation of apigenin loaded PLGA nanoparticles was also checked by accelerated stability study in different temperature and humidity conditions [Silva et al, 2015]. Nanoparticle structures were maintained in first month of this study but significantly softened over time in second and third months of the study. The polymeric matrix melted and the particle structures were deformed.

After administration of the drug loaded nanoparticles, depending on the different drug types and polymeric ratios, PLGA undergoes biodegradation through cleavage of ester links and monomers are formed. Since biodegradation pattern of PLGA depends on factors such as surface diffusion, bulk diffusion, surface erosion and bulk erosion, the release of the drug from the matrix also becomes unpredictable [Makadia et al, 2011]. Here prepared nanoparticles (ApNp3) showed a biphasic release pattern. ApNp3 had an initial burst release of apigenin (24% in 6 h) in PBS (pH. 7.4) followed by a sustained drug release pattern (52% in 60 days). Burst release might have occurred due to a comparatively faster release of drug molecules present close to the surface of the nanoparticles and a subsequent sustained release of drug occurred due to the release of drug molecules from the deeper region of the matrix as water content of the particles hydrolyses the polymers and allows the drug to diffuse slowly until complete solubilization of polymers occur [Ramchandani et al, 1998; Amann et al, 2010; Faisant et al, 2002]. A good linearity (as assessed by  $R^2$  value) has favored that drug diffusion followed Koresmeyer-Peppas kinetics with an anomalous diffusion pattern. Drug release was affected and altered by different pH values of the media. Apigenin released faster in acidic pH (both in pH 3 and 5) due to the faster hydrolysis of PLGA in acidic medium.

Earlier reports showed that apigenin has cytotoxic and anti-proliferative activity against human hepatocellular carcinoma (HCC) cells but the accurate mode of action remained unclear till date. However, studies also indicated that apigenin exerts its anti-cancer activity by inducing apoptosis, DNA damage, gene alteration and cell cycle arrest in a p<sup>53</sup>



modulating pathway [Chiang et al, 2006; Madunić et al, 2018; Zheng et al, 2008, Liu et al, 2017; Cai et al, 2011]. To determine the cytotoxic effect of ApNp3, we have performed MTT assay to find IC<sub>50</sub> of apigenin as well as apigenin nanoparticles. The cytotoxic effects of apigenin/ApNp3 were noted in two different types of HCC cells such as HepG2 and Huh-7 at two different time points (24 h and 48 h). IC<sub>50</sub> value of ApNp3 was recorded less than free apigenin in each case and the possible reason behind it was that due to smaller size range, nanoparticles had higher and rapid cellular uptake than free apigenin [Ahn et al, 1997]. After determining IC<sub>50</sub> values of the drug loaded nanoparticles, we did confocal microscopy to visualize the successful internalization of the particles inside the cell as well as quantified the cellular uptake by FACS. Uptake of FITC tagged apigenin nanoparticles (ApNp5) followed a time dependent pattern and in both the cell types, at 4h, the nucleus structures were seen to destroy (DAPI filter, **Figure 5.13**). This indicates the initial apoptotic phenomenon. FACS assay directly gives information of amount of cells entered in FITC filter area. As there was no other source of FITC in the total experimental procedure, the amount of FITC was directly proportional to the amount of ApNp5 entered inside the cells. More ApNp5 was detected and quantified over time by the FACS analysis.

Radiolabeling of drug loaded nanoparticles with <sup>99m</sup>Tc plays a very important role in the nanomedicine field due to its ability to convey direct information about biodistribution and *in-vivo* visualization of those nanoparticles [Psimadas et al, 2013; Stockhofe et al, 2014]. Radiolabeled technetium chloride was attached to the surface of nanoparticles (ApNp3) with the help of stannous chloride. All the radiolabeling parameters such as amounts of nanoparticle suspension and time of incubation were standardized to achieve labeling purity that ranged between 90–92% and was verified by TLC [Gaonkar et al, 2017]. After *in-vivo* administration of the compound to the experimental animals, the bioimaging was done in a predetermined time interval. In our study, <sup>99m</sup>Tc-ApNp3 was found to accumulate predominantly in liver (the targeted organ in this study) of normal experimental animals. There was a preferential hepatic distribution of ApNp3 than free apigenin (API). Further, apigenin loaded radiolabeled nanoparticles were also found to reach the livers of animals with HCC due to their nano-size and predominantly accumulated in hepatic tissue. Although the average particle sizes were 200 nm (ApNp3) and 300 nm (FITC-ApNp5) respectively, for two different formulations, they had size distribution ranges varied from

30-500 nm. Hence some of the smaller particles might have eliminated faster which were visualized in the kidney. Numbers of published reports also showed that various nanocarriers size ranging from 150-250 nm and labeled with  $^{99m}\text{Tc}$ , were detected in kidney and urinary bladder as well as in urine [Yu and Zheng, 2015; Polyak et al, 2011].

The biodistribution data obtained from radiolabeled ApNp3/apigenin was further supported by the data obtained by LC-MS/MS study. A selective, rapid and sensitive technique of LC-MS/MS was developed to determine the concentration of apigenin from free drug suspension as well as apigenin loaded nanoparticles. This method was established in such a way that very less quantity of apigenin was also be detected in mice plasma and hepatic tissue samples taken at different time points to determine the biodistribution and pharmacokinetic parameters of apigenin. Various pharmacokinetic parameters in mice plasma and liver (up to 72 h) showed much higher AUC and lower clearance rate of ApNp3 in comparison with API in both plasma and liver. This could be possibly responsible for more bioavailability of apigenin from ApNp3 than API. Difference in half-lives also suggests that apigenin from nanoparticles (half-life of apigenin from ApNp3 in plasma and hepatic circulation were  $70.7\pm 4.3$  and  $25.1\pm 1.1$  h respectively) followed a sustained release pattern. Plasma and hepatic clearance values reveal that ApNp3 caused reduction of apigenin clearance predominantly and assisted its longer presence in the body. Plasma protein binding of apigenin was predominantly long and release of drug from the plasma protein was comparatively much slower, hence  $t_{1/2}$  of the drug in the blood was comparatively more than its value in liver. Moreover, our negatively charged nanoparticles might have a much longer circulation half-life in plasma as surface charge plays a vital role on *in-vivo* behavior of nanoparticles. Initially nanoparticles taken up by the liver maintained the hepatic level of the drug. However, faster hepatic metabolism and elimination of larger nanoparticles and very slow distribution of plasma protein bound drug to liver at the extended period could be responsible for shorter hepatic half life of the drug in animals [Cao *et al*, 2011; Gradolatto et al, 2004; Blanco et al, 2015].

The treatment of hepatocellular carcinoma remains a great challenge due to unpredictability of this disease. Thus, drug metabolizing enzymes play a key role to detect the stage of HCC. Here we have chosen four tumor marker enzymes and measured their

activity in various treatment groups to get an idea about the effect of apigenin on HCC. Cytochrome P-450 (CYP) is an iso-enzyme which is extensively required in phase-I metabolism and has very important role in biotransformation of different exogenous and endogenous compounds in liver. CYP is selected as tumor marker enzyme as it is proved as marker for HCC and expression CYP decreases in rat liver carcinogenesis. Glutathione-S-transferase (GST) and uridyl phosphate glucoronyl transferase (UDPGT) are two enzymes of phase-II metabolism which are mainly used to detoxify xenobiotics and external toxic materials. In general, GST and UDPGT contents get increased in the HCC tumor tissue significantly than the normal hepatic condition. Therefore these two enzymes are used as marker protein for detection of chemical toxicity and carcinogenesis in liver. Antioxidant enzymes such as superoxide dismutase (SOD) are mainly required for counterbalancing the oxidative stress inside the hepatocytes and protect the cellular environment against DNA damages due to chemical carcinogen treatment. Studies reported that a decreased expression of SOD was noted in carcinogenic hepatic tissues than the normal ones. The low activity of this enzyme may be due to the depletion of antioxidant defense mechanism against overwhelming free radical generation in HCC [Aliya et al, 2003; Liaw et al, 1998; Yan et al, 2015; Lu et al 2015]. Hence we have selected these markers to identify any biochemical changes occurred in tumors and the non-tumor hepatic tissue upon the treatment of ApNp3 and we found that the apigenin content varied in tumor and non-tumor tissues upon ApNp3 application. Interestingly, we found that modulation of these enzyme activities and iso-enzyme (cyt P-450) content predominantly varied in the tumor area upon nanoparticle treatment as compared to free apigenin treatment. This may be due to the EPR effect of ApNp3 in the solid tumors.

Extensive morphological examinations of hepatocellular carcinoma were done with the help of various diagnostic imaging techniques over the past two decades. These studies revealed that there are biological markers such as ground glass hepatocytes, hyperplastic nodules, nodular lesions or altered hepatic foci that can distinguish a HCC liver from the normal ones. Occurrences of multiple nodules are the fundamental characteristics of advanced stage of HCC that can be detected by macroscopic investigations. The number, site of occurrence and size of the nodules also give an idea about the stage and progression of the disease [Kojiro M, 2009; Schlageter et al, 2014; Mathai et al, 2013].

Histomorphologic investigations depict a stepwise development of HCC. Advanced stage of HCC showed complete neovascularisations with destroyed cellular architecture, picnotic nucleus and ground glass appearances, absence of hepatic portal veins etc. Hematoxylin-eosin (HE) staining was used here to visualize the hepatic tissue structures of HCC control groups and compared it to other treatment groups as well as with normal control livers. Significant anti-cancer potential of the optimized nanoparticles containing apigenin (ApNp3) in rats bearing HCC was observed. The efficiency of this formulation was achieved in controlling the tumor incidence and HAF. Predominant lower incidence of HCC development and a gross reduction of HAF upon ApNp3 treatment showed potential antitumor effect of apigenin loaded in nanoparticles on HCC development *in-vivo*. Free apigenin also improved the tissue structure, but not to the extent of ApNp3 mediated improvement. ApNp3 could have acted either on delaying the progress of development of HCC or on regenerating the damage of hepatic tissue towards normal, clearly seen in histopathology study. Presence of apigenin in the tumor area thus could be beneficial for controlling the proliferation of preneoplastic and neoplastic cells, hindering tumor formation. Apigenin has a significant role in tumor suppression by maintaining level of p53-WAF1/p21 pathway in hepatocellular carcinoma [McVean et al, 2000; Chiang et al, 2006]. Apigenin loaded nanoparticles and free apigenin had no noticeable effect on normal liver. Blank nanoparticles also had no effect on normal liver, suggesting that PLGA has no considerable toxic effect in liver at all. Longer availability of apigenin as it released slowly from the nanoparticles and had a much lower clearance rate than free apigenin may be a responsible factor for such potential role of apigenin from ApNp3 than the free drug.

Thus, apigenin nanoparticles may serve as a successful line of treatment against HCC or as an adjuvant therapy to improve this disease state and can provide us a new therapeutic option to treat hepatocellular carcinoma patients. Further investigation in the area is warranted.

# Chapter 7

## *Summary*

## 7. Summary

Hepatocellular carcinoma (HCC) is one of the most common malignancies, resulting from various types of lifestyle diseases as well as from hepatitis B and C virus infection. In this disease, the normal hepatic environment gets destroyed, leading to liver cirrhosis and ultimately resulting in early and advanced stage of HCC. Currently, liver transplantation, liver resection and chemotherapy with sorafenib are the major therapeutic lines of treatment available for HCC. Although, depending on severity and stage of the disease, the quality of life gets affected significantly. From the past two decades scientists are studying more and more new chemotherapeutic agents to combat this deadly disease but successful treatment cannot be guaranteed till now. Natural products, on the other hand, have shown to possess many interesting effects on various kinds of diseases and are being studied and screened extensively for their activities. Bioflavonoids are such naturally occurring bioactive compounds which possess certain biological activities and are abundantly found in many natural sources including common vegetables and fruits which we consume daily. Apigenin is such a biologically active flavonoid found in many common dietary products and has been proved to have many types of biological actions including anti-hypertensive, anti-diabetes, anti-oxidant and anti-cancer activities. Apigenin induces apoptotic cell death and cell cycle arrest and exerts its anti-proliferative, tumor-suppressive activities against various types of cancer growth. However, apigenin, as a chemotherapeutic agent, has poor bioavailability and gets cleaved in gastrointestinal track when absorbed orally. Further, it is a hydrophobic chemical, and difficult to administer via intra-venous route due to its poor solubility issues.

Keeping all these things in mind we have prepared and optimized a novel drug delivery system (nanoparticles) which would deliver sufficient amount of apigenin in hepatocellular carcinogenic environment to delay the progress of HCC *in-vitro* and *in-vivo*.

Polymeric nanoparticles have got attentions in last few years as a unique drug delivery strategy that can deliver various therapeutics agents, proteins, enzymes *etc.* to target site of many diseases. Due to its nanosized range and ability to incorporate both hydrophilic and hydrophobic substances, nanoparticles have gained much popularity in field of targeted drug delivery. Poly-lactic-co-glycolic acid (PLGA) is a USA-FDA approved biodegradable

polymer which is extensively used as the carrier for nanoparticles and apigenin was incorporated inside PLGA core to develop a sustained release dosage form. Here, PLGA nanoparticles, loaded with apigenin as a therapeutic agent, were modified and characterized according to the need of the study. We have monitored the particle size, surface charge and polydispersity index which favored for a successful drug delivery to the hepatic cells. The surface morphology of the nanoparticles was checked by field emission scanning electron microscopy, atomic force microscopy and transmission electron microscopy and the particles were found to be spherical in shape and homogeneously distributed with a size range 150-300 nm. Fourier transform infrared spectroscopy showed no chemical interactions between drugs and the excipients took place. The stability of the nanoparticles was checked by accelerated stability study and hydrolytic stability study. Hydrolytic degradation of nanoparticles was found maximum in acidic pH medium and on the other hand, thermal softening of nanoparticles was seen in higher temperature conditions. Drug release was performed in three different pH mediums including PBS (pH 7.4) which mimics the blood pH, citric acid buffer (pH 3) which resembles the gastric environment and acetic acid buffer (pH 5) which mimics pH of tumor microenvironment. The prepared nanoparticles showed a sustained drug release pattern in PBS and a comparatively faster drug release in acidic mediums.

The effects of the apigenin loaded nanoparticles (ApNp) were tested in human hepatocellular carcinoma cells (*in-vitro*) as well as experimental animals bearing HCC (*in-vivo*). *In-vitro* cytotoxicity by ApNp as well as apigenin suspension (free drug) was measured in two different types of cells HepG2 and Huh-7. ApNps showed a much higher cytotoxicity than free drug in both the types of cells. Cellular uptake of nanoparticles was visualized and quantified by confocal microscopy and fluorescence activated cell sorting (FACS) respectively. In both of these studies, a higher cellular uptake was notified in a time dependent manner. Pharmacokinetic parameters of apigenin (released from the formulation and free apigenin) were determined by quantifying the amounts of apigenin in plasma and liver tissue samples of balb/c mice. For this study we have developed a novel mobile phase system for eluting apigenin by LC-MS/MS. A much higher bioavailability of apigenin from ApNp was noted in comparison with the free drug. An experimental animal model of HCC (in Sprague-Dawley rats) was prepared by the standard chemical

carcinogenesis technique and animals from different groups were treated with ApNp as well as free drug. Biodistribution of ApNp/free drug was visualized and quantified in experimental mice and rats (normal mice, normal rats and HCC bearing rats) by radiolabeling and gamma scintigraphy study. The highest concentration and accumulation of radiolabeled ApNp were found in hepatic area of those animals compared to free drug which followed a non organ-specific distribution pattern. Further, the experimental rats from the different groups of HCC model were subjected to different treatment with ApNp and free drug to find out the tumor-suppressive effect of apigenin against HCC *in-vivo*. The rats were sacrificed; livers were dissected out and studied by macroscopic investigation as well as microscopic imaging. Four different tumor marker enzyme activities were also assessed using those experimental liver samples. From these studies, it was clearly observed that apigenin from ApNp was able to control the severity and delay the progression of HCC in a significant way when compared to untreated group and free drug group. Thus, apigenin may have a successful tumor-suppressive and tumor cell anti proliferative effect to control hepatocellular carcinoma and can be used as a therapeutic agent with or without other available treatments for this disease.



## Chapter 8

### *Conclusion*

### **Conclusion**

Apigenin loaded nanoparticles (ApNp) suitable for hepatic delivery, were prepared and optimized. In this experimental study, lower dosing frequency and more site specific accumulation were ensured using ApNp than apigenin suspension. Predominant uptake of ApNp by human hepatocellular carcinoma cells reveals that the nanoparticles could be internalized successfully by the target cells. Biodistribution of nanoparticles showed that maximum amount of ApNp localized in hepatic region and the clearance rate was predominantly low. Further, ApNp remarkably delayed the progress of HCC by effectively reducing tumor incidence and development of altered hepatic foci in rats. Thus, apigenin nanoparticles may serve as a successful line of treatment against HCC or as an adjuvant therapy to improve this disease state and can provide us a new therapeutic option to treat hepatocellular carcinoma patients. Further study is warranted.

## *References*

## References

---

- Abouelmagd SA, Sun B, Chang AC, Ku YJ, Yeo Y. Release kinetics study of poorly water-soluble drugs from nanoparticles: are we doing it right? *Mol Pharm*. **2015**, 12 (3): 997–1003.
- Ahn S, Seo E, Kim K, Lee SJ. Controlled cellular uptake and drug efficacy of nanotherapeutics. *Scientific Reports*. **1997**, 3, 1-10. DOI: 10.1038/srep01997.
- Alcorn T. Mongolia's struggle with liver cancer. *Lancet*. **2011**, 377(9772):1139–1140.
- Alexis F, Pridgen E, Molnar LK, Farokhzad OC. Factors affecting the clearance and biodistribution of polymeric nanoparticles. *Mol Pharm*. **2008**, 5, 505–515.
- Ali F, Rahul, Naz F, Jyoti S, Siddique YH. Health functionality of apigenin: A review. *International Journal of Food Properties*. **2017**, 20 (6), 1197–1238.
- Aliya S, Reddanna P, Thyagaraju K. Does glutathione S-transferase Pi (GST-Pi) a marker protein for cancer? *Mol Cell Biochem*. **2003**, 253 (1-2), 319-27.
- Altekruse SF, McGlynn KA, Reichman ME. Hepatocellular carcinoma incidence, mortality, and survival trends in the United States from 1975 to 2005. *J Clin Oncol*. **2009**, 27, 1485-1491.
- Amann LC, Gandal MJ, Lin R, Liang Y, Siegel SJ. In vitro-in vivo correlations of scalable PLGA risperidone implants for the treatment of schizophrenia. *Pharm Res*. **2010**, 27, 1730–1737.
- Anderson JM, Shive SM. Biodegradation and biocompatibility of PLA and PLGA microspheres. *Adv. Drug Deliv. Rev*. **1997**, 28, 5–24.
- Anjana C, Sharmila S, Balasubramaniyan V. Endothelial dysfunction in non-alcoholic fatty liver disease. *Reactive Oxygen Species*. **2018**, 5(13), 1–14.
- Anzola M. Hepatocellular carcinoma: role of hepatitis B and hepatitis C viruses proteins in hepatocarcinogenesis. *J Viral Hepat*. **2004**, 11, 383-393.
- Arvizo RR, *et al*. Modulating pharmacokinetics, tumor uptake and biodistribution by engineered nanoparticles. *PLoS ONE*. **2011**, 6:e24374.
- Avgoustakis K. Polylactic-Co-Glycolic Acid (PLGA). *Encyclopedia of Biomaterials and Biomedical Engineering*. **2005**, 1-11.
- Aw-Yong PY, Gan PH, Sasmita AO, Mak ST, Ling AP. Nanoparticles as carriers of phytochemicals: Recent applications against lung cancer. *Int. J. Res. Biomed. Biotechnol*. **2018**, 7, 1–11.

## References

---

- Badran, M. Formulation and in vitro evaluation of flufenamic acid loaded deformable liposome for improved skin delivery. *Digest J. Nanomater. Biostruct.* **2014**, 9, 83–91.
- Bahari, LA. Hamishehkar, H. The impact of variables on particle size of solid lipid nanoparticles and nanostructured lipid carriers; a comparative literature review. *Adv. Pharm. Bull.* **2016**, 6, 143.
- Balez R, Steiner N, Engel M, Muñoz SS, Lum JS, Wu Y, Wang D, Vallotton P, Sachdev P, O'Connor M, Sidhu K, Münch, Ooi L. Neuroprotective effects of apigenin against inflammation, neuronal excitability and apoptosis in an induced pluripotent stem cell model of Alzheimer's disease. *Sci Rep.* **2016**, 12(6), 31450.
- Barichello JM, Morishita M, Takayama K, Nagai T. Encapsulation of hydrophilic and lipophilic drugs in PLGA nanoparticles by the nanoprecipitation method. *Drug Dev Ind Pharm.* **1999**, 25, 471- 6.
- Barraud L, Merle P, Soma E, Lefrancois L, Guerret S, Chevallier M, *et al.* Increase of doxorubicin sensitivity by doxorubicin-loading into nanoparticles for hepatocellular carcinoma cells in vitro and in vivo. *J Hepatol.* **2005**, 42, 736–743.
- Basu S, Mukherjee B, Chowdhury SR, Paul P, Choudhury R, Kumar A. Mondal L, Hossain CM, Maji R. Colloidal gold-loaded, biodegradable, polymer-based stavudine nanoparticle uptake by macrophages: An in vitro study. *Int J Nanomedicine.* **2012**, 7, 6049–6061.
- Bevilacqua L *et al.* Identification of compounds in wine by HPLC tandem mass spectrometry. *Ann Chim.* **2004**. (<http://www.ncbi.nlm.nih.gov/pubmed/15506618>)
- Bharali DJ, Mousa SA. Emerging nanomedicines for early cancer detection and improved treatment: current perspective and future promise, *Pharm. Ther.* **2010**, 128, 324–335.
- Bhattacharyya D, Singh, S. Nanotechnology, big things from a tiny world: a review. *Int. J. u- and e-Serv, Sci. Technol.* 2009, 2 (3), 29–38.
- Birt DF, Hendrich S, Wang W. Dietary agents in cancer prevention: flavonoids and isoflavonoids. *Pharmacol Ther.* **2001**. Pubmed/11578656.
- Bobo D, Robinson KJ, Islam J, Thurecht KJ, Corrie SR. Nanoparticle-Based Medicines: A Review of FDA-Approved Materials and Clinical Trials to Date. *Pharm Res.* **2016**, 33(10), 2373-87.
- Bralet MP, Régimbeau JM, Pineau P, Dubois S, Loas G, Degos F, Valla D, Belghiti J, Degott C, Terris B. Hepatocellular carcinoma occurring in nonfibrotic liver: epidemiologic and histopathologic analysis of 80 French cases. *Hepatology.* **2000**, 32, 200-204.

## References

---

- Brough C, Miller DA, Ellenberger D, Lubda D, Williams RO. Use of polyvinyl alcohol as a solubility enhancing polymer for poorly water-soluble drug delivery (Part 2). *AAPS PharmSciTech.* **2016**, 17(1), 180-90.
- Brough C, Miller DA, Keen JM, Kucera SA, , Lubda D, Williams RO. Use of polyvinyl alcohol as a solubility-enhancing polymer for poorly water soluble drug delivery (Part 1). *AAPS PharmSciTech.* **2016**, 17(1), 167-79.
- Bryant R, Laurent A, Tayar C, van Nhieu JT, Luciani A, Cherqui D. Liver resection for hepatocellular carcinoma. *Surg Oncol Clin N Am.* **2008**, 17, 607–633.
- Cai J, Zhao XL, Liu AW, Nian H, Zhang SH. Apigenin inhibits hepatoma cell growth through alteration of gene expression patterns. *Phytomedicine.* **2011**, 18, 366-373.
- Calvo P, Remunan-Lopez C, Vila-Jato JL, Alonso MJ. Novel hydrophilic chitosan-polyethylene oxide nanoparticles as protein carriers. *J. Appl. Polymer Sci.* **1997**, 63, 125-132.
- Cao H, Chen L, Xiao J. Binding Citrus flavanones to human serum albumin: effect of structure on affinity. *Mol Biol Rep.* **2011**, 38, 2257–2262.
- Cha CH, Ruo L, Fong Y, Jarnagin WR, Shia J, Blumgart LH *et al.* Resection of hepatocellular carcinoma in patients otherwise eligible for transplantation. *Ann Surg.* **2003**, 238, 315–321.
- Chatterjee R, Mitra A. An overview of effective therapies and recent advances in biomarkers for chronic liver diseases and associated liver cancer. *Int. Immunopharmacol.* **2015**, 24, 335–345.
- Chen M, Liu X, Fahr A. Skin penetration and deposition of carboxyfluorescein and temoporfin from different lipid vesicular systems: In vitro study with finite and infinite dosage application. *Int. J. Pharm.* **2011**, 408, 223–234.
- Chen M, Wang X, Zha D, Cai F, Zhang W, He Y, Huang Q, Zhuang H, Hua ZC. Apigenin potentiates TRAIL therapy of non-small cell lung cancer via upregulating DR4/DR5 expression in a p53-dependent manner. *Sci Rep.* **2016**, 6, 35468.
- Cheng MR, Li Q, Wan T, *et al.* Galactosylated chitosan/5-fluorouracil nanoparticles inhibit mouse hepatic cancer growth and its side effects. *World J Gastroenterol.* **2012**, 18 (42), 6076–6087.
- Chiang LC, Ng LT, Lin IC, Kuo PL, Lin CC. Anti-proliferative effect of apigenin and its apoptotic induction in human Hep G2 cells, *Cancer Lett.* **2006**, 237, 207–214.

## References

---

- Choi EJ, Kim GH. Apigenin causes G (2)/M arrest associated with the modulation of p21 (Cip1) and Cdc2 and activates p53-dependent apoptosis pathway in human breast cancer SK-BR-3 cells. *J Nutr Biochem.* **2009**, 20, 285–290.
- Clarke S. Development of Hierarchical Magnetic Nanocomposite Materials for Biomedical Applications. Thesis, Dublin City University, Northside, Dublin, **2013**.
- Colombo M and Maisonneuve P. Controlling liver cancer mortality on a global scale: Still a long way to go. *Journal of Hepatology.* **2017**, 216-217.
- Conn J, Oyasu R, Welsh M, Beal JM. Vicryl (polyglactin 910) synthetic absorbable sutures. *American Journal of surgery.* **1974**, 128, 19–23.
- Crespy D, Stark M, Hoffmann-Richter C, Ziener U, Landfester K. Polymeric nanoreactors for hydrophilic reagents synthesized by interfacial polycondensation on miniemulsion droplets. *Macro- molecules.* **2007**, 40, 3122–35.
- Danaei M, Dehghankhold M, Ataei S, Hasanzadeh Davarani F, Javanmard R, Dokhani A, Khorasani S, Mozafari MR. Impact of particle size and polydispersity index on the clinical applications of lipidic nanocarrier systems. *Pharmaceutics.* **2018**, 18; 10(2) E57. doi: 10.3390/pharmaceutics10020057.
- Danhier F, Feron O, Pr at V. To exploit the tumor microenvironment: passive and active tumor targeting of nanocarriers for anti-cancer drug delivery. *J Control Release.* **2010**, 148(2),135–146.
- Das S, Das J, Samadder A, Paul A, Khuda-Bukhsh AR. Efficacy of PLGA-loaded apigenin nanoparticles in Benzo [a] pyrene and ultraviolet-B induced skin cancer of mice: Mitochondria mediated apoptotic signaling cascades. *Food and Chemical Toxicology.* **2013**, 62, 670–680.
- Das S, Das J, Samadder A, Paul A, Khuda-Bukhsh AR. Strategic formulation of apigenin-loaded PLGA nanoparticles for intracellular trafficking, DNA targeting and improved therapeutic effects in skin melanoma in vitro. *Toxicol. Lett.* **2013**, 223, 124.
- Davaran S, Rashidi MR, Khandaghi R, Hashemi M. Development of a novel prolonged-release nicotine transdermal patch. *Pharmacol Res.* **2005**, 51(3), 233–7.
- Devulapally R, Foygel K, Sekar TV, Willmann JK, Paulmurugani R. Gemcitabine and Antisense-microRNA Co-encapsulated PLGA-PEG Polymer Nanoparticles for Hepatocellular Carcinoma Therapy. *ACS Appl Mater Interfaces.* **2016**, 8(49), 33412–33422.

## References

---

- Dhanasekaran R, Limaye A, Cabrera R. Hepatocellular carcinoma: current trends in worldwide epidemiology, risk factors, diagnosis, and therapeutics. *Hepat Med.* **2012**, 4, 19–37.
- Digumarthy SR, Sahani DV, Saini S. MRI in detection of hepatocellular carcinoma (HCC). *Cancer Imaging.* **2005**, 5, 20–24.
- Ding SM, Zhang ZH, Song J, Cheng XD, Jiang J, Jia XB. Enhanced bioavailability of apigenin via preparation of a carbon nanopowder solid dispersion. *Int J Nanomedicine.* **2014**, 9, 2327-33. doi: 10.2147/IJN.S60938.
- Drexler KE, *Engines of Creation: The coming era of nanotechnology.* New York: Anchor Books, **1986**.
- Drury DR, Wick AN. Chemistry and metabolism of L (þ) and D (–) lactic acids. *Am. J. Physiol.* **1956**, 184, 1061–1069.
- Dutta L, Mukherjee B, Chakraborty T, Das MK, Mondal L, Bhattacharya S, Gaonkar RH, Debnath MC. Lipid-based nanocarrier efficiently delivers highly water soluble drug across the blood–brain barrier into brain. *Drug Deliv.* **2018**, 25(1), 504–516.
- Ekman B, Sjöholm I. Improved stability of proteins immobilized in microparticles prepared by modified emulsion polymerization technique. *J Pharm Sci.* **1978**, 67, 693 - 6.
- Erbetta CDC, Alves RJ, Resende JM, de Souza Freitas RF, de Sousa RG. Synthesis and Characterization of Poly (D, L-Lactide-co-Glycolide) Copolymer. *Journal of Biomaterials and Nanobiotechnology.* **2012**, 3, 208-225.
- Evason KJ, Grenert JP, Ferrell LD, Kakar S. Atypical hepatocellular adenoma-like neoplasms with  $\beta$ -catenin activation show cytogenetic alterations similar to well-differentiated hepatocellular carcinomas. *Hum Pathol,* **2013**, 44, 750-758.
- Faisant N, Siepmann J, Benoit JP. PLGA-based microparticles: Elucidation of mechanisms and a new, simple mathematical model quantifying drug release. *Eur J Pharm Sci.* **2002**, 15, 355–366.
- Fattal E, Youssef M, Couvreur P, Andremont A. Treatment of experimental salmonellosis in mice with ampicillin-bound nanoparticles. *Antimicrob Agents Chemother.* **1989**, 33, 1540–1543.
- Fattovich G, Stroffolini T, Zagni I, Donato F. Hepatocellular carcinoma in cirrhosis: incidence and risk factors. *Gastroenterology.* **2004**, 127, S35-S50.



## References

---

- Ferlay, J. *et al.* GLOBOCAN 2012 v1.0, Cancer Incidence and Mortality Worldwide. IARC Cancer Base No. 11. Lyon, France: International Agency for Research on Cancer. 2013.
- Fessi H, Puisieux F, Devissaguet JP, Ammoury N, Benita S. Nanocapsule formation by interfacial deposition following solvent displacement. *Int J Pharm.* **1989**, 55, R1- R4.
- Fischer AH, Jacobson KA, Rose J, Zeller R. Hematoxylin and eosin staining of tissue and cell sections. *CSH Protoc.* **2008**, doi: 10.1101/pdb.prot4986.
- Gaonkar RH, Gangul S, Dewanjee S, Sinha S, Gupta A, Ganguly S, Chattopadhyay D, Debnath MC. Garcinol loaded vitamin E TPGS emulsified PLGA nanoparticles: preparation, physicochemical characterization, in vitro and in vivo studies. *Scientific Reports.* **2016**, 7, 1-14.
- Gentile P, Chiono V, Carmagnola I, Hatton PV. An Overview of Poly (lactic-co-glycolic) Acid (PLGA)-Based Biomaterials for Bone Tissue Engineering. *Int. J. Mol. Sci.* **2014**, 15, 3641-3659.
- Gentile P, Chiono V, Carmagnola I, Hatton PV. An Overview of Poly (lactic-co-glycolic) Acid (PLGA)-Based Biomaterials for Bone Tissue Engineering. *Int J Mol Sci.* **2014**, 15(3), 3640–3659.
- Ghosh MK, Patra F, Ghosh S, Hossain CM, Mukherjee B. Antisense oligonucleotides directed against insulin-like growth factor-II messenger ribonucleic acids delay the progress of rat hepatocarcinogenesis. *J Carcinog.* **2014**, 13 (2): 1-17.
- Gilding, D.K.; Reed, A.M. Biodegradable polymers for use in surgery-polyglycolic poly (lactic acid) homo- and copolymers: 1. *Polymer* **1979**, 20 (12), 137–143.
- Gradolatto A, Basly JP, Berges R, Teyssier C, Chagnon MC, Siess MH, Lavier MCC. Pharmacokinetics and metabolism of apigenin in female and male rats after a single oral administration. *Drug Metab. Dispos.* **2004**, 33, 49-54.
- Griffiths LA, Smith GE. Metabolism of apigenin and related compounds in the rat. Metabolite formation in vivo and by the intestinal microflora in vitro. *Biochem J.* **1972**, 128(4), 901–911.
- Gu FX, Karnik R, Wang AZ, *et al.* Targeted nanoparticles for cancer therapy. *Nano Today.* **2007**, 2(3), 14–21.
- Gunasekaran T, Haile T, Nigusse T, Dhanaraju MD. Nanotechnology: an effective tool for enhancing bioavailability and bioactivity of phytomedicine. *Asian Pac J Trop Biomed.* **2014**, 4, S1–S7.

## References

---

- Hamidi M, Azadi, A Rafiei P, Ashrafi H. A pharmacokinetic overview of nanotechnology-based drug delivery systems: an adme-oriented approach. *Therapeutic Drug Carrier Systems*. **2013**, 30(5), 435–467.
- Hans ML and Lowman AM. Biodegradable nanoparticles for drug delivery and targeting. *Current Opinion in Solid State and Materials Science*. 2002, 6(4), 319-327.
- Hickey JW, Santos JL, Williford JM, Mao HQ. Control of Polymeric Nanoparticle Size to Improve Therapeutic Delivery. *J Control Release*. **2015**, 219, 536–547.
- Hollman PC, Katan MB. Health effects and bioavailability of dietary flavonols *Free Radic Res*. **1999**. <http://www.ncbi.nlm.nih.gov/pubmed/10694044>.
- Hootegeem AV, Verslype C, Steenbergen WV. Sorafenib-induced liver failure: a case report and review of the literature. *Case Reports in Hepatology*. **2011**, 2011, 1-4. doi:10.1155/2011/941395.
- Hoshyar N, Gray S, Han H, Bao G. The effect of nanoparticle size on in vivo pharmacokinetics and cellular interaction. *Nanomedicine (Lond)*. **2016**, 11(6), 673–692
- Houchin ML, Topp EM. Chemical degradation of peptides and proteins in PLGA: a review of reactions and mechanisms, *J Pharm Sci*. **2008**, 97, 2395e2404.  
<https://www.spectrumchemical.com/MSDS/P2152-AGHS.pdf>
- Hu XY, Liang JY, Guo XJ, Liu L, Guo YB. 5-Fluorouracil combined with apigenin enhances anticancer activity through mitochondrial membrane potential ( $\Delta\Psi_m$ )-mediated apoptosis in hepatocellular carcinoma. *Clin Exp Pharmacol Physiol*. **2015**, 42(2), 146-53.
- Hyon SH, Jamshidi K, Ikada Y. Synthesis of polylactides with different molecular weights. *Biomaterials*. **1997**, 18 (22), 1503–1508.
- Jain NK, Jain SK. Development and in vitro characterization of galactosylated low molecular weight chitosan nanoparticles bearing doxorubicin. *AAPS PharmSciTech*. **2010**, 11, 686–697.
- James AM, Ambrose EJ, Lowick JH. Differences between the electrical charge carried by normal and homologous tumour cells. *Nature*. **1956**, 177(4508),576–577.
- Jarnagin W, Chapman WC, Curley S, D'Angelica M, Rosen C, Dixon E, Nagorney D. Surgical treatment of hepatocellular carcinoma: expert consensus statement. *HPB (Oxford)*. **2010**, 12(5), 302-10. doi: 10.1111/j.1477-2574.2010.00182.x.

## References

---

- Jeetah R, Bhaw-Luximon A, Jhurry D. Nanopharmaceutics: phytochemical-based controlled or sustained drug-delivery systems for cancer treatment. *J Biomed Nanotechnol.* **2014**, 10(9),1810-40.
- Jeyabal PV, Syed MB, Venkataraman M, Sambandham JK, Sakthisekaran D. Apigenin inhibits oxidative stress-induced macromolecular damage in N-nitrosodiethylamine (NDEA)-induced hepatocellular carcinogenesis in Wistar albino rats. *Mol Carcinog.* **2005**, 44,11–20.
- Jyothi U. Jadeja MP, Tambe P, Vu K, Yuan B, Nguyen KT. Nanomaterials for photo-based diagnostic and therapeutic applications. *Theranostics.* **2013**, 3(3), 152–166.
- Keles H, Naylor A, Clegg F, Sammon C. Investigation of factors influencing the hydrolytic degradation of single PLGA microparticles. *Polymer Degradation and Stability.* **2015**, 119, 228e241.
- Kenley RA, Lee MO, Mahoney TR, Sanders LM, Poly (lactide-co-glycolide) decomposition kinetics in vivo and in vitro, *Macromolecules.* 1987, 20, 2398e2403.
- Kew MC. Hepatic Iron Overload and Hepatocellular Carcinoma. *Liver Cancer.* **2014**; 3:31–40 (DOI: 10.1159/000343856).
- Kim BR, Jeon YK, Nam MJ. A mechanism of apigenin-induced apoptosis is potentially related to anti-angiogenesis and anti-migration in human hepatocellular carcinoma cells. *Food Chem Toxicol.* **2011**, 49, 1626–1632.
- Kim EY, Yu JS, Yang M, Kim AK. Sub-Toxic Dose of Apigenin Sensitizes HepG2 Cells to TRAIL through ERK-Dependent Up-Regulation of TRAIL Receptor DR5. *Mol Cells.* **2013**, 35(1), 32–40.
- Kim, HY, Kim OH, Sung MKJ. Effects of Phenol-Depleted and Phenol-Rich Diets on Blood Markers of Oxidative Stress, and Urinary Excretion of Quercetin and Kaempferol in Healthy Volunteers. *Journal of the American College of Nutrition.* **2003**, 22, 217–223.
- Kirpotin DB, Drummond DC, Shao Y, *et al.* Antibody targeting of long-circulating lipidic nanoparticles does not increase tumor localization but does increase internalization in animal models. *Cancer Res.* **2006**, 66(13), 6732–6740.
- Kojiro M. *Pathology of Hepatocellular Carcinoma.* Hoboken: Wiley, **2009**, 1-184
- Kumar P, Singh AK, Raj V, Rai A, Keshari AK, Kumar D, Maity B, Prakash A, Maiti S, Saha S. Poly(lactic-co-glycolic acid)-loaded nanoparticles of betulinic acid for improved treatment of hepatic cancer: characterization, in vitro and in vivo evaluations. *Int J Nanomedicine.* **2018**, 13, 975–990.

## References

---

- Kumar V, Bhatt PC, Rahman M, Kaithwas G, Choudhry H, Al-Abbasi FA, Anwar F, Verma A. Fabrication, optimization, and characterization of umbelliferone  $\beta$ -D-galactopyranoside-loaded PLGA nanoparticles in treatment of hepatocellular carcinoma: *in vitro* and *in vivo* studies. *Int J Nanomedicine*. **2017**, 11, 12:6747-6758.
- Lee Y, Sung B, Kang YJ, Kim DH, Jang JY, Hwang SY, Kim M, Lim HS, Yoon JH, Chung HY, Kim ND. Apigenin-induced apoptosis is enhanced by inhibition of autophagy formation in HCT116 human colon cancer cells. *Int J Oncol*. **2014**, 44, 1599–606.
- Lefort EC and Blay J. Apigenin and its impact on gastrointestinal cancers. *Mol Nutr Food Res*. **2013**, 57, 126–144.
- Li B, Robinson DH, Birt DF. Evaluation of Properties of Apigenin and [G-3H] Apigenin and Analytic Method Development. *Journal of Pharmaceutical Sciences* 1997, 86 (6):721-5
- Li FR, Yan WH, Guo YH, Qi H, Zhou HX. Preparation of carboplatin- Fe@C-loaded chitosan nanoparticles and study on hyperthermia combined with pharmacotherapy for liver cancer. *Int J Hyperthermia*. **2009**, 25, 383–391.
- Li G, Chi CW, Shao XF, Fang CH. Application of molecular imaging technology in evaluating the inhibiting effect of apigenin *in-vivo* on subcutaneous hepatocellular carcinoma. *Biochemical and Biophysical Research Communications*. **2017**, 487(1), Pages 122-127.
- Li HL, Ji WB, Zhao R, Duan WD, Chen YW, Wang XQ, Yu Q, Luo Y, Dong JH. Poor prognosis for hepatocellular carcinoma with transarterial chemoembolization pre-transplantation: retrospective analysis. *World J Gastroenterol*. **2015**, 21 (12), 3599-3606.
- Liaw KY, Lee PH, Wu FC, Tsai JS, Lin-Shiau SY. Zinc, copper, and superoxide dismutase in hepatocellular carcinoma. *Am J Gastroenterol*. **1997**, 92(12), 2260-3.
- Lippman SM, Hong WK. Cancer prevention science and practice. *Cancer Res*. **2002**, 62, 5119-25.
- Liu CY, Chen KF, Chen PJ. Treatment of Liver Cancer. *Cold Spring Harb Perspect Med*. 2015; 5(9): a021535. doi: 10.1101/cshperspect.a021535
- Liu R, Ji P, Liu B, Qiao H, Wang X, Zhou L, Deng T, Ba Y. Apigenin enhances the cisplatin cytotoxic effect through p53-modulated apoptosis. *Oncol Lett*. **2017**, 13(2), 1024-1030.
- Livraghi T, Meloni F, Di Stasi M, Rolle E, Solbiati L, Tinelli C *et al*. Sustained complete response and complications rates after radiofrequency ablation of very early hepatocellular carcinoma in cirrhosis: Is resection still the treatment of choice? *Hepatology*. 2008, 47, 82–89.

## References

---

- Longmire M, Choyke PL, Kobayashi H. Clearance properties of nano-sized particles and molecules as imaging agents: considerations and caveats. *Nanomedicine (Lond)*. 2008, 3, 703–717.
- Lu DS, Yu NC, Raman SS, Limanond P, Lassman C, Murray K *et al*. Radiofrequency ablation of hepatocellular carcinoma: treatment success as defined by histologic examination of the explanted liver. *Radiology*. **2005**, 234, 954–960.
- Lu L, Garcia CA, Mikos AG. In vitro degradation of thin poly (D,L-lactic-co-glycolic acid) films. *J Biomed Mater Res*. **1999**, 46, 236–244.
- Lu L, Zhou J, Shi J, Peng XJ, Qi XX, Wang Y, Li FY, Zhou FY, Liu L, Liu ZQ. Drug-metabolizing activity, protein and gene expression of udp-glucuronosyltransferases are significantly altered in hepatocellular carcinoma patients. *PLoS One*. **2015**, 10(5), e0127524.
- Madunić V, Madunić J, Antunović M, Paradžik M, Garaj-Vrhovac V, Breljak D, Marijanović I, Gajski G. Apigenin, a dietary flavonoid, induces apoptosis, DNA damage, and oxidative stress in human breast cancer MCF-7 and MDA MB-231 cells. *Naunyn Schmiedebergs Arch Pharmacol*. **2018**, 391(5), 537-550.
- Maeda H. The enhanced permeability and retention (EPR) effect in tumor vasculature: the key role of tumor-selective macromolecular drug targeting. *Adv Enzyme Regul*. **2001**, 41, 189–207.
- Maeda, H. Toward a full understanding of the EPR effect in primary and metastatic tumors as well as issues related to its heterogeneity. *Adv. Drug Deliv. Rev*. **2015**, 91, 3–6.
- Maggioni D, Garavello W, Rigolio R, Pignataro L, Gaini R, Nicolini G. Apigenin impairs oral squamous cell carcinoma growth in vitro inducing cell cycle arrest and apoptosis. *Int J Oncol*. **2013**, 43, 1675–82.
- Maji R, Dey NS, Satapathy BS, Mukherjee B, Mondal S. Preparation and characterization of tamoxifen citrate loaded nanoparticles for breast cancer therapy. *Int J Nanomedicine*. **2014**, 9, 3107-3118.
- Makadia HK, Siegel SJ. Poly Lactic-co-Glycolic Acid (PLGA) as Biodegradable Controlled Drug Delivery Carrier. *Polymers (Basel)*. **2011**, 3(3), 1377–1397.
- Manasadeepa R, Paul P, Mukherjee B. Pressure-sensitive mucoadhesive polymer-based dental patches to treat periodontal diseases: an in vitro study. *Drug Deliv*, **2013**, 20(6), 258–267
- Mandal D , Shaw TK, Dey G, Pal MM , Mukherjee B, Bandyopadhyay AK , Mandal M. Preferential hepatic uptake of paclitaxel-loaded poly-(D-L-lactide-co-glycolide)

## References

---

nanoparticles-A possibility for hepatic drug targeting: Pharmacokinetics and biodistribution. *Int. J. Biol. Macromol.* **2018**, 112, 818–830.

Marsh JW, Dvorchik I. Liver organ allocation for hepatocellular carcinoma: are we sure? *Liver Transpl.* **2003**, 9, 693–696.

Masarudin MJ, Cutts SM, Evison BJ, Phillips DR, Pigram PJ. Factors determining the stability, size distribution, and cellular accumulation of small, monodisperse chitosan nanoparticles as candidate vectors for anticancer drug delivery: application to the passive encapsulation of [<sup>14</sup>C]-doxorubicin. *Nanotechnol Sci Appl.* **2015**, 8, 67–80.

Masood F. Polymeric nanoparticles for targeted drug delivery system for cancer therapy. *Materials Science and Engineering.* **2016**, 60 (1), 569-578.

Mathai AM, Alexander J, Kuo FY, Torbenson M, Swanson PE, Yeh MM. Type II ground-glass hepatocytes as a marker of hepatocellular carcinoma in chronic hepatitis B. *Hum Pathol.* **2013**, 44(8), 1665-71.

Mazzaferro V, Regalia E, Doci R, Andreola S, Pulvirenti A, Bozzetti F *et al.* Liver transplantation for the treatment of small hepatocellular carcinomas in patients with cirrhosis. *N Engl J Med.* **1996**, 334, 693–699.

McGlynn KA, Petrick JL, London WT. Global epidemiology of hepatocellular carcinoma: an emphasis on demographic and regional variability, *Clin Liver Dis.* **2015**; 19(2), 223–238.

McKay DL, Blumberg JB. A review of the bioactivity and potential health benefits of chamomile tea (*Matricaria recutita* L.) *Phytother Res.* **2006**, 20(7), 519-30

McVean M, Xiao H, Isobe K, Pelling J.C, Increase in wildtype p53 stability and transactivational activity by the chemopreventive agent apigenin in keratinocytes, *Carcinogenesis.* **2000**, 21, 633–639.

Meißner T, Potthoff A, Richter V. Suspension characterization as important key for toxicological investigations. *J Phys Conf Ser.* **2009**, 170 (1), 1-6.

Merle P, Si Ahmed S, Habersetzer F, Abergel A, Taieb J, Bonyhay L, *et al.* Phase study of intra-arterial hepatic (IAH) delivery of doxorubicin-transdrug (DT) for patients with advanced hepatocellular carcinoma (HCC). *J Clin Oncol.* **2006** [ASCO annual meeting proceedings Part I. 2006; 24, No. 18S: 14094].

Middleton, E. Kandaswami, C. Theoharides, T.C. The Effects of Plant Flavonoids on Mammalian Cells: Implications for Inflammation, Heart Disease, and Cancer. *Pharmacological Reviews.* **2000**, 52, 673–751.

## References

---

- Mittal S, El-Serag HB. Epidemiology of hepatocellular carcinoma: consider the population. *J Clin Gastroenterol.* **2013**, 47, S2-S6.
- Mozafari MR, Pardakhty A, Azarmi S, Jazayeri JA, Nokhodchi A, Omri A. Role of nanocarrier systems in cancer nanotherapy. *J. Liposome Res.* **2009**, 19, 310–321.
- Mu L, Feng S. A novel controlled release formulation for the anticancer drug paclitaxel (Taxol®): PLGA nanoparticles containing vitamin E TPGS. *J Control Release.* **2003**, 86(1), 33–48.
- Mukherjee S, Ray S, Thakur R S. Solid Lipid Nanoparticles: A Modern Formulation Approach in Drug Delivery System. *Indian J Pharm Sci.* **2009**, 71(4), 349–358.
- Nair KL, Jagadeeshan S, Nair SA, Kumar GS. Biological evaluation of 5-fluorouracil nanoparticles for cancer chemotherapy and its dependence on the carrier, PLGA. *Int J Nanomed.* **2011**, 6, 1685–1697
- Niwa T, Takeuchi H, Hino T, Kunou N, Kawashima Y. Preparation of biodegradable nanoparticles of water-soluble and insoluble drugs with D, L-lactide/ glycolide copolymer by a novel spontaneous emulsification solvent diffusion method, and the drug release behavior. *J. Control.Release.* **1993**, 25, 89-98.
- Pan Z and Ding J. Poly (lactide-co-glycolide) porous scaffolds for tissue engineering and regenerative medicine. *Interface Focus.* **2012**, 366-377.
- Pandey P, Rahman M, Bhatt PC, Beg S, Paul B, Hafeez A, Al-Abbasi FA, Nadeem MS, Baothman O, Anwar F, Kumar V. Implication of nano-antioxidant therapy for treatment of hepatocellular carcinoma using PLGA nanoparticles of rutin. *Nanomedicine (Lond).* **2018**, 13(8), 849-870.
- Park H, Yang J, Lee J, Haam S, Choi IH, Yoo KH. Multifunctional nanoparticles for combined doxorubicin and photothermal treatments. *ACS Nano.* **2009**, 3(10), 2919–2926.
- Park TG. Degradation of poly (lactic- co-glycolic acid) microspheres: Effect of copolymer composition. *Biomaterials.* **1995**, 16, 1123–1130.
- Patel D, Shukla S, Gupta S. Apigenin and cancer chemoprevention: progress, potential and promise (review) *Int J Oncol.* **2007**. (<http://www.ncbi.nlm.nih.gov/pubmed/17143534>) (2007)
- Phillips MA, Gran ML, Peppas NA. Targeted nanodelivery of drugs and diagnostics. *Nano Today.* **2010**, 5(2), 143–159.

## References

---

- Piktel E, Niemirowicz K, Wątek M, Wollny T, Deptuła P, Bucki R. Recent insights in nanotechnology-based drugs and formulations designed for effective anti-cancer therapy. *J Nanobiotechnology*. **2016**, 14(1), 39. doi: 10.1186/s12951-016-0193-x.
- Pitt CG, Gu Z. Modification of the rates of chain cleavage of poly (ε-caprolactone) and related polyesters in the solid state. *J. Controlled Release*. **1987**, 4, 283–292.
- Polyak A, Palade EA, Balogh L, Posteny Z, Haasz V, Janoki G, Janoki GA. In vitro and biodistribution examinations of Tc-99m-labelled doxorubicin-loaded nanoparticles. *Nuclear Medicine Review*. **2011**, 14, 55-62.
- Prabhu RH, Patravale VB, Joshi MD. Polymeric nanoparticles for targeted treatment in oncology: current insights. *International Journal of Nanomedicine*. **2015**, 10, 1001–1018.
- Prasad M *et al.* Nanotherapeutics: An insight into healthcare and multi-dimensional applications in medical sector of the modern world. *Biomedicine & Pharmacotherapy*. **2018**, 97, 1521–1537.
- Psimadas D, Bouziotis P, Georgoulas A, Valotassiou V, Tsotakos T, Loudos G. Radiolabeling approaches of nanoparticles with <sup>99m</sup>Tc. *Contrast Media Mol. Imaging*. **2013**, 8, 333–339.
- Quintanar-Guerrero D, Allemann E, Fessi H, Doelker E. Preparation techniques and mechanism of formation of biodegradable nanoparticles from preformed polymers. *Drug Dev Ind Pharm*. **1998**, 24, 1113-28.
- Ramchandani M, Robinson D. In vitro and in vivo release of ciprofloxacin from PLGA 50:50 implants. *J Control Release*. **1998**, 54,167–175.
- Reddy LH, Couvreur P. Nanotechnology for therapy and imaging of liver diseases. *J Hepatol*. **2011**, 55(6), 1461-6.
- Reis CP, Neufeld RJ, Ribeiro AJ, Veiga F. Nanoencapsulation I. Methods for preparation of drug-loaded polymeric nanoparticles. *Nanomedicine: Nanotechnology, Biology, and Medicine*. **2006**, 2, 8– 21
- Riis T, Bauer-Brandl A, Wagner T, Kranz H. pH-independent drug release of an extremely poorly soluble weakly acidic drug from multiparticulate extended release formulations. *Eur J Pharm Biopharm*. **2007**, 65(1), 78–84.
- Rizvi SAA, Saleh AM. Applications of nanoparticle systems in drug delivery technology. *Saudi Pharmaceutical Journal*. **2018**, 26, 64–70.
- Roncalli M. Hepatocellular nodules in cirrhosis: focus on diagnostic criteria on liver biopsy. A Western experience. *Liver Transpl*. **2004**, 10, S9-S15



## References

---

- Ross JA, Kasum CM. Dietary flavonoids: bioavailability, metabolic effects, and safety. *Annu Rev Nutr.* **2002**. (pubmed/12055336)
- Rowe RC, Sheskey PJ, Owen SC, Association AP. Handbook of pharmaceutical excipients. London: Pharmaceutical press; **2006**.
- Sadat SM, Jahan ST, Haddadi A. Effects of size and surface charge of polymeric nanoparticles on in vitro and in vivo applications. *J. Biomater. Nanobiotechnol.* **2016**, 7, 91.
- Sahoo SK, Panyam J, Prabha S, Labhasetwar V. Residual polyvinyl alcohol associated with poly (D, L-lactide-co-glycolide) nanoparticles affects their physical properties and cellular uptake. *J Control Release.* **2002**, 82(1), 105–14.
- Sak K. Cytotoxicity of dietary flavonoids on different human cancer types. *Pharmacogn Rev.* **2014**, 8(16), 122–146.
- Sanoff HK, Chang Y, Lund JL, O'Neil BH, Dusetzina SB. Sorafenib Effectiveness in Advanced Hepatocellular Carcinoma. *Oncologist.* **2016**, 21(9), 1113-20.
- Sanyal AJ, Yoon SK, Lencionic R. The etiology of hepatocellular carcinoma and consequences for treatment. *The Oncologist.* **2010**, 15 (4), 14–22.
- Satapathy BS, Mukherjee B, Baishya R, Debnath MC, Dey NS, Maji R. Lipid nanocarrier-based transport of docetaxel across the blood brain barrier. *RSC Adv.* **2016**, 6, 85261–85274.
- Saunders D, Seidel D, Allison M, Lyratzopoulos G. Systematic review: the association between obesity and hepatocellular carcinoma - epidemiological evidence. *Aliment Pharmacol Ther.* **2010**, 31(10), 1051–1063.
- Schlageter M, Terracciano LM, D'Angelo S, Sorrentino P. Histopathology of hepatocellular carcinoma, *World J Gastroenterol.* **2014**, 20(43), 15955-15964.
- Schneider A, Hommel G, Blettner M. Linear Regression Analysis. *Dtsch Arztebl Int.* **2010**, 107(44), 776–782.
- Shaw TK, Mandal D, Dey G, Pal MM, Paul P, Chakraborty S, Ali KA, Mukherjee MB, Bandyopadhyay AK, Mandal M. Successful delivery of docetaxel to rat brain using experimentally developed nanoliposome: a treatment strategy for brain tumor. *Drug Deliv.* **2017**, 24 (1), 346–357.
- Shin HR, Oh JK, Masuyer E, *et al.* Epidemiology of cholangiocarcinoma: an update focusing on risk factors. *Cancer Sci.* **2010**, 101, 579-585.

## References

---

- Shukla S and Gupta S. Apigenin: A Promising Molecule for Cancer Prevention. *Pharm Res.* **2010**, 27(6), 962–978.
- Silva FM, Hechenleitner AAW, Irache JM, de Oliveira AJA, Pineda EAG. Study of Thermal Degradation of PLGA, PLGA Nanospheres and PLGA/Maghemite Superparamagnetic Nanospheres. *Materials Research.* **2015**, 18(6), 1400-1406.
- Singhvi G, Sing M. Review: in-vitro drug release characterization models. *International Journal of Pharmaceutical Studies and Research.* **2011**, 2 (1), 77-84.
- Smith RJ. Nutrition and metabolism in hepatocellular carcinoma. *Hepatobiliary Surg Nutr.* **2013**, 2 (2), 89-96.
- Stockhofe K, Postema JM, Schieferstein H, Ross TL. Radiolabeling of Nanoparticles and Polymers for PET Imaging. *Pharmaceuticals (Basel).* **2014**, 7(4), 392-418.
- Sung B, Chung HY, Kim ND. Role of Apigenin in Cancer Prevention via the Induction of Apoptosis and Autophagy. *J Cancer Prev.* **2016**, 21, 216-226.
- Tang X, Lyu Y, Xie D, Li A, Liang Y, Zheng D, Therapeutic Effect of Sorafenib-Loaded TPGS-b-PCL Nanoparticles on Liver Cancer. *Journal of Biomedical Nanotechnology.* **2018**, 14(2), 396-403.
- Taniguchi N. **1974**. On the basic concept of “nano-technology”, Proceedings of the International Conference of Production Engineering (Tokyo: Japan Society of Precision Engineering).
- Tanimoto A, Kuribayashi S. Application of superparamagnetic iron oxide to imaging of hepatocellular carcinoma. *Eur J Radiol.* **2006**, 58, 200–216.
- Thanoo B, Sunny M, Jayakrishnan A. Controlled release of oral drugs from cross-linked polyvinyl alcohol microspheres. *J Pharm Pharmacol.* **1993**, 45(1), 16–20
- The International Agency for Research on Cancer. **2010**, 1-418.. WHO Classification of Tumours of the Digestive System (IARC WHO Classification of Tumours). 4th ed. In: Bosman FT, Carneiro F, Hruban RH, Theise ND, editors. Publisher: World Health Organization.
- The International Consensus Group for Hepatocellular Neoplasia. Pathologic diagnosis of early hepatocellular carcinoma: a report of the international consensus group for hepatocellular neoplasia. *Hepatology.* **2009**, 49, 658-664.
- Thoppil RJ, Bhatia D, Barnes KF, Haznagy-Radnai E, Hohmann J, Darvesh AS, Bishayee A. Black currant anthocyanins abrogate oxidative stress through Nrf2-mediated antioxidant

## References

---

- mechanisms in a rat model of hepatocellular carcinoma. *Curr. Cancer Drug Targets.* **2012**, 12, 1244–1257.
- Torre LA, Bray F, Siegel RL, Ferlay J, Tieuulent JL, Jemal A. Global cancer statistics, 2012. *Ca Cancer J Clin.* **2015**, 65 (2), 87–108.
- Tracy MA, Ward KL, Firouzabadian L, Wang Y, Dong N, Qian R, Zhang Y. Factors affecting the degradation rate of poly (lactideco- glycolide) microspheres in vivo and in vitro *Biomaterials.* **1999**, 20, 1057–1062.
- Tran S, DeGiovanni PJ, Piel B, Rai P. Cancer nanomedicine: a review of recent success in drug delivery. *Clin Transl Med.* **2017**, 6(1), 44.
- Ulery BD, Nair LS, Laurencin CT. Biomedical Applications of Biodegradable Polymers. *J Polym Sci B Polym Phys.* **2011**, 49(12), 832–864.
- Valdameri G, Trombetta-Lima M, Worfel PR, Pires AR, Martinez GR, Noletto GR, Cadena SM, Sogayar MC, Winnischofer SM, Rocha ME. Involvement of catalase in the apoptotic mechanism induced by apigenin in HepG2 human hepatoma cells. *Chem Biol Interact.* **2011**, 193(2), 180-9.
- Vigano L, Tayar C, Laurent A, Cherqui D. Laparoscopic liver resection: a systematic review. *J Hepatobiliary Pancreat Surg.* **2009**, 16, 410–421.
- Wang C, Su L, Wu C, Wu J, Zhu C, Yuan G. RGD peptide targeted lipid-coated nanoparticles for combinatorial delivery of sorafenib and quercetin against hepatocellular carcinoma. *Drug Dev Ind Pharm.* **2016**, 42(12), 1938-1944.
- Wang IK, Lin-Shiau LY, Lin JK, Induction of apoptosis by apigenin and related flavonoids through cytochrome c release and activation of caspase-9 and caspase-3 in leukaemia HL-60 cells, *Eur. J. Cancer.* **1999**, 35, 1517–1525.
- Wang T, Bai J, Jiang X, Nienhaus GU. Cellular uptake of nanoparticles by membrane penetration: a study combining confocal microscopy with FTIR spectroelectrochemistry. *ACS Nano.* **2012**, 28, 6(2), 1251-9.
- Wang W, Heideman L, Chung CS, Pelling JC, Koehler KJ, Birt DF, Cell cycle arrest at G2/M and growth inhibition by apigenin in human colon carcinoma cell lines, *Mol. Carcinog.* 2000, 28, 102–110.
- Wang X, Ouyang Y, Liu J, Zhu M, Zhao G, Bao W, *et al.* Fruit and vegetable consumption and mortality from all causes, cardiovascular disease, and cancer: systematic review and dose-response meta-analysis of prospective cohort studies. *BMJ.* **2014**, 349, g4490.

## References

---

Weledji EP, Orock GE, Ngowe MN, Nsagha DS. How grim is hepatocellular carcinoma? *Annals of Medicine and Surgery*. **2014**, 3, 71-76.

Winterton LC, Lally JM, Sentell KB, Chapoy LL. The elution of poly (vinyl alcohol) from a contact lens: the realization of a time release moisturizing agent/artificial tear. *J Biomed Mater Res B Appl Biomater*. **2007**, 80B(2), 424–32.

Wong MCS *et al.* International incidence and mortality trends of liver cancer: a global profile. *Sci. Rep*. **2017**, 7, 45846.

WP International. Terminology of nodular hepatocellular lesions. *Hepatology*. **1995**, 22, 983-993.

Wu W, Zu Y, Wang L, Wang L, Wang H, Li Y, Wu M, Zhao X, Fu Y. Preparation, characterization and antitumor activity evaluation of apigenin nanoparticles by the liquid antisolvent precipitation technique. *Drug Deliv*. **2017**, 24(1), 1713-1720.

[www.wikipedia.com](http://www.wikipedia.com)

Xiao JB, Cao H, Wang YF, Zhao JY, Wei XL. Glycosylation of dietary flavonoids decreases the affinities for plasma protein. *J Agric Food Chem*. **2009**, 57, 6642–6648.

Xu Y, Xin Y, Diao Y, Lu C , Fu J, Luo L, Yin Z. Synergistic Effects of Apigenin and Paclitaxel on Apoptosis of Cancer Cells. *PLoS ONE*, **2011**, 6 (12), e29169.

Yadav HKS, Nagavarma BVN, Ayaz A, Vasudha LS, Shivakumar HG. Different techniques for preparation of polymeric nanoparticles- a review. *Asian J Pharm Clin Res*. **2012**, 5 (3), 16-23.

Yan T, Lu L, Xie C, Chen J, Peng X, Zhu L, Wang Y, Li Q, Shi J, Zhou F, Hu M, Liu Z. Severely impaired and dysregulated cytochrome p450 expression and activities in hepatocellular carcinoma: implications for personalized treatment in patients. *Mol Cancer Ther*. **2015**, 14(12), 2874-86.

Yan X, Qi M, Li P, Zhan Y, Shao H. Apigenin in cancer therapy: anticancer effects and mechanisms of action. *Cell Biosci*. **2017**, 7, 50.

Yao C, *et al.* Highly biocompatible zwitterionic phospholipids coated upconversion nanoparticles for efficient bioimaging. *Anal Chem*. **2014**, 86:9749–9757.

Yatvin MB, Kreutz W, Horwitz BA, Shinitzky M. pH-sensitive liposomes: possible clinical implications. *Science*. **1980**, 210(4475), 1253–1255.

York P. Strategies for particle design using supercritical fluid technologies. *Pharm Sci Technol Today*. **1999**, 2, 430–40.

## References

---

- Yu M and Zheng J. Clearance pathways and tumor targeting of imaging nanoparticles. *ACS Nano*. **2015**, 9, 6655–6674.
- Yuan JM, Govindarajan S, Arakawa K, Yu MC. Synergism of alcohol, diabetes, and viral hepatitis on the risk of hepatocellular carcinoma in blacks and whites in the U.S. *Cancer*. **2004**, 101(5), 1009–1017.
- Yuan YY, *et al.* Surface charge switchable nanoparticles based on zwitterionic polymer for enhanced drug delivery to tumor. *Adv Mater*. **2012**, 24, 5476–5480.
- Zeng P, Liu B, Wang Q, Fan Q, Diao J, Tang J, Fu XQ, Sun XG. Apigenin attenuates atherogenesis through inducing macrophage apoptosis via inhibition of akt ser473 phosphorylation and downregulation of plasminogen activator inhibitor-2. *Oxidative Medicine and Cellular Longevity*. **2015**, 1-12.
- Zetterlund PB, Kagawa Y, Okubo M. Controlled/living radical polymerization in dispersed systems. *Chem Rev*. **2008**, 108, 3747–94.
- Zhai Y, Guo S, Liu C, Yang C, Dou J, Li L, Zhai G. Preparation and in vitro evaluation of apigenin-loaded polymeric micelles. *Colloid Surf*. **2013**, A 429, 24
- Zhang J, Liu D, Huang Y, Gao Y, Qian S. Biopharmaceutics classification and intestinal absorption study of apigenin. *Int J Pharm*. **2012**, 436(1–2), 311–317.
- Zhang J, Saltzman M. Engineering biodegradable nanoparticles for drug and gene delivery. *Chem. Eng. Prog*. **2013**, 109 (3), 25–30.
- Zheng PW, Chiang LC, Lin CC. Apigenin induced apoptosis through p53-dependent pathway in human cervical carcinoma cells. *Life Sci*. **2005**, 76(12), 1367-79.
- Zhou Q, Sun X, Zeng L, Liu J, Zhang Z. A randomized multicenter phase II clinical trial of mitoxantrone-loaded nanoparticles in the treatment of 108 patients with unresected hepatocellular carcinoma. *Nanomed Nanotech Biol Med*. **2009**, 5, 419–423.
- Zhou Y, Li Y, Zhou T, Zheng S, Li S, Li HB. Dietary natural products for prevention and treatment of liver cancer. *Nutrients*. **2016**, 8, 1-23.
- Zolnik BS, Burgess DJ. Effect of acidic pH on PLGA microsphere degradation and release. *J Control Release*. **2007**, 122, 338–344.

# *Appendix*



ELSEVIER



## Apigenin loaded nanoparticle delayed development of hepatocellular carcinoma in rats

Sanchari Bhattacharya, M.Pharm<sup>a</sup>, Laboni Mondal, M.Pharm<sup>a</sup>, Biswajit Mukherjee, Ph.D<sup>a,\*</sup>,  
Lopamudra Dutta, M.Pharm<sup>a</sup>, Iman Ehsan, M.Pharm<sup>a</sup>, Mita C. Debnath, Ph.D<sup>b</sup>,  
Raghuvir H. Gaonkar, M.Pharm<sup>b</sup>, Murari M. Pal, M.Pharm<sup>a</sup>, Subrata Majumdar, Ph.D<sup>c</sup>

<sup>a</sup>Department of Pharmaceutical Technology, Jadavpur University, Kolkata, West Bengal, India

<sup>b</sup>Infectious Diseases and Immunology Division, CSIR-Indian Institute of Chemical Biology, Kolkata, West Bengal, India

<sup>c</sup>Division of Molecular Medicine, Bose Institute, Kolkata, West Bengal, India

Received 30 April 2018; accepted 5 May 2018

### Abstract

Hepatocellular carcinoma (HCC) is one of the major causes of cancer related death globally. Apigenin, a dietary flavonoid, possesses anti-tumor activity against HCC cells *in-vitro*. Development, physicochemical characterization of apigenin loaded nanoparticles (ApNp), biodistribution pattern and pharmacokinetic parameters of apigenin upon intravenous administration of ApNp, and effect of ApNp treatment in rats with HCC were investigated. Apigenin loaded nanoparticles had a sustained drug release pattern and successfully reached the hepatic cancer cells *in-vitro* as well as in liver of carcinogenic animals. ApNp predominantly delayed the progress of HCC in chemical induced hepatocarcinogenesis in rats. Quantification of apigenin by liquid chromatography–mass spectroscopy (LC-MS/MS) showed that apigenin availability significantly increased in blood and liver upon ApNp treatment. Apigenin loaded nanoparticle delivery substantially controlled the severity of hepatocellular carcinoma and could be a future hope for lingering the survival in hepatic cancer patients.

© 2018 Elsevier Inc. All rights reserved.

**Key words:** Apigenin nanoparticles; Hepatocellular carcinoma; Pharmacokinetics; Gamma scintigraphy; Histopathology; LC-MS/MS

Hepatocellular carcinoma (HCC) is one of the most common malignant solid tumors with a very poor prognosis<sup>1</sup> and survival rate<sup>2</sup> in humans and HCC-related death has been reported as the second highest among the all cancer related deaths worldwide.<sup>3</sup> Treatment of this life-threatening disease includes surgical (liver resection and transplantation) and non-surgical (chemotherapy) techniques.<sup>4</sup> Liver cirrhosis is the most common underlying cause leading to HCC related deaths in patients.<sup>5</sup> Dietary supplements along with the medicines are always under research

to combat this serious health condition and improve patient-compliance.<sup>6</sup> Drug resistance and drug-induced toxicity in patients and often failure of early detection of HCC make it very tough to get cure.<sup>7</sup> Dietary supplements have been reported to improve the condition of HCC in patients as they possess anti-proliferative and anti-tumor effect on malignancies including HCC.<sup>8</sup> Apigenin is a dietary flavonoid found in various vegetable sources such as parsley leaves, chamomile tea, celery, kumquats, dried Mexican oregano, peppermint, vinespinach *etc.*<sup>9</sup> It has effective chemo-preservative and/or tumor-suppressive activity<sup>10</sup> against many kinds of carcinomas such as prostate, oral, skin<sup>11</sup>, colon, breast, lung, pancreatic, colorectal<sup>9</sup> and hepatic cancer *in-vitro*.<sup>12</sup> Many reports suggest that apigenin induces apoptosis in liver cancer cells and may play a vital role in the treatment of HCC.<sup>13–15</sup> Apigenin, after the oral administration, is cleaved, absorbed and gets distributed inside the gastrointestinal lumen, and thus, bioavailability of apigenin is much less when administered orally.<sup>16</sup> Further, free apigenin has a very high level of protein binding (10,000 times more than the

Funding Source: This work was supported by Department of Science and Technology (Government of India), Grant no. DST/Inspire Fellowship/2012/691.

Disclosure: The authors of this article have no conflicts of interest to declare.

\*Corresponding author at: Department of Pharmaceutical Technology, Jadavpur University, Kolkata 700032, India.

E-mail addresses: [biswajit.mukherjee@jadavpuruniversity.in](mailto:biswajit.mukherjee@jadavpuruniversity.in), [biswajit55@yahoo.com](mailto:biswajit55@yahoo.com). (B. Mukherjee).

<https://doi.org/10.1016/j.nano.2018.05.011>

1549-9634/© 2018 Elsevier Inc. All rights reserved.

other flavonoids) and its release from the protein bound stage is extremely slow<sup>17,18</sup>. Thus, parenteral administration of free apigenin is also difficult. Nanoparticles are excellent drug delivery systems (DDS) for delivering hydrophobic/hydrophilic drug moieties, flavonoids, vaccines, genes, protein *etc.* to the target site of delivery. Poly lactic co-glycolic acid (PLGA) based polymeric nanoparticles gained most popularity in this field due to their non-toxic and biodegradable nature<sup>19</sup> and PLGA has been approved by the United States Food and Drug Administration<sup>20</sup> (US FDA) for use in intravenous drug delivery in human. Hence we prepared apigenin loaded PLGA-nanoparticle to deliver significant amount of apigenin in liver to inhibit liver cancer growth and the efficacy of apigenin was investigated both *in vitro* and *in vivo*.

## Methods

### Materials

Apigenin (4', 5, 7-trihydroxyflavone, M.W 270.24) and PLGA {MW 50,000-75,000; poly (lactide-co-glycolide) ratio 85:15} were procured from Sigma-Aldrich Co, St Louis, MO, USA. Polyvinyl alcohol was purchased from S D Fine-Chemicals limited, Mumbai, India. Fluorescein isothiocyanate 98% (FITC) was purchased from HiMedia Laboratories, Mumbai, India. Dimethylsulfoxide (DMSO) and dichloromethane (DCM) were procured from Merck Life Science Pvt. Ltd, Bengaluru, India. All other chemicals used in this study were of analytical grade.

### Cell culture and animals

Two different human hepatocellular carcinoma cell lines (HepG2 and Huh-7) were purchased from National Centre for Cell Science (NCCS), Pune, India. Cell lines were maintained in Dulbecco's Modified Eagle's Medium (DMEM) supplemented with 10% fetal bovine serum (FBS, Sigma-Aldrich Co), 100 U/ml penicillin, 100 U/ml streptomycin and kept in 5% CO<sub>2</sub> incubator (MCO-15AC; Sanyo, Tokyo, Japan) at 37 °C.

Balb/c mice and Sprague–Dawley rats of either sex were procured from National Institute of Nutrition, Hyderabad, India and all the animal studies were conducted as per the guidelines of the Animal Ethics Committee (AEC), Jadavpur University, Kolkata.

Outline methodologies are given below. Each study protocol in details is given in the supplementary file.

### Preparation of nanoparticles

Apigenin loaded nanoparticles (ApNp) were prepared by multiple emulsion solvent evaporation technique as described by Maji et al.<sup>21</sup> For FITC labeled ApNp, FITC was dissolved in the drug solution at a concentration of 5 mg/ml.<sup>21</sup> Blank particles were prepared using the same process without the incorporation of apigenin in the organic phase.

### Fourier transform infrared spectroscopy

Fourier transform infrared (FTIR) spectroscopy was used to investigate interactions between apigenin and the excipients

selected for the formulation, by the method as described by Maji et al.<sup>21</sup>

### Surface characteristics of nanoparticles

Surface morphology of the nanoparticles was investigated by field emission scanning electron microscope (FESEM), transmission electron microscope (TEM) and atomic force microscopy (AFM).

### Particle size assessment

A small amount of lyophilized ApNp was taken in 2 ml of Milli-Q water and sonicated for 15 min followed by vortexing for few min. Size distribution, average particle size, polydispersity index (PDI) and zeta potential of the different formulations were determined by Zetasizer nano ZS 90 and analyzed by the instrument Data Transfer Assistance (DTA) software (Malvern Zetasizer Limited, Malvern, UK) by a dynamic light scattering method at 25 °C.

### Physicochemical characterization of nanoparticles

Drug loading and loading efficiency were determined in weight % by the procedure described by Maji et al.<sup>21</sup> using the following formulas:

$$\text{Actual drug loading (weight \%)} = \left( \frac{\text{Amount of drug present in nanoparticles}}{\text{Total amount of nanoparticles sample analyzed}} \right) \times 100 (\%)$$

$$\begin{aligned} \text{Drug loading efficiency (\%)} \\ &= \left( \frac{\text{Actual drug loading}}{\text{Theoretical drug loading}} \right) \\ &\times 100 (\%) \end{aligned}$$

### Stability study

A stability study was performed to understand the effect of temperature and relative humidity (RH) on apigenin loaded nanoparticles. Fixed amounts of ApNp3 were weighed and kept in zone III at 4–8 °C (in refrigerator), 30 °C, 75% RH and 40 °C, 75% RH for 30, 60 and 90 days as per the International Conference on Harmonization (ICH) guidelines (ICH, 2003). Samples were withdrawn and FTIR-spectra, FESEM photograph and drug loading were checked for those samples at 30, 60 and 90 days.

### In-vitro drug release study

In-vitro drug release study was performed in phosphate buffer saline (PBS, pH 7.4), citrate buffer (pH 3) and acetate buffer (pH 5) for 60 days using a cumulative drug release method as reported by Abouelmagd et al.<sup>22</sup>

### Hydrolytic stability study

Hydrolytic stability of ApNp3 was determined as described by Mandal et al.<sup>23</sup> at different pH buffers (citrate buffer pH 3, acetate buffer pH 5, phosphate buffer pH 7.4, bicarbonate buffer pH 10) for 30 days.



Weight variations were measured for each sample over time according to the formula,

$$\text{Weight change (\%)} = (W_0 - W_t) / W_0 \times 100$$

Where  $W_0$  and  $W_t$  represent the initial weight and weight at time  $t$ , respectively.

*In-vitro* stability of ApNp3 in mouse serum (blood was collected by heart puncture technique and serum was prepared) was investigated in the above mentioned procedure for 24 h. The actual weight of the nanoparticles in mouse serum was calculated by subtracting control sample (serum without ApNp3) weight from test sample (serum with ApNp3) weight.

#### Cytotoxicity study by MTT assay

The time-dependent cytotoxic effect of ApNp3 on HepG2 and Huh-7 cells was determined using 3-(4, 5-dimethylthiazol-2-yl)-2, 5-diphenyltetrazolium bromide (MTT dye), (Sigma-Aldrich Co, St. Louis, MO) as per reported method.<sup>24</sup>

% cell viability

$$= (\text{Absorbance of test sample} / \text{absorbance of positive control sample}) \times 100$$

#### Cellular uptake studies on HepG2 cells in-vitro

Cellular uptake of FITC labeled ApNp3 (ApNp5) was investigated in two types of human hepatocellular carcinoma cells, namely, HepG2 and Huh-7. Internalization of ApNp5 was visualized by confocal microscopy and quantification of the amount of ApNp5 inside the cells was determined by fluorescence activated cell sorter (FACS).

#### Radiolabeling of apigenin and apigenin loaded nanoparticles and biodistribution and gamma scintigraphy study

Radiolabeling of apigenin and ApNp3 with technetium (<sup>99m</sup>Tc) chloride was performed according to the procedure described by Gaonkar et al<sup>25</sup> and Satapathy et al.<sup>26</sup> Biodistribution and gamma scintigraphy study of the radiolabeled ApNp3 and radiolabeled apigenin were performed to have direct information about localization of apigenin/ApNp3 in experimental animals.

#### Pharmacokinetic study and hepatic accumulation of apigenin by LC-MS/MS method

The pharmacokinetic study and hepatic accumulation of apigenin were performed in plasma and liver samples collected from balb/c mice (body weight 25-30 g). Naringenin<sup>27</sup> was used as the internal standard for this study.

#### Histopathological investigation of carcinogenic rat livers

Male Sprague–Dawley rats (140-150 g bodyweight) were divided into six groups each containing six rats and chemically induced hepatocellular carcinoma in rats was developed as per the protocol published by Ghosh et al.<sup>28</sup> Schematic diagram of

hepatocarcinogenesis model along with treatment schedule with free apigenin/ApNp3 (single i.v. dose of 20 mg/kg bodyweight per week)<sup>29</sup> in rats is given in Supplementary Figure 1.

#### Enzyme assays

Hepatic cytosolic and microsomal fractions were prepared (from both normal/tumor surrounding tissues/ tumor tissues) as reported by Das et al<sup>30</sup> and Ghosh et al<sup>28</sup> and cytochrome P-450 (cyt p-450) content<sup>31</sup>, UDP-glucuronyl transferase (UDPGT) and glutathione-S-transferase (GST) activities<sup>32</sup> were determined.

#### Statistical analysis

The data were statistically analyzed by one-way ANOVA followed by Tukey's multiple comparison test, and statistical significance was considered at  $P < 0.05$ .

## Results

#### Fourier-transform infrared spectroscopy (FTIR) study

Presence of the characteristic peaks of apigenin [at wave number 1243  $\text{cm}^{-1}$ , responsible for C-C (O) –C stretching], PLGA (at wave number 2948  $\text{cm}^{-1}$ , responsible for –OH stretching) and PVA (at wave number 3426  $\text{cm}^{-1}$ , responsible for –OH stretching) in their physical mixture suggests that no chemical interaction took place between the drug and the excipients. However, absence of the characteristic peak of apigenin (at wave number 1243  $\text{cm}^{-1}$ ) in apigenin loaded nanoparticles (Supplementary Figure 2) indicates that apigenin distribution occurs inside the polymeric nanoparticle scaffolds and no free apigenin was available on the surface of the nanoparticles.

#### Determination of surface characteristics

FESEM photographs (Figure 1, A and B) of ApNp3 showed that prepared particles were in nanosize range, homogeneously and thickly distributed and had smooth outer surface. The surface morphology was further confirmed by 3D AFM picture (Figure 1, C) where it showed that height of the particles varied between 10 and 14 nm. TEM images of ApNp3 (Figure 1, D) showed that drug particles were scatteredly distributed throughout the polymeric nanoparticle body. Average particle sizes of ApNp3 and ApNp5 were 270 nm (Figure 1, E) and 325 nm (Figure 1, F) respectively and PDI values for those formulations were 0.260 and 0.409 respectively. The zeta potential values were –4.84 mV (Figure 1, G) and –4.1mV (Figure 1, H) for ApNp3 and ApNp5 respectively. FESEM images of ApNp3 kept at 30 °C, 75% relative humidity and 40 °C, 75% relative humidity clearly showed the effect of temperature on surface morphology of the particles as the polymeric surface structure softened over time for the samples stored at 30 °C and 40 °C as compared to the freshly prepared samples (Figure 1, I). Sample stored at 4-8 °C was found to maintain the structure of the particles.

#### Drug loading and drug loading efficiency

In this study, percentage of drug loading increased with an increasing amount of apigenin incorporated in nanoparticles. It

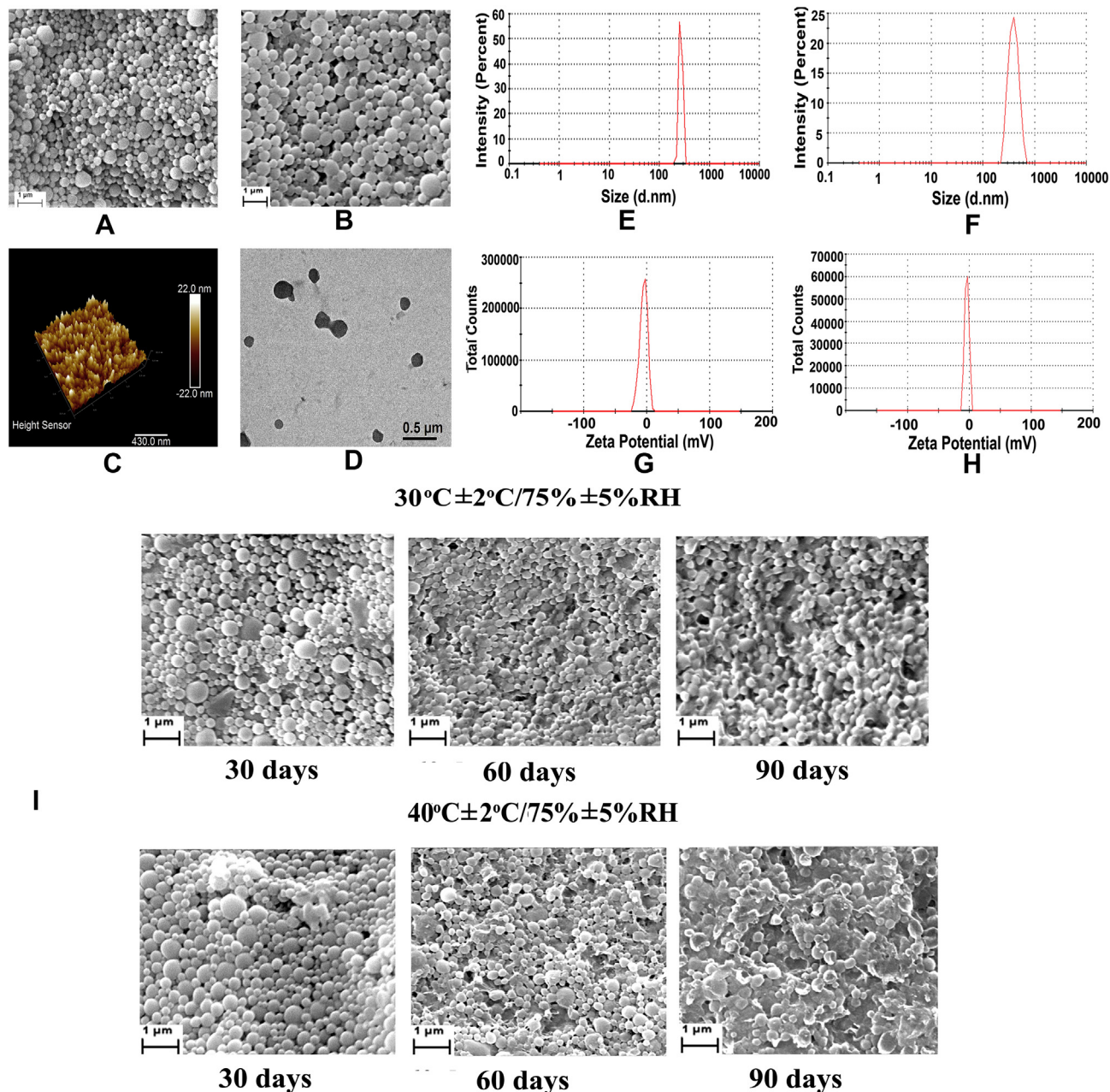


Figure 1. Morphology, size distribution and zeta potential of some selected experimental formulations. Morphology of ApNp3 (stored at 4–8 °C) was showed by FESEM (A and B), AFM (C) and TEM (D). Particle size distribution of ApNp3 (E), particle size distribution of ApNp5 (F) and zeta potential of ApNp3 (G), zeta potential of ApNp5 (H), FESEM images of ApNp3 stored at 30 °C, 75% relative humidity and 40 °C, 75% relative humidity are indicated respectively.

varied from ApNp1 (drug loading, 2.098%) to ApNp3 (drug loading, 19.14%) as shown in Supplementary Table 1. Further, ApNp4 showed a nearly similar drug loading (19.09%) to ApNp3 despite an increase in amount of drug incorporated in the formulation. Drug loading efficiency was found to increase with the increase of amount of drug for ApNp3. Hence we have chosen ApNp3 for further investigation.

Stability of ApNp3 stored at 4–8 °C, 30 °C, 75% RH and 40 °C, 75% RH for 30, 60 and 90 days was evaluated. When the stored samples were compared with the fresh formulation, by FTIR spectroscopy (data not shown) and FESEM, the formula-

tion stored at 4–8 °C was found to have similar FTIR spectra and the formulation structure was found to be maintained. The other formulations were also found to have similar FTIR spectra but deformed structurally due to softening of polymer with higher temperature.

#### *In-vitro drug release and kinetic study*

A variable *in-vitro* drug release pattern in different pH buffers was observed (Figure 2, A). After 60 days of the study, in PBS (pH 7.4) average percentage cumulative drug release was noted

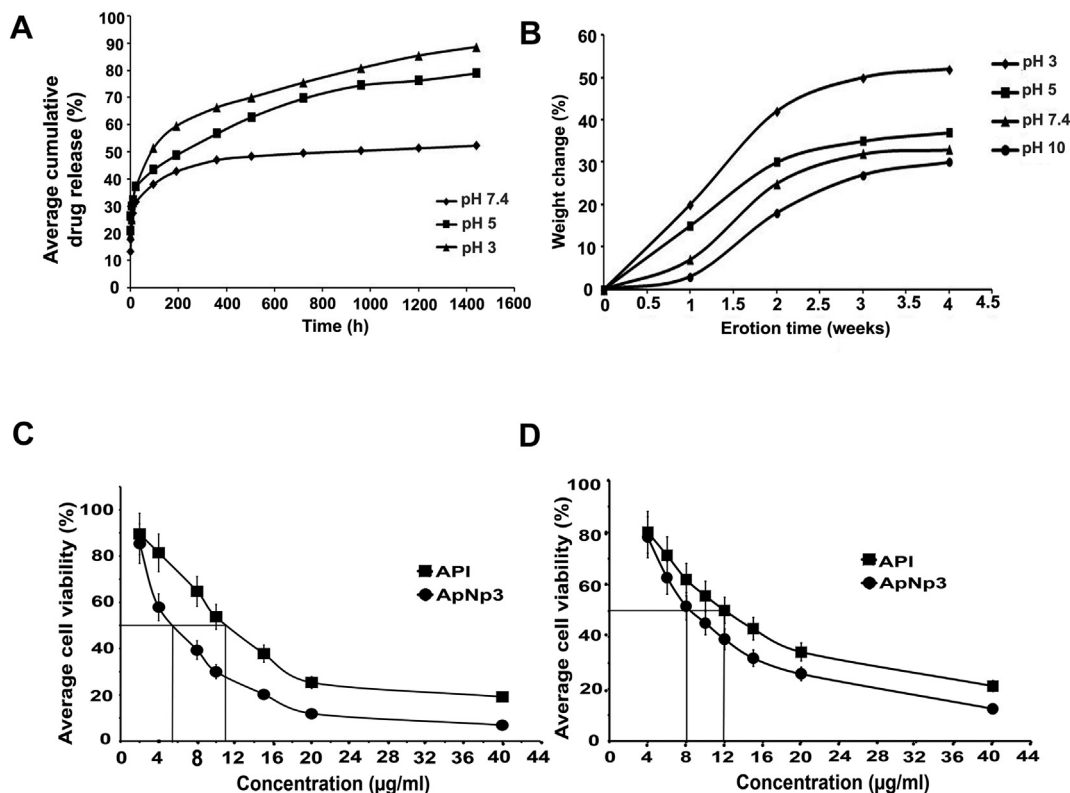


Figure 2. (A) *In vitro* drug release profile of ApNp3 in different pH (pH 3, 5 and 7.4) media. (B) Weight variation of nanoparticles in buffers of different pH. *In vitro* cytotoxicity of ApNp3 and API was determined in (C) HepG2 and (D) Huh-7 cells.

as 52.43% from ApNp3. Drug release was more in lower pH mediums. The cumulative drug release was reported as 79.06% and 88.54% in pH 5 and pH 3 respectively. To evaluate the drug-release kinetic pattern in PBS, release data were assessed using zero order, first order, Hixon–Crowell, Korsmeyer–Peppas, and Higuchi kinetic models. Various regression co-efficient ( $R^2$ ) values for the kinetics were tabulated (Table 1). The corresponding plot (log cumulative percent drug release versus log time) of ApNp3 followed the Korsmeyer–Peppas equation with a good linearity ( $R^2 = 0.9634$ ). The release exponent ( $n$ ) value for our formulation was 0.17 which suggests apigenin release followed anomalous diffusion pattern.<sup>33</sup>

#### Hydrolytic stability study

The stability of nanoparticles altered in different pH. Weight loss was found to increase with the decrease pH of medium (Figure 2, B). After 4 weeks of study, the mass loss of ApNp3 in pH 10, pH 7.4, pH 5 and pH 3 was  $30.35\% \pm 0.48\%$ ,  $33.87\% \pm 0.93\%$ ,  $37.45\% \pm 1.13\%$  and  $52.01\% \pm 1.97\%$  respectively. The weight loss of ApNp3 was  $2.8\% \pm 0.13\%$  after 24 h in mouse serum (graph not shown).

#### *In-vitro* cytotoxicity

*In-vitro* cytotoxicity of apigenin suspension (API, free drug) and ApNp3 in hepatocellular carcinoma cells was determined by MTT assay. Earlier reports suggest that apigenin successfully reduced cell viability and proliferation of HepG2<sup>34</sup> and Huh-7 cells.<sup>35</sup> In this study, we found that ApNp3 had an  $\text{IC}_{50}$  value

much lower than that of API. In HepG2 cells,  $\text{IC}_{50}$  value of ApNp3 was 5.5  $\mu\text{g/ml}$  and that of API was 11  $\mu\text{g/ml}$  (Figure 2, C). Again, in case of Huh-7 cells,  $\text{IC}_{50}$  value of ApNp3 was 8.5  $\mu\text{g/ml}$  and that of API was 12  $\mu\text{g/ml}$  (Figure 2, D).

#### Cellular uptake determination and quantification

The confocal images showed time dependent uptake of FITC labeled apigenin loaded formulation (ApNp5) by the HepG2 and Huh-7 cells *in-vitro* (Figure 3).

A quantitative measurement by FACS analysis showed that FITC signals were directly proportional to the amount of ApNps incorporated in HepG2 and Huh-7 cells incubated with ApNp5 at 0.5 h, 2 h and 6 h, along with an enhancement of uptake of FITC-nanoparticles in cells with time, as compared to untreated (control) cells (Figure 4). Cellular uptake of drug through ApNp3 in both the cell types was found to be predominantly more as compared to those cells treated with API when analyzed by LC-MS/MS (data not shown).

#### Gamma scintigraphy and biodistribution

$^{99\text{m}}\text{Tc-API}/^{99\text{m}}\text{Tc-ApNp3}$  was visualized by gamma scintigraphy in different animals (mice/rats) and the investigation showed that labeled ApNp3 accumulated predominantly in liver than  $^{99\text{m}}\text{Tc-API}$  (Figure 5, A). Further, predominant time-dependent accumulations were detected in intestine, thymus gland, stomach and urinary bladder (Figure 5, A, a and b) of mice. However, in case of  $^{99\text{m}}\text{Tc-ApNp3}$  administration,

Table 1

Average particle size, PDI and zeta potentials of ApNp3 and drug release data tested on various release kinetics models.

Formulation code	Z-average (d-nm) <sup>a</sup>	PDI <sup>a,b</sup>	Zeta potential (mV)	<i>In-vitro</i> kinetic model on which drug release data were assessed	Corresponding kinetic equation with $R^2$ value
ApNp3	270	0.409±0.05	−4.21±1	Zero Order	$y=0.0267x+28.64$ , $R^2 = 0.6361$
				First Order	$y=0.0002x+1.85$ , $R^2 = 0.6915$
				Higuchi	$y=1.0288x+22.79$ , $R^2=0.8452$
				Hixson–Crowell	$y=0.0006x+4.140$ , $R^2 = 0.6733$
				Korsmeyer–Peppas	$y=0.1732x+1.217$ , $R^2=0.9648$ ( $n=0.17$ ) <sup>c</sup>

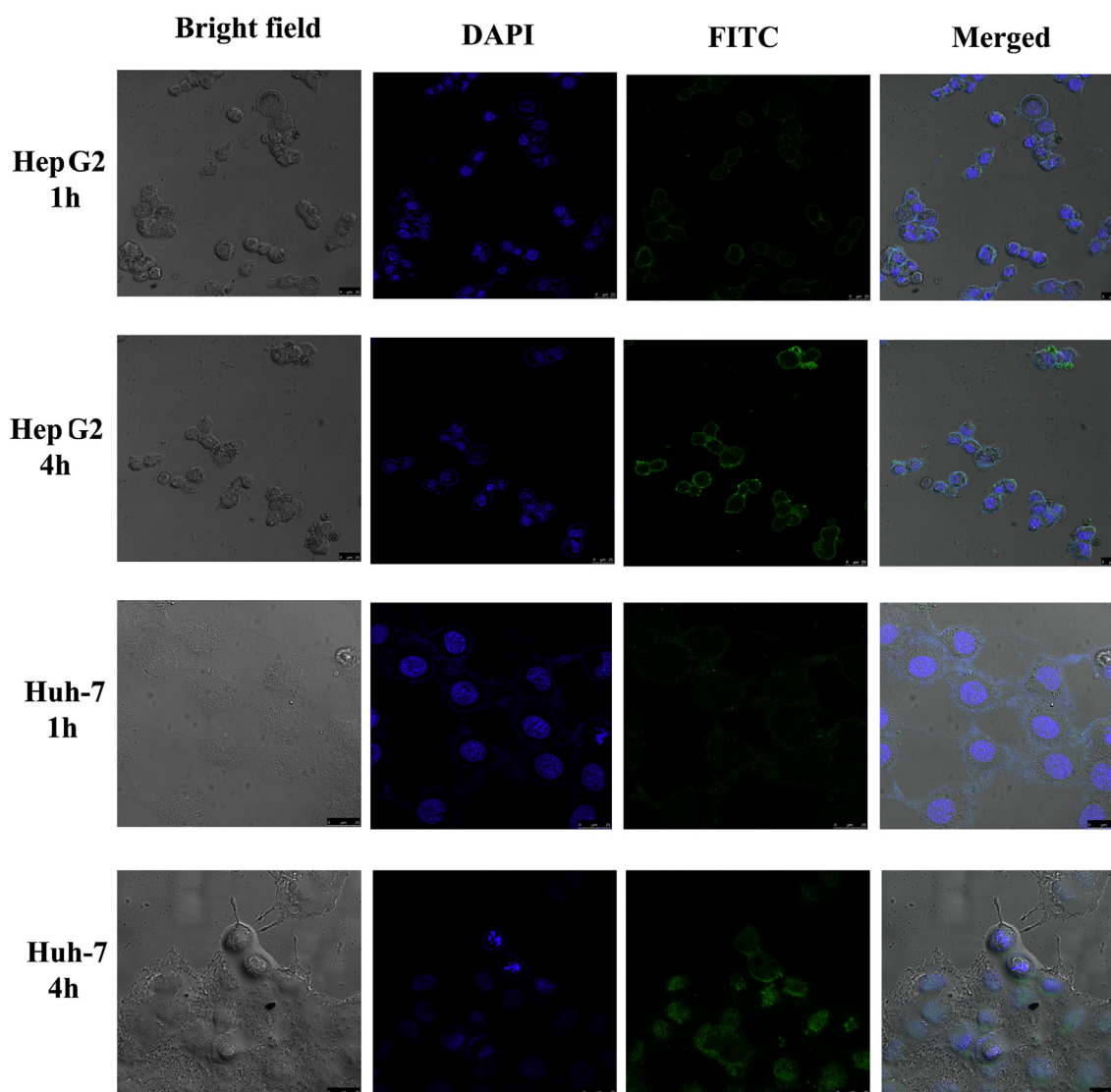
<sup>a</sup> Data show mean ±SD (n = 3).<sup>b</sup> PDI, polydispersity index.<sup>c</sup>  $n$ =release exponent.

Figure 3. Cellular uptake of FITC labeled ApNp3 (ApNp5) in HepG2 and Huh-7 cells observed by confocal microscopy at 1 h and 4 h respectively.

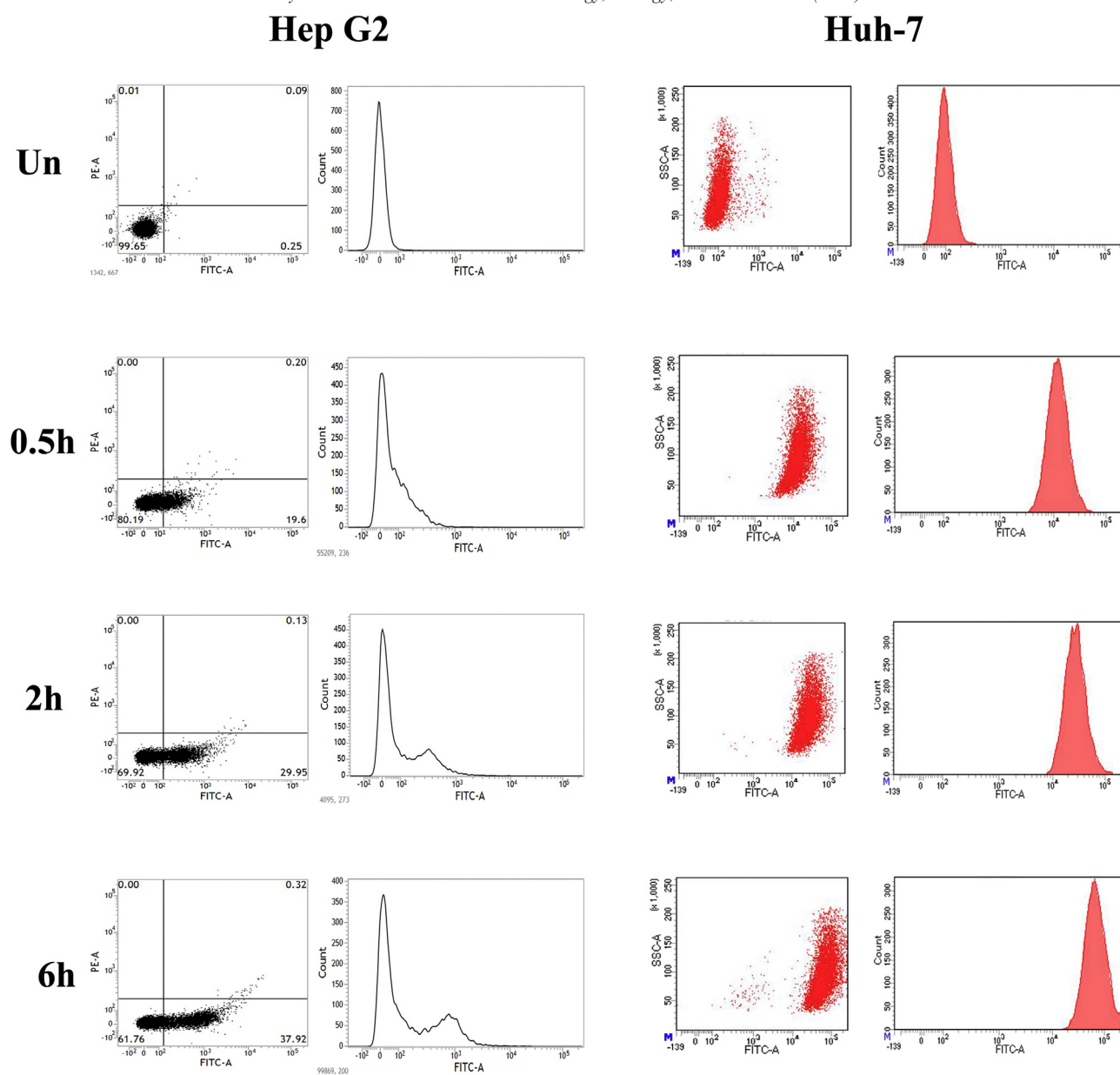


Figure 4. Time-dependent and quantitative measurement of cellular uptake of ApNp5 (FITC-ApNp3) in HepG2 and Huh-7 cells by FACS at 0.5 h, 2 h and 6 h against untreated cells (Un).

prominent time-dependent accumulations in liver, urinary bladder as well as in intestinal region were noticed (Figure 5, A, f and g). When radiolabeled  $^{99m}\text{Tc}$ -API /  $^{99m}\text{Tc}$ -ApNp3 was administered in normal rats by tail vein, a quick and time-dependent distribution of labeled ApNp3 was observed in liver and the clearance of labeled nanoparticles through urinary bladder was very less (Figure 5, A, h and i) as compared to that of  $^{99m}\text{Tc}$ -API in mice. Administration of  $^{99m}\text{Tc}$ -API in rats showed distribution in kidneys, and elimination through urinary track via urinary bladder (Figure 5, A, c and d). When rats with HCC were treated with  $^{99m}\text{Tc}$ -ApNp3 /  $^{99m}\text{Tc}$ -API, predominant localization of  $^{99m}\text{Tc}$ -ApNp3 was seen inside the enlarged (most likely due to inflammation) liver and its surrounding organs (at 4 h) and its clearance through urinary bladder was remarkably low

(Figure 5, A, e and j). Biodistribution of  $^{99m}\text{Tc}$ -API and  $^{99m}\text{Tc}$ -ApNp3 was examined in various organs of balb/c mice. Substantial uptake of  $^{99m}\text{Tc}$ -ApNp3 was observed in hepatic region compared to  $^{99m}\text{Tc}$ -API. At both the time points (2 h and 6 h), radiolabeled nanoparticles had much higher residence time in blood and lower distribution in kidney than  $^{99m}\text{Tc}$ -API (Table 2).

#### LC-MS/MS study

Graphical representations of the plasma profile and the hepatic accumulation of apigenin upon ApNp3/API administrations were given in Figure 5, B, a and B, b, respectively. In case of plasma, ApNp3 was found to maintain a steady blood level of predominantly more amount of drug even up to 72 h (period of the study).

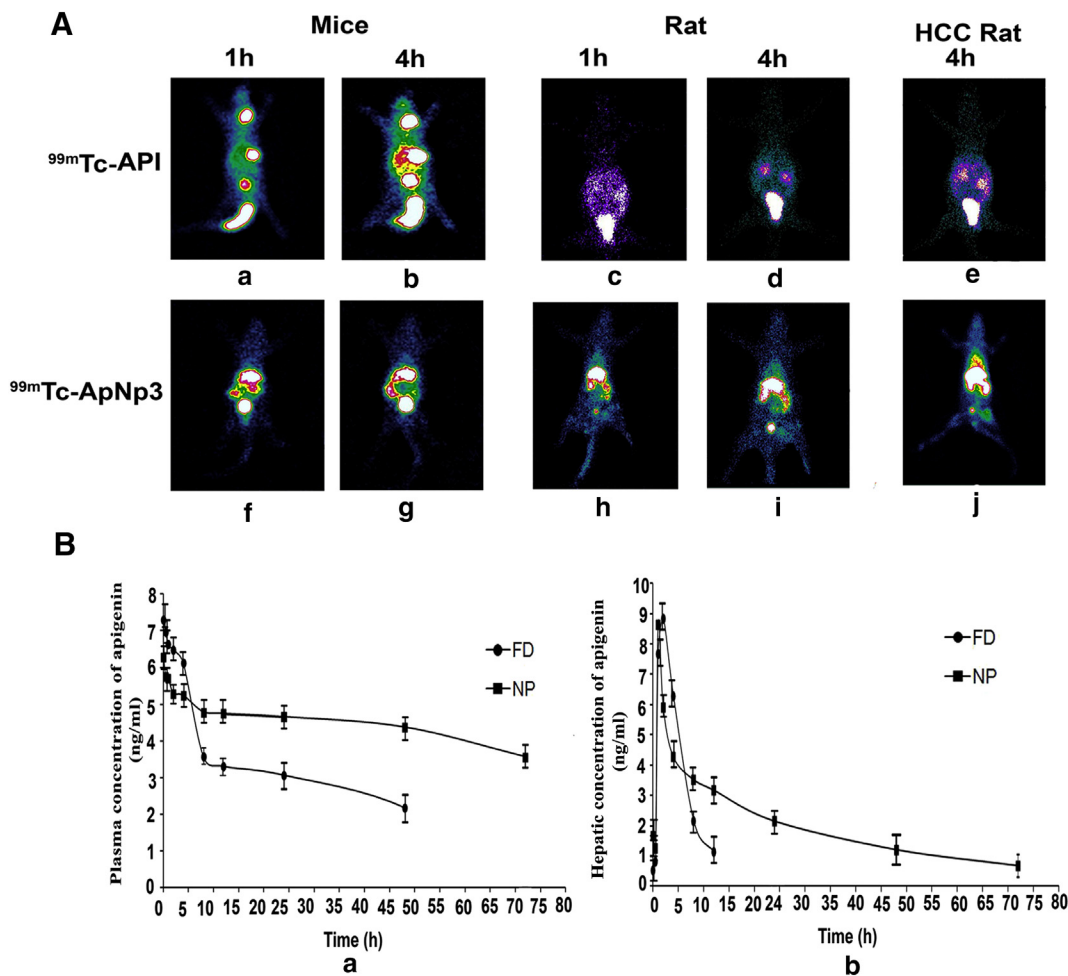


Figure 5. Gamma scintigraphic images of radiolabeled ApNp3/API localization in animals treated with radiolabeled ApNp3/API (A) and plasma concentration and hepatic concentration of apigenin in animals treated with ApNp3/API (B). (A) Time dependent biodistribution and accumulation of  $^{99m}\text{Tc-API}$  in mice at 1 h (a) and 4 h (b); in rats at 1 h (c) and 4 h (d); in rats with HCC at 4 h (e) along with the accumulation of  $^{99m}\text{Tc-ApNp3}$  in mice at 1 h (f) and 4 h (g); in rats at 1 h (h) and 4 h (i); rats with HCC at 4 h (j). (B) Plasma (a) and hepatic (b) concentration of apigenin upon i.v bolus injection (at a dose of 1mg/kg body weight) of ApNp3 (NP) and API (FD) were shown.

Table 2  
Biodistribution of apigenin in mice that received i.v.<sup>a</sup> injection of  $^{99m}\text{Tc-ApNp3}/^{99m}\text{Tc-API}$ .<sup>b</sup>

Organ/ Tissue	$^{99m}\text{Tc-ApNp3}$		$^{99m}\text{Tc-API}$	
	2 h	6 h	2 h	6 h
Heart	0.597 ± 0.058 <sup>c</sup>	0.421 ± 0.049	0.315 ± 0.051	0.284 ± 0.056
Blood	2.230 ± 0.095	1.806 ± 0.087	0.829 ± 0.099	0.631 ± 0.087
Liver	42.15 ± 1.213	54.151 ± 1.191	22.456 ± 1.311	20.561 ± 1.197
Lung	0.747 ± 0.213	1.285 ± 0.222	1.215 ± 0.192	0.997 ± 0.213
Spleen	0.378 ± 0.054	0.721 ± 0.034	1.531 ± 0.049	1.745 ± 0.057
Kidney	2.912 ± 0.211	2.451 ± 0.189	3.990 ± 0.212	4.785 ± 0.191
Intestine	6.160 ± 1.431	8.751 ± 1.212	21.556 ± 1.198	25.612 ± 1.199
Muscle	0.125 ± 0.003	0.156 ± 0.002	0.287 ± 0.007	0.215 ± 0.002

<sup>a</sup> i.v., intra-venous.

<sup>b</sup>  $^{99m}\text{Tc-ApNp3}$ , radiolabeled apigenin loaded nanoparticle;  $^{99m}\text{Tc-API}$ , radiolabeled apigenin.

<sup>c</sup> Data show mean ±SD (n = 4).

In case of hepatic concentration of apigenin, apigenin from suspension was detected up to 12 h, but the concentration could not be detected in liver at 24 h. In case of ApNp3, the hepatic concentration of drug was detectable up to 72 h (time period of

the investigation) which showed maintenance of a steady level of hepatic concentration of apigenin by ApNp3. Hepatic  $t_{\text{max}}$  (time to reach maximum concentration) values were very close for ApNp3 and API (about 1-2 h) suggesting rapid uptake of API

Table 3

Plasma and hepatic pharmacokinetic parameters of apigenin from ApNp3<sup>a</sup> and API<sup>b</sup> after intravenous bolus administration of API and ApNp3 with an equivalent amount of drug in balb/c mice.

Parameters	Plasma values of drug upon API administration <sup>c</sup>	Plasma values of drug upon ApNp3 administration	Hepatic values of drug upon API administration	Hepatic values of drug upon ApNp3 administration
Elimination $t_{1/2}$ (h)	39.8 ± 2.1	70.7 ± 4.3	3.8 ± 0.9	25.1 ± 1.
$C_{max}$ (ng/ml)	7.31 ± 1.3	6.29 ± 2.5	8.48 ± 2.78	8.66 ± 1.99
<sup>d</sup> AUC <sub>0-t</sub>	164.6 ± 12.2	338.6 ± 31.67	47.87 ± 4.9	124.13 ± 2.24
AUC <sub>0-inf</sub>	289.9 ± 23.5	701.7 ± 55.31	55.9 ± 4.7	168.2 ± 14
CL (L/h/kg)	3.45 ± 0.75	1.43 ± 0.43	17.9 ± 1.54	5.9 ± 0.88
MRT <sub>last</sub> (h)	20 ± 3.7	33.7 ± 2.24	4.8 ± 1.02	18 ± 2.01
V <sub>ss</sub> (L/kg)	196.5 ± 17.6	151.5 ± 11	113.9 ± 13.6	209.9 ± 17.8

<sup>a</sup> ApNp3, apigenin loaded nanoparticles.

<sup>b</sup> API, suspension of apigenin.

<sup>c</sup> Data show mean ±SD (n = 4).

<sup>d</sup> Units of AUC in plasma is h ng/ml, and in hepatic tissue h ng/g respectively.

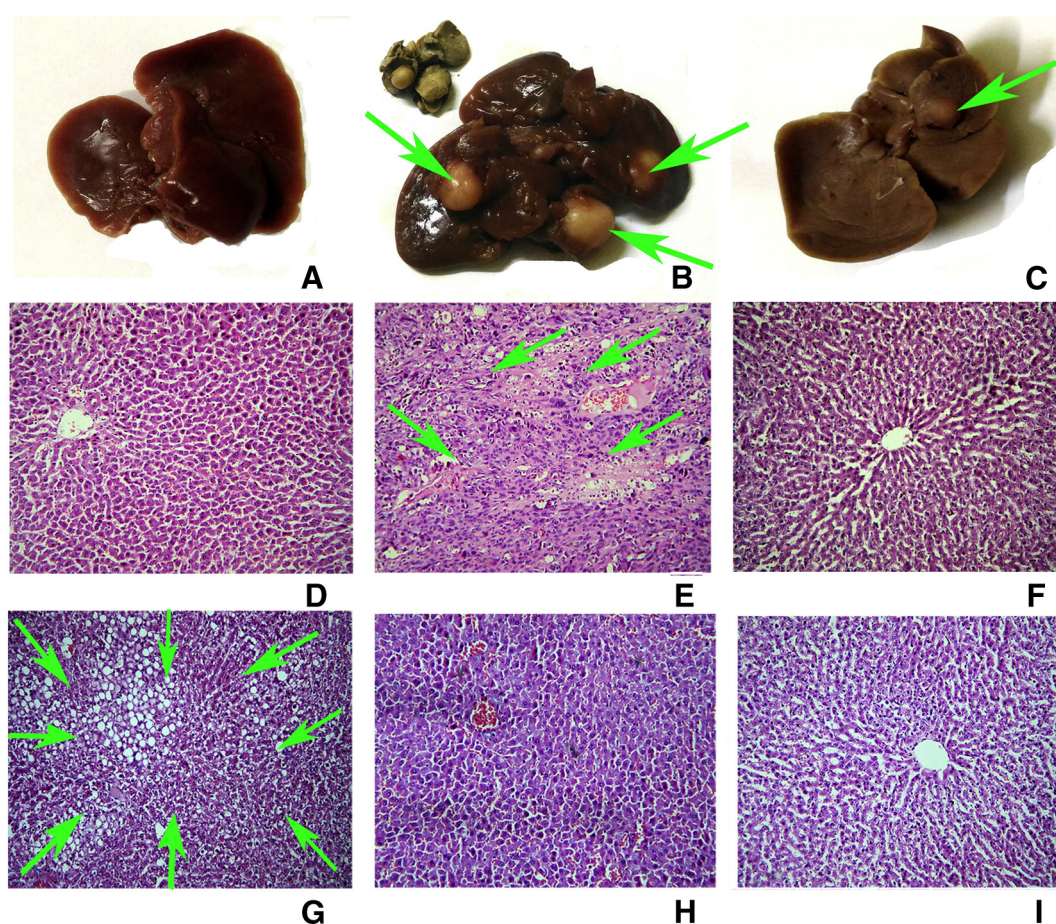


Figure 6. Macroscopic and microscopic images (in 10× magnifications) of liver of the experimental animals. Macroscopic images of livers of normal rats (A), carcinogen control rats (B) and carcinogen treated rats treated with ApNp3 (C). Microscopic images of liver section of normal rats (D), carcinogen treated rats (E), carcinogen treated animals treated with ApNp3 (F), carcinogen treated animals treated with API (G), normal animals treated with ApNp3 (H), and normal animals treated with API (I).

and the nanoparticles by liver. The plasma and liver pharmacokinetic data of apigenin from ApNp3 and from API (Table 3) showed that administration of ApNp3 by i.v. route enhanced plasma half-life of drug by 75% and hepatic half-life of it by 6.6 times in the experimental animals. Values of maximum concentration of drug ( $C_{max}$ ) in plasma and in liver were more

or less similar for API and ApNp3. Plasma as well as hepatic AUC values markedly increased upon ApNp3 administration from 1.5 to 3 times respectively as compared to those for API. Further, the values of the mean residence time of apigenin (from ApNp3) in plasma and in liver were found to increase by 1.68 and 3.03 times respectively, compared to API.

Table 4

A quantitative data on the effect of API/ApNp3 treatment of hepatic tumor incidences, number and total area of hepatic altered foci (HAF).

Groups	Number of rats developed HCC per total number of experimental rats per group	Tumor incidences (%)	Number of HAF <sup>a</sup> /cm <sup>2</sup> of hepatic tissue <sup>b</sup>	Total area of lesion (%)
A	0/6	-	-	-
B	6/6	100	79.57 ± 6.08 <sup>b</sup>	57.76 ± 1.45
C	2/6	66	21.98 ± 3.34 <sup>c</sup>	12.38 ± 0.98 <sup>c</sup>
D	-	-	-	-
E	-	-	-	-
F	5/6	83	56.43 ± 5.8 <sup>c</sup>	36.73 ± 4.65 <sup>c</sup>

<sup>a</sup> HAF: hepatic altered foci.<sup>b</sup> Values represent mean ±SD (*n*=6 for each group).<sup>c</sup> *P*<0.05 when compared against Group B.

### In-vivo HCC model

**Macroscopic and histopathology study.** Macroscopic images of liver tissues from group A, B and C animals revealed that treatment with apigenin nanoparticles (20 mg/kg single i.v. dose/week) for 12 weeks successfully controlled the tumor development in carcinogen treated rats (Figure 6, C). The hyperplastic nodules (HN) and preneoplastic and neoplastic hepatic altered foci lesions (HAF)<sup>30</sup> were clearly visible in HCC rats without any treatment (Figure 6, B) and upon intravenous treatment with ApNp3, the sizes of the nodules and number of lesions were markedly reduced (Figure 6, C). In the carcinogen control animals (Figure 6, E), tumor formation and scattered lesions with cells of ground glass appearance<sup>36</sup> were visible in the liver and normal hepatic architecture was lost. There were focal lesions and tumor formation visible in HCC. Cellular death and cells with pyknotic nucleus were also observed as compared to the normal liver architecture (Figure 6, D). Treatment of apigenin nanoparticles (ApNp3) in carcinogenic animals (Figure 6, F) was found to hold the hepatocellular architecture predominantly towards normal as compared to the carcinogenic animals treated with free drug (Figure 6, G). There was no distinguishable change in hepatocellular architecture in normal animals treated with blank nanoparticle (data not shown), ApNp3 (Figure 6, H) and free drug (Figure 6, I). A quantitative measurement of the effect of ApNp3 and free apigenin on HAF lesions and total area of the lesions (Table 4) showed that ApNp3 predominantly reduced number and total area of lesions and cancer incidence compared to API treatment.

**Marker enzyme assay.** Cytochrome P-450 (cyt p-450) content, glutathione-S-transferase (GST) activity in cytosolic fraction and, UDP-glucuronyl transferase (UDPGT) activity in microsomal hepatic fraction of the experimental animals were tabulated in Supplementary Table 2. In our study, cyt P-450 content was found to reduce in group B (HCC control) animals both in tumor tissues as well as in tumor surrounding tissue in comparison with the normal rats (Group A). ApNp3 treated HCC animals (Group C) markedly increased cyt P-450 content in the tumor area when compared with group B (HCC) animals. On the other hand, GST and UDPGT activities were found to increase predominantly in tumor areas of group B rats in comparison with the normal rats. Activities of the two enzymes significantly

decreased in tumor area after the ApNp3 treatment in group C rats indicating the effect of apigenin nanoparticles in repairing or delaying the progress of HCC in rats.

### Discussion

In recent times apigenin has gained much popularity as a naturally occurring flavonoid which has much lower intrinsic toxicity on normal cells compared to cancer cells while used as a tumor-suppressive agent.<sup>37</sup> There are very few reports published to date, which showed tumor suppressive effect of apigenin against HCC *in-vivo*.<sup>14, 38–40</sup> All these studies indicated a much higher dosing of apigenin required to acquire the therapeutic activity. To the best of our knowledge, this is the first report showing that apigenin nanoparticles successfully delayed the progress of HCC. Another uniqueness of our study was that the investigation showed *in-vivo* localization of apigenin-loaded nanoparticle as well as their tissue distribution by gamma scintigraphy. The investigations further support the hypothesis that site specific (liver) delivery of ApNp may ensure a successful treatment to control the progress of HCC.

FTIR data indicated the absence of chemical reaction (electrovalent or covalent type reactions) and rather suggested for physical interactions that might be involved in the formation of structure of the nanoparticles.

Developed nanoparticles were of spherical shape, smooth surface and within a size range of 250–400 nm which fulfills the primary requirements for efficient drug delivery to the target site as large particles (more than 150 nm) are mainly accumulated in liver.<sup>41</sup> A lower PDI value suggests a narrow range of size distribution of particles.<sup>42</sup> Nanoparticles with zeta potential ranging from –30 mV to +30 mV, have a tendency to settle down quickly as compared to those having zeta potential range >+30 mV or <–30 mV which generally form colloidal dispersion.<sup>43, 44</sup> But the particles with zeta potential values ranging from –30 mV to +30 mV never settle down so quickly that they would not be administered intravenously. They should be stored in a powder form (at 4–8 °C) and suspended in saline solution or water for injection and shaken well before administration. ApNp3 had 19.14% drug loading and was found to be stable at least for 90 days (period of study) at 4–8 °C.

A variable hydrolytic degradation of nanoparticles was observed in different pH buffers. Nanoparticles were found to



be more stable in bicarbonate buffer (pH 10) and PBS (pH 7.4) in comparison with acetate (pH 5) and citrate (pH 3) buffers. ApNp3 was stable in mouse serum at least for 24 h.

ApNp3 had an initial burst release of apigenin (24% in 6 h) in PBS (pH. 7.4) followed by a sustained drug release pattern (52% in 60 days). Burst release might have occurred due to a comparatively faster release of drug molecules present close to the surface of the nanoparticles and a subsequent sustained release of drug occurred due to the release of drug molecules from the deeper region of the matrix as the drug molecules had to traverse more distance through the tortuous complex network pathways through the polymeric matrix.<sup>19</sup> A good linearity (as assessed by  $R^2$  value) has favored that drug diffusion followed Korsmeyer–Peppas kinetics with an anomalous diffusion pattern.<sup>3</sup> Drug release was affected and altered by different pH values of the medium. Apigenin released fast in acidic pH (both in pH 3 and 5) due to the degradation of PLGA in acidic media.

FITC labeled ApNp3 showed much higher cytotoxicity in Hep-G2 and Huh-7 cells in comparison to free apigenin due to higher cellular uptake and a sustained release of drug over time as supported by confocal microscopic data, flow cytometric images and quantification by LC-MS/MS. Concisely, the nanoparticles were internalized more by the hepatocellular carcinoma cells in a time-dependent manner.

<sup>99m</sup>Tc-ApNp3 was found to accumulate predominantly in liver (the targeted organ in this study). The findings support the fact that there was a preferential hepatic distribution of ApNp3 than free apigenin (API). Further, apigenin loaded radiolabeled nanoparticles were also found to reach the livers of animals with HCC due to their nano-size and predominantly accumulated in hepatic tissue. Although the average particle sizes were 200 nm (ApNp3) and 400 nm (FITC-ApNp5) respectively, for two different formulations, they had size distribution ranges that varied from 30 to 500 nm. Hence some of the smaller particles might have eliminated faster which were visualized in the figure. However, numbers of published reports also showed that various nanocarriers size ranging from 150 to 250 nm and labeled with <sup>99m</sup>Tc, were detected in kidney and urinary bladder as well as in urine.<sup>45, 46</sup>

The biodistribution data obtained from radiolabeled ApNp3/apigenin were further supported by the data obtained by LC-MS/MS determination. Various pharmacokinetic parameters in mice plasma and liver (up to 72 h) showed much higher AUC and lower clearance rate of ApNp3 in comparison with API in both plasma and liver. This could be possibly responsible for more bioavailability of apigenin from ApNp3 than API. Difference in half-lives also suggests that apigenin from nanoparticles (half-life of apigenin from ApNp3 in plasma and hepatic circulation were  $70.7 \pm 4.3$  and  $25.1 \pm 1.1$  h respectively), followed a sustained release pattern. Plasma and hepatic clearance values reveal that ApNp3 caused reduction of apigenin clearance predominantly and assisted its longer presence in the body. Plasma protein binding of apigenin is predominantly long and release of drug from the plasma protein is comparatively much slower.<sup>17, 18</sup> Hence  $t_{1/2}$  of the drug in the blood was comparatively more than its value in liver. Initially nanoparticles taken up by the liver maintained the hepatic level of the drug. However, faster hepatic metabolism and elimination of larger nanoparticles and very slow distribution of plasma protein bound drug to liver at the

extended period could be responsible for shorter hepatic half-life of the drug in animals.

Significant anti-cancer potential of the optimized nanoparticles containing apigenin (ApNp3) in rats bearing HCC was observed. The efficiency of this formulation was achieved in controlling the tumor incidence and HAF. Predominant lower incidence of HCC development and a gross reduction of HAF upon ApNp3 treatment showed potential antitumor effect of apigenin loaded in nanoparticles on HCC development *in-vivo*.<sup>47, 48</sup> Free apigenin also improved the tissue structure, but not to the extent of ApNp3 mediated improvement. ApNp3 could have acted either on delaying the progress of development of HCC or on regenerating the damage of hepatic tissue towards normal, clearly seen in histopathology study. Presence of apigenin in the tumor area thus could be beneficial for controlling the proliferation of preneoplastic and neoplastic cells, hindering tumor formation.<sup>47, 48</sup> Apigenin has a significant role in tumor suppression by maintaining level of tumor suppressor gene p<sup>53</sup> in humans.<sup>10</sup> Apigenin loaded nanoparticles and free-apigenin had no noticeable effect on normal liver. Blank nanoparticles also had no effect on normal liver, suggesting that PLGA has no toxic effect in liver at all. Longer availability of apigenin as it released slowly from the nanoparticles and had a much lower clearance rate than free apigenin may be a responsible factor for such potential role of apigenin from ApNp3 than the free drug.

Cyt P-450, GST and UDPGT are well known tumor markers and have been extensively used to evaluate the progress of hepatic tumor development.<sup>26, 28, 48, 49</sup> Hence we have selected these markers to identify any biochemical changes occurred in tumors and the surrounding non-tumor hepatic tissue upon the treatment of ApNp3, as we found that the apigenin content varied in tumor and non-tumor surrounding tissues upon ApNp3 application. Interestingly, we found that modulation of these enzyme activities and iso-enzyme (cyt P-450) content predominantly varied in the tumor area upon nanoparticle treatment as compared to free apigenin treatment. This may be due to the enhanced permeability and retention (EPR) effect of ApNp3 in the solid tumors.<sup>50</sup> Thus, apigenin nanoparticles may serve as a successful line of treatment against HCC or as an adjuvant strategy to improve this disease state and can provide us a new therapeutic option to treat hepatocellular carcinoma patients. Further investigation in the area is warranted.

## Appendix A. Supplementary data

Supplementary data to this article can be found online at <https://doi.org/10.1016/j.nano.2018.05.011>.

## References

- Li HL, Ji WB, Zhao R, Duan WD, Chen YW, Wang XQ, et al. Poor prognosis for hepatocellular carcinoma with transarterial chemoembolization pre-transplantation: retrospective analysis. *Gastroenterol* 2015;**21**(12):3599-606.
- Weledji EP, Oroock GE, Ngowe MN, Nsagha DS. How grim is hepatocellular carcinoma? *Ann Med Surg* 2014;**3**:71-6.
- Torre LA, Bray F, Siegel RL, Ferlay J, Tieulent JL, Jemal A. Global cancer statistics, 2012. *Clin* 2015;**65**(2):87-108.

4. Jarnagin W, Chapman WC, Curley S, D'Angelica M, Rosen C, Dixon E, et al. Surgical treatment of hepatocellular carcinoma: expert consensus statement. *HPB* 2010;**12**:302-10.
5. Sanyal AJ, Yoon SK, Lencioni R. The etiology of hepatocellular carcinoma and consequences for treatment. *Oncologist* 2010;**15** (4):14-22.
6. Smith RJ. Nutrition and metabolism in hepatocellular carcinoma. *Hepatobiliary Surg Nutr* 2013;**2**(2):89-96.
7. Hootegem AV, Verslype C, Steenberg W. Sorafenib-induced liver failure: a case report and review of the literature. *Case Rep Hepatol* 2011;**2011**:1-4, <https://doi.org/10.1155/2011/941395>.
8. Zhou Y Li Y, Zhou T, Zheng S, Li S, Li HB. Dietary natural products for prevention and treatment of liver cancer. *Nutrients* 2016;**8**:1-23.
9. Sung B, Chung HY, Kim ND. Role of apigenin in cancer prevention via the induction of apoptosis and autophagy. *J Cancer Prev* 2016;**21** (4):216-26.
10. Chinembiri TN, du Plessis LH, Gerber M, Hamman JH, du Plessis J. Review of natural compounds for potential skin cancer treatment. *Molecules* 2014;**19**:11679-721.
11. Das S, Das J, Samadder A, Paul A, Khuda-Bukhsh AR. Strategic formulation of apigenin-loaded PLGA nanoparticles for intracellular trafficking, DNA targeting and improved therapeutic effects in skin melanoma in vitro. *Toxicol Lett* 2013;**223**:124-38.
12. Qin Y, Zhao D, Zhou HG, Wang XH, Zhong WL, Chen S, et al. Apigenin inhibits nf- $\kappa$ b and snail signaling, emt and metastasis in human hepatocellular carcinoma. *Oncotarget* 2016;**7**(27):41421-31.
13. Chiang LC, Ng LT, Lin IT, Kuo PL, Lin CC. Anti-proliferative effect of apigenin and its apoptotic induction in human hep g2 cells. *Cancer Lett* 2006;**237**:207-14.
14. Takagaki N, Sowa Y, Oki T, Nakanishi R, Yogosawa S, Sakai T. Apigenin induces cell cycle arrest and p21/waf1 expression in a p53-independent pathway. *Oncol* 2005;**26**:185-9.
15. Cai J, Zhao XL, Liu AW, Nian H, Zhang SH. Apigenin inhibits hepatoma cell growth through alteration of gene expression patterns. *Phytomedicine* 2011;**18**:366-73.
16. Lefort EC, Blay J. Apigenin and its impact on gastrointestinal cancers. *Mol Nutr Food Res* 2013;**57**:126-44.
17. Cao H, Chen L, Xiao J. Binding citrus flavanones to human serum albumin: effect of structure on affinity. *Mol Biol Rep* 2011;**38**:2257-62.
18. Gradolatto A, Basly JP, Berges R, Teyssier C, Chagnon MC, Siess MH, et al. Pharmacokinetics and metabolism of apigenin in female and male rats after a single oral administration. *Drug Metab Dispos* 2004;**33**:49-54.
19. Das PJ, Paul P, Mukherjee B, Mazumder B, Mondal L, Baishya R, et al. Pulmonary delivery of voriconazole loaded nanoparticles providing a prolonged drug level in lungs: a promise for treating fungal infection. *Mol Pharm* 2015;**12**:2651-64.
20. Mirakabad MST, Koshki KN, Akbarzadeh A, Yamchi MR, Milani M, Zarghami N, et al. PLGA-based nanoparticles as cancer drug delivery systems. *Cancer Prev* 2014;**15**(2):517-35.
21. Maji R, Dey NS, Satapathy BS, Mukherjee B, Mondal S. Preparation and characterization of tamoxifen citrate loaded nanoparticles for breast cancer therapy. *Nanomed* 2014;**9**:3107-18.
22. Abouelmagd SA, Sun B, Chang AC, Ku YJ, Yeo Y. Release kinetics study of poorly water-soluble drugs from nanoparticles: are we doing it right? *Mol Pharm* 2015;**12**(3):997-1003.
23. Mandal D, Shaw TK, Dey G, Pal MM, Mukherjee B, Bandyopadhyay AK, et al. Preferential hepatic uptake of paclitaxel-loaded poly-(D,L-lactide-co-glycolide) nanoparticles — a possibility for hepatic drug targeting: Pharmacokinetics and biodistribution. *Biol Macromol* 2018;**112**:818-30.
24. Shaw TK, Mandal D, Dey G, Pal MM, Paul P, Chakraborty S, et al. Successful delivery of docetaxel to rat brain using experimentally developed nanoliposome: a treatment strategy for brain tumor. *Drug Deliv* 2017;**24**(1):346-57.
25. Gaonkar RH, Gangul S, Dewanjee S, Sinha S, Gupta A, Ganguly S, et al. Garcinol loaded vitamin E TPGS emulsified PLGA nanoparticles: preparation, physicochemical characterization, *in vitro* and *in vivo* studies. *Sci Rep* 2016;**7**:1-14.
26. Satapathy BS, Mukherjee B, Baishya R, Debnath MC, Dey NS, Maji R. Lipid nanocarrier-based transport of docetaxel across the blood brain barrier. *RSC Adv* 2016;**6**:85261-74.
27. Dong X, Lan W, Yin X, Yang C, Wang W, Ni J. Simultaneous determination and pharmacokinetic study of quercetin, luteolin, and apigenin in rat plasma after oral administration of matricaria chamomilla l. extract by HPLC-UV. *Evid Based Complement Alternat Med* 2017:1-7.
28. Ghosh MK, Patra F, Ghosh S, Hossain CM, Mukherjee B. Antisense oligonucleotides directed against insulin-like growth factor-II messenger ribonucleic acids delay the progress of rat hepatocarcinogenesis. *J Carcinog* 2014;**13**(2):1-17.
29. Hu XY, Liang JY, Guo XJ, Liu L, Guo YB. 5-Fluorouracil combined with apigenin enhances anticancer activity through mitochondrial membrane potential ( $\Delta\Psi_m$ )-mediated apoptosis in hepatocellular carcinoma. *Clin Exp Pharmacol Physiol* 2015;**42**(2):146-53.
30. Das T, Patra F, Mukherjee B. Effect of antisense oligomer in controlling c-raf.1 overexpression during diethylnitrosamine-induced hepatocarcinogenesis in rat. *Cancer Chemother Pharmacol* 2010;**65**:309-18.
31. Omura T, Sato R. The carbon monoxide-binding pigment of liver microsomes. I. Evidence for its hemoprotein nature. *J Biol Chem* 1964;**239**:2370-8.
32. Ahn D, Putt D, Kresty L, Stoner GD, Fromm D, Hollenberg PF. The effects of dietary ellagic acid on rat hepatic and esophageal mucosal cytochromes P450 and phase II enzymes. *Carcinogenesis* 1996;**17** (4):821-8.
33. Singhvi G, Sing M. Review: in-vitro drug release characterization models. *Pharm Stud Res* 2011;**2**(1):77-84.
34. Kim EY, Yu JS, Yang M, Kim AK. Sub-toxic dose of apigenin sensitizes HepG2 cells to TRAIL through ERK-dependent up-regulation of TRAIL receptor DR5. *Mol Cells* 2013;**35**(1):32-40.
35. Kim BR, Jeon YK, Nam MJ. A mechanism of apigenin-induced apoptosis is potentially related to anti-angiogenesis and anti-migration in human hepatocellular carcinoma cells. *Food Chem Toxicol* 2011;**49**:1626-32.
36. Mathai AM, Alexander J, Kuo FY, Torbenson M, Swanson PE, Yeh MM. Type II ground-glass hepatocytes as a marker of hepatocellular carcinoma in chronic hepatitis B. *Hum Pathol* 2013;**44**(8):1665-71.
37. Madunić J, Madunić IV, Gajski G, Popić J, Garaj-Vrhovac V. Apigenin: A dietary flavonoid with diverse anticancer properties. *Cancer Lett* 2018, <https://doi.org/10.1016/j.canlet.2017>.
38. Jeyabal PVS, Syed MB, Venkataraman M, Sambandham JK, Sakthisekara D. Apigenin inhibits oxidative stress-induced macromolecular damage in N-nitrosodiethylamine (NDEA)-induced hepatocellular carcinogenesis in Wistar albino rats. *Mol Carcinog* 2005;**44**:11-20.
39. Singh JP, Selvendiran K, Banu SM, Padmavathi R, Sakthisekaran D. Protective role of apigenin on the status of lipid peroxidation and antioxidant defense against hepatocarcinogenesis in Wistar albino rats. *Phytomedicine* 2004;**11**(4):309-14.
40. Shukla S, Gupta S. Apigenin: A promising molecule for cancer prevention. *Pharm Res* 2010;**27**(6):962-78.
41. Blanco E, Shen H, Ferrari M. Principles of nanoparticle design for overcoming biological barriers to drug delivery. *Nat Biotechnol* 2015;**33** (9):941-51.
42. Masarudin MJ, Cutts SM, Evison BJ, Phillips DR, Pigram PJ. Factors determining the stability, size distribution, and cellular accumulation of small, monodisperse chitosan nanoparticles as candidate vectors for anticancer drug delivery: application to the passive encapsulation of [ $^{14}$ C]-doxorubicin. *Nanotechnol Sci Appl* 2015;**8**:67-80.
43. Meißner T, Potthoff A, Richter V. Suspension characterization as important key for toxicological investigations. *J Phys Conf Ser* 2009;**170** (1):1-6.
44. Basu S, Mukherjee B, Chowdhury SR, Paul P, Choudhury R, Kumar A, et al. Colloidal gold-loaded, biodegradable, polymer-based stavudine

- nanoparticle uptake by macrophages: AN in vitro study. *Nanomed* 2012;**7**:6049-61.
45. Yu M, Zheng J. Clearance pathways and tumor targeting of imaging nanoparticles. *ACS Nano* 2015;**9**:6655-74.
  46. Polyak A, Palade EA, Balogh L, Posteny Z, Haasz V, Janoki G, et al. In vitro and biodistribution examinations of Tc-99m-labelled doxorubicin-loaded nanoparticles. *Nucl Med Rev* 2011;**14**:55-62.
  47. Schlageter M, Terracciano ML, D'Angelo S, Sorrentino P. Histopathology of hepatocellular carcinoma. *Gastroenterol* 2014;**20**(43):15955-64.
  48. Yan X, Qi M, Li P, Zhan Y, Shao H. Apigenin in cancer therapy: anti-cancer effects and mechanisms of action. *Cell Biosci* 2017;**7**:1-16.
  49. Yan T, Lu L, Xie C, Chen J, Peng X, Zhu L, et al. Severely impaired and dysregulated cytochrome P450 expression and activities in hepatocellular carcinoma: implications for personalized treatment in patients. *Mol Cancer Ther* 2015;**14**(12):2874-86.
  50. Kobayashi H, Watanabe R, Choyke PL. Improving conventional enhanced permeability and retention (EPR) effects; what is the appropriate target. *Theranostics* 2014;**4**(1):81-9.



## Lipid-based nanocarrier efficiently delivers highly water soluble drug across the blood–brain barrier into brain

Lopamudra Dutta, Biswajit Mukherjee, Tapash Chakraborty, Malay Kumar Das, Laboni Mondal, Sanchari Bhattacharya, Raghuvir H. Gaonkar & Mita Chatterjee Debnath

To cite this article: Lopamudra Dutta, Biswajit Mukherjee, Tapash Chakraborty, Malay Kumar Das, Laboni Mondal, Sanchari Bhattacharya, Raghuvir H. Gaonkar & Mita Chatterjee Debnath (2018) Lipid-based nanocarrier efficiently delivers highly water soluble drug across the blood–brain barrier into brain, *Drug Delivery*, 25:1, 504-516, DOI: [10.1080/10717544.2018.1435749](https://doi.org/10.1080/10717544.2018.1435749)

To link to this article: <https://doi.org/10.1080/10717544.2018.1435749>



© 2018 The Author(s). Published by Informa UK Limited, trading as Taylor & Francis Group.



[View supplementary material](#)



Published online: 09 Feb 2018.



[Submit your article to this journal](#)



Article views: 296



[View related articles](#)



[View Crossmark data](#)

## Lipid-based nanocarrier efficiently delivers highly water soluble drug across the blood–brain barrier into brain

Lopamudra Dutta<sup>a</sup>, Biswajit Mukherjee<sup>a</sup> , Tapash Chakraborty<sup>b</sup>, Malay Kumar Das<sup>b</sup>, Laboni Mondal<sup>a</sup>, Sanchari Bhattacharya<sup>a</sup>, Raghuvir H. Gaonkar<sup>c</sup> and Mita Chatterjee Debnath<sup>c</sup>

<sup>a</sup>Department of Pharmaceutical Technology, Jadavpur University, Kolkata, India; <sup>b</sup>Department of Pharmaceutical Sciences, Dibrugarh University, Dibrugarh, India; <sup>c</sup>Infectious Diseases and Immunology Division, CSIR-Indian Institute of Chemical Biology, Kolkata, India

### ABSTRACT

Delivering highly water soluble drugs across blood–brain barrier (BBB) is a crucial challenge for the formulation scientists. A successful therapeutic intervention by developing a suitable drug delivery system may revolutionize treatment across BBB. Efforts were given here to unravel the capability of a newly developed fatty acid combination (stearic acid:oleic acid:palmitic acid = 8.08:4.13:1) (ML) as fundamental component of nanocarrier to deliver highly water soluble zidovudine (AZT) as a model drug into brain across BBB. A comparison was made with an experimentally developed standard phospholipid-based nanocarrier containing AZT. Both the formulations had nanosize spherical unilamellar vesicular structure with highly negative zeta potential along with sustained drug release profiles. Gamma scintigraphic images showed both the radiolabeled formulations successfully crossed BBB, but longer retention in brain was observed for ML-based formulation (MGF) as compared to soya lecithin (SL)-based drug carrier (SYF). Plasma and brain pharmacokinetic data showed less clearance, prolonged residence time, more bioavailability and sustained release of AZT from MGF in rats compared to those data of the rats treated with SYF/AZT suspension. Thus, ML may be utilized to successfully develop drug nanocarrier to deliver drug into brain across BBB, in a sustained manner for a prolong period of time and may provide an effective therapeutic strategy for many diseases of brain. Further, many anti-HIV drugs cannot cross BBB sufficiently. Hence, the developed formulation may be a suitable option to carry those drugs into brain for better therapeutic management of HIV.

### ARTICLE HISTORY

Received 7 December 2017  
Revised 23 January 2018  
Accepted 29 January 2018

### KEYWORDS



Nanosize lipid carrier; blood–brain barrier; gamma scintigraphy; pharmacokinetics; biodistribution


### Introduction

Blood–brain barrier (BBB), a complex tight endothelial vascular lining, is the main hindrance of most chemicals for free diffusion and penetration into the brain from blood stream of body for maintaining homeostasis in brain (Seju et al., 2011; Martins et al., 2012). BBB acts as a safeguard of brain from exogenous toxic agents as well as rejecter of essential therapeutic agents (Hu et al., 2009). Nearly 100% of large molecular drugs and about 98% of drugs consisting of small molecules are unable to cross BBB to provide therapeutic outcome (Wilson et al., 2008; Hu et al., 2017). Various novel drug delivery systems such as nanoparticles, nanoliposomes (NLs), micelles, dendrimers, quantum dots, and nanoemulsions are applied to overcome the limitations (Li et al., 2017). Nowadays, nanosize drug delivery into brain across BBB is an emerging field of pharmaceutical research. In the current study, we have selected lipid-based nanoliposomal drug carrier to deliver drug into brain. NLs can deliver hydrophobic as well as hydrophilic drug efficiently due to their special structure. Due to some important properties such as biodegradability, biocompatibility, low toxicity, ability of

enhancement of therapeutic index and efficacy of drug, enhancement of stability of drug through encapsulation, and non-immunogenicity, the liposomal drug delivery is a choice as a drug carrier (Akbarzadeh et al., 2013).

It is always an enormous challenge for formulation scientists to deliver highly water soluble drug into brain across BBB and the same is true for many other large molecules. In the present study, we have selected a highly water soluble drug zidovudine (AZT), 1-[(2R,4S,5S)-4-azido-5-(hydroxymethyl)oxolan-2-yl]-5-methylpyrimidine-2,4-dione (Figure 1(A)), as a model water-soluble drug to deliver across BBB into brain. AZT is a highly water soluble drug (25 mg/ml at 25 °C). Therefore, it has been used as a representative water soluble active pharmaceutical ingredient or drug in a number of reports (Jain et al., 2008; Nayak et al., 2009; Singh et al., 2010; Christopher et al., 2014). It is expected that the physical characteristics provided by AZT would be similar for many other hydrophilic drugs. Hence, we have considered AZT as a water soluble model drug in the present study. AZT, nucleoside reverse transcriptase inhibitor, is also a part of combination therapy 'highly active antiretroviral treatment (HAART)' for anti-HIV treatment (Bergshoeff et al., 2004; Mu et al., 2016).

**CONTACT** Biswajit Mukherjee  biswajit.mukherjee@jadavpuruniversity.in, biswajit55@yahoo.com  Department of Pharmaceutical Technology, Jadavpur University, Kolkata 700032, West Bengal, India

 Supplemental data for this article can be accessed [here](#).

© 2018 The Author(s). Published by Informa UK Limited, trading as Taylor & Francis Group.

This is an Open Access article distributed under the terms of the Creative Commons Attribution License (<http://creativecommons.org/licenses/by/4.0/>), which permits unrestricted use, distribution, and reproduction in any medium, provided the original work is properly cited.

AZT due to its strong hydrophilicity is unable to cross BBB sufficiently to reach brain, resulting in inadequate concentration of AZT for therapeutic efficacy (Rautio et al., 2008; Weiss et al., 2009). Thus, delivering AZT in brain could be utilized for better management of HIV as in HIV infected patients, at very early stage (up to 10 days of post HIV infection), neuro-invasion can arise and HIV infected circulated monocytes in blood stream can easily enter into brain (Ivey et al., 2009).

Here, by trial and error method we developed several lipids using various mixtures of three fatty acids present in many edible lipids (Kittiphoom, 2012). Out of them we have selected the best combination [stearic acid (SA):oleic acid (OA):palmitic acid (PA) = 8.08:4.13:1] (ML) on the basis of its consistency to develop the nanocarrier. We also compared the efficacy of this formulation with soya lecithin (SL)-based formulation developed by us.

The prime objective of this investigation was to evaluate the capability of ML as base component for the development

of nanocarrier to deliver highly water soluble drug into brain across BBB. Further, its efficiency was evaluated by comparing with SL-based drug nanocarrier.

## Materials and methods

AZT was obtained as a gift sample from Cipla Ltd. (Goa, India). Cholesterol (CHO), fluorescein isothiocyanate (Isomer I) (FITC), SL, fetal bovine serum (FBS) and minimum essential medium Eagle (MEM) were procured from HiMedia Laboratories Pvt. Ltd. (Mumbai, India). SA, OA, and PA were purchased from Sigma-Aldrich (Bangalore, India) and butylated hydroxytoluene (BHT) was obtained from Qualigens Fine Chemicals (Mumbai, India). U-87 MG cells were procured from National Center for Cell Science (Pune, India). All other chemicals used were of analytical grade.

## Animals

Sprague-Dawley rats (male:female ratio 2:1) having body weight 200–250 g were utilized for biodistribution investigation, plasma and brain pharmacokinetic study and only male Sprague-Dawley rats of body weight 200–250 g were used for gamma scintigraphy study. Animal experiments were carried out upon receiving approval of the Animal Ethics Committee, Jadavpur University, Kolkata. Animals were accommodated in the university animal house after keeping them in polypropylene cages. The temperature ( $22 \pm 1^\circ\text{C}$ ) and humidity ( $55 \pm 5\%$ ) were maintained in the animal house with 12 h light/dark cycle. The animals had free access of standard diet (Dey et al., 2016) and drinking water.

## Fourier-transform infrared spectroscopy (FTIR)

FTIR was conducted to determine possible interaction (if any) between the drug and the excipients. For ML-based formulation, pure drug (AZT), CHO, ML, BHT, physical mixture (PM) of CHO, ML, BHT, physical mixture (PMD) of CHO, ML, BHT and drug AZT, lyophilized formulation without drug (MGB) and lyophilized formulation with drug (MGF) and for SL-based formulation, AZT, CHO, SL, BHT, physical mixture (PM-1) of CHO, SL, BHT, physical mixture (PMD-1) of CHO, SL, BHT and AZT, lyophilized formulation without drug (SYB) and lyophilized formulation with drug (SYF) were scanned at  $4000\text{--}400\text{ cm}^{-1}$  using FTIR instrument (JASCO International Co. Ltd., FTIR 4200, Tokyo, Japan) using their pellets formed by mixing with potassium bromide (KBr) at 1:100 ratio and compressing with a hydraulic press (Sahana et al., 2010).

## Preparation of NLS

Fatty acids at the selected ratio were dissolved in small quantity of chloroform and chloroform was evaporated under vacuum to get the lipid formed from the fatty acids.

NLS were prepared by lipid layer hydration technique by varying different process parameters (Rudra et al., 2010). Specific weighed amounts of excipients CHO, lipids (ML for MGF/SL for SYF, respectively) (Supplementary Table 1) and

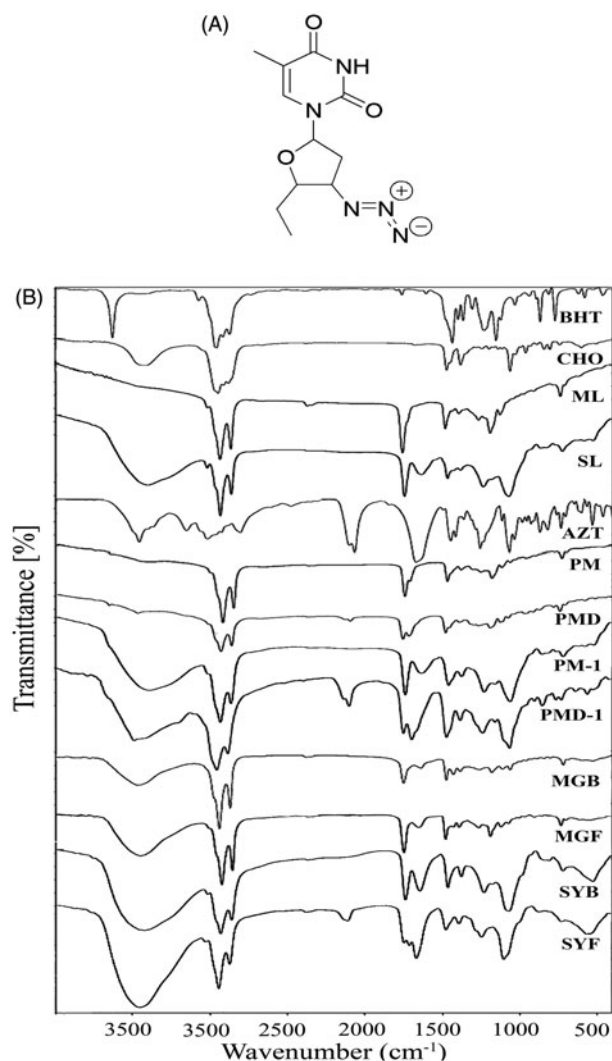


**Figure 1.** (A) Chemical structure of zidovudine (AZT). (B) Fourier transform infrared spectroscopy (FTIR)-spectra of BHT (butylated hydroxytoluene), CHO (cholesterol), ML (lipid), SL (soya lecithin), AZT (zidovudine), PM (physical mixture of BHT, CHO, ML), PMD (physical mixture of BHT, CHO, ML, and drug), PM-1 (physical mixture of BHT, CHO, SL), PMD-1 (physical mixture of BHT, CHO, SL, and drug), MGB (ML-based lyophilized formulation without drug), MGF (ML-based lyophilized formulation with drug), SYB (SL-based lyophilized formulation without drug), and SYF (SL-based lyophilized formulation with drug).

BHT (1% w/v as antioxidant) were taken in 250 ml round bottom flask and adequate quantity of chloroform was added within the flask with vigorous shaking to dissolve the excipients. The flask was set up in a rotary vacuum evaporator (Rotavap, model PBU-6, Superfit Continental Pvt. Ltd., Mumbai, India) fitted with an A3S aspirator (Eyela, Rikakikaic, Ltd., Taguig City, Philippines) and a circulating water bath (Spac N service, Kolkata, India) at 5 °C and was rotated at 145 rpm rotation speed at 40 °C in water bath to evaporate the organic solvent and to form thin film of lipid layer on the inside-wall of the flask. For complete elimination of the residual chloroform, the flask was kept overnight in a vacuum desiccator. The weighed amount of AZT was dissolved in phosphate buffer (pH 7.4), and the mixture was taken in the flask. The flask was then fitted in a rotary vacuum evaporator with rotation speed at 145 rpm and at 40 °C in a water-bath for complete dispersion of thin lipid film in the aqueous phase. The dispersion was sonicated at  $30 \pm 3$  kHz in a bath type sonicator (Trans-o-Sonic, Mumbai, India) for 1 h with cold water. To form vesicles, the round bottom flask was kept at room temperature for 1.5 h and stored overnight at 4 °C. The preparation was centrifuged at 5000 rpm for 15 min at 4 °C to separate the larger vesicles and the obtained supernatant was again centrifuged (at 16,000 rpm for 45 min in a cold centrifuge at 4 °C) (3K30 Sigma Lab Centrifuge, Merrington Hall Farm, Shrewsbury, UK) to precipitate NLs. The obtained precipitate was re-suspended in fresh phosphate buffer (pH 7.4) and precipitated again number of times to wash the NLs. NLs were collected in a petridish and lyophilized for 12 h (Laboratory Freeze Dryer, Instrumentation India Ltd., Kolkata, India) to get dry product. Blank NLs (MGB, SYB) were prepared by the same procedure without using AZT. Fluorescent NLs were prepared using the same process as described above except the step where fluorescent marker FITC was used. FITC stock solution (0.4% w/v) was prepared in a mixture of chloroform and ethanol at volume 3:1 ratio and a volume of 100  $\mu$ l was mixed into the organic phase (chloroform) during the initial mixing of preparation (Shaw et al., 2017).

## Characterization of NL

### Evaluation of drug loading

MGF/SYF (5 mg) was taken in a mixture of phosphate buffer (pH 7.4) and ethanol at a ratio of 5:1 and sonicated and vortex-mixed. After centrifugation (at 16,000 rpm for 15 min at 4 °C), the supernatant was collected and measured at 265 nm using UV/VIS spectrophotometer (Model Intech-295, Gentaur GmbH, Aachen, Germany). The same procedure was performed for MGB/SYB. Absorbance for drug was obtained by deducting the absorbance obtained from NLs without drug and from that of NLs with drug (Satapathy et al., 2016). Each study was conducted thrice. The percentage of drug loading was calculated using the following formula:

$$\text{Percentage of drug loading} = \frac{\text{Amount of AZT in NLs}}{\text{Amount of NLs taken}} * 100 \quad (1)$$

### Percentage of yield determination

To determine the yield of NLs from the utilized total amount of raw materials of NLs preparation, lyophilized dried NLs of each batch were weighed and the percentage of yield was calculated by using the following equation as mentioned earlier (Sahana et al., 2010).

$$\text{Percentage of yield} = \frac{\text{Amount of NLs obtained}}{\text{Total amount of drug and excipients used}} * 100 \quad (2)$$

### Evaluation of size distribution and zeta potential

By utilizing the dynamic light scattering (DLS) technology in a Zetasizer Nano ZS90 (Malvern Instrument, Malvern, UK), average size of NLs, size distribution pattern, polydispersity index (PDI) and zeta potential of the experimental formulations were determined.

### Field emission scanning electron microscopy (FESEM) for surface morphology analysis

FESEM was used to investigate the surface morphology of NLs. The lyophilized NLs were placed on an adhesive tape of carbon over a stub by spreading smoothly and then dried through vacuum and coated with platinum using a platinum coater instrument (JEOL, Tokyo, Japan). After that the samples were observed at various magnifications with the help of FESEM (Model-JSM-6700F; JEOL, Tokyo, Japan) (Dey et al., 2016).

### Cryo-transmission electron microscopy (Cryo-TEM) study

Cryo-TEM study was performed to observe morphology and lamellarity of NLs. About 1.5 mg lyophilized formulation was taken in a microcentrifuge tube and 1 ml of Milli-Q water was added into it. The suspension was vortexed followed by sonication for a few minutes to prevent agglomeration. The NLs suspension (4  $\mu$ l) was put on a clean grid, blotted away the excess (if any) with the help of filter paper and vitrified instantly by dipping into liquid ethane. The grid was stored in liquid nitrogen till shifting under the electron microscope (Tecnaï Polara, version 4.6 FEI Tecnaï G2, Eindhoven, Netherlands) which was operated at 300 kV equipped with an FEI Eagle 4 K  $\times$  4 K charge-coupled device (CCD) camera for capturing the images (Fox et al., 2014).

## In vitro investigations

### In vitro drug release study

*In vitro* drug release study was conducted in freshly prepared phosphate buffer (pH 7.4) and in 50% serum [serum:phosphate buffer (pH 7.4) = 1:1] individually as drug release media at room temperature (for phosphate buffer as media) and at 37 °C (for 50% serum as media) (in physiological mimicking condition), for 24 h. Drug release media (50 ml) were taken in a glass beaker (100 ml). Lyophilized formulation (5 mg) was weighed accurately and reconstituted in 1 ml of the

respective drug release media and was placed into a dialysis bag (Himedia Dialysis Membrane – 110, Mumbai, India) (Dey et al., 2016). The dialysis bag was tightly knotted at the two ends with cotton thread and hanged centrally into the beaker containing drug release medium (in such a way so that the formulation portion inside the bag immersed within the media) using a laboratory ring stand with clamp kit. The beaker was put on a magnetic stirrer maintaining stirring at 300 rpm using a magnetic bead. From the beaker, 1 ml media was withdrawn at various predetermined time intervals and same volume of fresh media was replaced immediately into the beaker. All the collected samples were analyzed using UV-VIS spectrophotometer at 265 nm with phosphate buffer or 50% serum as blank according to requirement. In case of serum sample, protein was precipitated as mentioned under LC-MS/MS study. The drug concentration at any individual time point was calculated with the help of calibration curve. For 50% serum as drug release media, total experiment was conducted maintaining aseptic condition in all respect under laminar air flow hood.

#### **In vitro drug release kinetic study**

*In vitro* drug release data were applied in various kinetic models such as zero order (percentage cumulative drug release versus time), first order (log of percentage cumulative amount of drug remained to release versus time), Higuchi model (percentage cumulative drug release versus square root of time), Hixson–Crowell's model (cube root of percentage cumulative amount of drug remained to release versus time), Korsmeyer–Peppas's model (log of percentage cumulative drug release versus log of time) to predict the drug release pattern of the optimized formulations. The highest correlation coefficient value ( $R^2$ ) from all the tested models was utilized to select the suitable kinetic pattern (Das et al., 2015).

#### **In vitro cellular uptake study**

To investigate the cellular uptake ability of NLs by U-87 MG cells, confocal laser scanning microscopy study was executed. In six well culture plates, U-87 MG cells were seeded on coverslips ( $3 \times 10^4$ ) and cultivated using MEM containing 10% FBS for 24 h. These cells were treated with FITC-MGF/FITC-SYF suspension at a concentration of 100  $\mu$ g/ml. At different time points (i.e. 0.25 h, 1 h, 3 h) of incubation, the cells were washed thrice and fixed applying paraformaldehyde aqueous solution (4%). They were cleaned by using freshly prepared phosphate buffer (pH 7.4) after 5 min of fixation. Then, coverslips were collected cautiously and mounted on the glass slide. After complete air drying, the slides were placed individually under a confocal laser scanning microscope (Model: IX81, Olympus Singapore Pte Ltd., Singapore) and the images were snapped (Maji et al., 2014).

#### **Stability study**

Stability testing of the lyophilized formulations was performed as per ICH guidelines (Sahana et al., 2010).

### **In vivo investigations**

#### **Radiolabeling of AZT and AZT loaded NLs**

According to the tin (II) chloride reduction method as described earlier (Das et al., 2015; Satapathy et al., 2016), radiolabeling of AZT and AZT loaded MGF/SYF was performed with technetium-99m ( $^{99m}\text{Tc}$ ). At first, 5 mg of AZT was dissolved in 0.5 ml ethanol and AZT loaded NLs (equivalent to 5 mg of AZT) were suspended in 0.5 ml of nitrogen purged water. The aqueous  $^{99m}\text{Tc}$ -pertechnetate ( $^{99m}\text{TcO}_4^-$ ) (40–100 MBq) was incorporated to them followed by addition of 25  $\mu$ l of aqueous stannous chloride dihydrate ( $\text{SnCl}_2 \cdot 2\text{H}_2\text{O}$ ) (2 mg/ml) solution. At room temperature, they were incubated for 15 min. The radiolabeled efficiencies were then assessed with the help of ascending thin layer chromatography by applying silica gel coated aluminum strips (Merck, Darmstadt, Germany) as stationary phase and methyl ethyl ketone as mobile phase. The sheets were dried after developing the spots and they were cut into five strips (1 cm each). These were analyzed quantitatively through counting using a well type gamma counter at 140 keV (Electronic Corporation of India, model LV4755, Hyderabad, India).

#### **Gamma scintigraphy**

For providing direct evidence of location of radiolabeled NLs as well as free drug within the body of experimental rats, gamma scintigraphy imaging was performed. Only male Sprague-Dawley rats (body weight 200–250 g) were utilized in this study. After dividing the total rats into three groups,  $^{99m}\text{Tc}$  labeled AZT/ $^{99m}\text{Tc}$  labeled MGF/ $^{99m}\text{Tc}$  labeled SYF was injected (100  $\mu$ l) through femoral vein of rats of the respective group. Using the intramuscular injection of ketamine hydrochloride (1 ml), rats were anesthetized and fixed on a board in the posterior position for imaging. At predetermined time interval (1 h and 5 h of post injection), static images were snapped with the help of planar gamma camera (GE Infinia Gamma Camera equipped with Xeleris Workstation, GE, Cleveland, OH).

#### **Biodistribution study**

Sprague-Dawley rats (body weight 200–250 g) were utilized for performing the biodistribution of radiolabeled AZT and NLs (MGF, SYF). By applying ketamine (30–50 mg/kg) intramuscularly, rats were anesthetized and cannulation was done in the femoral vein of animals using polyethylene (PE-50) catheter tubes. All the experimental animals were well-hydrated by administering (2 ml) normal saline (0.9% NaCl (w/v) in water) through intraperitoneal route for 1 h.  $^{99m}\text{Tc}$  labeled AZT/ $^{99m}\text{Tc}$  labeled MGF/ $^{99m}\text{Tc}$  labeled SYF was injected at 0.03 ml volume (10–15 MBq/kg) via intravenous (i.v.) route through the cannula. The animals were sacrificed at 1 h and 5 h post injection. The organs and tissues such as heart, liver, lung, spleen, muscle, intestine, stomach, kidney, and brain were removed followed by washing using normal saline. The collected organs and tissues were dried up immediately using blotting paper (if applicable) and taken into the preweighed counting vials. Blood was collected using heart



puncture process. With the help of a well-type gamma scintillation counter along with an injection standard, the corresponding radioactivity of the samples was measured and percentage of injected dose per gram (% ID per g) of tissue or organ was utilized for expressing the results.

### **In vivo plasma and brain pharmacokinetic study**

*In vivo* plasma and brain pharmacokinetic study was performed to compare the distribution of AZT from free drug suspension and NLS (MGF, SYF) and observe the ability of NLS to cross BBB in Sprague-Dawley rats. The animals were distributed into four groups. AZT suspension was injected in animals of one group through i.v. route as per dose. Another group of animals was injected MGF and the third group was treated with SYF intravenously with an equivalent amount of AZT with respect to free drug in suspension. Tail vein was selected to administer the injection for all animals of each batch. The fourth group remained as control (untreated). For plasma pharmacokinetic study, blood samples were collected by terminal cardiac puncture of each animal following anesthesia, at a predetermined time interval such as 0.25 h, 0.5 h, 1 h, 2 h, 4 h, 6 h, 8 h, 10 h, 12 h, 24 h, and 48 h of post i.v. injection and kept the sample immediately into a microcentrifuge tube having EDTA solution. For plasma collection, the blood samples were centrifuged at 5000 rpm for 6 min using cold centrifuge (HERMLE Labortechnik GmbH, Wehingen, Germany) and the plasma was preserved at  $-80^{\circ}\text{C}$  till further analysis (Dey et al., 2016).

For brain kinetic study, at a predetermined time interval (0.5 h, 1 h, 2 h, 4 h, 6 h, 8 h, 10 h, 12 h, and 24 h of post i.v. injection), rats were dissected and brains were separated followed by washing with Milli-Q water. *In situ* blood perfusion (Takasato et al., 1984) was done before collection of brain in the experiment. Then, the collected brains were kept into cryogenic tubes and stored at  $-80^{\circ}\text{C}$  till LC-MS/MS study.

### **LC-MS/MS study**

Evaluation of AZT concentration in plasma and brain was performed by using LC-MS/MS technique (Shaw et al., 2017). Briefly, plasma sample/homogenized brain tissue was first mixed with ice cold acetonitrile (plasma/tissue homogenate: cold acetonitrile was 1:3 by volume) containing internal standard followed by vortex-mixed for 10 min and centrifuged (at 4000 rpm for 15 min at  $4^{\circ}\text{C}$ ) for efficient extraction of AZT by protein precipitation method (Gautam et al., 2013). The supernatant for each sample was collected. The supernatant (100  $\mu\text{l}$ ) of each sample was mixed with 100  $\mu\text{l}$  water and loaded into LC-MS/MS (LC: Shimadzu Model 20AC, MS: AB-SCIEX, Model: API4000, Software: Analyst 1.6). Elution was done with the help of YMC Triat C18 column ( $2.1 \times 30\text{ mm}$ ,  $5\ \mu\text{m}$ ). Gradient elution technique of two mobile phases (mobile phase A: 0.1% formic acid in water and mobile phase B: 0.1% formic acid in 80:20 acetonitrile/water) was conducted with injection volume: 20  $\mu\text{l}$ , flow rate 0.8 ml/min and total run time was 3.0 min in each case.

### **Calculation of PK parameter**

AZT concentrations in plasma and brain were plotted against time. By utilizing NCA toolbox of Phoenix-WinNonlin software (Certara, Daresbury, UK), various PK parameters such as area under the concentration-time curve from time of injection to a determined time point ( $\text{AUC}_{0-t}$ ), area under the first moment curve ( $\text{AUMC}_{0-t}$ ), clearance (Cl), time taken for maximum blood concentration to drop in half-life ( $t_{1/2}$ ), steady state volume of distribution ( $V_{ss}$ ), mean residence time (MRT), etc. were determined.

### **Statistical analysis**

Statistical calculations of various data were conducted by applying one-way analysis of variance (ANOVA) through Tukey-Kramer's multiple comparisons test with the help of GraphPad InStat (version 3.06) software (La Jolla, CA). The probability value ( $p$ )  $< .05$  at 95% confidence interval was recognized as statistically significant.

## **Results**

### **FTIR analysis**

Drug-excipient interaction was investigated through FTIR spectroscopy to determine any interaction between the functional groups of drug (AZT) and the excipients of a formulation (Basu et al., 2012). When the FTIR spectra of the physical mixture of the drug and the excipients (ML, CHO) were compared with those of the physical mixture of the excipients without drug, the lyophilized formulation with or without drug and each of the excipients, the presence of the characteristic peaks of the drug (at  $2083\text{ cm}^{-1}$ ), ML (at  $2922\text{ cm}^{-1}$ , at  $2852\text{ cm}^{-1}$ , and at  $721\text{ cm}^{-1}$ ) and CHO (at  $1373\text{ cm}^{-1}$ ) was observed (Figure 1(B)).

Likewise, during the comparison of the FTIR spectra of the drug, SL and CHO, the presence of the characteristic peak of the drug was observed at  $2083\text{ cm}^{-1}$  in the physical mixture. The characteristic peaks of SL (at  $2928\text{ cm}^{-1}$  and at  $1462\text{ cm}^{-1}$ ) and CHO (at  $1373\text{ cm}^{-1}$ ) were also observed in the physical mixture of the drug and the excipients (Figure 1(B)).

The findings suggest the absence of any chemical interaction between the drug and the excipients for both the formulations (ML based, MGF and SL based, SYF). However, minor shifting of some of the peaks of the excipients in formulations (from  $2922\text{ cm}^{-1}$  to  $2920\text{ cm}^{-1}$ ,  $2852\text{ cm}^{-1}$  to  $2851\text{ cm}^{-1}$ , and from  $721\text{ cm}^{-1}$  to  $719\text{ cm}^{-1}$  in ML-based formulation and CHO from  $3415\text{ cm}^{-1}$  to  $3436\text{ cm}^{-1}$  in case of SL-based formulation) was observed. The observations suggest that physical interactions existed between the molecules of the excipients. The interaction might be responsible to provide the structure of the formulation and for sustained drug release from the formulations. In case of the ML formulation, the peak of the drug was not observed. The finding suggests that the drug was encapsulated entirely in the formulation and there was the absence of drug molecules on the surface of the formulation. For SL formulation, presence of the peak of the drug was found to shift from  $2084\text{ cm}^{-1}$

to  $2096\text{ cm}^{-1}$ . The finding indicates that the shifting of the peak of the drug might be due to physical interaction between the drug and the excipients. Further, the drug molecules were also present in the lipid bilayers and might retain in the formulation due to the physical interaction between the drug and the excipients.

In case of SL formulation, a shifting of wave number from  $2084\text{ cm}^{-1}$  to  $2096\text{ cm}^{-1}$  might be due to the formation of weak bond (such as hydrogen bond, van der Waals force of attraction or dipole moment) between methyl group of the drug and OH group of CHO. The wave number ranging from  $3415\text{ cm}^{-1}$  to  $3436\text{ cm}^{-1}$  is the strong intensity stretching vibration zone of OH group. The wave number ranging from  $2084\text{ cm}^{-1}$  to  $2096\text{ cm}^{-1}$  is the stretching vibration zone of C=C of the drug. Further, the wave number regions,  $2922\text{--}2920\text{ cm}^{-1}$  and  $2852\text{--}2851\text{ cm}^{-1}$ , are the strong intensity stretching vibration regions of  $\text{CH}_2$ , CH, and  $\text{CH}_3$  and the region  $721\text{--}719\text{ cm}^{-1}$  is the variable to weak intensity bending vibration region of out of plane OH bending. Hence, there might be physical interaction by formation of weak bonds (hydrogen bond, van der Waals force of attraction or dipole moment) responsible for minor shifting of peaks.

### Physico-chemical characterization of NLS

We initially varied the different process parameters such as temperature and speed of hydration, duration of sonication, time and speed of centrifugation, duration of freeze drying and ratio of the constituents to optimize the preparation process and to select the formulations. The best two formulations (MGF, SYF) were selected based on drug loading, particle size, zeta potential, FESEM, and Cryo-TEM data and investigated for further study.

### Percentage of drug loading and yield

The percentage of drug loading of MGF was  $5.7 \pm 0.37\%$  with  $60.87 \pm 5.92\%$  yield capacity but SYF had  $7.00 \pm 0.23\%$  drug loading with yield capacity of  $54.34 \pm 4.79\%$  (Supplementary Table 1). Every experiment was repeated thrice to establish the reproducibility.

### Size, size distribution, and zeta potential

Liposomal size, surface morphology, and the lamellarity of liposome have been assessed by particle size analyzer, FESEM, and Cryo-TEM, respectively. FESEM figures showed that the average size of the lyophilized liposome varied for MGF and SYF. When the liposomes were assessed by particle size analyzer, it showed the average size  $24.37 \pm 2.2\text{ nm}$  for MGF (Figure 2(A)) and  $33.75 \pm 3.7\text{ nm}$  for SYF (Figure 2(B)), with their PDI  $0.26 \pm 0.02$  and  $0.25 \pm 0.06$ , respectively. When the lamellarity was checked by Cryo-TEM, average size of the vesicles was found to be  $30.75 \pm 1.8\text{ nm}$  for MGF and  $40.43 \pm 2.4\text{ nm}$  for SYF with the intact lamellarity. The size was little bit higher as compared to the lyophilized liposome and the liposome analyzed by particle size analyzer. Since for Cryo-TEM analysis, the lyophilized liposomes were suspended for longer time as compared to particle size analysis by

particle size analyzer, the average size was enhanced marginally due to the entrapment of water in the core area of the liposomal vesicles. However, all the methods of analysis showed that the size was below  $50\text{ nm}$ . Zeta potential of both the formulations was observed as negative,  $-71.5 \pm 6.5\text{ mV}$  (Figure 2(C)) and  $-70.8 \pm 7.0\text{ mV}$  (Figure 2(D)) for MGF and SYF, respectively. The statistical analysis of data of average size for both the formulations and the variation in PDI showed that there was an insignificant variation ( $p > .05$ ) in size distribution, but a significant variation of particle size between MGF and SYF. MGF showed smaller size particles compared to SYF. Zeta potential showed nearly same value for both the formulations.

### FESEM study

Three images of FESEM at different magnifications namely  $60,000\times$ ,  $120,000\times$ , and  $300,000\times$  were captured for MGF to establish the shape, size, and distribution pattern of the formulation. The MGF had nanosize structure with smooth surface and was homogeneously distributed at  $60,000\times$  and  $120,000\times$  magnification (Figure 2(E,F)). At  $300,000\times$  magnification, MGF was found to be spherical structure having nanosize with smooth surface and a homogeneous distribution pattern (Figure 2(G)). The FESEM image at  $100,000\times$  magnification of SYF revealed that the liposomes were also in nanosize (about  $30\text{ nm}$ ), spherical shape with smooth surface and homogenous distribution (Figure 2(H)).

### Cryo-TEM study

Cryo-TEM study was performed to visualize the internal structure of NLS. Nanosize unilamellar vesicles were found in the Cryo-TEM images for both the types of NLS (Figure 2(I,J)). MGF had smaller size lyophilized vesicles than the size of SYF vesicles.

### In vitro investigations

#### In vitro drug release study

*In vitro* drug release study was conducted for both the formulations (MGF and SYF) to compare *in vitro* drug release patterns of both the formulations in two different release media. The data were plotted as percentage of cumulative drug release against time measured in hour (h) (Figure 2(K,L)). From the results, it appeared that cumulative  $73.43\%$  and cumulative  $82.21\%$  of AZT released from MGF in phosphate buffer media and in  $50\%$  serum, respectively, whereas cumulative  $82.48\%$  (phosphate buffer as media) and cumulative  $84.51\%$  ( $50\%$  serum as media) of AZT released from SYF over a period of 24 h. Drug release was to an extent slower from MGF than SYF. However, a steady and sustained drug release pattern was observed for both the formulations.

#### Drug release kinetics analysis

To understand the drug release kinetic patterns, data were plotted using various kinetic equations and the

corresponding correlation coefficients (represented here as  $R^2$  values) were determined (Supplementary Table 2). Data gave good linearity in Korsmeyer–Peppas's kinetic model for both the formulations [ $R^2 = 0.9742$  (phosphate buffer as drug release media) and  $R^2 = 0.9780$  (50% serum as drug release media) for MGF and  $R^2 = 0.9752$  (phosphate buffer as drug release media) and  $R^2 = 0.9751$  (50% serum as drug release media) for SYF] as compared to the other kinetic models tested. The release exponent values ( $n$ ) were 0.8387 and 0.8561 for MGF and SYF in phosphate buffer drug release media where as in 50% serum ' $n$ ' values were 0.7539 for MGF and 0.8179 for SYF, respectively. The ' $n$ ' values indicated non-Fickian diffusion pattern of release of drug from NLs in both types of drug release media.

### In vitro cellular uptake study

*In vitro* cellular uptake study of NLs was conducted in U-87 MG human glioblastoma cells by using fluorescent NLs to inspect the uptake ability of NLs in brain cells using confocal microscopy. From the results, it revealed that both the types of fluorescent NLs (FITC-MGF, FITC-SYF) were internalized by the cells (Figure 3(A,B)) and were localized in cytoplasm as well as nucleus. Cellular uptake of FITC-MGF increased with time till 3 h of the study (Figure 3(A)). However, for FITC-SYF, the cellular uptake was more in 1 h than 0.25 h and then decreased at 3 h (total duration of the study) (Figure 3(B)). By both confocal and conventional fluorescence microscopies, FITC treated cells were shown to internalize FITC in a time-dependent manner (Cole et al., 1990). Thus, addition of FITC in media alone as a control

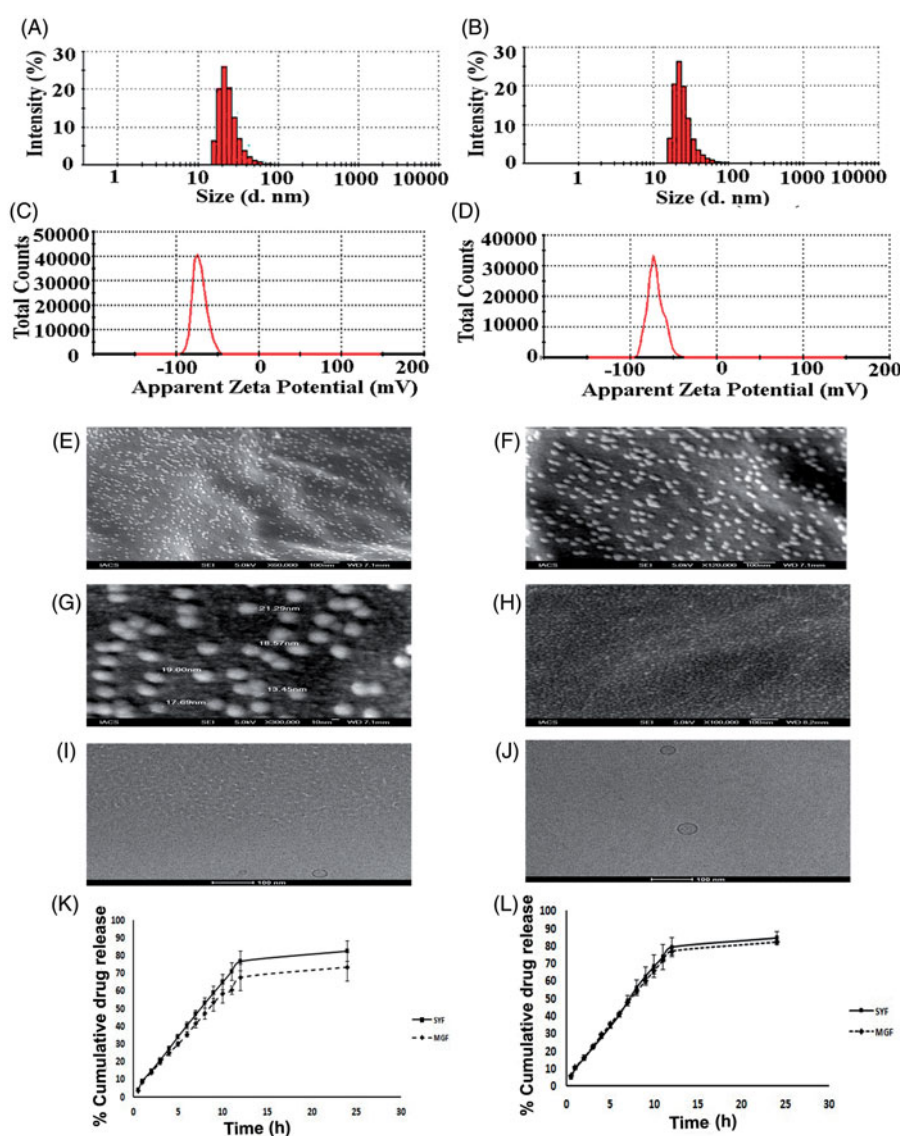


**Figure 2.** Particle size distribution of (A) MGF and (B) SYF. Zeta potential of (C) MGF and (D) SYF. Field emission scanning electron microscopy (FESEM) images of (E) MGF at magnification of 60,000 $\times$ , (F) MGF at magnification of 120,000 $\times$ , (G) MGF at magnification of 300,000 $\times$ , (H) SYF at magnification of 100,000 $\times$ . Cryo-transmission electron microscopy (Cryo-TEM) images of (I) MGF and (J) SYF. Scale bar for Cryo-TEM image: 100 nm. (K) *In vitro* drug release profiles of MGF and SYF in phosphate buffer (pH 7.4). (L) *In vitro* drug release profiles of MGF and SYF in 50% serum. Data show mean  $\pm$  SD ( $n = 3$ ). SD: standard deviation.

sample to treat cells would provide results which can mislead the actual findings of the FITC-labeled formulations. Hence, no FITC control was run.

### Stability study

FTIR spectra of the stored NLs (MGF, SYF) were compared with those of the freshly prepared formulations. No distinguish changes in spectrum were observed for the formulations stored at 4 °C. However, NLs stored at 25 °C showed the deformation of structure (data not shown), although drug assay results did not significantly vary the quantity of drug loaded in the formulation. Further, FTIR, DSC (Supplementary Figure 1), UV-visible spectroscopy, LC-MS/MS analysis of free drug, encapsulated drug and drug released showed that drug remained in the active form after encapsulation and released, and in the same active form.

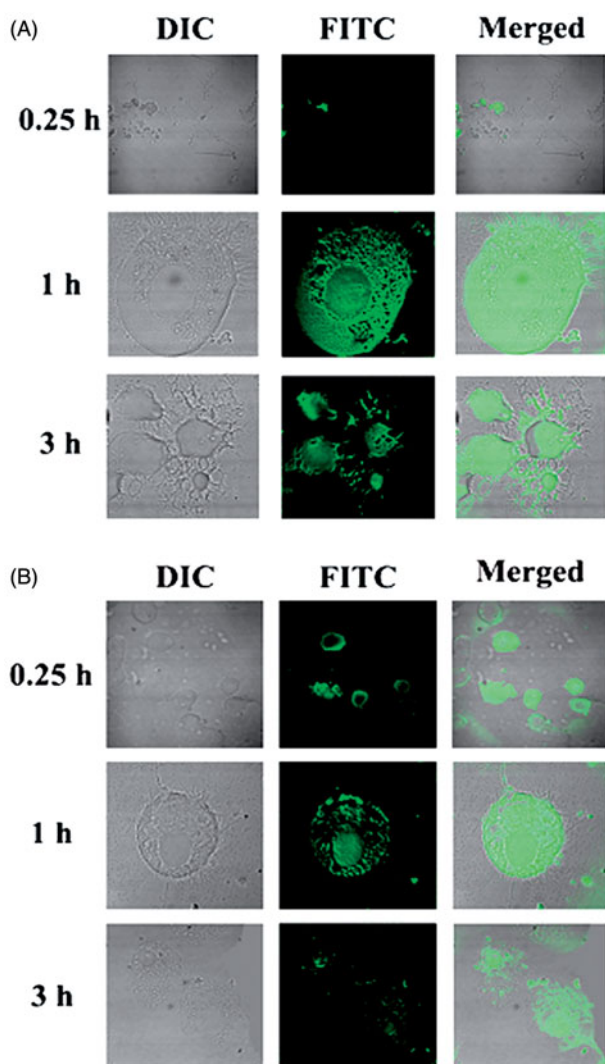


**Figure 3.** Investigation of *in vitro* cellular uptake of MGF and SYF by confocal microscopy. (A) *In vitro* cellular uptake study of fluorescein isothiocyanate labeled MGF (FITC-MGF) in U-87 MG human glioblastoma cells at various time points (0.25 h, 1 h, 3 h). (B) *In vitro* cellular uptake study of fluorescein isothiocyanate labeled SYF (FITC-SYF) in U-87 MG human glioblastoma cells at various time points (0.25 h, 1 h, 3 h). DIC: differential interference contrast images of U-87 MG human glioblastoma cells.

### In vivo analysis

#### Gamma scintigraphy

The gamma scintigraphy was performed to investigate the ability of the NLs to cross BBB after the administration of  $^{99m}\text{Tc}$  labeled MGF,  $^{99m}\text{Tc}$  labeled SYF and  $^{99m}\text{Tc}$  labeled free drug (AZT) in different groups of Sprague-Dawley rats, respectively. The radioactivity signals were observed (Figure 4) and assessed in brain as well as in different organs (Supplementary Table 3) of the experimental animals which received radiolabeled NLs/AZT. The study showed that NLs were able to cross BBB and reached in brain. In animals treated with radiolabeled MGF, the intensity of signals in brain tissue was higher at 1 h as compared to 5 h (Figure 4(I)). The signals were stronger in brain at 1 h than 5 h in the animals received radiolabeled SYF (Figure 4(II)). At 5 h, the signals were stronger in the brain tissue of animals treated with radiolabeled MGF compared to radiolabeled SYF. In  $^{99m}\text{Tc}$  labeled free drug (AZT)-treated animals, very weak signal was noticed at 1 h and 5 h in brain tissue (Figure 4(III)) which indicated poor permeation of free AZT through BBB.

#### Biodistribution study

Biodistribution studies were conducted by administering  $^{99m}\text{Tc}$  labeled MGF,  $^{99m}\text{Tc}$  labeled SYF, and  $^{99m}\text{Tc}$  labeled free drug (AZT) in Sprague-Dawley rats through i.v. route at 1 h and 5 h after injection. In different organs including brain, accumulation of radiolabeled NLs as well as free drug was measured and data were reported as percentage of injected dose per gram (% ID per g) of tissue or organ (Supplementary Table 3). The values of residence time of radiolabeled formulation MGF/SYF in blood were 2.90-fold, 3.09-fold higher at 1 h and 4.08-fold, 3.94-fold greater than that of radiolabeled AZT at 5 h, respectively. On the other hand, kidney accumulation was distinctively more in free drug than NLs at 1 h as well as 5 h. Further, at 1 h, kidney accumulation of radiolabeled SYF was 2.75 time less than MGF but at 5 h this was 31.91% higher as compared to MGF. Enhancement of brain uptake values (by 18 folds and 19 folds, respectively, at 1 h and 36 times and 23 times, respectively, at 5 h, for MGF and SYF) was observed as compared to the brain uptake values of labeled AZT at those respective time points. Although brain uptake of  $^{99m}\text{Tc}$  labeled MGF was slightly less in values than those of SYF at 1 h but it was 56.52% higher compared to SYF at 5 h (Supplementary Table 3). For this reason, brain/blood ratio was 0.48 for MGF at 5 h which was greater than the value at 1 h whereas it was 0.32 for SYF at 5 h. Brain/blood ratio was predominantly higher for NLs compared to free AZT (Supplementary Table 3).

#### In vivo plasma pharmacokinetic study

The plasma pharmacokinetic study was performed to observe the changes of pharmacokinetic parameters in Sprague-Dawley rats after i.v. administration of MGF/SYF/free AZT suspension. The mean plasma concentration of

drug from MGF/SYF was higher than that of AZT in animals which had received AZT suspension, at the different experimental time points. The plasma concentration of AZT from MGF was comparatively higher than that of SYF after 4 h (Figure 5(A)).  $AUC_{0-t}$  value for MGF was reasonably greater than those of SYF as well as free drug suspension (Table 1).  $AUMC_{0-t}$  values of drug in rats received MGF/SYF were 13.76-fold/8.25-fold respectively greater than  $AUMC_{0-t}$  value as detected in animals received free drug suspension. Half-life ( $t_{1/2}$ ) value of AZT from MGF was 8.44-fold higher than that of free AZT suspension and 1.27-fold higher than that of SYF, suggesting a predominantly sustained drug release from MGF. MRT values were 5.10-fold and 3.25-fold higher for MGF and SYF respectively than the MRT value found in rats treated with AZT suspension. This suggests maximally prolonged blood residence time of MGF among the experimental formulations. A predominant variation in  $V_{ss}$  values was also noticed for MGF (about two times greater than the value obtained from rat treated with AZT suspension and 1.5 times greater than the value obtained from rat treated with SYF). There was 63.21% decreased clearance of AZT from MGF as compared to free AZT suspension. Data revealed that MGF provided most favorable pharmacokinetic profile of AZT as compared to SYF and free AZT suspension.

### In vivo brain pharmacokinetic study

Till 24 h (the total duration of the study), AZT level was detectable in brain from MGF/SYF (Figure 5(B)). However, AZT could not be detected in the brain of rats treated with AZT suspension after 10 h of the study. AZT level in brain was found to be maximum from SYF followed by MGF in 0.5 h. The values were five- and four-fold higher respectively as compared to the values detected in animals treated with AZT suspension at 0.5 h. AZT level was 25% higher in the brain of rats treated with SYF as compared to MGF at 0.5 h. With the increasing duration of time, AZT levels were decreasing in all the cases. Interestingly, at 4 h of the investigation the values of AZT concentration in brain were almost same in rats treated with SYF/MGF. However, from then on, till 24 h of the study, AZT levels in brain were found to be more (46.76% more in value at 6 h, 263.75% more in value at 24 h) in rats treated with MGF as compared to those treated with SYF. Treatment of AZT through MGF enhanced  $AUMC_{0-t}$  value by 50.99% and MRT value by 49.14% as compared to the rats treated with SYF. The data were also substantiated by clearance values (Table 1).

### Discussion

The present investigation was intended to understand the capability of ML to act as base material of lipid nanocarrier

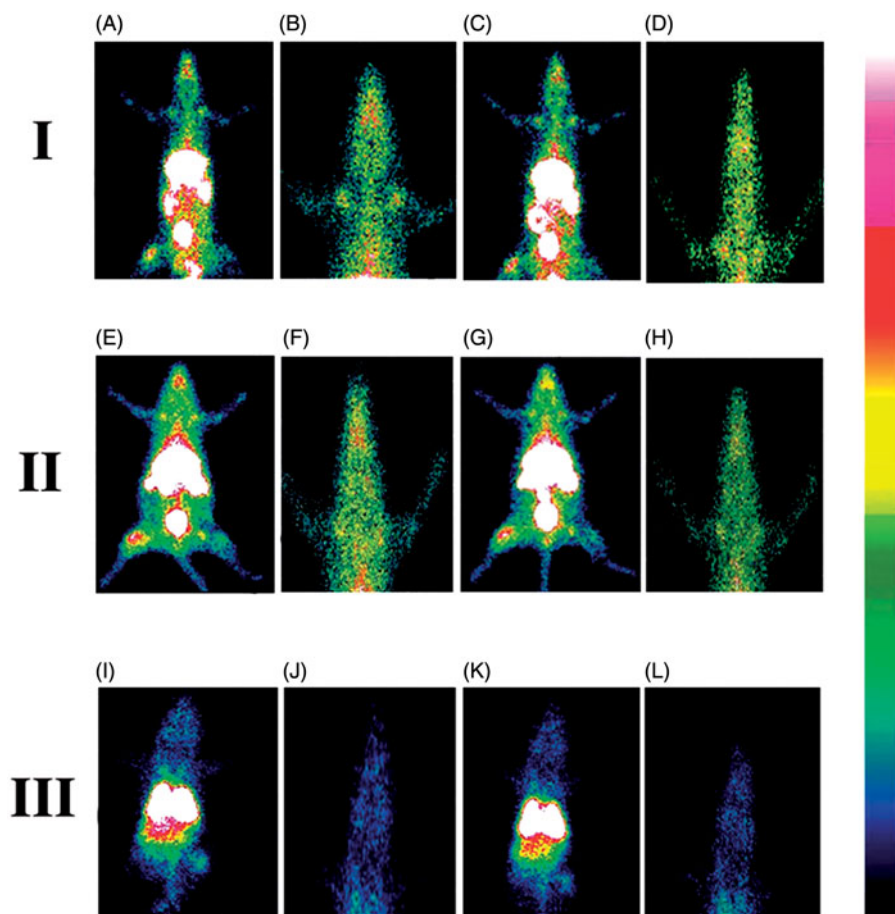


**Figure 4.** Gamma scintigraphy images of rats after receiving radiolabeled MGF/radiolabeled SYF/radiolabeled AZT. (I) rats received  $^{99m}\text{Tc}$  labeled MGF at 1 h (A, B) and at 5 h (C, D) post i.v. injection; (II) rats received  $^{99m}\text{Tc}$  labeled SYF at 1 h (E, F) and at 5 h (G, H) post i.v. injection; (III) rats received  $^{99m}\text{Tc}$  labeled free drug at 1 h (I, J) and at 5 h (K, L) post i.v. injection. A, C, E, G, I, and K are whole animal image; B, D, F, H, J, and L are magnified brain part.

to deliver water soluble drug through BBB to brain. Continuous tight junctions of endothelial cells of brain capillaries and several transmembrane proteins seal the paracellular pathways and effectively block the free diffusion of polar solutes (such as AZT) from blood along these potential paracellular pathways, causing denial of access to brain interstitial fluid (Ballabh et al., 2004; Abbott, 2005). Blood–brain barrier

predominantly impedes entry from blood to brain of virtually all molecules, other than those that are small and lipophilic (e.g. nanoliposome) or those (such as essential nutrients, precursors and cofactors) that enter the brain through active transport mechanism (Alavijeh et al., 2005; Agrawal et al., 2017). Thus, lipophilicity and size of nanoliposome tend to lead higher permeation across BBB as compared to the polar drug or comparatively polar phospholipid vesicles. Since AZT is a highly water soluble drug that does not cross BBB efficiently (Rautio et al., 2008; Weiss et al., 2009) and the nano-size lipid vesicles have been shown to permeate through BBB effectively (Masserini, 2013; Vieira & Gamarra, 2016; Li et al., 2017), we developed two types of NLs (MGF and SYF) applying lipid layer hydration technique by using ML/SL. A comparative physicochemical and biopharmaceutical analysis on those two types of formulations were also performed.

FTIR data analysis revealed that there was no chemical interaction between the drug and the excipients. However, there were some physical interactions between the drug and excipients and between the molecules of excipients. Such physical interactions might have a role to form the spherical nanostructure of the drug carrier (Rudra et al., 2010) and to retain the drug in the lipid layer, causing slower diffusion of drug through the membrane (Rudra et al., 2010). Again, absence of peak of AZT in the lyophilized ML-based NLs was due to the entire encapsulation of AZT in the formulation. Presence of peak of AZT in SYF suggests the availability of free drug on the surface of the formulation.

Various process parameters such as temperature and speed of hydration, duration of sonication, time and speed of centrifugation, duration of freeze drying and ratio of the constituents were optimized to develop formulations with maximum drug loading, homogeneous and uniform particle size, desirable zeta potential value and smooth surface structure, among the experimental formulations. Out of the various experimental formulations, the best optimized formulation of each category (MGF/SYF) was selected and reported here.

Lower drug loading was observed in MGF as compared to SYF. AZT is a highly water soluble drug (Singh et al., 2010; Nath et al., 2011). SYF had hydrophobic phospholipid

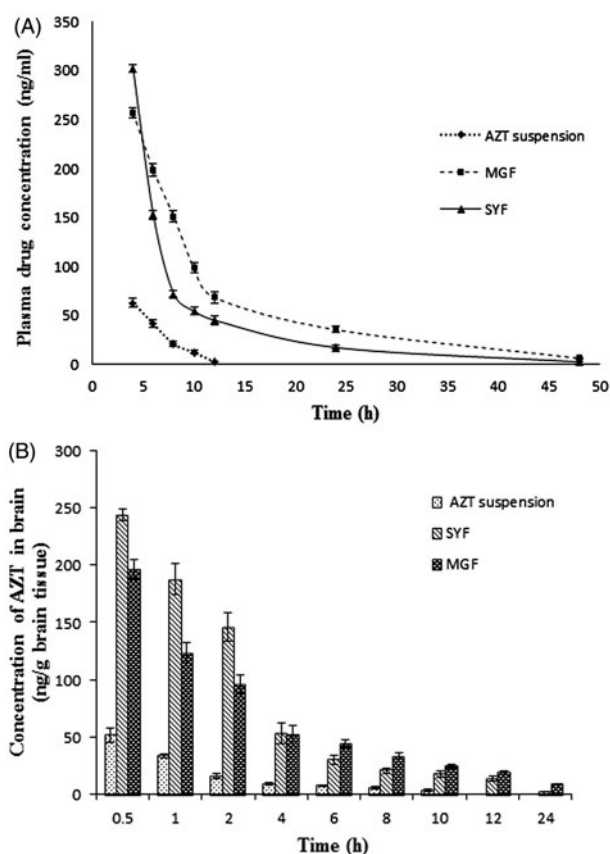


**Figure 5.** *In vivo* pharmacokinetic parameters in plasma and brain. (A) Plasma concentration of AZT–time profiles after i.v. administration of MGF/SYF/free drug (AZT) suspension in rats. (B) Concentration of AZT in brain after i.v. administration of MGF/SYF/AZT suspension in rats represented by bar diagram. Data showed mean  $\pm$  SD ( $n = 3$ ). SD of each point was represented by error bar. SD: standard deviation represented by deviation bar.

**Table 1.** Plasma and brain pharmacokinetic parameters of AZT after i.v. administration of MGF/SYF/free drug (AZT) suspension in rats.

Pharmacokinetic parameters	AZT suspension	MGF	SYF
<b>Plasma pharmacokinetic profile</b>			
$t_{1/2}$ (h)	1.15 $\pm$ 0.04	9.71 $\pm$ 0.21 <sup>a,b</sup>	7.64 $\pm$ 0.08 <sup>a</sup>
AUC <sub>0–t</sub> (h ng ml <sup>–1</sup> )	2003.27 $\pm$ 24.63	5405.57 $\pm$ 151.03 <sup>a</sup>	5107.23 $\pm$ 153.91 <sup>a</sup>
AUMC <sub>0–t</sub> (h <sup>2</sup> ng ml <sup>–1</sup> )	2529.70 $\pm$ 188.70	34806.50 $\pm$ 2475.71 <sup>a,b</sup>	20881.90 $\pm$ 1198.92 <sup>a</sup>
Cl (L h <sup>–1</sup> kg <sup>–1</sup> )	2.99 $\pm$ 0.04	1.10 $\pm$ 0.03 <sup>a</sup>	1.17 $\pm$ 0.03 <sup>a</sup>
MRT (h)	1.26 $\pm$ 0.08	6.43 $\pm$ 0.28 <sup>a,b</sup>	4.09 $\pm$ 0.24 <sup>a</sup>
$V_{ss}$ (L kg <sup>–1</sup> )	3.83 $\pm$ 0.19	7.88 $\pm$ 0.19 <sup>a,b</sup>	5.03 $\pm$ 0.38 <sup>a</sup>
<b>Brain pharmacokinetic profile</b>			
AUC <sub>0–t</sub> (h ng ml <sup>–1</sup> )	141.17 $\pm$ 12.08	888.23 $\pm$ 28.67 <sup>a</sup>	875.73 $\pm$ 53.86 <sup>a</sup>
AUMC <sub>0–t</sub> (h <sup>2</sup> ng ml <sup>–1</sup> )	386.53 $\pm$ 35.11	5396.33 $\pm$ 236.87 <sup>a,b</sup>	3574.03 $\pm$ 290.51 <sup>a</sup>
MRT (h)	2.73 $\pm$ 0.06	6.07 $\pm$ 0.15 <sup>a,b</sup>	4.07 $\pm$ 0.06 <sup>a</sup>
Cl (L h <sup>–1</sup> kg <sup>–1</sup> )	37.33 $\pm$ 4.66	5.9 $\pm$ 0.17 <sup>a</sup>	6.73 $\pm$ 0.35 <sup>a</sup>

$t_{1/2}$ : half-life; AUC<sub>0–t</sub>: area under the concentration–time curve from time of injection ( $t = 0$ ) to a determined time point; AUMC<sub>0–t</sub>: area under the first moment curve; Cl: clearance; MRT: mean residence time;  $V_{ss}$ : steady state volume of distribution.

Note: Data were expressed as mean  $\pm$  SD of three separate observations.

<sup>a</sup>Data were significantly different ( $p < .05$ ) where MGF and SYF were compared with AZT suspension. It was assessed by one-way analysis of variance (ANOVA) through Tukey–Kramer’s multiple comparisons test.

<sup>b</sup>Data were significantly different ( $p < .05$ ) where MGF was compared with SYF. It was assessed by one-way analysis of variance (ANOVA) through Tukey–Kramer’s multiple comparisons test.

and CHO. Presence of phosphate group in SL makes it comparatively more hydrophilic than ML (Jones, 2008). Presence of SA, OA, and PA possibly caused comparatively less partitioning of drug into the lipid layer causing less drug loading in MGF. Yield of SYF was nearly about 6% less as compared to MGF and the possible reason may be the recovery problem due to slightly stickiness of SYF for presence of SL (Das et al., 2015).

Nanosize SYF had larger size (38.49% larger) than MGF. This could be because of the presence of phospholipid in SYF. Phospho moiety owing to the hydrophilic nature of the phosphate group (Jones, 2008) might have been pulled with more tension by water molecules toward the bulk of the liquid during the formation of the liposomal structure, resulting in comparatively larger size. PDI values of both the formulations were nearly similar. PDI value is a very crucial indicator for size distribution, stability, and uniformity of NLS (Masarudin et al., 2015). Lower PDI value signifies more monodisperse pattern with better stability of NLS. On the other hand, higher PDI value indicates aggregation of particles with low stability (Masarudin et al., 2015). The PDI value 0.1–0.25 is desirable for uniform distribution but the value more than 0.5 is an indication of poor homogeneity (Gharib et al., 2014). In our study, both the formulations were mostly uniform in size and homogeneously distributed. Zeta potential is also considered as a parameter for confirmation of physical stability (Dey et al., 2016; Shaw et al., 2017). If electric charge of NLS surface is high, then zeta potential of NLS will also show high value. This means strong repellent forces among the vesicles of NLS are able to inhibit agglomeration of NLS in suspension. Normally, zeta potential value (more than +30 mV or less than –30 mV) indicates good stability of NLS in colloidal dispersion (Dey et al., 2016). In our study, nearly similar zeta potential values (about –70 mV) were achieved for MGF and SYF. This denotes that both the formulations had prolonged and better physical stability in colloidal suspension. The negatively charged NLS are removed slowly than the positive one, which suggests longer blood residence time of negatively charged drug carriers (Satapathy et al., 2016). Thus, both the experimental formulations are expected to possess extended blood residence time.

FESEM provides information related to 3D structure as well as surface property (Tripathi et al., 2017). FESEM study reveals that both the formulations had spherical structure with smooth surface and they were homogeneously distributed with nonappearance of any agglomerate.

The Cryo-TEM images show that MGF/SYF had unilamellar spherical nanosize structure with an intact lamellarity. Lipid layer was present at the external side and aqueous part was enclosed by the lipid layer. Dark spot in the inner aqueous core and dark outer layer revealed the presence of hydrophilic drug in a suspended condition in the aqueous core as well as in the outer lipid layer.

Drug was found to release in a slower and more sustained manner from MGF compared to SYF in both types of drug release media. This could be due to the lipid composition of the NLS. SYF fundamentally consisted of phospholipid which contains polar phosphoryl and basic groups and they make the phospholipid more hydrophilic (Jones, 2008) than the ML which does not contain any phospholipid. Since AZT is a

highly water soluble drug (Singh et al., 2010; Nath et al., 2011), it seems to permeate more through phospholipid than the ML.

The drug release pattern from both the NLS in phosphate buffer media as well as 50% serum was best fitted (based on  $R^2$  value) with Korsmeyer–Peppas's kinetic model. Release component ( $n$ ) value suggests for an anomalous non-Fickian diffusion pattern of drug molecules (Pattnaik et al., 2012). Further, Korsmeyer–Peppas's kinetic model suggests that AZT release from the experimental NLS followed diffusion and erosion process (Pattnaik et al., 2012).

Cellular uptake of both the NLS in U-87MG human glioblastoma cells showed that NLS were localized in the cytoplasm and in the nucleus after internalization by the cells. But FITC-MGF was intense in cells in a time dependent manner whereas FITC-SYF concentration in cells initially increased (at 1 h as investigated) and then decreased with the time (at 3 h, total duration of the investigation). Possibly phospholipid vesicles were metabolized faster than MGF by glioma cells (Carnielli et al., 1998; Klein, 2002).

At 4°C, absence of changes in spectra for formulations indicates that there was no physico-chemical reaction occurred between the drug and the excipients during storage condition. So, drug remains as a stable form in stored formulation during storage condition at 4°C. At 25°C, although FTIR spectra did not significantly vary for the experimental formulations, the deformity of structures of NLS forced us to reject the consideration of 25°C to store the formulation. However, drug assay showed that the drug was stable in the formulation at 25°C.

We performed gamma scintigraphic investigation and brain pharmacokinetic study to compare the capability of MGF and SYF to cross BBB. Gamma scintigraphic images gave clear picture of localization of radiolabeled NLS/radiolabeled AZT in whole body of the experimental rats. From the gamma scintigraphic images, it revealed that both the radiolabeled NLS were capable to cross BBB and reached in brain. The intensity of signal in brain was stronger at 1 h as compared to 5 h for both MGF and SYF (as observed from signal intensity bar given with the photograph). At 5 h, the signal intensity of MGF in brain was more pronounced than that of SYF, suggesting longer retention of radiolabeled MGF than radiolabeled SYF in brain after crossing BBB. Very weak signal at 1 h and 5 h for  $^{99m}\text{Tc}$  labeled free drug (AZT) signifies poor ability of AZT to cross BBB. Both the NLS successfully crossed BBB possibly due to their nano-vesicular structure (Li et al., 2017) and longer retention of MGF in brain compared to SYF might be due to the variable lipid characteristics of MGF than SYF which had phospholipid in its structure.

In biodistribution study, radiolabeled MGF obtained from brain/blood ratio maintained its level persistently as compared to radiolabeled SYF, suggesting MGF was able to provide sustaining drug level in brain and blood better than SYF. Application of MGF showed presence of more amount of drug in brain with the increasing duration of the experiment as compared to that of SYF owing to an increased presence of MGF in brain. The presence of more MGF in brain/blood ratio as compared to SYF might be due to the sustained drug release and less clearance of drug through

liver and kidney as compared to those of SYF. Predominant hepatic clearance of free AZT is also noteworthy to mention. The investigation reported that it is possible for a compound to possess a long half-life in blood, but a short half-life in brain or even not to permeate BBB at all (Dawson et al., 2001). Hence, if a drug or formulation remains longer time in blood, it does not necessarily provide enhanced brain level of the drug (Dawson et al., 2001; Vieira & Gamarra, 2016). On the other hand, almost all things injected in blood must go into liver and liver does not have any barrier like BBB. Hence, the access of drug/formulation takes place much faster with a greater amount in liver than brain. Thus, MGF can tackle the short elimination half-life, low bioavailability, frequent dosing and dose-dependent toxicity of AZT (Mandal & Tenjarla, 1996; Blum et al., 1988; Oh et al., 1998; Thomas & Panchagnula, 2003) more effectively than SYF.

After i.v. administration, at 4 h, SYF showed more drug level in blood as compared to MGF. It dropped sharply with the increasing duration till 8 h which indicates rapid distribution of SYF compared to MGF. However, MGF showed slow distribution and significantly ( $p < .05$ ) longer blood residence time as compared to SYF which also increased  $t_{1/2}$  value of AZT.  $AUC_{0-48}$  and  $AUMC_{0-48}$  were significantly more for MGF. It could be due to the longer MRT and less renal clearance of MGF compared to SYF. Reports suggest that longer MRT and less renal clearance increase AUMC and AUC (Dey et al., 2016; Satapathy et al., 2016).

Drug concentration in brain was initially 25% more for SYF than MGF. The drug level in brain from MGF/SYF eventually reduced with the duration. At 4 h, the drug level in brain from MGF/SYF was more or less same. Interestingly, brain drug concentration from SYF dropped sharply after 4 h whereas it dropped in a much slower manner for MGF till 24 h of the study where brain drug level was about 260% more than that obtained from SYF. One of the most important features of brain is that it is completely separated from blood by BBB. In our study, blood perfusion was done before collection of brain from the animals to estimate drug in brain. Blood perfusion precludes the presence of drug in brain vasculatures and rather suggests its accumulation in brain, as drug has to cross BBB to reach brain endothelial cells (Ballabh et al., 2004; Abbott, 2005; Alavijeh et al., 2005). Thus, *in situ* perfusion provides a measure of brain uptake and the brain/plasma ratio of the drug (as done in the present study) provides a partial measure (Takasato et al., 1984; Abbott, 2005; Alavijeh et al., 2005). Since both the studies have been done, it supports that drug reached in brain. It is also an indicative of cross of the drug-loaded formulations through BBB. Sustained drug release, less clearance, and enhanced MRT of MGF in brain could be responsible for such enhancement. These further reflected in the enhanced availability of drug in brain from MGF compared to SYF. Lipid composition of MGF might be responsible for such variation.

## Conclusions

In the study, nanosize drug delivery systems were developed successfully utilizing ML/SL to deliver AZT in brain across BBB.

Both the formulations had sustained drug release profiles. *In vivo* gamma scintigraphy study and brain pharmacokinetic investigation revealed that both the formulations sufficiently reached brain through BBB, but MGF had better pharmacokinetic profile than that of SYF with respect to sustained drug release, prolonged blood residence time as well as brain residence time and increased  $t_{1/2}$ . Thus, ML may be utilized as a new and effective carrier material to deliver AZT effectively in brain. ML could be an emerging pharmaceutical for developing various therapeutic strategies to deliver drugs to brain and other organs. However, further studies are warranted in the area.

## Disclosure statement

The authors declare that the content of this article has no conflict of interest.

## Funding

The authors are very grateful to the Department of Biotechnology (DBT), Govt. of India, for providing the financial support (sanction no. BT/504/NE/TBP/2013) to execute this work.

## ORCID

Biswajit Mukherjee  <http://orcid.org/0000-0002-7854-9680>

## References

- Abbott NJ. (2005). Dynamics of CNS barriers: evolution, differentiation, and modulation. *Cell Mol Neurobiol* 25:5–23.
- Agrawal M, Ajazuddin, Tripathi DK, et al. (2017). Recent advancements in liposomes targeting strategies to cross blood–brain barrier (BBB) for the treatment of Alzheimer's disease. *J Control Release* 260:61–77.
- Akbarzadeh A, Rezaei-Sadabady R, Davaran S, et al. (2013). Liposome: classification, preparation, and applications. *Nanoscale Res Lett* 8:102.
- Alavijeh MS, Chishty M, Qaiser MZ, et al. (2005). Drug metabolism and pharmacokinetics, the blood–brain barrier, and central nervous system drug discovery. *Neurotherapeutics* 2:554–71.
- Ballabh P, Braun A, Nedergaard M. (2004). The blood–brain barrier: an overview: structure, regulation, and clinical implications. *Neurobiol Dis* 16:1–13.
- Basu S, Mukherjee B, Chowdhury SR, et al. (2012). Colloidal gold-loaded, biodegradable, polymer-based stavudine nanoparticle uptake by macrophages: an *in vitro* study. *Int J Nanomedicine* 7:6049–61.
- Bergshoeff AS, Fraaij PLA, Verweij C, et al. (2004). Plasma levels of zidovudine twice daily compared with three times daily in six HIV-1-infected children. *J Antimicrob Chemother* 54:1152–4.
- Blum MR, Liao SH, Good SS, Miranda P. (1988). Pharmacokinetics and bioavailability of zidovudine in humans. *Am J Med* 85:189–94.
- Carnielli VP, Verlato G, Pederzini F, et al. (1998). Intestinal absorption of long-chain polyunsaturated fatty acids in preterm infants fed breast milk or formula. *Am J Clin Nutr* 67:97–103.
- Christopher GVP, Raghavan CV, Siddharth K, et al. (2014). Formulation and optimization of coated PLGA – zidovudine nanoparticles using factorial design and *in vitro* *in vivo* evaluations to determine brain targeting efficiency. *Saudi Pharm J* 22:133–40.
- Cole L, Coleman J, Evans D, Hawes C. (1990). Internalisation of fluorescein isothiocyanate and fluorescein isothiocyanate-dextran by suspension-cultured plant cells. *J Cell Sci* 96:721–30.
- Das PJ, Paul P, Mukherjee B, et al. (2015). Pulmonary delivery of voriconazole loaded nanoparticles providing a prolonged drug level



- in lungs: a promise for treating fungal infection. *Mol Pharm* 12:2651–64.
- Dawson DA, Wadsworth G, Palmer AM. (2001). A comparative assessment of the efficacy and side effect liability of neuroprotective compounds in experimental stroke. *Brain Res* 892:344–50.
- Dey NS, Mukherjee B, Maji R, Satapathy BS. (2016). Development of linker-conjugated nanosize lipid vesicles: a strategy for cell selective treatment in breast cancer. *Curr Cancer Drug Targets* 16:357–72.
- Fox CB, Mulligan SK, Sung J, et al. (2014). Cryogenic transmission electron microscopy of recombinant tuberculosis vaccine antigen with anionic liposomes reveals formation of flattened liposomes. *Int J Nanomedicine* 9:1367–77.
- Gautam N, Bathena SPR, Chen Q, et al. (2013). Pharmacokinetics, protein binding, and metabolism of a quinoxaline urea analog as a NF- $\kappa$ B inhibitor in mice and rats by LC–MS/MS. *Biomed Chromatogr* 27:900–9.
- Gharib A, Faezizadeh Z, Namin SARM, Saravani R. (2014). Preparation, characterization and *in vitro* efficacy of magnetic nanoliposomes containing the artemisinin and transferrin. *Daru* 22:44.
- Hu K, Li J, Shen Y, et al. (2009). Lactoferrin-conjugated PEG-PLA nanoparticles with improved brain delivery: *in vitro* and *in vivo* evaluations. *J Control Release* 134:55–61.
- Hu X, Yang F, Liao Y, et al. (2017). Cholesterol-PEG comodified poly (N-butyl) cyanoacrylate nanoparticles for brain delivery: *in vitro* and *in vivo* evaluations. *Drug Deliv* 24:121–32.
- Ivey NS, MacLean AG, Lackner AA. (2009). Acquired immunodeficiency syndrome and the blood–brain barrier. *J Neurovirol* 15:111–22.
- Jain S, Tiwary AK, Jain NK. (2008). PEGylated elastic liposomal formulation for lymphatic targeting of zidovudine. *Curr Drug Deliv* 5:275–81.
- Jones ML. (2008). Lipids. In: Bancroft JD, Gamble M, eds. *Theory and practice of histological techniques*. Philadelphia: Churchill Livingstone Elsevier, 187–216.
- Kittiphoom S. (2012). Utilization of mango seed. *Int Food Res J* 19:1325–35.
- Klein CJ. (2002). Nutrient requirements for preterm infant formulas. *J Nutr* 132:1395S–577S.
- Li X, Tsibouklis J, Weng T, et al. (2017). Nano carriers for drug transport across the blood–brain barrier. *J Drug Target* 25:17–28.
- Maji R, Dey NS, Satapathy BS, et al. (2014). Preparation and characterization of tamoxifen citrate loaded nanoparticles for breast cancer therapy. *Int J Nanomedicine* 9:3107–18.
- Mandal TK, Tenjarla S. (1996). Preparation of biodegradable microcapsules of zidovudine using solvent evaporation: effect of the modification of aqueous phase. *Int J Pharm* 137:187–97.
- Martins S, Tho I, Reimold I, et al. (2012). Brain delivery of camptothecin by means of solid lipid nanoparticles: formulation design, *in vitro* and *in vivo* studies. *Int J Pharm* 439:49–62.
- Masarudin MJ, Cutts SM, Evison BJ, et al. (2015). Factors determining the stability, size distribution, and cellular accumulation of small, mono-disperse chitosan nanoparticles as candidate vectors for anticancer drug delivery: application to the passive encapsulation of [ $^{14}$ C]-doxorubicin. *Nanotechnol Sci Appl* 8:67–80.
- Masserini M. (2013). Nanoparticles for brain drug delivery. *ISRN Biochem* 2013:1–18.
- Mu L, Zhou R, Tang F, et al. (2016). Intracellular pharmacokinetic study of zidovudine and its phosphorylated metabolites. *Acta Pharm Sin B* 6:158–62.
- Nath B, Nath LK, Kumar P. (2011). Preparation and *in vitro* dissolution profile of zidovudine loaded microspheres made of Eudragit RS 100, RL 100 and their combinations. *Acta Pol Pharm* 68:409–15.
- Nayak UY, Gopal S, Mutalik S, et al. (2009). Glutaraldehyde cross-linked chitosan microspheres for controlled delivery of zidovudine. *J Microencapsul* 26:214–22.
- Oh SY, Jeong SY, Park TG, Lee JH. (1998). Enhanced transdermal delivery of AZT (zidovudine) using iontophoresis and penetration enhancer. *J Control Release* 51:161–8.
- Pattnaik G, Sinha B, Mukherjee B, et al. (2012). Submicron-size biodegradable polymer-based didanosine particles for treating HIV at early stage: an *in vitro* study. *J Microencapsul* 29:666–76.
- Rautio J, Laine K, Gynther M, Savolainen J. (2008). Prodrug approaches for CNS delivery. *AAPS J* 10:92–102.
- Rudra A, Deepa RM, Ghosh MK, et al. (2010). Doxorubicin-loaded phosphatidylethanolamine-conjugated nanoliposomes: *in vitro* characterization and their accumulation in liver, kidneys, and lungs in rats. *Int J Nanomedicine* 5:811–23.
- Sahana B, Santra K, Basu S, Mukherjee B. (2010). Development of biodegradable polymer based tamoxifen citrate loaded nanoparticles and effect of some manufacturing process parameters on them: a physicochemical and *in-vitro* evaluation. *Int J Nanomedicine* 5:621–30.
- Satapathy BS, Mukherjee B, Baishya R, et al. (2016). Lipid nanocarrier-based transport of docetaxel across the blood brain barrier. *RSC Adv* 6:85261–74.
- Seju U, Kumar A, Sawant KK. (2011). Development and evaluation of olanzapine-loaded PLGA nanoparticles for nose-to-brain delivery: *in vitro* and *in vivo* studies. *Acta Biomater* 7:4169–76.
- Shaw TK, Mandal D, Dey G, et al. (2017). Successful delivery of docetaxel to rat brain using experimentally developed nanoliposome: a treatment strategy for brain tumor. *Drug Deliv* 24:346–57.
- Singh S, Dobhal AK, Jain A, et al. (2010). Formulation and evaluation of solid lipid nanoparticles of a water soluble drug: zidovudine. *Chem Pharm Bull* 58:650.
- Takasato Y, Rapoport SI, Smith QR. (1984). An *in situ* brain perfusion technique to study cerebrovascular transport in the rat. *Am J Physiol* 247:H484–93.
- Thomas NS, Panchagnula R. (2003). Transdermal delivery of zidovudine: effect of vehicles on permeation across rat skin and their mechanism of action. *Eur J Pharm Sci* 18:71–9.
- Tripathi KM, Castro M, Feller JF, Sankar SK. (2017). Characterization of metal, semiconductor, and metal-semiconductor core–shell nanostructures. In: Gupta RK, Misra M, eds. *Metal Semiconductor Core–Shell Nanostructures for Energy and Environmental Applications*. Netherlands: Elsevier, 51–78.
- Vieira DB, Gamarra LF. (2016). Getting into the brain: liposome-based strategies for effective drug delivery across the blood–brain barrier. *Int J Nanomedicine* 11:5381–414.
- Weiss N, Miller F, Cazaubon S, Couraud PO. (2009). The blood–brain barrier in brain homeostasis and neurological diseases. *Biochim Biophys Acta* 1788:842–57.
- Wilson B, Samanta MK, Santhi K, et al. (2008). Targeted delivery of tacrine into the brain with polysorbate 80-coated poly(n-butylcyanoacrylate) nanoparticles. *Eur J Pharm Biopharm* 70:75–84.



# Comparison of Enhanced Solubility Profile Analysis of Thermodynamic Parameters and Pharmacokinetic Profile Related to Tamoxifen Citrate Solubilisation



Laboni Mondal, Biswajit Mukherjee\*, Shreyasi Chakraborty, Sanchari Bhattacharya, Iman Ehsan, Soma Sengupta and Murari M Pal

Department of Pharmaceutical Technology, Jadavpur University, India

Received Date: June 14, 2018; Published Date: July 09, 2018

\*Corresponding author: Biswajit Mukherjee, Department of Pharmaceutical Technology, Jadavpur University, Kolkata, West Bengal, India, Email: biswajit55@yahoo.com

## Abstract

The aim of this study was to investigate the improvement of solubility of a poorly water soluble drug tamoxifen citrate (TC) by various methods such as cosolvency, micellisation, and complexation. Cosolvents (ethanol, polyethylene glycol-400), surfactants [polyoxyethylene sorbitan monooleate (Tween-80), poloxamer-407 and poloxamer-188], and cyclodextrins [ $\beta$ -cyclodextrin (BCD) and hydroxypropyl- $\beta$ -cyclodextrin (HPBCD)] were used as solubilizing agents in this study. Solubility improvement approaches showed variable degrees of solubility improvement of TC. Among the solubilizing agents used, the modified  $\beta$ -cyclodextrin was found to be the most effective. The solubility of TC was enhanced to  $6.31 \text{ mmolL}^{-1}$  in water (about 7.1 fold solubility improvement) using 0.05% m/v hydroxy propyl- $\beta$ -cyclodextrin. Different thermodynamic parameters, enthalpy and entropy, were analyzed for solubility enhancement of TC with different cyclodextrins which showed enthalpy not the entropy was the driving force for TC solubilisation. The less positive enthalpy of BCD complexation than HPBCD complexation signifies the higher solubilising efficacy of HPBCD. Pharmacokinetic study was performed using HPBCD as solubility enhancer at its optimized concentration which also resulted in improved bioavailability when compared to the bioavailability obtained with free tamoxifen.

**Keywords:** Tamoxifen citrate; Solubility; Cosolvent; Surfactant; Cyclodextrin; Pharmacokinetic

## Introduction

Tamoxifen citrate (TC) is an antiestrogenic drug and is first choice treatment of breast cancer in both pre- and post-menopausal women. The antiestrogenic effects may be related to its ability to compete with estrogen for binding sites in target tissues such as breast [1]. Chemically, TC is the isomer of a triphenylethylene derivative. The chemical name is (Z) 2-[4-(1,2-diphenyl-1-butenyl) phenoxy]-N,N-dimethylethanamine-2-hydroxy-1,2,3-propane tricarboxylate. Following a single oral dose of 20 mg tamoxifen, an average peak plasma concentration of  $40 \mu\text{g L}^{-1}$  (range 35 to 45  $\text{ng ml}^{-1}$ ) occurred in 4-7 h after dosing [2,3] and this indicates poor bioavailability of the drug. Poorly water-soluble drugs often provide limited bioavailability if dissolution is the rate-limiting step in overall oral absorption process [4]. Since TC is poorly soluble in water (equilibrium solubility in water at 37 °C is 0.5  $\text{mg ml}^{-1}$ ) [5], it is, therefore, important to improve its solubility to ameliorate its bioavailability [6].

Although there has been enormous amount of research works performed using different techniques of solubilisation,

yet a comparative profile is very scarce. In this study, the effect of different solubilisation approaches such as micellar solubilisation, complexation by cyclodextrins and cosolvency on the aqueous solubility of TC has been presented in a comparative approach. An attempt has been made to provide an insight into the mechanism of solubilisation of TC particularly by complexation based on analysing thermodynamic parameters, since complexation was found to be the most successful approach among the methods tried.

## Experimental

### Materials

Poly (ethylene glycol) 400 (SRL Pvt. Ltd., Mumbai, India),  $\beta$ -cyclodextrin (Hi Media Laboratories Pvt. Ltd., Mumbai, India), tween-80 (S.d. Fine Chemical Limited, Mumbai, India), absolute ethanol (Merck Ltd., Mumbai, India) were obtained commercially. Hydroxypropyl- $\beta$ -cyclodextrin, poloxamer-407, poloxamer-188 were purchased from Sigma-Aldrich, Bengaluru, India. TC (Khandelwal Laboratories Pvt. Ltd., Mumbai, India) was a gift sample.

### Phase Solubility Study

In each of the different approaches (cosolvency, micellisation, and complexation) of solubilisation, solubility of TC was determined by placing an excess amount of TC (10 mg) in water (5 ml), in different test tubes containing increasing concentrations (Table 1) of various cosolvents, surfactants and the complexation agents so that the total volume in each case remained to 5 ml. Three sets of sample vials were prepared for each particular solubilising agent. The test tubes were shaken mechanically in a shaker water bath at 37°C for 48 h. At equilibrium (after 2 days, as preliminary studies showed that this period of time was sufficient to ensure saturation at 37°C), aliquots were removed, centrifuged for 10 min at 10000 rpm. After proper dilution with water the samples were analyzed spectrophotometrically at 275 nm using Shimadzu UV/Vis spectrophotometer (Japan) [7] taking appropriate blank solution. The cosolvents used were ethanol, poly (ethylene glycol) 400 and glycerine. The surfactants were polyoxyethylene sorbitan monooleate (Tween 80), poloxamer-407 and poloxamer-188. The complexation ligands were  $\beta$ -cyclodextrin (BCD) and hydroxypropyl- $\beta$ -cyclodextrin (HPBCD).

### Thermodynamic Parameters for Different Cyclodextrin Concentrations

Thermodynamic analysis was performed by measuring the solubility measurement with BCD and HPBCD concentration (0.05% m/v to 0.5% m/v) at different temperatures (300, 310 and 320 K) (Tables 2&3). Rest of the procedure was same as the phase solubility study. Gibbs and van't Hoff equations were used to estimate the thermodynamic parameters, enthalpy ( $\Delta H^\circ$ ), entropy ( $\Delta S^\circ$ ) and Gibbs free energy ( $\Delta G^\circ$ ).

The general form of van't Hoff equation for calculation of thermodynamic parameters:

$$\ln K = \Delta S^\circ/R - \Delta H^\circ/RT$$

or

$$\log K = -(\Delta H^\circ / 2.303R) 1/T + \Delta S^\circ / 2.303R$$

The Gibbs equation gives the values of ( $\Delta H^\circ$ ) and ( $\Delta S^\circ$ ) and therefore, the values of ( $\Delta G^\circ$ ) were calculated in each case from the equation.

$$\Delta G^\circ = \Delta H^\circ - T \Delta S^\circ$$

For a plot of  $\ln K$  versus  $1/T$ , slope =  $-\Delta H^\circ/R$  and intercept =  $\Delta S^\circ/R$  were calculated.

Where,  $K$  (equilibrium constant) represents either  $S$  (drug inherent solubility) or  $K_{1:1}$  (equilibrium constant considering 1:1 complex formation). The values of  $S$  were initially estimated from the phase solubility diagrams) [8].

### Pharmacokinetic Study by LC-MS/MS

Swiss albino mice (either sex, 25-30 g) were purchased from registered breeders, and were given normal standard diet with tap water ad libitum. Animals were kept under a 12 hrs light

dark cycle. The animals were maintained in this condition for at least one week prior to the experiment. All experiments were conducted as per the guidelines of the animal ethics committee (AEC), Jadavpur University, Kolkata.

Animals were divided into two groups (10 animals in each group) and fasting condition for at least 24 h prior to the experiment. Animals from the free drug group (FD) were given tamoxifen citrate at 10 mg/kg oral dose and animals of the test group (CD) were given HPBCD (as a solubility enhancer at the concentration of 0.5% w/v) along with TC in an equivalent oral dose of 10 mg/kg, mixing in water. After oral dosing mice were anaesthetized with diethyl ether. Blood samples were collected by heart puncture technique at various time points from 0.25 h, 0.5 h, 1h, 2 h, 4 h, 8h and 24 h. Blood samples were centrifuged at 6000 rpm for 5 min and plasma were collected and stored at -80°C until further study by LC-MS/MS.

### LC-MS/MS Assay

Working stocks of TC were prepared by serial dilution in HPLC grade methanol. Working stocks and blank plasma were spiked to prepare calibration control (CC) and quality control (QC) samples. Liquid liquid extraction (LLE) technique was used for the extraction of CC, QC and test samples.

The plasma concentrations of TC in both the groups were determined by LC-MS/MS assay using a method described by Choi and Kang [9]. At first, 0.05 ml butyl paraben (IS) of concentration 8 $\mu$ g/ml in methanol was added to 0.2 ml acetonitrile and 0.2 ml of plasma sample. This mixture was vortexed and centrifuged at 13,000 rpm for 10 min and 0.05 ml of the supernatant was loaded to LC-MS/MS (LC: Shimadzu Model 20AC, MS: AB-SCIEX, Model: API 4000, Software: Analyst 1.6) for analysis. Plasma data were plotted against time and PK parameters were determined by WinNonlin software (Certara,UK).

## Results and Discussion

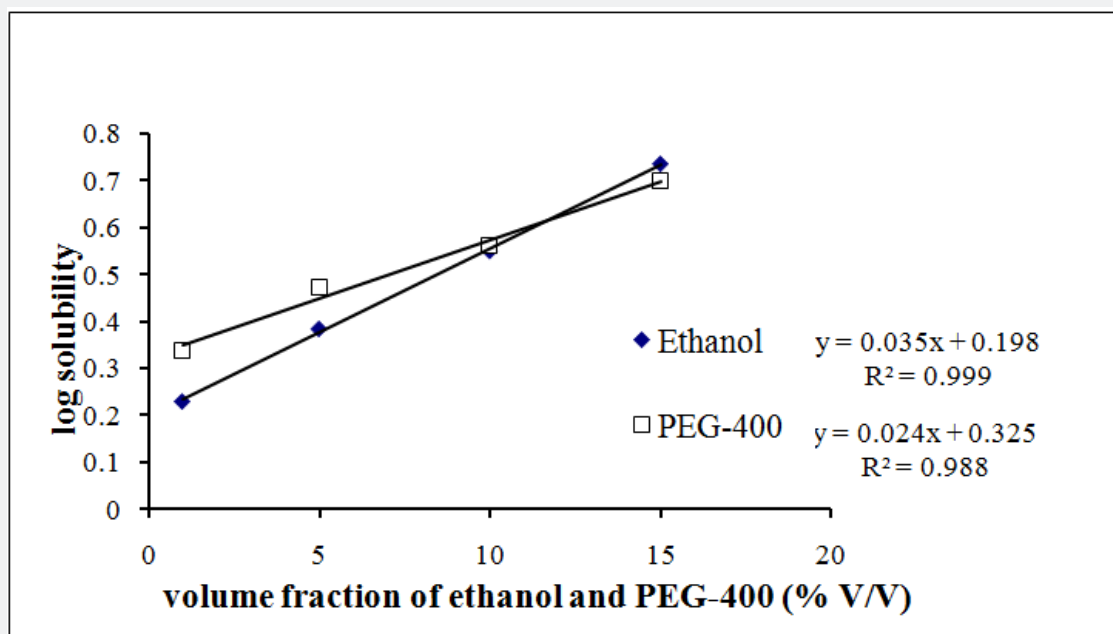
### Cosolvency

Figure 1 shows straight lines in semi-logarithmic plot of TC solubility vs. volume fractions of the experimental cosolvents. Solubility study of TC with different concentrations of the cosolvents, ethanol and PEG-400 at 37°C showed that efficiency of ethanol (15% V/V) as cosolvent was higher (6.10-fold) than that of 15% PEG-400 (5.62-fold) compared to the inherent solubility of TC in water.

Cosolvents are widely used in pharmaceutical industry for solubilisation purpose. They work by reducing hydrogen bond density of aqueous system and create a less polar environment in bulk [10]. This results in more solubilisation of sparingly soluble or less soluble drug molecules. Cosolvents generally possess non-polar regions which do not interact strongly with water and they decrease the capability of water molecules to squeeze out non-polar solutes from the aqueous system [11]. A relationship between the total drug solubility ( $D_{tot}$ ) and

cosolvent concentration (C) in a drug-cosolvent-solvent mixture has been described by using the equation,  $\log D_{tot} = \log D_u + \sigma C$  [12,13] where,  $D_u$  and  $\sigma$  are drugs solubility in water and cosolvent solubilisation power, respectively. The value of  $\sigma$  is

inversely correlated with the polarities of both the solute and the cosolvent. The more non-polar the solvent and the solute, the larger is the  $\sigma$  value [14].



**Figure 1:** Effect of cosolvency (by ethanol and PEG- 400) on tamoxifen solubility at 37°C

Figure1 shows straight lines in semi-logarithmic plot of TC solubility vs volume fractions of the experimental cosolvents. The findings suggest exponential increase in TC solubility with the increasing concentration of the cosolvent, ethanol and PEG-400. Both ethanol and PEG-400 obey 1<sup>st</sup> order solubilisation kinetic. For a single non-polar solute, cosolvent solubilisation power ' $\sigma$ ' depends only on cosolvent polarity [14]. Table 1 indicates

that solubility enhancement of TC follows the cosolvent order as: EtOH ( $\sigma$ : 0.036) > PEG-400 ( $\sigma$ : 0.025). The less polar is the cosolvent, the more effective it is at disrupting hydrogen bonding interactions in water molecules [15]. In the present study, more efficient improvement of solubility of TC by ethanol may be because ethanol is the less polar solvent than PEG-400 [14].

**Table 1:** Solubilisation parameters for tamoxifen citrate.

Solubilizing agent	Concentration	Dependence of $D_{tot}$ on $D_u$
Ethanol (% v/v)	1, 5, 10, 15	$\sigma$ : 0.036
PEG-400 (% v/v)	1, 5, 10, 15	$\sigma$ : 0.025
Tween- 80 (mmol L <sup>-1</sup> )	0.8246, 2.0615, 4.123, 8.24	$\kappa$ : 0.97
Poloxamer- 407 (mmol L <sup>-1</sup> )	0.082, 0.205, 0.409, 0.818	$\kappa$ : 2.28
Poloxamer- 188 (mmol L <sup>-1</sup> )	0.12, 0.29, 0.58, 1.16	$\kappa$ : 0.25
BCD (mmol L <sup>-1</sup> )	0.4404, 0.8809, 2.202, 4.404	$K_{1:1}$ = 0.48
HPBCD (mmol L <sup>-1</sup> )	0.357, 0.71428, 1.785, 3.5714	$K_{1:1}$ = 0.68

$D_{tot}$  - total drug solubility in a mixed solvent and cosolvent concentration (C).  $D_u$  - drug solubility in water. BCD:  $\beta$ -cyclodextrin; HPBCD: hydroxyl propyl- $\beta$ -cyclodextrin.

### Micellization

Figure 2 shows the effects of poloxamer-407, poloxamer-188 and Tween 80 on solubility profiles of TC, respectively which

indicates that TC solubility was enhanced in the surfactant order as: poloxamer-407 (5.36-fold) > Tween80 (5.30-fold) > poloxamer-188 (3.20-fold).

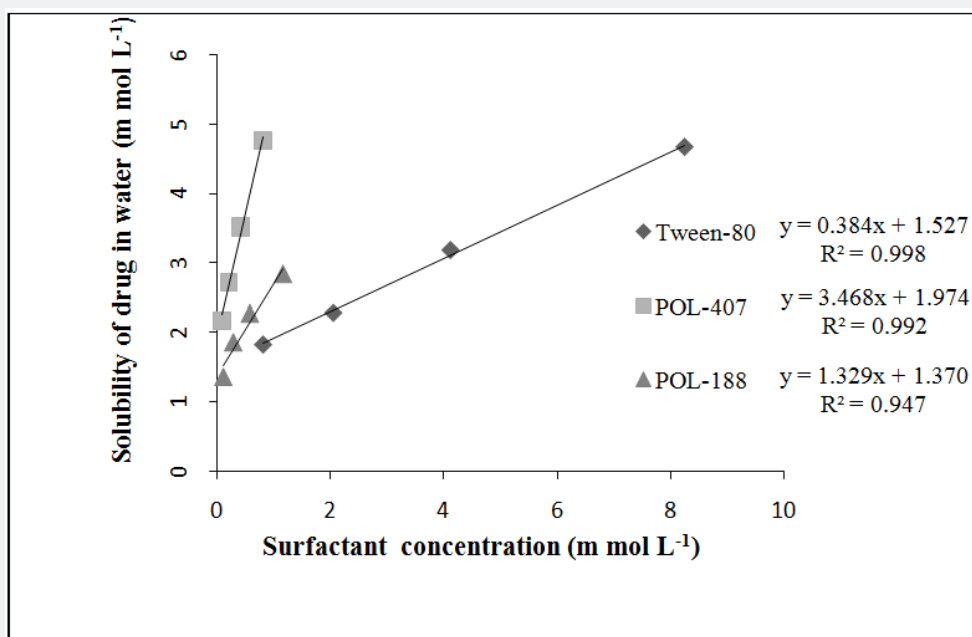


Figure 2: Effect of surfactants (Tween-80, POL-407, POL-188) on tamoxifen solubility at 37°C

Micelle formation is one of the important mechanisms to solubilise solutes. Incorporation of solute molecules to the micelles depends on the degree of non-polarity of solutes and their micellar partitioning performances [11]. The more non-polar the solute, the more likely it is to be incorporated near the nonpolar core or center of micelles [11]. Researchers have described a relationship of micellar surfactant concentration and solubility of solute (drug) [15,16]. Total drug solubility ( $D_{tot}$ ) depends on inherent solubility ( $D_u$ ) and concentration of micellar surfactant ( $S$ ) (i.e., the total surfactant concentration minus the critical micellar concentration) and is presented by  $D_{tot} = D_u + \kappa D_u S$  [10], where  $\kappa$  is micellar partition coefficient. Product of  $\kappa$  and  $D_u$  reflects number of surfactant molecules required to solubilise one solute molecule [14].

Table 1 indicates that TC solubility was enhanced in the following sequences: poloxamer-407 ( $\kappa$ : 2.28) > Tween-80 ( $\kappa$ : 0.97) > poloxamer-188 ( $\kappa$ : 0.25). Poloxamer-407 was found to improve the solubility of TC maximally among the surfactants tested. Due to higher micellar partitioning, more non-polar TC molecules were incorporated in the poloxamer-407 micelles.

### Complexation

Figure 3 shows a linear relationship between TC solubility with different concentration of BCD and HPBCD used to solubilize TC. HPBCD showed higher solubilisation of TC than natural BCD. The solubility improvement of TC was about 5.8-fold with 0.5% m/v BCD and 7.1-fold with 0.5% m/v HPBCD compared to the original solubility of TC in water.

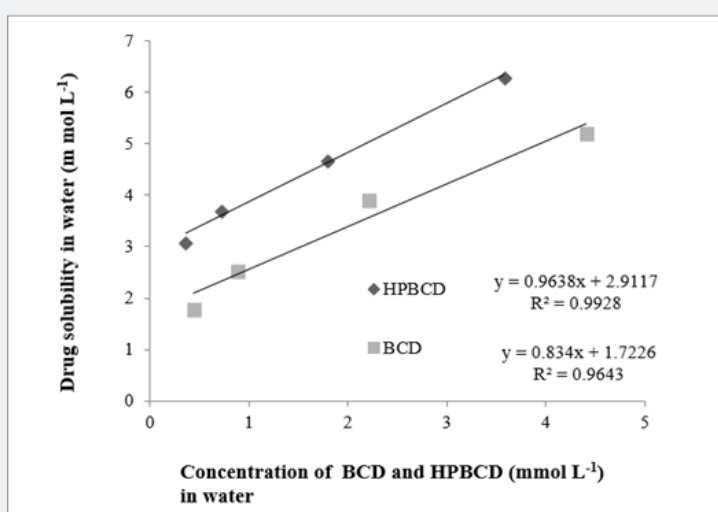


Figure 3: Effect of complexation (by BCD and HPBCD) on tamoxifen citrate solubility at 37°C

The solubility of TC with different cyclodextrins has been described using the following equation,  $D_{tot} = D_u + KD_uL$  [14], where L is the total ligand concentration, and K is the complexation constant/ solubilisation capacity of the drug-ligand complex.  $D_{tot}$  and  $D_u$  have been described earlier. Table 1 shows that the solubilisation capacity  $K_{1:1}$  of HPBCD (0.68) is slightly greater than that of natural BCD (0.48). The modified  $\beta$ -cyclodextrins have been widely used and reportedly have higher solubilisation capacity than natural BCD for most drugs [17,18]. Complexation constant or solubilising capacity, K, depends on the geometry and polarity of the solute molecules and compatibility between the solute and the cyclodextrin cavity [15].

Except for differences in size, the overall geometries of the cyclodextrins are similar. Each having a torus equals to the length of the appropriate number of glycosides. The derivatized cyclodextrins are characterized by the nature, position and degree of the substituents and there they differ in the available sites. Size and structure of the molecules are important for formation of inclusion compounds. Structurally smaller drug insertion (as compared to CD cavity) is not energetically favored and for appropriately larger solutes, they can fill most of the CD cavity and form the more stable complexes. Thus, TC solubilisation capacity of HPBCD is higher by forming HPBCD-TC inclusion complex than that of BCD. Again, equilibrium analysis of drug cyclodextrin complex within the experimental

concentration range (data not shown) was found to be of 1:1 stoichiometry which has been reported to happen with a low ligand concentration, as at higher ligand concentration higher order complexes are formed [14]. In conclusion, HPBCD is a better complexation ligand for TC than natural BCD.

### Thermodynamic Parameters

Thermodynamic parameters calculated are shown in Table 1. It shows the effect of increasing experimental temperatures and concentrations of both the cyclodextrins on TC solubilisation. The solubility of TC was increased with both the conditions. TC solubility was characterized by a negative  $\Delta G^\circ$ , indicative of spontaneous dissolution and positive  $\Delta H^\circ$  indicative of endothermic dissolution [19]. Van der Waal interactions, hydrogen bonding, hydrophobic interactions, release of high-energy water molecules from the cavity of cyclodextrin and release of strain energy in the ring of cyclodextrin structure etc. are the known driving forces for the formation of cyclodextrin inclusion complexes with foreign molecules [20]. These interactions cause conformational changes in cyclodextrin structure, dissolution to complex stability and drug solubility. Breakdown of water structure around a solute creates a higher positive  $\Delta S^\circ$  and a positive  $\Delta H^\circ$  known to be governed by hydrophobic interaction [21]. In the present study dissolution thermodynamics of TC in aqueous BCD and HPBCD were characterized by a positive  $\Delta H^\circ$  (Figures 4&5), indicative of endothermic dissolution [19].

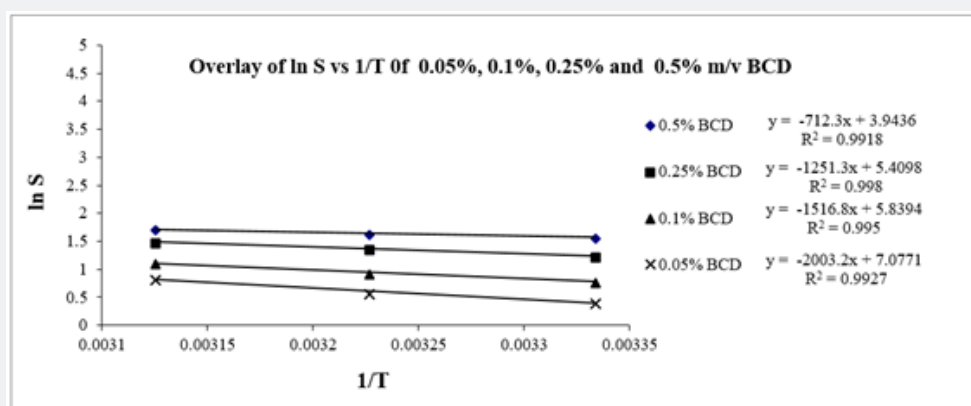


Figure 4: Overlay of ln S (of TC) vs 1/T of different concentrations of BCD

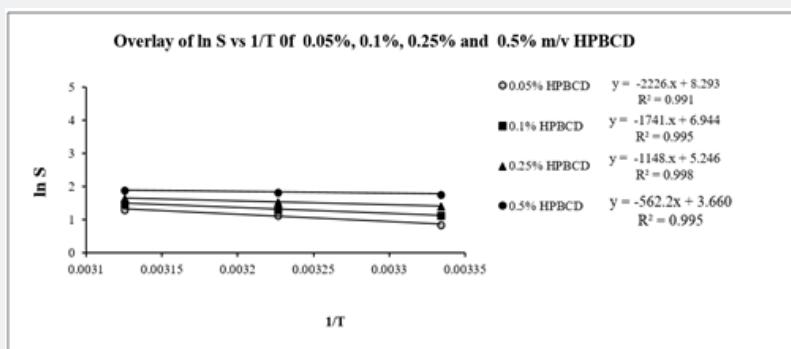


Figure 5: Overlay of ln S (of TC) vs 1/T of different concentrations of HPBCD

Reports suggests that complex formation with BCD and HPBCD yields negative or positive  $\Delta H^\circ$  and negative or positive  $\Delta S^\circ$  [22]. In our study both BCD and HPBCD complex formations resulted in positive  $\Delta H^\circ$  as well as positive  $\Delta S^\circ$ . Breakdown of water structure around TC creates a large positive  $\Delta S^\circ$  and a positive  $\Delta H^\circ$  (Tables 2&3), apparently governed by hydrophobic

interactions [23]. Positive  $\Delta S^\circ$  for TC may be attributed to transfer of TC from polar aqueous medium to nonpolar cavities of CDs [18]. Positive  $\Delta H^\circ$  indicates endothermic dissolution thermodynamics of TC in aqueous BCD and HPBCD. In this experiment, the enthalpy difference ( $\Delta H^\circ$ ) decreased with the increasing concentrations of BCD and HPBCD.

**Table 2:** Enthalpy-Entropy data of tamoxifen citrate-BCD complexation.

Concentration of cyclodextrin (% m/v)	Slope	Enthalpy( $\Delta H^\circ = \text{slope} \times R$ ) $\text{kJ mol}^{-1}$	Intercept	ENTROPY ( $\Delta S^\circ = \text{intercept} \times R$ ) $\text{kJ mol}^{-1} \text{K}^{-1}$
0.5	-712.3	5.922276	3.9436	0.032788
0.25	-1251.3	10.40368	5.4098	0.044979
0.1	-1516.8	12.61113	5.8394	0.048551
0.05	-2003.2	16.65521	7.0771	0.058841

**Table 3:** Enthalpy-Entropy data of Tamoxifen citrate-HPBCD complexation.

Concentration of cyclodextrin (% m/v)	Slope	Enthalpy( $\Delta H^\circ = \text{slope} \times R$ ) $\text{kJ mol}^{-1}$	Intercept	ENTROPY ( $\Delta S^\circ = \text{intercept} \times R$ ) $\text{kJ mol}^{-1} \text{K}^{-1}$
0.5	-562.25	4.67	3.66	0.03
0.25	-1148.3	9.54	5.25	0.043
0.1	-1741.1	14.47	6.94	0.058
0.05	-2226.7	18.51	8.29	0.069

This is favourable for a thermodynamic process to happen and in this case, enthalpy was the driving force for complexation of TC with BCD and HPBCD. The entropy difference ( $\Delta S^\circ$ ) decreased with (Tables 2&3) increasing BCD and HPBCD concentrations. The entropy was not the driving force for complexation of TC with CDs. With respect to the HPBCD, the complexation of natural BCD with TC is characterized by less positive enthalpy, the contribution from which the solubility improvement profile of TC with BCD is lesser than HPBCD.

### Pharmacokinetic Assay

The study result of pharmacokinetic assay by LC-MS/MS was represented by the plasma concentration-time profile (Figure 6). The pharmacokinetic parameters of tamoxifen as a free drug (FD) and along with a solubility enhancer HPBCD (HCD) (Table 4) revealed that Area under the curve (AUC) and maximum concentration reached ( $C_{\text{max}}$ ) for tamoxifen was much higher in case of CD than FD which indicated that cyclodextrin had a clear effect on improving the bioavailability of tamoxifen

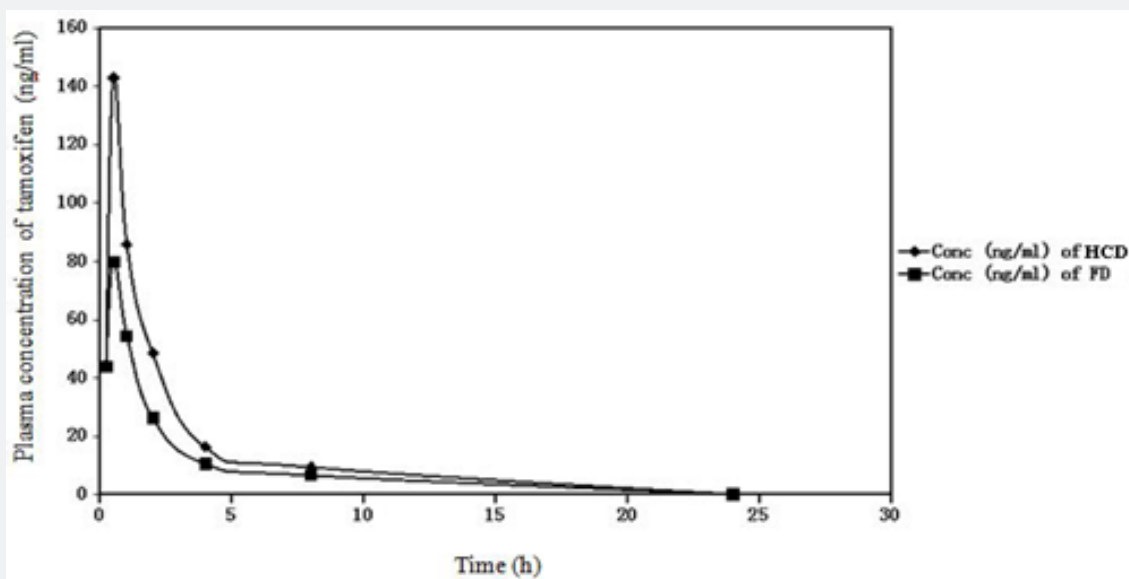


**Figure 6:** Plasma concentration time curves of tamoxifen as a free drug (FD) and along with a solubility enhancer HPBCD (HCD)

**Table 4:** Pharmacokinetic parameters of tamoxifen after oral administration of tamoxifen (10mg/kg) with HCD in mice

Parameters	Plasma values of Tamoxifen upon oral administration	
	HCD	FD
Half-life (h)	3.28	2.75
C <sub>max</sub> (ng/ml)	143	79.9
T <sub>max</sub> (h)	0.5	0.5
AUC <sub>0-t</sub>	275.6	171.6
AUC <sub>0-inf</sub>	313.4	203.4
CL (L/h/kg)	108.9	166.6
MRT <sub>inf</sub> (h)	2.97	2.91

Mean±SD (n=6), AUC; area under the plasma concentration time curve from 0 h to infinity, C<sub>max</sub>; peak concentration, T<sub>max</sub>; time to reach the peak concentration, MRT; mean residence time; CL; total body clearance. HCD; hydroxy propyl β cyclodextrin added to tamoxifen, FD; tamoxifen as a free drug.

On other hand, clearance rate was higher for FD in comparison with HCD which may be due to the faster elimination of tamoxifen when administered alone (FD) than with a solubility enhancer (HCD). After in vivo administration, free tamoxifen due to its poor solubility was absorbed less but eliminated quickly after absorption. On the other hand, tamoxifen-HPBCD complex was absorbed faster and distributed in the system with a slower elimination.

### Conclusion

The water solubility of TC was increased 7.1-fold in the presence of 0.5% m/v HPBCD, compared to 0.5% m/v natural BCD (increase 5.8-fold). Thermodynamic parameters derived from TC solubility in the presence of various concentrations of BCD and HPBCD at several temperatures reveal that the solubility of TC increased with an increase in temperature. Besides, TC-BCD complex formation was a characteristic of a very strong hydrophobic interaction. Furthermore, pharmacokinetic study was also representing the similar observation with higher Area under the plasma concentration-time curve and peak plasma concentrations of TC, when administered along with HPBCD. However, clinical trial will be needed to conclude the simultaneous oral administration of cyclodextrin along with tamoxifen to enhance the bioavailability in human.

### Acknowledgement

We acknowledge the funding agency University Grants Commissions, Government of India and Indian Council of Medical Research (ICMR), Grant number: Nan/BMS -45/6/2013 for providing the necessary grants for the study.

### Disclosure

The authors report no conflicts of interest in this work.

### References

- JK Sarmah, SK Bhattacharjee, R Mahanta (2009) Preparation of cross-linked guar gum nanospheres containing tamoxifen citrate by single step emulsion in situ polymer cross-linking method. *J Incl Phenom Macrocycl Chem* 65(3-4): 329-334.

- MMT Buckley, KL Goa (1989) Tamoxifen: a reappraisal of its pharmacodynamic and pharmacokinetic properties and therapeutic use, *Drugs* 37(4): 451-490.
- EA Lien, E Solheim, OA Lea (1989) Distribution of 4-hydroxy-N-desmethyl tamoxifen and other tamoxifen metabolites in human biological fluids during tamoxifen treatment. *Cancer Res* 49(8): 2175-2183.
- VM Rao, J Haslam, VJ Stella (2001) Controlled and complete release of a model poorly water-soluble drug, prednisolone, from hydroxypropyl methylcellulose matrix tablets using (SBE) (7m)-beta-cyclodextrin as a solubilizing agent. *J Pharm Sci* 90(7): 807-816.
- Indian Pharmacopoeia (1996) Ministry of Health and Family Welfare, Government of India, Published Delhi, India, p. 1.
- SM Ahmed (1998) Improvement of solubility and dissolution of 19-Norprogesterone via inclusion complexation, *Jour. Inclusion. Phen Mol Recog Chem* 30(2): 111-125.
- S Sehra, AS Dhake (2005) Formulation and evaluation of sustained release microspheres of poly-lactide-co-glycolide containing tamoxifen citrate, *J Microencapsul* 22(5): 521-528.
- Al Omari, MM Zughul, MB Davies, JED Badwan (2006) Sildenafil/cyclodextrin complexation: stability constants, thermodynamics, and guest-host interactions probed by 1H-NMR and molecular modeling studies, *J. Pharm. Biomed. Anal.* 41(3): 857-865.
- JS Choi, KW Kang (2008) Enhanced tamoxifen bioavailability after oral administration of tamoxifen in rats pretreated with naringin, *Arch Pharm Res.* 31(12): 1631-1636.
- SH Yalkowsky (1999) *Solubility and Solubilization in Aqueous Media*, Oxford University Press, New York, USA.
- Y Ran, L Zhao, Q Xu, SH Yalkowsky (2001) Solubilization of Cyclosporin A, *AAPS Pharm Sci Tech* 2(1): 2.
- S H Yalkowsky, TJ Roseman, NY Dekker Solubilization of drugs by cosolvents. In *Techniques of Solubilization of Drugs*, New York 1981.
- SH Yalkowsky, SH, JT Rubino (1985) Solubilization of cosolvents I: organic solutes in propylene glycol-water mixtures, *J. Pharm. Sci* 74(4): 416.
- J Swarbrick, JC Boylan (2002) *Encyclopedia of Pharmaceutical Technology*, 2<sup>nd</sup> edition, Informa Health Care, Volume 3.
- L Zhao, P Li, SH Yalkowsky (1999) Solubilization of fluasterone, *J. Pharm. Sci.* 88(10): 967-969.



16. D Attwood, AT Florence, Surfactant systems, New York, Chapman and Hall, 1983.
17. J Pitha, J Milecki, H Fales, L Pannel, K Uekama (1986) Hydroxypropyl- $\beta$ -cyclodextrin: preparation and characterization: effects on solubility of drugs. *Int J Pharm* 29(1): 73-82.
18. K. Uekama, M Otagiri (1987) Cyclodextrins in therapeutic drug carrier systems, in *CRC Critical Reviews in Therapeutic Drug Carrier Systems*, 3(1):1-40.
19. Z Zuo, G Kwon, B Stevenson, J Diakur, LL Wiebe (2000) Flutamide - hydroxypropyl- $\beta$ -cyclodextrin complex: formulation, physical characterization, and absorption studies using the caco-2 in vitro model, *J. Pharm. Pharm. Sci* 3(2): 220-227.
20. M Komiyama, LM Bender (1983) Importance of apolar binding in complex formation of cyclodextrins with adamantanecarboxylate, *J Am Chem Soc* 100(7): 2259-2260.
21. T Loftsson, E M Brewster (1996) Pharmaceutical application of cyclodextrins: Drug solubilization and stabilization, *J. Pharm. Sci.* 85(10): 1017-1025.
22. IV Terekhova, TV Volkova, GL Perlovich (2006) Experimental analysis of complex formation of Niflumic acid with  $\beta$ -cyclodextrins. *J Incl Phen Macro Chem* 55(3-4): 335-340.
23. A Martin (1993) *Physical Pharmacy*, (4th edn), Lea & Febiger, Philadelphia, USA, pp. 274-277.



This work is licensed under Creative Commons Attribution 4.0 License  
DOI: [10.19080/NAPDD.2018.03.555624](https://doi.org/10.19080/NAPDD.2018.03.555624)

**Your next submission with Juniper Publishers  
will reach you the below assets**

- Quality Editorial service
- Swift Peer Review
- Reprints availability
- E-prints Service
- Manuscript Podcast for convenient understanding
- Global attainment for your research
- Manuscript accessibility in different formats  
( Pdf, E-pub, Full Text, Audio)
- Unceasing customer service

Track the below URL for one-step submission  
<https://juniperpublishers.com/online-submission.php>



( / )

Search for...

Search

**Search in:**  All  Article  Chapter  eBook

[Purchase PDF](#)

## Variation of Pharmacokinetic Profiles of Some Antidiabetic Drugs from Nanostructured Formulations Administered Through Pulmonary Route

**Author(s):** Biswajit Mukherjee, Paramita Paul, Ankan Choudhury, Sanchari Bhattacharya, Ruma Maji, Lopamudra Dutta.

**Journal Name:** Current Drug Metabolism

**Volume 17 , Issue 3 , 2016**

**DOI :** 10.2174/1389200216666151015115503 (<https://doi.org/10.2174/1389200216666151015115503>)

[🏠 Journal Home \(/node/592\)](#)



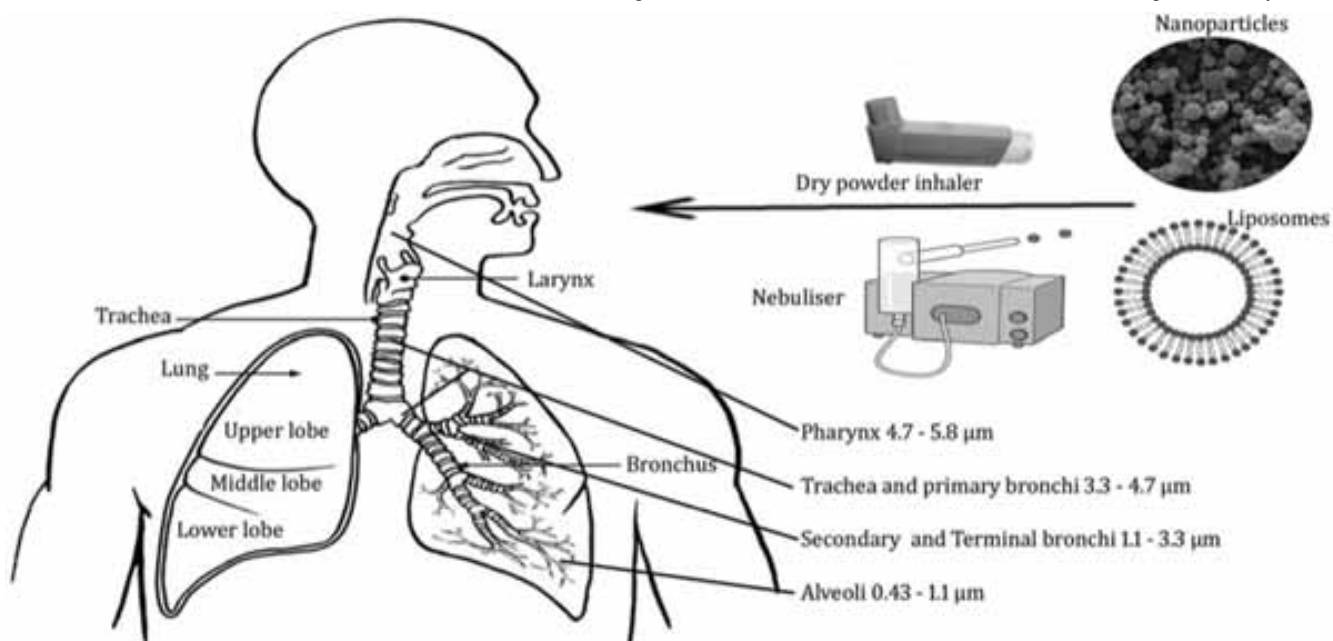
**IN VITRO DDI REGULATORY COMPARISON  
DISCUSSION & REFERENCE POSTER AVAILABLE**  
SEKISUI XENOTECH 25 YEARS OF ADME/DMPK/DDI EXPERTISE

(<http://bit.ly/2Dn8qOc>)

### Graphical Abstract:

### Abstract:

Background: Diabetes is a chronic disease that occurs when the pancreas does not produce enough insulin, or when the body cannot effectively use the insulin it produces. WHO projects that diabetes death will be doubled between 2005 and 2030, where 347 million people worldwide had diabetes as per the



report of 2013. The increase in the prevalence of diabetes is due to three influences - lifestyle, ethnicity, and age.

**Methods:** The present review summarizes the pharmacokinetic parameters and challenges in the field of nanoparticles and nanoliposomes of insulin and other antidiabetic drugs given through pulmonary route to treat diabetes effectively.

**Results:** Current challenges in diabetes management include optimizing the use of the already available therapies to ensure adequate glycemic condition, blood pressure, lipid control and to reduce complications. At present, several pieces of research have been focusing on new management options for diabetes. Among these options, the use of nanomedicine is becoming an eye catching and most promising one. Currently, nanoparticles and nanoliposomes are thrust areas of research to treat any deadly disease like diabetes. These drug delivery systems ultimately result in longer circulation half-lives, improved drug pharmacokinetics, and reduced side effects of therapeutically active substances that may be insulin and non-insulin.

**Conclusions:** Thus, the pulmonary route is the most promising alternative route of drug delivery since it is non-invasive and lungs have a large surface area, richly supplied by the capillary network, for absorption of drugs.

**Keywords:** Antidiabetics, diabetes, insulin, nanoliposomes, nanoparticles, pulmonary.

[Mark Item](#)
[Purchase PDF](#)
[Rights & Permissions](#)
[Print](#)
[Export](#)
[Cite as](#)

Other

### Article Details

VOLUME: 17

ISSUE: 3

Year: 2016

Page: [271 - 278]

Pages: 8

DOI: 10.2174/1389200216666151015115503

(<https://doi.org/10.2174/1389200216666151015115503>)

Price: \$58

### Article Metrics

PDF: 20

HTML: 3

## Related Article(s)

Limonin, A Citrus Limonoid, had no Apparent Effect on Cognitive Dysfunction in Mice with Chronic Cerebral Hypoperfusion

(<http://www.eurekaselect.com/node/109350/?trendmd-shared=4>)

Immunology, Endocrine & Metabolic Agents in Medicinal Chemistry (Discontinued)

Diabetes Therapy: Novel Patents Targeting the Glucose-Induced Insulin Secretion

(<http://www.eurekaselect.com/node/93703/?trendmd-shared=4>)

Recent Patents on DNA & Gene Sequences (Discontinued)

History, Prevalence and Assessment of Limited Joint Mobility, from Stiff Hand Syndrome to Diabetic Foot Ulcer Prevention: A Narrative Review of the Literature

(<http://www.eurekaselect.com/node/154964/?trendmd-shared=4>)

Current Diabetes Reviews

Status of Acetylcholinesterase and Butyrylcholinesterase in Alzheimer's Disease and Type 2 Diabetes Mellitus

(<http://www.eurekaselect.com/node/125556/?trendmd-shared=4>)

CNS & Neurological Disorders - Drug Targets

Effects of Resveratrol and ACE Inhibitor Enalapril on Glucose and Lipid Profiles in Mice

(<http://www.eurekaselect.com/node/154558/?trendmd-shared=4>)

Protein & Peptide Letters

Efficacy of Pentoxifylline in the Management of Microalbuminuria in Patients with Diabetes

(<http://www.eurekaselect.com/node/66356/?trendmd-shared=4>)

Current Diabetes Reviews

Adiponectin as a Regulator of Vascular Redox State: Therapeutic Implications

(<http://www.eurekaselect.com/node/88209/?trendmd-shared=4>)

Recent Patents on Cardiovascular Drug Discovery (Discontinued)

Hormones and the Autonomic Nervous System are Involved in Suprachiasmatic Nucleus Modulation of Glucose Homeostasis

(<http://www.eurekaselect.com/node/55801/?trendmd-shared=4>)

Current Diabetes Reviews

Design of Novel Biphenyl-2-thioxothiazolidin-4-one Derivatives as Potential Protein Tyrosine Phosphatase (PTP)-1B Inhibitors Using Molecular Docking Study

(<http://www.eurekaselect.com/node/134097/?trendmd-shared=4>)

Letters in Drug Design & Discovery

Metabolic Syndrome: Clinical Features Leading to Therapeutic Strategies

(<http://www.eurekaselect.com/node/80734/?trendmd-shared=4>)

Vascular Disease Prevention

Type 2 Diabetes and Risk for Functional Decline and Disability in Older Persons

(<http://www.eurekaselect.com/node/71578/?trendmd-shared=4>)

Current Diabetes Reviews

Basic and Clinical Aspects of Gene Therapy for Retinopathy Induced by Diabetes

(<http://www.eurekaselect.com/node/55569/?trendmd-shared=4>)

Current Gene Therapy

Retinoids as Critical Modulators of Immune Functions: New Therapeutic Perspectives for Old Compounds

(<http://www.eurekaselect.com/node/84431/?trendmd-shared=4>)

Endocrine, Metabolic & Immune Disorders - Drug Targets

Identification of Lipid Species Linked to the Progression of Non-alcoholic Fatty Liver Disease

(<http://www.eurekaselect.com/node/130168/?trendmd-shared=4>)

Current Drug Targets

Growth Hormone and Insulin-Like Growth Factor-I as an Endocrine Axis in Alzheimers Disease

(<http://www.eurekaselect.com/node/82739/?trendmd-shared=4>)

Endocrine, Metabolic & Immune Disorders - Drug Targets

Molecular and Pharmacological Characterization of Hamster HCA1 and HCA2

(<http://www.eurekaselect.com/node/134546/?trendmd-shared=4>)

Immunology, Endocrine & Metabolic Agents in Medicinal Chemistry (Discontinued)

The Treatment of Cardiovascular Disease Continuum: Focus on Pharmacologic Management and RAS Blockade

(<http://www.eurekaselect.com/node/71524/?trendmd-shared=4>)

Current Clinical Pharmacology

Osteoporosis and its Association with Non-Gonadal Hormones Involved in Hypertension, Adiposity and Hyperglycaemia

(<http://www.eurekaselect.com/node/115598/?trendmd-shared=4>)

Current Drug Targets

Potential Application of Biliverdin Reductase and its Fragments to Modulate insulin/IGF-1/MAPK/PI3-K Signaling Pathways in Therapeutic Settings

(<http://www.eurekaselect.com/node/72590/?trendmd-shared=4>)

Current Drug Targets

Mechanisms Involved in the Protective Effects of Metformin Against Nonalcoholic Fatty Liver Disease

(<http://www.eurekaselect.com/node/98519/?trendmd-shared=4>)

Current Medicinal Chemistry

(/terms/termandcondition.html?1)

© 2018 Bentham Science Publishers (<http://www.eurekaselect.com/136826/page/terms-and-conditions>)





( / )

Search for...

Search

**Search in:**  All  Article  Chapter  eBook

[Purchase PDF](#)

## Is Type 2 Diabetes Mellitus a Predisposal Cause for Developing Hepatocellular Carcinoma?

**Author(s):** Biswajit Mukherjee, Sanchari Bhattacharya, Samrat Chakraborty, Bhabani Sankar Satapathy, Niladri Shekhar Dey, Tapan Kumar Shaw.

**Journal Name:** Current Diabetes Reviews

**Volume 11 , Issue 2 , 2015**

**DOI :** 10.2174/1573399811666150115110747 (<https://doi.org/10.2174/1573399811666150115110747>)

[Journal Home \(/node/587\)](#)

11<sup>th</sup> october  
2018

# World Obesity Day

**AVAIL 20% DISCOUNT QUOTE "BSPMD2018"**



### Abstract:

Hepatic cancer stands as one of the frontier causes of cancer related mortality worldwide. Among the several risk factors already established, type 2 diabetes is now considered as one of the important risks in progression of liver cancer. Studies have shown that likelihood of occurrence of liver cancer is many folds higher in patients diagnosed with type II diabetes compared to patients without diabetes. Liver plays an important role in metabolism of glucose in our body, so may be type II diabetes as it is an important epiphenomenon of hepatic diseases such as liver cirrhosis, liver failure, fatty liver, chronic hepatitis and hepatocellular carcinoma. Some reports suggested that extensive change in enzyme structures in

molecular level in diabetic patients may lead to liver function damage and hence accelerate hepatic cancer. Other strong links between these two diseases are “non alcoholic fatty liver diseases” and “nonalcoholic steatohepatitis” which are metabolic disorders caused by type II diabetes and eventually develops hepatocellular carcinoma. However, it still remains unanswered whether prevention of diabetes would effectively lower the chances of developing liver cancer or eliminating diabetes from the population would effectively reduce the liver cancer incidence. In this review, we will primarily focus on the molecular link between type2 diabetes and hepatic cancer and investigate underlying mechanism to establish type II diabetes as predisposed cause of hepatic cancer.

**Keywords:** Diabetes mellitus, hepatocellular carcinoma, molecular mechanism, risk factors, TNF- $\alpha$ , IL-6.

[Mark Item](#)
[Purchase PDF](#)
[Rights & Permissions](#)
[Print](#)
[Export](#)
[Cite as](#)

Other

### Article Details

VOLUME: 11

ISSUE: 2

Year: 2015

Page: [64 - 70]

Pages: 7

DOI: 10.2174/1573399811666150115110747

(<https://doi.org/10.2174/1573399811666150115110747>)

Price: \$58

### Article Metrics

PDF: 26

## Related Article(s)

Neural Pathways and Neuropeptides Mediate the Therapeutic Actions of DPP IV Inhibitors in Type-2 Diabetes

(<http://www.eurekaselect.com/node/89978/?trendmd-shared=4>)

Recent Patents on Endocrine, Metabolic & Immune Drug Discovery (Discontinued)

SGLT-2 Inhibition: Novel Therapeutics for Reno-and Cardioprotection in Diabetes Mellitus

(<http://www.eurekaselect.com/node/161335/?trendmd-shared=4>)

Current Diabetes Reviews

Gut Microbiota as a Therapeutic Target for Metabolic Disorders

(<http://www.eurekaselect.com/node/156280/?trendmd-shared=4>)

Current Medicinal Chemistry

Food Applications for Flaxseed and its Components: Products and Processing

(<http://www.eurekaselect.com/node/95529/?trendmd-shared=4>)

Recent Patents on Food, Nutrition & Agriculture



Hyperglycemic Hyperosmolar State Associated with Low-Dose Quetiapine Treatment in a Patient with Bipolar Disorder

(<http://www.eurekaselect.com/node/75366/?trendmd-shared=4>)

Current Drug Safety

Associations between Adiponectin Gene Variability, Pro-inflammatory and Angiogenetic Markers: Implications for Microvascular Disease

Development in Type 2 Diabetes Mellitus?

(<http://www.eurekaselect.com/node/158869/?trendmd-shared=4>)

Current Vascular Pharmacology

Therapeutic Potential of Caffeic Acid Phenethyl Ester (CAPE) in Diabetes

(<http://www.eurekaselect.com/node/147487/?trendmd-shared=4>)

Current Medicinal Chemistry

Editorial [Hot Topic: Novel Peptides and Proteins in Diabetes Mellitus (Guest Editors: Po Sing Leung and Marc de Gasparo)]

(<http://www.eurekaselect.com/node/83898/?trendmd-shared=4>)

Current Protein & Peptide Science

Vitamin D Deficiency and Oxidative Stress in Type 2 Diabetic Population of India

(<http://www.eurekaselect.com/node/141488/?trendmd-shared=4>)

Cardiovascular & Hematological Agents in Medicinal Chemistry

Diabetes, Sexual Dysfunction and Therapeutic Exercise: A 20 Year Review

(<http://www.eurekaselect.com/node/72031/?trendmd-shared=4>)

Current Diabetes Reviews

Clinical Significance of the New Cardiovascular Risk Markers in Diabetes Mellitus

(<http://www.eurekaselect.com/node/129666/?trendmd-shared=4>)

Current Diabetes Reviews

Polyphenols-Rich Natural Products for Treatment of Diabetes

(<http://www.eurekaselect.com/node/124175/?trendmd-shared=4>)

Current Medicinal Chemistry

Design of Novel Biphenyl-2-thioxothiazolidin-4-one Derivatives as Potential Protein Tyrosine Phosphatase (PTP)-1B Inhibitors Using Molecular Docking Study

(<http://www.eurekaselect.com/node/134097/?trendmd-shared=4>)

Letters in Drug Design & Discovery

Protective Role of Diabetes Mellitus on Abdominal Aortic Aneurysm Pathogenesis: Myth or Reality?

(<http://www.eurekaselect.com/node/131754/?trendmd-shared=4>)

Current Vascular Pharmacology

Is Metabolic Syndrome X a Disorder of the Brain?

(<http://www.eurekaselect.com/node/82533/?trendmd-shared=4>)

Current Nutrition & Food Science

Microvascular Endothelial Dysfunction in Obesity and Hypertension

(<http://www.eurekaselect.com/node/107756/?trendmd-shared=4>)

Current Pharmaceutical Design

Homology-Based Design for Selective GSK-3 Peptide Inhibitors: Patent Applications and Type 2 Diabetes Mellitus

(<http://www.eurekaselect.com/node/115973/?trendmd-shared=4>)

Current Signal Transduction Therapy

Atherogenic Index of Plasma is Associated with Body Fat Level in Type 2 Diabetes Mellitus Patients

(<http://www.eurekaselect.com/node/158793/?trendmd-shared=4>)

Current Vascular Pharmacology

A Review on Natural Products for Controlling Type 2  
Diabetes with an Emphasis on their Mechanisms  
of Actions

([http://www.eurekaselect.com/node/113909/?  
trendmd-shared=4](http://www.eurekaselect.com/node/113909/?trendmd-shared=4))

Current Diabetes Reviews

Testosterone as Potential Effective Therapy in  
Treatment of Obesity in Men with Testosterone  
Deficiency: A Review

([http://www.eurekaselect.com/node/76619/?  
trendmd-shared=4](http://www.eurekaselect.com/node/76619/?trendmd-shared=4))

Current Diabetes Reviews

(</terms/termandcondition.html?1>)

© 2018 Bentham Science Publishers (<http://www.eurekaselect.com/136826/page/terms-and-conditions>)



# Size Dependent Variations of Phospholipid Based Vesicular Drug Carriers in Systemic Drug Activity

Biswajit Mukherjee\*, Laboni Mondal, Samrat Chakraborty, Paramita Paul, Ankan Choudhury, Sanchari Bhattacharya and Chowdhury M. Hossain

Department of Pharmaceutical Technology, Jadavpur University, Kolkata-700032, India



**Abstract:** Lipid based vesicular drug delivery system, one of the emerging technologies designed for addressing the delivery challenges of conventional drug delivery methods, has widespread applications in chemotherapeutics, immunotherapeutics, recombinant DNA technology, membrane biology and also as a diagnostic tool in different biological field. The enclosed phospholipid bilayer spherical structure, typically known as liposome, is a versatile vesicular delivery system to carry hydrophilic/hydrophobic drug generally efficiently to the site of action leading to reduced non-specific toxicity and improved bioavailability of the therapeutic moiety. Efficacy of drug encapsulated in liposome depends mainly on the circulation amount of liposome and its residence time, *in vivo* drug release, drug accumulation in the target site and uptake of the formulation in the reticuloendothelial system. Liposomal formulation factors that dictate those actions are liposomal size (hydrodynamic diameter), surface charge, lipid composition and steric stabilization. Variation in liposomal size shows around 100 fold alterations in pharmacokinetic parameters and systemic activity while the other factors such as surface charge, lipid composition and steric stabilization bring only about 10 fold changes in those properties. The findings indicate the critical role of vesicular size in liposomal efficacy. In the present review the effect of size-variation of liposome on systemic activity of drug as well as its pharmacokinetic profile will be discussed to understand the rational designing of liposomal preparation to maximize therapeutic activity of a drug at desired magnitude and to provide a wide range of product applications such as immunological vaccines, chemotherapy, antimicrobial therapy etc.

**Keywords:** Drug delivery, liposomes, phospholipid, pharmacokinetics, size, vesicles.

## INTRODUCTION

Lipid based vesicular drug delivery systems have gained attention of researchers around the globe due to their enormous potential as carriers for drugs, nutrients and other bio-active agents. Among the lipid-based vesicular drug delivery systems, liposome has been exploited heavily as drug delivery system. It was the pioneering work by Alec Bangham and their colleagues which first described these swollen, spherical phospholipid systems as a model membrane system [1]. Since then myriads of enclosed phospholipid bilayer structures, initially called 'banghosome' and then 'liposome', were reported [2]. Later, the work of another pioneer, Gregory Gregoriadis, established the concept that eventually described the potential of liposome as drug delivery system [2]. Almost over the last five decades, liposomal technology has experienced great advancement in drug loading of various potent drugs, homogenization of size of the carrier, prolongation of drug circulation time, innovation of triggered drug release, optimization for nucleic acid containment in liposomes, development of ligand targeted drug delivery and incorporation of multiple drugs in such formulation. These resulted in numerous clinical trials for the development of a

plethora of liposomal formulations to deliver drugs of diverse nature such as anticancer, antifungal, antibiotics, anti-inflammatory, genetic medicines for gene therapy etc [3].

Liposomes consist of small artificial spherical vesicles made up of cholesterol (Chol) and natural non-toxic phospholipids. Phosphoglycerides and sphingolipids together with their hydrolytic products are being utilized for the preparation of liposomal formulations. Depending on the composition and nature of intracellular delivery, liposomes can be classified into five different categories such as (a) conventional liposome, (b) pH-sensitive liposome, (c) cationic liposome (d) immunoliposome and (e) long-circulating liposome [4, 5].

Vesicle sizes and number of bilayers control a number of important parameters, such as drug circulation half-life and the extent of drug encapsulation of liposomal formulations. Therefore, on the basis of these parameters, liposomes are also classified as (a) small (20-100 nm) unilamellar vesicle (SUV), (b) large (100-1000 nm) unilamellar vesicle (LUV), (c) giant (> 1000 nm) unilamellar vesicle (GUV), (d) oligo-lamellar vesicle (OLV) of size 100-500 nm and (e) multi-lamellar vesicle (MLV) of size > 500 nm.

Liposomes serve to play as one of the essential vehicles in drug delivery and offer numerous advantages as mentioned below.

\*Address correspondence to this author at the Department of Pharmaceutical Technology, Jadavpur University, Kolkata-700032, India; Tel./Fax: +91-33-24146677; E-mail: biswajit55@yahoo.com

- (i) They exhibit biocompatibility, biodegradability and also induce less toxicity and immunogenicity in both systemic and non-systemic administration [1, 2, 4].
- (ii) They potentiate efficacy, therapeutic index as well as systemic stability of drug via encapsulation, thus improving the pharmacokinetic profile of drug molecules [1, 2, 4].
- (iii) They are flexible enough to couple with site-specific ligands and thus reduce the systemic toxicity [2].
- (iv) Liposomes protect encapsulated DNA from enzymatic and other metabolic processes and hence are capable of delivering even large DNA sequences [2].
- (v) They are capable of delivering both hydrophilic and hydrophobic drugs [6].

The proper control over the rate of drug release is extremely vital for liposomal formulation to become effective as a drug carrier. A drug is effective only when it is released and the therapeutic outcome of the drug depends on its bioavailability. Therefore, designing of liposome and optimization of drug release from it are vital issues for delivering drug at the diseased site and making them bioavailable within its therapeutic window for a sufficient time period at a desired rate to achieve optimum therapeutic activity.

Rapid clearance of conventional liposomes by mononuclear phagocyte system (MPS) is an important concern. Liposomal uptake by the MPS organs such as spleen and liver reduce the availability of the drug to the other tissues of the body and is also responsible for imposing toxicity to those MPS organs. Initially several techniques were adopted for prolonging the systemic circulation time of conventional liposome through the inhibition of MPS uptake by using large empty (without drug) liposomes [4]. Extensive research on liposomal carriers has proved that surface properties, size and lipid composition should be engineered properly in order to avoid the MPS uptake. The decrease in the degree of opsonization by serum proteins results in potentiation of circulating drug half-life in serum. Thus, modification of surface of liposomal carriers has been attempted to optimize the pharmacokinetic profile for better therapeutic outcome. Size of the liposome is another important determinant for blood circulation of drug. Several investigations have proved that the decrease in the size of liposomes results in decreased recognition of the carrier by complement system (series of blood glycoproteins that promote phagocytosis) of the blood causing decrease in MPS uptake. Therefore, the focus of present day research in the field of liposome is on the development of nanoscale lipid vesicles (nanoliposome) [2].

The delivery of drug cargo across the cell membrane to the intracellular site is another huge concern associated with liposomal carriers. Hydrophobic weak bases such as doxorubicin or viscristine have gained their entry through passive diffusion due to their concentration gradient whereas small hydrophilic molecules take the aid of the cell membrane transporters for their transport. Some liposomal carriers also require some modifications to deliver their payloads to the intracellular sites [2]. There are several ways through which liposomal carriers have gained their access to the intracellular sites as mentioned below.

- (i) Liposomes are taken up by macrophages through endocytosis.
- (ii) Liposomal carriers enriched with fusogenic lipid and membrane active peptides attached to the liposomal surface either fuse with or disintegrate the cell membrane more effectively, resulting in efficient intracellular drug delivery.
- (iii) Liposomes conjugated with different target specific ligands are endocytosed by those target receptor sites and release the entrapped drug in the endosomal compartment [6].

Size of liposomes is found to have very significant impact to improve therapeutic index of entrapped drug by reducing the Reticulo Endothelial System (RES) uptake while prolonging the circulation time in blood [6]. Liposomal carrier of 100-200 nm would be ideal for delivering drug to tumor as reported in literatures [4].

Size of liposome also plays a very crucial role for the development of efficient liposomal vaccine delivery system. It determines the degree and type of immune response generated upon administration of liposomal vaccine. Large size liposome is more superior to the smaller ones for the development of successful liposomal vaccine to achieve better therapeutic activity. This is due to the fact that the large size liposomal carriers are more readily phagocytosed and the processed peptides are presented to major histocompatibility complex II (MHCII) for generation of immune response [7].

Liposomal size is a crucial determinant factor because it has profound effect on the systemic activity. Therefore, proper designing of method for development of liposomal formulation of desired size is essential for different therapeutic applications. While formulating the liposome for drug delivery, our main goal should be to avoid/ or reduce its uptake by MPS, to achieve better blood circulation half-life and the pharmacokinetic profile of entrapped drug [1]. In case of liposome containing anti-cancer drug, vesicular size should be such that it helps liposome not only to escape the RES but also enables them to pass through pores of the leaky vasculature to exploit the benefit of active or passive targeting strategies. Another interesting fact is that large size liposomal carriers are preferable for the delivery of protein/peptide antigens (vaccine) as the goal is to achieve rapid phagocytosis of liposomal carriers to develop strong immune response as soon as possible. Therefore, in case of vaccine delivery, liposomes not only act as a carrier but also serve as an adjuvant. Moreover, care should be taken while developing liposomes of smaller size to increase the benefit of targeting to specific cell/tissue. Size should be above the cut off size (5.5 nm) for renal excretion in order to prevent rapid excretion through urine. Presently, researchers are more concentrating on the development of better targeting strategies to increase the therapeutic index as well as to decrease the toxicity of entrapped drugs [8]. However, it should be kept in mind that development of more efficient targeting strategies does not end the task. The development of optimal sized liposomes is also equally important to utilize the advantages of targeting strategies as much as possible. Therefore, the present review is intended to describe the size dependent physiological behavior and therapeutic applications, of liposome as a drug carrier system.

## FACTORS AFFECTING THE PHARMACOKINETIC PARAMETERS OF LIPID VESICLES

### Size and Its Relation with the Other Factors

Efficient biodistribution and target specific delivery of drug are the two key problems in drug therapy that can be tactfully managed by the use of liposomal drug delivery system [9]. Liposome, like other drug delivery systems, has a varying systemic activity influenced by its uptake, circulation time, permeability and clearance from the system [9, 10].

One of the first aspects of liposome that affects its systemic disposition is its size. Based on the several research investigations related to the role of liposomal size to the total body clearance ( $CL_{tot}$ ) of liposome, Harashima described a scattered plot created from moment analysis of blood disappearance data of liposome to depict a variation in  $CL_{tot}$  of different liposomes against their sizes [11]. The regression analysis has determined that  $\log CL_{tot}$  varies fairly linearly to the  $\log$  size with  $r^2$  (regression coefficient,  $r$ ) value of 0.478 and a probability value ( $P$ )  $\leq 0.001$ . A group of researchers has also compared  $CL_{tot}$  of liposomes against the other formulation parameters like surface charge, composition and steric stabilization, but the variations explained by those factors were marginal compared to that attributed to size [10]. In fact, the variation  $CL_{tot}$  due to these factors ranged within only 10-folds, while that due to size was more than 100-folds. This clearly indicates the importance of liposomal size in determining its clearance and thus the systemic activity of the drug entrapped in it. The disappearance of drug from blood or its total clearance is, as we know, directly proportional to the uptake of liposomes from the blood circulation. It has been seen that an increase in size causes quicker uptake by the RES for liposomes having similar lipid composition [11-13]. Distearoylglycerophosphocholine (DSPC)/Chol (3:2) vesicles (400 nm) show faster clearance (around 7.5 times) than those with a size of 200 nm which also have a clearance (around 5 times) faster rate than the SUVs of half of their size [13]. Another such study of the relation between size and liposome composition was done with egg phosphatidylcholine (EPC) and hydrogenated EPC (HEPC) SUVs, each of them stabilized with dicetyl phosphate (DCP) and Chol at 5:1:4 molar ratios. EPC liposomal species have more propensity to depend on their size than its hydrogenated species. The EPC liposomal species in 24 h accumulated more in tumor and RES uptake data varied more sharply as compared to the HEPC SUVs due to the variation of the mean liposome size from 100 to 200 nm [14]. The inclusion of PEG-DSPE (Polyethyleneglycolated distearoylglycero phosphoethanolamine) in the liposome composition however resulted in clearance rates that were relatively independent of the change in size in the range of 80 to 250 nm for most of the liposomal compositions [15, 16].

Relationship of charge and size is more intricate. Aggregation of non-stabilized neutral liposomes increases the effective size and thus a rapid body clearance occurs via a size-dependent mechanism, through the RES or Kupffer cells [15, 16, 17]. Existence of charge causes interparticulate repulsion that overrides the problem of aggregation without the need of sterical stabilization. But again the inclusion of charges has its own set of complications. Generally the negatively

charged vesicles show a faster clearance rate. Neutral non-sterically stabilized liposomes have a considerably narrow clearance window for providing optimal drug level in the circulation. Thus along with the charge factor, liposomes should be small enough (preferably 100 nm) to negate the liposomal aggregation [18]. Phagocytosis and pinocytosis are the main mechanisms that are responsible for the uptake of large and small liposomes respectively [10, 19-21]. The systemic aggregation of liposomes can highly alter the uptake mechanisms and hence fate of the liposomes is dependent on the variation of the original size because of their aggregation. Conjugation of chemicals like PEG to the surface of liposomes causes strong interbilayer repulsion that can overcome the existing force of attraction (such as van der Waals force) and subsequently avoids aggregation and stabilizes the formulation [22]. Surface modification has been reported to only cause a very slight increase of an overall diameter of the liposome, depending on the grafting density of the molecules. Only 5nm extension from the lipid surface was observed by X-ray analysis of PEG 1900 conjugated lipid bilayers [22]. This avoids a serious handicap for size-dependent uptake and clearance mechanisms. Monosialotetrahexosylganglioside (GM1), another candidate for steric stabilization, has less effect on the interbilayer separation compared with PEG. The phenomenon of enhanced steric barrier decreased with decreasing PEG chain length ( $M_w$  120 and 750) than at higher PEG lengths ( $M_w$  1900 and 5000). However, the steric barrier produced by low molecular weight PEGs was still significantly greater than that produced by GM1 [23].

Pharmacokinetic distribution curve associated with liposomal distribution are often bi-phasic in nature and can be represented by the following formula:

$$C = Ae^{-\alpha t} + Be^{-\beta t}$$

In the formula,  $C$  represents the concentration of liposomes in the blood,  $A$  and  $B$  represent the initial concentrations for each of the compartments (mentioned below) and  $\alpha$  and  $\beta$  represent the disappearance rate constants associated with the compartments A and B respectively. The peripheral tissue compartment (B) slowly equilibrates to the blood compartment (A). This phenomenon may be due to the presence of a size-dependent transcapillary transport through the intercellular pores and/or the endocytosis or exocytosis by the endothelial or parenchymal cells [24]. This may explain the correlation of size to that of systemic distribution and hence activity. The size-dependence of the systemic activity of liposomes, specially antitumor activity, can thus be seen as a delicate balance between the tendency of vesicles to be transported in interstitial spaces and tendency of being cleared from circulation by various uptake mechanisms, which represent the hypothetical secondary compartment. Phagocytotic uptake through complement receptors, C3 and C5, activates macrophagic cascade more in vesicles larger than 400 nm [11]. The enhanced uptake was inhibited by anti-C3 serum and K76-COOH (C5a inhibitor) respectively, establishing size being the predominant factor in hepatocytic uptake of liposomes [11]. In liver, the liposome reaches from the periportal region to the central vein through the sinusoids. During this journey, the liposome is phagocytosed or taken up by the hepatocytes in a size dependent manner. The density of fenestrae on the surface of the hepatic sinusoid

increases whereas the mean diameter of those fenestrae decreases along the direction of the flow of blood thus making the hepatic sinusoids more porous near the hepatic venule [25]. This gradient is also present in the distribution of Kupffer cells along the hepatic sinusoids as more of these cells are found in the periportal region, having larger size and higher phagocytotic activity, than in the centrilobular region [45]. Therefore, liposomes of diameter larger than 100 nm are preferentially taken up via phagocytosis and hence do not reach the hepatocytes. Whereas, smaller liposomes are taken up by both hepatocytes and Kupffer cells as well, which indicates the importance of size in sorting of liposomes in hepatic circulation [24].

The presence of a discontinuous endothelium and a lack of efficient lymphatic drainage in the tumor vasculature during angiogenesis facilitates extravasation and accumulation of liposomal formulations into the interstitium, mimicking a sustained drug-release system. This preferential accumulation of liposomes in the tumor area is known as the Enhanced Permeation and Retention (EPR) [26]. In normal conditions, the tight junctions between capillary endothelial cells do not permit the liposomes to extravasate from the blood-stream. This may be the reason behind the improved therapeutic effects of anti-cancer drugs when encapsulated in liposomes [17]. This EPR effect is optimal when the diameter of the liposome is in the range of 90-200 nm. [17]. This indicates the possibility of this optimum size being used as a tool for "passive targeting" of liposomes for tumor targets along with steric stabilization. Liposomes of reduced size can avoid recognition by blood phagocytotic complement receptors [4]. Again EPR is not seen in vesicles below a certain size range, attributed mainly to the hepatic parenchymal uptake as the sinusoidal fenestrations have a mean diameter of around 100 nm. In a study, 40 nm HEPC liposomes showed much longer circulation time but poor accumulation in tumor sites than the liposomes of 100 nm in size [27]. It is a conventional knowledge that prolonging the circulation time in the blood of small liposomes increases their chance of encountering leaky vessels and permeating into the tumor interstitial spaces [17, 27]. But this study showed that the systemic circulation time may not correspond directly to the accumulation of liposomes in tumor. The enhanced circulation time for the liposomes (40 nm size) may be due to the tendency of RES to forgo uptake of smaller liposomes as the small size prevents the liposomes to interact with the blood components and hence are not recognized by either the hepatic parenchymal or Kupffer cells [28-30]. But the liposomal accumulation in tumor may be due to a balance in the influx and efflux of liposomes between the vascular space and tumor. Liposomes of 100 nm are more preferentially accumulated in tumor sites as the discontinuity of the adjoining capillary walls is not large enough to allow them to be effluxed into the vasculature [27]. Liposomal interaction with the structures present in the interstitial spaces which comprise of mainly collagen and elastic fiber network [31] and the presence of leaky capillaries, enable easy transmission of all liposomes into the interstitial space which enhances their accumulation. While, the liposomes of 40 nm size are small enough to be effluxed from the interstitial area back to the vascular spaces more readily than the liposomes of 100 nm, resulting in evidently high AUC and blood residence time of the 40 nm vesicles [27]. The following figure

(Fig. 1) summarizes the phenomenons that were described above regarding the systemic distribution of liposomes of different sizes.

Some studies involving DSPC/Chol liposomes with DSPE-PEG grafting showed similar results. Liposome in the size range of 100 to 200 nm (median being 120 nm) was found to accumulate efficiently in all the examined tumor cells such as C1300, Ehrlich, Colon 26 and S180 [17]. This seconds the idea that liposomes with an optimal size range extravasate more frequently into the interstitium by exploiting the gaps between adjacent endothelial cells and other discontinuities in the vasculature during angiogenesis. Thus liposome with that size range can be employed for efficient tumor targeting through EPR effect [17, 32-35].

The correlation of size and activity is however inverse of the conventional wisdom when it comes to immunoliposomes. For developing liposomal vaccines, size and sometimes lamellarity are critical to their adjuvant activities [8, 19]. On studying the effect of monopalmitoylglycerol (MPG)-DCP-Chol liposomes of varying sizes (namely 100, 155, 225 and 560 nm) Brewer *et al.* [36] established that though all tested formulations induced similar anti-OVA IgG1 levels whereas significantly higher IgG2a and IFN- $\gamma$  productions were associated with only the larger vesicles. Further, no differential macrophagic uptake was seen for liposomes having diameter between 155 nm to 225 nm [36]. The results were mirrored in another study in which influenza A hemagglutinin was given through liposomes of either 250 nm or 980 nm in diameter [37]. The immune response to dimethyldioctadecylammonium (DDA)-tetrahalose-6,6'-dibehenate (TDB) vesicles of <200 nm, 700 nm, and 1500 nm size containing antigen derived from *M. tuberculosis*, also showed that vesicles of larger size had the tendency to accumulate more in the draining lymph node and the vesicles of 700 nm average diameter showed the greatest IFN- $\gamma$  secretion by restimulated splenocytes [38]. In another study, rgp63, a major surface glycoprotein of *Leishmania*, was encapsulated in Dipalmitoylphosphatidylcholine (DPPC) liposomes of 100, 400, 1000 nm sizes and injected subcutaneously into BALB/c mice and the rate of protection and immune response against leishmaniasis were recorded and evaluated [8]. On the basis of footpad lesion size and splenic parasite burden, it was seen that the liposomes with over 400 nm size were more capable of combating the infection on immunization and they also exhibited highest production of IFN- $\gamma$  and the highest IgG2a and IgG1 ratio. Another interesting fact was that immunization through 100 nm liposome induced largely Th1 type response whereas that through liposome greater than 400 nm size produced mostly Th2 type response [8].

#### DEPENDENCY OF DRUG SYSTEMIC ACTIVITY ON LIPOSOMAL SIZE

Liposomal drug delivery systems have the potential to selectively target diseased site and to control the drug release rate from them. Understanding of the kinetics of encapsulated drug is essential for any efficient formulation including liposome. It demands a discussion on the role of the size of the phospholipid vesicular drug carrier (typically liposome) on different parameters determining the drug systemic activity.

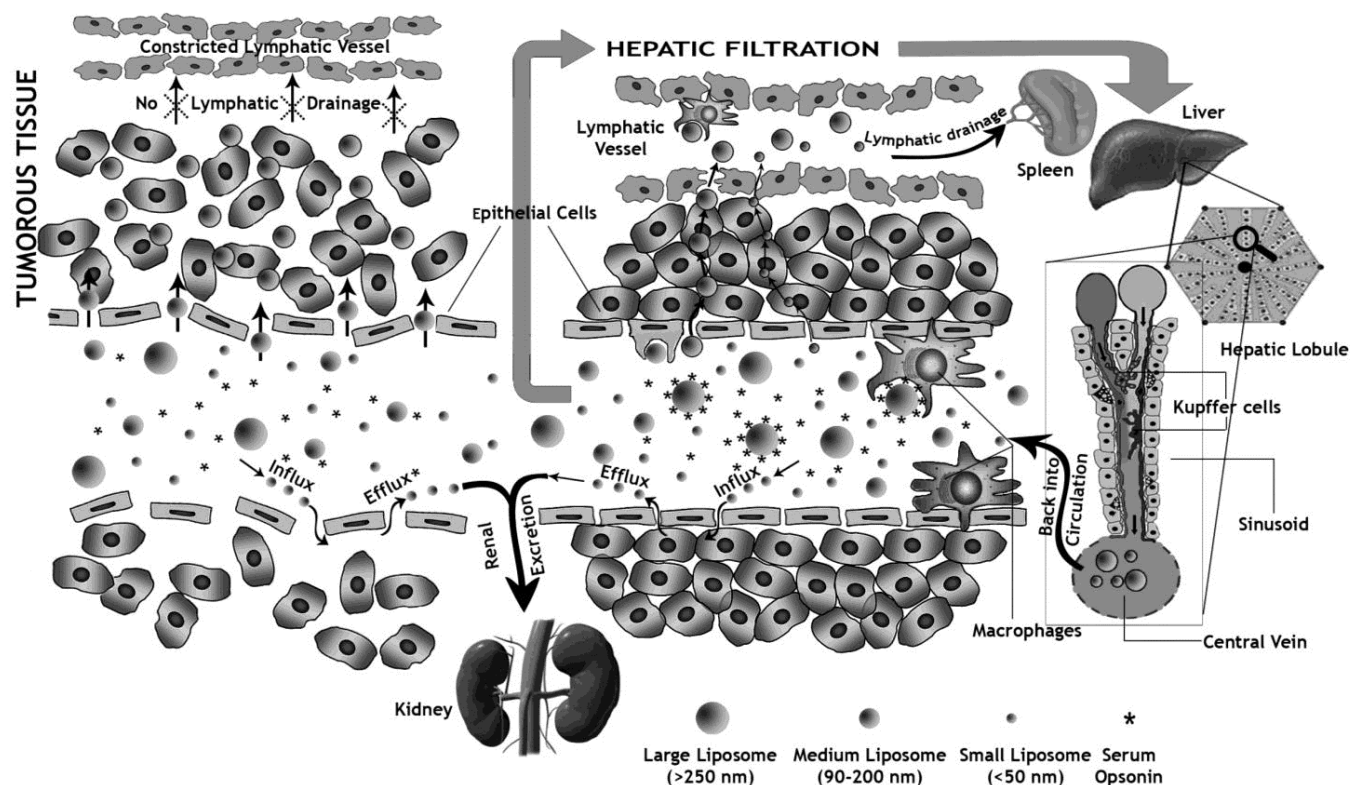


**Fig. (1).** Distributive behavior of liposomes of different sizes depicting the activities of the liposomes in a healthy vascular tissue with a continuous epithelial lining (right) against that in a tumorous tissue having poor lymphatic supply and blood vessels with discontinuous epithelium (left) [9, 11, 25-30].

### Size Dependent Extravasations of Liposome Across Capillary Endothelium

Liposome size is an important factor determining the distribution of liposomes across the capillary walls. The capillary wall is the main hindrance to the permeation of nanoliposomes, and thus also to the efficacy of these therapeutic vesicles. Physiological evidences suggest that the water filled small pores (4 nm) present in the capillary walls are the passage route for the small hydrophilic molecules [39]. Besides that, extremely less number of nonselective pathways only permit the macromolecules in the range of 25-30 nm, which indicates the restricted passage for larger liposomal vesicles having diameter > 25 nm. Probably this may be the cause of the limitation of distribution of commonly used liposomes. Exception is shown in leaky blood vessels, which are prevalent in tumorous tissues, inflamed tissues and sinusoidal tissues [11].

Poste *et al.* [40] have examined the ability of liposomes of variable sizes to cross anatomically different classes of capillaries. They have demonstrated the limited transport of liposome across the open sinusoidal capillaries (as in liver) following i.v. injection but not in the case of organs with continuous capillaries (as in lungs). In this particular study, the liposomes were injected through intravenous route in C57NL/6N mice for evaluating the ability of those liposomes to penetrate into the capillaries. Ultrastructural and cell fractionation studies revealed more efficient penetration of smaller unilamellar vesicles (30-80 nm) across liver sinu-

soids than the larger multilamellar vesicles (500-10000 nm) [40].

When compared between classical liposomes (CL) and stealth liposomes (SL), injected through both subcutaneous (s.c.) and intraperitoneal (i.p.) routes, SL having diameter below 120 nm showed size dependent absorption profile after s.c. application, where CL (either large or small size) were unable to enter the circulation after both s.c. or i.p. route. However, above 120 nm size, SL retained in the site of administration but did not enter the systemic circulation [41].

Collagen fibers of the capillary wall may offer a biophysical marker for the extravagation of liposomes, as this component of capillary wall affects leakiness in healthy or tumor vasculature. Yokoi *et al.* [42] studied the effect of collagen structure on diffusion flux of free doxorubicin (DOX) in comparison to 80 nm doxorubicin-loaded pegylated liposome (DOX-PLD) on tumor vasculature. The results of this study suggests that while the delivery of DOX and DOX-PLD to the same tumor phenotype is determined by their pharmacokinetics, the extravasation of DOX-PLD to different tumor phenotypes is determined by the collagen content. [42]. The accumulation and elimination of drugs in tumor are governed by the permeability of microvasculature. Similarly, the liposome accumulation in tumor is also controlled by the tumor perfusion, extravasation into the tissue and transport within the interstitium. The EPR effect causes the extravasation (through leaky endothelium of the tumor microvasculature, liposomal transcytosis through vascular

endothelial cells) and accumulation of drug, resulting in deposition of most of the liposomes [43]. Most of the liposomal formulations can accumulate 'passively' at the more permeable sites, when their size are in the ultrafilterable range (<200 nm in diameter) [7].

### Liposome Size and MPS Uptake

Liposomes are cleared from the circulation due to the Monuclear Phagocytosis System (MPS) in liver and spleen. The clearance of foreign drug and microorganisms from blood is done chiefly by the MPS. Malfunction of the MPS may cause infections and thus increase mortality [44].

Majority of Kupffer cells, the cells responsible for greater hepatic phagocytic activity are present in the hepatic sinusoids though their activity is uneven. As discussed before, the Kupffer cells are larger in the periportal region and show higher phagocytotic tendencies while the cells located in the centrilobular region have limited activities [45]. These cells can remove foreign and endogenous substances from the systemic circulation through pinocytosis and receptor-mediated endocytosis.

Removal of foreign and endogenous substances from the systemic circulation by the non parenchymal cells of liver is performed through Receptor mediated endocytosis (RME or pinocytosis) [46]. The study of Roger *et al.* [47] re-established that internalization of small compounds (in the mean diameter range of approximately 100-200 nm) are mediated through RME where as larger vesicles are engulfed by phagocytosis. Based on these physiological evidences, it can be assumed that larger liposomes are unable to reach hepatocytes as they are taken up via phagocytosis but smaller one are taken up by both the hepatocytes and Kupffer cells, as already stated. Immunoglobulins and the complements, blood proteins associated with the MPS uptake, are known as major opsonins for the uptake of large vesicles [48]. These proteins are present on the phagocytic cell surface to enhance phagocytosis. The complement system, an immediate host defense against invading pathogens, represents a possible candidate for the major dominant factor in the clearance of liposomes. Nanocarriers undergo rapid clearance by MPS cells after i.v. injection, as they are rapidly opsonised by complement proteins [49].

Liposome size is an important factor in relation with the MPS uptake. Rapid uptake of MLV with a diameter of 200-1000 nm by MPS has been shown to be dependent on their size rather than lipid composition and surface charge [11]. The opsonization of the liposomes by blood components are more pronounced for vesicles with diameter larger than 400 nm and hence the tendency of being taken up by MPS is higher for them. In the case of CL, size and their distribution in MPS cells show an inverse relationship. However, the clearance of SL (by addition of PEG-DSPE into the liposome composition) shows no dependency on size within 80-250 nm [16, 50]. Above this size range, the SLs are increasingly taken up by spleen though in contrast, higher hepatic uptake was seen in case of large CL since uptake into the spleen occurs only after the liver gets saturated with the liposomes. For example, ganglioside coated liposomes were observed to depend on size (liver accumulation for the particle size < 70 nm, and accumulation in spleen for particle size

> 200 nm), while size independent accumulation in liver was seen for identical liposomes made of only phosphatidylserine [7, 51].

### Effect of Size on Release of Liposomal Drug

*In vivo* drug release from liposomal formulations determines the extent of drug accumulation, activity as well as their toxicity. To be therapeutically active, the drugs should retain in the liposomes for a definite time period.

Yamauchi *et al.* [52] correlated the variation of drug release from liposomes with particle size. They reported that release of doxorubicin, a well retained drug in liposomal carriers, was slow and was unaffected by liposomal size while in case of vincristine, a readily releasable drug, showed size dependent release from the liposomal carriers. In the larger liposomes (>120 nm) vincristine retained well in the liposome, but smaller liposomes (approximately 50 nm) released drug more rapidly. They explained that in case of small liposomes, the greater curvature of the vesicle and loose packing of drug between the membrane lipids are responsible for releasing the drug readily than the larger liposomes. They also suggested that below 120 nm the liposomes were unilamellar whereas above 120 nm they are composed of multilamellar vesicles where the drug retention is more favorable. They concluded that larger liposomal formulation of the rapidly releasing drug such as vincristine could improve the efficacy of drug clinically [52].

Nagayasu *et al.* [53] studied the size-dependent *in vivo* release of daunorubicin from different liposomal formulations into the blood circulation, after administration in the rats. The mean vesicle sizes of these liposomes, prepared with HEPC or EPC with cholesterol were adjusted to about 50 and 100 nm. When they compared the two different formulations (HEPC-liposomes and EPC-liposomes) of same size (either 50 nm each or 100 nm each), HEPC-liposomes (50 nm) released the drug gradually (cumulative percent release of the drug reached 40% after 240 min) after intravenous administration, whereas EPC-liposomes released a detectable amount of drug within 5 min and more than 90% of the drug was released within 60 min. After administration, no drug was released for 240 min from HEPC-liposomes having 100 nm diameters. The findings suggest the important role played by both vesicle size and lipid composition on *in vivo* release of drug from liposome.

### Clearance and Liposome Size

Vesicle size is intrinsically related to the rate of its clearance from the blood circulation, and it is a conventional knowledge that smaller liposomes (<300 nm) are retained for a longer period than the larger ones [54]. MPS uptake and the nature of drug release from liposomes are predominant factors for the determination of rate of clearance of liposomal drugs from blood circulation. Variation in liposomal clearance due to the variation of mean diameter of the vesicles is more than 100 folds while the variation produced by other variables (such as surface charge, lipid composition, dose etc.) is around 10 folds [24]. Generally elimination of larger liposomes from blood circulation is faster than the smaller ones [55]. A tentative cut-off size for such effect can be considered at 200 nm, below which vesicles have less



propensity of being removed by the RES. In a similar study involving nobilicide-A (Nob) loaded liposomes that were prepared by extrusion through a pore filter (220 nm) and injected in rats, the greatest presence of Nob-liposomes was found to occur in liver, followed by spleen [56]. This strongly indicates that the size range is perfect to facilitate uptake of liposomes by both the organs, which are the part of the RES.

Renal clearance plays a relatively small role as only vesicles smaller than 5.5 nm are susceptible to it and this may serve as the lower limit for liposomal preparation [57]. A trend of liposomal clearance depending on size was also seen by Mirahmadi *et al.* [58] They showed a direct relation between size and clearance rate by intraperitoneal injection of  $^{99m}\text{Tc}$ -HMPAO (Hexamethyl-propylene-amine-oxime) radio labeled liposomes in mice. For all the formulations used in the experiment, the respective maximum blood concentration levels of  $^{99m}\text{Tc}$ -HMPAO was achieved 2 h after injection with a maximum concentration of ~50% of Initial Dose/g of body weight of the mouse (ID/g) for 100 nm vesicles against 12% ID/g for 400 nm liposomes, and less than 5% ID/g for the 1000 and 3000 nm vesicles. As evident, the highest blood concentration level was produced by the liposomes of 100 nm size and that level was detected even after 24 h of administration, creating an overall AUC which was 8.06 times higher than the AUC generated by free  $^{99m}\text{Tc}$ -HMPAO [58].

When liposomes are injected intravenously, they come in contact with serum proteins (opsonins) which generally bind to foreign vesicles thus permitting the quick recognition by phagocytes. This type of liposome-serum protein interaction has a crucial role in the liposome clearance [60]. Influence of liposomal size on their uptake in the Gastrointestinal Tract (GIT) using DPPC liposomes was observed in an *in vitro* experiment involving Caco-2 cell line [59]. Liposomes of varying size from ~40 nm to over 250 nm were used. The disposition of larger vesicles was recognized and rapidly uptaken by the colonic macrophages and hence cleared at a faster rate.

Harashima *et al.* [11] demonstrated the extent of size dependency of liposomal opsonisation. No size dependent difference has been observed in the extraction of unopsonised liposomes. Thus, the opsonisation of liposomes is dependent on size; and hepatic uptake of liposomes is dependent on opsonisation. The small liposomes generally do not bind the opsonin, as reported by Liu *et al.* [34] when pretreatment of empty liposomes was done in the serum. Physicochemical properties of liposomes are also altered by plasma proteins, which result in altered stability and clearance properties in the biological milieu [61].

Protein binding values indicate the probability of recognition of liposomes by MPS and clearance from the circulation. The systemic circulation half-lives of smaller unilamellar liposomes showed an inverse relationship with the total blood protein (PB) content [62]. When the clearance kinetics between the CL and SL (containing PEG or GM1) were compared in the size range of around 100 nm with the formulation given in low doses, SL showed first order elimination whereas the elimination curve of CL resembled the Michaelis-Menten type kinetics [12, 63]. Longest half lives in circulation was produced with both GM1 conjugated

liposomes [34] and PEG containing liposomes [64] in the size range of 100-200 nm. Reduction of GM1 liposome uptake by MPS was due to decreased blood protein absorption on the liposomal surface [62]. However, the decrease in the extent of liposome below the diameter of 100 nm size range in the blood circulation may be attributed to the elevated hepatic parenchymal uptake because the smaller liposomes are capable of passing through the pores of liver sinusoidal capillaries (which has an average diameter of 100 nm) and have more chances of interaction with the hepatic parenchyma [34, 41]. Another study done with  $^{99m}\text{Tc}$ -HMPAO involved vesicles of various phospholipids of two different size ranges- about 100 nm and about 1000 nm, with the smaller liposomes showed much higher concentrations (from 4 to 12 times varying with composition) in blood compared to their large counterparts and the free  $^{99m}\text{Tc}$ -HMPAO label which were not detectable after 7 h of i.p. injection into mice. On pegylation, the 1000 nm vesicles showed higher plasma AUCs than the nonpegylated forms. However, pegylation often seems to destabilize them due to micellisation or lipid packing defects and bilayer instability at submicellar concentrations [65]. Some predominant trends derived from different studies related to size dependent changes in systemic activity of liposomal drug delivery systems are given in Table 1.

## IMPACT OF LIPOSOME SIZE ON DIFFERENT THERAPEUTIC APPLICATIONS

### Tumor Therapy

Liposomal size is an important factor that has effect on therapeutic activity of liposomal antitumor drugs and their targeting efficiency to tumors. As already told, higher endothelial cell gap (approximately 100-600 nm) in tumor vasculatures than that of the normal tissue (< 6 nm) causes easier extravasation of small size liposomes (less than 200 nm) to tumor cells by EPR effect. Liposomes (>200 nm) remain in the tumor tissue for longer time and more promptly facilitate ligand-receptor interaction by adhering to the target cells [72]. Uchiyama *et al.* [27] studied the interaction of different sized liposomes (40-400 nm) composed of EPC or HEPC, dicetyl phosphate and cholesterol with the tumor cells to investigate the effect of size on such interactions. They concluded that the highest tumor uptake clearance (CL<sub>TU</sub>) values, the greatest tumor accumulation and AUC were exhibited by liposomes of approximately 100 nm size. They demonstrated that uptake of smaller liposomes (50 nm) by tumor cells was more (4-fold) than that of 100 nm liposomes. This may be due to increased endocytosis in tumor. But the enhanced localisation of 100 nm liposomes may be due to the increased tendency of the smaller liposomes (50 nm) to be effluxed readily from the sites and hence suggesting a size-dependent pattern for accumulation of liposome in the tumor [27]. Kibria *et al.* [72] reported an exceptional influence of vesicle size in targeted delivery of DOX through liposomes. They compared the therapeutic effect of DOX-loaded, RGD (Arginylglycylaspartic acid, a tripeptide) modified PEGylated liposomes of both small (~100 nm in diameter) and large size (~300 nm) against Doxil (a clinically used DOX-loaded PEG-liposomes, ~100 nm) in DOX resistant OSRC-2 renal cell carcinoma tumor xenografts. Despite the capability to target and extravasate tumor, Doxil and small size liposomes

**Table 1. Different practical examples of studies which show size dependent variation on the systemic activity of liposomal drug delivery systems.**

Detailed Liposomal content	Size of liposome prepared and used	Size related effect	Conclusion	Reference
<sup>14</sup> C-sucrose labeled liposomes of egg lecithin, phosphatidic acid, chol and $\alpha$ -tocopherol in the molar ratios of 4:1:5:0.1	48, 170, 460 and 720 nm	Peritoneal retention increases above a particular size.	No effect of liposomal size was seen on absorption from the peritoneal cavity. Effect would only be expected if the sizes were to be increased to the point that the entry of vesicles into lymphatic capillaries became restricted.	[66]
A lipid mixture composed of DSPC:Chol:DSPE-PEG (10:10:1). The lipid film was hydrated with saline containing <sup>125</sup> I-TI as a liposomal marker for the distribution study.	120, 400 nm	Circulation time and extravasation into solid tumor tissue were both increased with lowering of sizes.	PEG-liposomes (100-200 nm) showed the maximum prolonged circulation time and the greatest tumor accumulation in all the solid tumors. Although large PEG-liposomes (400 nm) showed a short circulation time in normal mice, the results in splenectomized mice indicated that they had an intrinsic prolonged circulation character <i>in vivo</i> . However, large PEG-liposomes could not extravasate into solid tumor tissue.	[67]
GM1 liposome (EPC/cholesterol/GM1 in 10:5:1), 1-O-palmitoyl-D-glucuronic acid (PGlcUA) liposome (DPPC/Chol/PGlcUA in 4:4:1), Conventional liposome (EPC or HEPC/cholesterol/DCP in 5:4:1)	GM1 liposome (30-555 nm), PGlcUA liposome (100-400 nm), conventional liposome (40-400 nm)	Blood circulation time and drug accumulation in tumor sites were increased by keeping the liposomes in a particular size range.	A size of 100 nm is suitable for retention of liposomes by tumor tissue.	[4]
DSPC/Chol/DMPG/DOX (100:100:60:16 mol)	150, 600 or 4000 nm	Tissue distribution and peritoneal dissemination were inversely proportional with size.	Large liposomes (4000 nm) remained in the abdominal cavity for a long time inducing cytotoxicity. Liposomes, both small and large in size appeared to be effective against solid tumors except in the abdominal cavity, and against peritoneal dissemination in the abdominal cavity, respectively.	[68]
EPC:EPG:Chol liposomes	40, 70 nm	Lymph node localization was slightly proportional to liposomal size.	Liposomes substantially larger than those with the mean size of 70 nm retained at the site of injection. Lymph node localization is much less dependent on liposome size.	[69]
Multilamellar vesicles of DSPC, Chol and DCP (molar ratio of 5:4:1)	410, 460, 510, 1200 nm	Drug targeting increased approximately three fold	The targeting of antimony to the bone marrow was improved (approximately three-folds) with the novel liposomal formulation of 410 nm, when compared to the large sized liposomes of 1200 nm containing meglumine antimoniate.	[70]
DSPC and Chol (molar ratio 2:1)	100, 400, 1000 and 3000 nm	Peritoneal retention increased	Highest retention rate was obtained with 1000 nm liposomes with an AUC value 15.51 times of that of <sup>99m</sup> Tc-HMPAO	[58]
Liposomes containing insulin and bile salts of Sodium Glycocholate (SGC), Sodium Taurocholate (STC) and Sodium Deoxycholate (SDC)	80, 150, 400, and 2000 nm	Hypoglycemic activity and oral bioavailability was directly proportional with the size of liposomes.	Liposomes with 80 nm vesicle size showed less oral bioavailability, which was especially significant in diabetic rats, than liposomes with bigger sizes of 150 nm and 400 nm.	[71]

failed to show antitumor activity through their EPR effect. However large size RGD-PEG- liposomes, with minimized EPR effect, reduced the tumor growth mainly due to its high anti-angiogenic activity on the tumor vasculature and

showed higher multivalent target receptor binding due to presence of higher number of RGD molecules on their surface than the smaller liposome, against the general trend.

Influence on extravasation and interstitial localization by vesicle size were studied using PEG-liposomes in various size ranges by Ishida *et al.* [67]. They reported that the liposomes with average size of 100-200 nm showed the highest circulation time and the greatest tumor accumulation.

### Ocular Drug Delivery

Size is an important phenomenon determining the efficacy of ocular drug delivery system. As compared to drug solutions, liposomes reduce solution drainage. Increase in liposomal size has been reported to restrict solution drainage to prolong contact time of drug [73]. However, increase in size should be within the limit of tolerable irritancy. Ophthalmic delivery of coumarin-6 improved greatly by reducing liposomal size to less than 100 nm and the correlation persisted on further reduction [74]. Tsukamoto *et al.* [75] showed that vesicles of 100 nm prepared for ophthalmic administration almost achieved 100 % drug loading efficiency when bromofenac was loaded using pH gradient method. Earlier studies by the same group [76] demonstrated the successful efficacy of 100 nm DSPC liposomes in delivering drugs to the posterior region of the eye. Therefore, it can be assumed that limiting liposome vesicle size to 100 nm is preferable for better ophthalmic drug therapy.

### Antibiotic Therapy

The distribution of antibiotic drugs is considerably influenced by the vesicle size of liposomes. MLV formulations (>1000 nm) are not often used in antibiotic carriers while SUVs (~100 nm) are highly efficacious for controlling bacterial infections [77]. Allahajan *et al.* [78] prepared clarithromycin loaded liposomes with different surface charges and investigated the efficacy and safety of these formulations against *Pseudomonas aeruginosa*, which was clinically isolated from the lungs of patients with cystic fibrosis. They reported that in case of liposomes, its size is a determining factor based on its anatomical target. Negatively charged liposomes containing clarithromycin possessed larger diameter than positively charged vesicles and this difference in size may be due to the inclusion of charge that increased the space between the adjacent bilayers. Bakker- Woudenberg *et al.* [79] determined the increased survival rate of rats after administering liposomal gentamicin than the free drug in the model of pneumonia. The formulated liposomes decreased the number of bacteria in infected lungs. In this study, localization of small-sized liposomes (100 nm) was more in the infected tissue than the larger liposomes (280 nm and 360 nm) as the larger ones were preferentially taken up by MPS organs.

### Vaccine Delivery

Cationic liposomes are widely applied as well-known vaccine carriers. Liposomal size is an important factor for their efficiency as carrier as there is an effect on the immunogenicity of liposome associated antigens. Carstens *et al.* [80] described the size-dependent immunogenicity of liposomal DNA vaccines given through subcutaneous route. The liposomes were composed of EPC, dioleoyl-phosphoethanolamine and 1,2-dioleoyl-3-trimethylammonium-propane (DOTAP) containing OVA-encoding pDNA. Liposomes of

two size range, 500 nm and 140 nm, were used to study the tissue distribution. Higher *in vitro* transfection efficiency and stronger activation of the important pathogen recognition receptor TLR9 were observed with the smaller liposomes, measured against naked pDNA. In a study Milicic *et al.* [81] showed by using cationic liposomes of DDA and TDB that the liposomes had different tendencies to induce humoral and cellular immunity depending on their size and lamellarity. In this study, small unilamellar liposomal formulation when conjugated with protein antigen showed significant cellular response as well as humoral adaptation in the size of about 600 nm than the larger multilamellar vesicles.

### Transdermal Delivery

A major obstacle in tropical/transdermal delivery is low percutaneous penetration of drug, owing to the hydrophobic environment of the skin. According to Khosravi-Darani *et al.* [2], nanotechnology among the other approaches, provides a significant result in overcoming transdermal barrier and thus enhances drug delivery across the skin. The nanosized elastic vesicles and ethosomes ensured the protection of stratum corneum (SC) against different nonionic surfactants through the visual detection of nontreated and treated SC (incubated with nanoliposomes and octyl glucoside). The size of the liposomes has great influence on the intact passage through the lipid rich outer layer of the skin (SC) to the deeper area. du Plessis *et al.* reported that the vesicles with the size of about 300 nm rather than smaller vesicles of about 60 nm had highest reservoir capacity in deeper skin strata [82]. Verma *et al.* [83] investigated the liposomal size dependent transport of fluorescent compound (both hydrophilic and lipophilic) into human skin. They used different liposomes with variation in different well-defined compositions and sizes. The confocal laser scanning microscopy study revealed that, smaller vesicles ( $\leq 300$  nm) delivered the drug to the deeper layer into the skin to some extent more in comparison with larger liposomes ( $\geq 600$  nm). Liposomes with the vesicle size ( $\leq 70$  nm) were able to deliver the contents maximum to the epidermis as well as in the dermis [83].

### Respiratory Drug Delivery

Extensive research has been done on liposomes for their pulmonary drug delivery as they are proved to be biocompatible, bio-degradable as well as non-toxic in nature. Chougule *et al.* [84] in their study have developed spray dried liposomal dry powder inhaler of dapsone. They showed that the liposome enhanced deep lung deposition, with maximum fine particle fraction (>75%) with the particle size 7.9  $\mu\text{m}$ . The formulations had a prolonged *in vitro* drug release (duration up to 16 h). Another significant effort to use of liposomes in pulmonary administration is to deliver insulin [85]. In the study, liposomes loaded with Insulin was aerosolized and delivered using ultrasonic nebulizer. The resultant vesicles were of 1  $\mu\text{m}$  in size approximately and suitably delivered insulin into the alveoli.

### CONCLUSION

Reports related to effect of liposome size on drug delivery are very limited. After reviewing the available informa-

tion, it may be concluded that liposomal size has a significant impact in the treatment of different diseases. Larger size liposomes increase their chances of being recognized by the RES system and fast systemic clearance through phagocytotic uptake. Smaller size of liposomes is selected for their cohesiveness, adhesiveness and EPR effect in various drug delivery applications, facilitating passive targeting. Very small liposomes (<50 nm) have a great tendency of being readily effluxed from their accumulation site due to their resemblance to endosomes in size, an effect which is highly subsidized if the size of the liposome is kept in a range of 100-120 nm. Thus, the potential benefit of liposomal drug delivery system can be achieved through the development of liposomal carrier of the desired optimal size. Therefore, more research in the area should be focused in future to gain optimum efficacy of drug delivery strategies by adjusting the size of liposomal carrier according to the need.

### CONFLICT OF INTEREST

The authors confirm that this article content has no conflicts of interest.

### ACKNOWLEDGEMENTS

Declared none.

### REFERENCES

- Sen, K.; Mandal, M. Second generation liposomal cancer therapeutics: Transition from laboratory to clinic. *Int. J. Pharm.*, **2013**, *448*, 28-43.
- Khosravi-Darani, K.; Mozafari, M. R. Nanoliposome Potentials in Nanotherapy: A Concise Overview. *Int. J. Nanosci. Nanotechnol.*, **2010**, *6(1)*, 3-13.
- Sawant, R. R.; Torchilin, V. P. Challenges in Development of Targeted Liposomal Therapeutics. *AAPS. J.*, **2012**, *14(2)*, 303-315.
- Nagayasu, A.; Uchiyama, K.; Kiwada, H. The size of liposomes: a factor which affects their targeting efficiency to tumors and therapeutic activity of liposomal antitumor drugs. *Adv. Drug. Deliv. Rev.*, **1999**, *40*, 75-87.
- Akbarzadeh, A.; Rezaei-Sadabady, R.; Davaran, S.; Joo, S. W.; Zarghami, N.; Hanifehpour, Y.; Samiei, M.; Kouhi, M.; Uchiyama, K.; Nagayasu, A.; Yamagiwa, Y.; Nishida, T.; Harashima, H.; Kiwada, H. Effects of the size and fluidity of liposomes on their accumulation in tumors: A presumption of their interaction with tumors. *Int. J. Pharm.*, **1995**, *121*, 195-203.
- Nejati-Koshki, K. Liposome: classification, preparation, and applications. *Nanoscale Res Lett*, **2013**, *8(102)*, 1-9.
- Allen, T.M.; Cullis, P.R. Liposomal drug delivery systems: From concept to clinical applications. *Adv. Drug Deliv. Rev.*, **2013**, *65*, 36-48.
- Badiee, A.; Jaafari, M.R.; Khamesipour, A.; Samiei, A.; Soroush, D.; Kheiri, M.T. The role of liposome charge on immune response generated in BALB/c mice immunized with recombinant major surface glycoprotein of Leishmania (rgp63). *Exp Parasitol*, **2009**, *121(4)*, 362-9.
- Taira, M.C.; Chiaramoni, N.S.; Pecuch, K.M.. Stability of liposomal formulations in physiological conditions for oral drug delivery. *Drug Deliv*, **2004**, *11*, 123-8.
- Immordino, M. L.; Dosio, F.; Cattelet, L. Stealth liposomes: review of the basic science, rationale, and clinical applications, existing and potential. *Int. J. Nanomedicine*, **2006**, *1(3)*, 297-315.
- Harashima, H.; Sakata, K.; Funato, K.; Kiwada, H. Enhanced hepatic uptake of liposomes through complement activation depending on the size of liposomes. *Pharm. Res*, **1994**, *11(3)*, 402-406.
- Hwang, K.J. (1987) Liposome pharmacokinetics. In: M.J. Ostro (Ed.), *Liposomes: from Biophysics to Therapeutics*. Marcel Dekker, New York, pp. 109-156
- Senior, J. H. Fate and behaviour of liposomes in vivo: A review of controlling factors. *CRC Crit. Rev. Ther. Drug. Carrier. Syst.*, **1987**, *3*, 123-193.
- Allen, T.M.; Everest, J.M. Effect of liposome size and drug release properties on pharmacokinetics of encapsulated drug in rats. *J. Pharmacol. Exp. Ther.*, **1983**, *226*, 539-544.
- Drummond, D. C.; Meyer, O.; Hong, K.; Kirpotin, D. B.; Papahadjopoulos, D. Optimizing Liposomes for Delivery of Chemotherapeutic Agents to Solid Tumors, *Pharmacol. Rev.*, **1999**, *51(4)*, 691-743.
- Woodle, M.C.; Matthey, K.K.; Newman, M. S.; Hidayat, J. E.; Collins, L.R.; Redemann, C.; Martin, F.J.; Papahadjopoulos, D. Versatility in lipid compositions showing prolonged circulation with sterically stabilized liposomes. *Biochim. Biophys. Acta*, **1992**, *1105*, 193-200.
- Maruyama, K. Intracellular targeting delivery of liposomal drugs to solid tumors based on EPR effects, *Adv. Drug Deliv. Rev.*, **2011**, *63*, 161-169.
- Ahl, P. L.; Bhatia, S.K.; Meers, P.; Roberts, P.; Stevens, R.; Dause, R.; Perkins, W. R.; Janoff, A.S. Enhancement of the in vivo circulation lifetime of L-a-distearoylphosphatidylcholine liposomes: Importance of liposomal aggregation versus complement opsonization. *Biochim. Biophys. Acta*, **1997**, *1329*, 370-382.
- Watson D.S.; Endsley, A. N.; Huang, L. Design considerations for liposomal vaccines: Influence of formulation parameters on antibody and cell-mediated immune responses to liposome associated antigens. *Vaccine*, **2012**, *30*, 2256-2272.
- Beaumier, P.L.; Hwang, K.J. Effects of liposome size on the degradation of bovine brain sphingomyelinicholesterol liposomes in the mouse liver. *Biochim. Biophys. Acta*, **1983**, *731*, 23-30.
- Chow, D. D.; Essien, H. E.; Padki, M.M.; Hwang, K.J. Targeting small unilamellar liposomes to hepatic parenchymal cells by dose effect. *J. Pharm. Exp. Ther.*, **1989**, *248*, 506-513.
- Needham, D.; McIntosh, T.J.; Lasic, D.D. Repulsive interactions and mechanical stability of polymer - grafted lipid membranes. *Biochim Biophys Acta*, **1992**, *1108*, 40-48.
- Mori, A.; Klibanov, A.L.; Torchilin, V.P.; Huang, L. Influence of the steric barrier activity of amphiphatic poly(ethyleneglycol) and ganglioside GM1 on the circulation time of liposomes and on the target binding of immunoliposomes in vivo. *FEBS Lett*, **1991**, *284*, 263-266.
- Harashima, H.; Kiwada, H. Liposomal targeting and drug delivery: kinetic consideration. *Adv. Drug. Deliv. Rev.*, **1996**, *19*, 425-444.
- Wisse, E.; de Zanger, R.B.; Charels, K.; Van der Smisse, P.; McCuskey, R.S. The liver sieve: considerations concerning the structure and function of endothelial fenestrate, the sinusoidal wall and the space of Disse. *Hepatology*, **1985**, *5*, 683-692.
- Maeda, H.; Sawa, T.; Konno, T. Mechanism of tumor targeted delivery of macromolecular drugs, including the EPR effect in solid tumor and clinical overview of the prototype polymeric drug SMANCS. *J. Controlled. Release*, **2001**, *74*, 47-61.
- Uchiyama, K.; Nagayasu, A.; Yamagiwa, Y.; Nishida, T.; Harashima, H.; Kiwada, H. Effects of the size and fluidity of liposomes on their accumulation in tumors: A presumption of their interaction with tumors. *Int. J. Pharm.*, **1995**, *121*, 195-203.
- Allen, T.M.; Chonn, A. Large unilamellar liposomes with low uptake into the reticuloendothelial system. *FEBS Lett*, **1987**, *223*, 42-46.
- Patel, H.M. Serum opsonins and liposomes: their interaction and opsonophagocytosis. *Crit. Rev. Ther. Drug Carrier Syst.*, **1992**, *9*, 39-90.
- Senior, J.; Crawly, J.C.W.; Gregoriadis, G. Tissue distribution of liposomes exhibiting long half-lives in the circulation after intravenous injection. *Biochim. Biophys. Acta*, **1992**, *839*, 1-8.
- Jain, R.K. Delivery of novel therapeutic agents in tumors: physiological barriers and strategies. *J. Natl. Cancer Inst.*, **1989**, *81*, 570-576.
- Yuan, F.; Leuning, M.; Huang, S.K.; Berk, D.A.; Papahadjopoulos, D.; Jain, K. Microvascular permeability and interstitial penetration of sterically stabilized (stealth) liposomes in a human tumor xenograft. *Cancer Res*, **1994**, *54*, 3352-3356.
- Maruyama, K.; Ishida, O.; Takizawa, T.; Moribe, K. *Adv. Drug Deliv. Rev.*, **1999**, *40*, 89-102.
- Liu, D.; Mori, A.; Huang, L.; Role of liposome size and RES blockade in controlling biodistribution and tumor uptake of GMI-

- Containing liposomes. *Biochim. Biophys. Acta*, **1992**, *1104*, 95-101.
- [35] Unezaki, S.; Maruyama, K.; Ishida, O.; Suginaka, A.; Hosoda, J.; Iwatsuru, M. Enhanced tumor targeting and improved antitumor activity of doxorubicin by longcirculating liposomes containing amphipathic poly(ethylene glycol). *Int. J. Pharm.*, **1995**, *126*, 41-48.
- [36] Brewer, J.M.; Tetley, L.; Richmond, J.; Liew, F.Y.; Alexander, J. Lipid vesicle size determines the Th1 or Th2 response to entrapped antigen. *J. Immunol.*, **1998**, *161*, 4000-4007.
- [37] Mann, J.F.; Shakir, E.; Carter, K.C.; Mullen, A.B.; Alexander, J.; Ferro, V. A. Lipid vesicle size of an oral influenza vaccine delivery vehicle influences the Th1/Th2 bias in the immune response and protection against infection. *Vaccine*, **2009**, *27*, 3643-3649.
- [38] Henriksen-Lacey, M.; Devitt, A.; Perrie, Y. The vesicle size of DDA:TDB liposomal adjuvants plays a role in the cell-mediated immune response but has no significant effect on antibody production. *J. Controlled Release*, **2011**, *154*(2), 131-137.
- [39] Tarbell, J. M. Mass transport in arteries and the localization of atherosclerosis. *Annu. Rev. Biomed Eng.*, **2003**, *5*, 79-118.
- [40] Poste, G.; Bucana, C.; Raz, A.; Bugelski, P.; Kirsh, R.; Fidler, I. J. Analysis of the fate of systemically administered liposomes and implications for their use in drug delivery. *Cancer Res.*, **1982**, *42*, 1412-1422.
- [41] Allen, T.M.; Austin, G.A.; Chonn, A.; Lin, L.; Lee, K.C. Uptake of liposomes by cultured mouse bone marrow macrophages: influence of liposome composition and size. *Biochim. Biophys. Acta*, **1991**, *1061*, 56-64.
- [42] Yokoi, K.; Kojic, M.; Milosevic, M.; Tanei, T.; Ferrari, M.; Ziemys, A. Capillary-wall collagen as a biophysical marker of nanotherapeutic permeability into the tumor microenvironment. *Cancer Res.*, **2014**, doi: 10.1158/0008-5472.CAN-13-3494.
- [43] Ait-Oudhia, S.; Mager, E. D.; Straubinger, R. M. Application of pharmacokinetic and pharmacodynamic analysis to the development of liposomal formulations for oncology. *Pharmaceutics*, **2014**, *6*, 137-174; doi:10.3390/pharmaceutics6010137.
- [44] Van Etten, E. W. M.; Ten Kate, M. T.; Snijders, S. V.; Bakker-Woudenberg, I. A. J. M. Administration of liposomal agents and blood clearance capacity of the mononuclear phagocyte system. *Antimicrob. Agents. Chemother.*, **1998**, *42* (7)1677-1681.
- [45] Brodt, P. *Liver Metastasis: Biology and Clinical Management*, Springer Science+Business Media: New York, 2011.
- [46] Mishra, N.; Yadav, N.P.; Rai, V.K.; Sinha, P.; Yadav, K.S.; Jain, S.; 2 Arora, S. Efficient Hepatic Delivery of Drugs: Novel Strategies and Their Significance. *BioMed Res. Int.*, **2013**, 1-20.
- [47] Roger, E.; Lagarce, F.; Garcion, E.; Benoit, J.P. Lipid nanocarriers improve paclitaxel transport throughout human intestinal epithelial cells by using vesicle-mediated transcytosis. *J. Controlled Release*, **2009**, *140*, 174-181.
- [48] Simberg, D.; Park, J.H.; Karmali, P. P.; Zhang, W. M.; Merkulov, S.; McCrae, K.; Bhatia, S. N.; Sailor, M.; Ruoslahti, E. Differential proteomics analysis of the surface heterogeneity of dextran iron oxide nanoparticles and the implications for their in vivo clearance. *Biomaterials*, **2009**, *30*, 3926-3933.
- [49] Salmasso, S.; Caliceti, P. Stealth Properties to Improve Therapeutic Efficacy of Drug Nanocarriers. *J. Drug Deliv.*, **2013**, 1-19.
- [50] Gabizon, A.; Papahadjopoulos, D. The role of surface charge and hydrophilic groups on liposome clearance in vivo. *Biochim Biophys Acta*. **1992**, *1103* (1), 94-100.
- [51] Jokerst, J.V.; Lobovkina, T.; Zare, R.N.; Gambhir, S.S. Nanoparticle PEGylation for imaging and therapy. *Nanomedicine(Lond)*, **2011**, *6*(4), 715-728.
- [52] Yamauchi, M.; Tsutsumi, K.; Abe, M.; Uosaki, Y.; Nakakura, M.; Aoki, N. Release of Drugs from Liposomes Varies with Particle Size. *Biol. Pharm. Bull.*, **2007**, *30*(5), 963-966.
- [53] Nagayasu, A.; Shimooka, T.; Kiwada, H. Effects of vesicle size on in vivo release of daunorubicin from hydrogenated egg phosphatidylcholine-based liposomes into blood circulation. *Biol. Pharm. Bull.*, **1995**, *18*, 1020-1023.
- [54] Bae, Y. H.; Park, K. Targeted drug delivery to tumors: Myths, reality and possibility. *J. Controlled Release*, **2011**, *153*, 198-205.
- [55] Senior, J. H. Fate and behavior of liposomes in vivo: a review of controlling factors. *Crit. Rev. Ther. Drug Carrier Syst.*, **1987**, *3*, 123-193.
- [56] Xiong, Y.; Jianming, J.; Guo, D. Bio-distribution and pharmacokinetics of nobilside A-loaded liposome following intravenous administration in rats. *J. Chromatogr.*, **2014**, *B: 962*, 132-140.
- [57] Ernsting, M. J.; Murakami, M.; Roy, A.; Li, S-D. Factors controlling the pharmacokinetics, biodistribution and intratumoral penetration of nanoparticles. *J. Controlled Release*, **2013**, *172*, 782-794.
- [58] Mirahmadi, N.; Babaei, M.H.; Vali, A.M.; Dadashzadeh, S. Effect of liposome size on peritoneal retention and organ distribution after intraperitoneal injection in mice. *Int. J. Pharm.*, **2010**, *383*, 7-13.
- [59] Ishida, T.; Harashima, H.; Kiwada, H. Liposome clearance. *Biosci. Rep.*, **2002**, *22*(2), 197-224.
- [60] Andar, A. U.; Hood, R. R.; Vreeland, W. N.; DeVoe, D. L.; Swaan, P.W. Microfluidic preparation of liposomes to determine particle size influence on cellular uptake mechanisms. *Pharm. Res.*, **2014**, *31*, 401-413.
- [61] Semple, S. C.; Chonn, A.; Cullis, P. R. Interactions of liposomes and lipid-based carrier systems with blood proteins: Relation to clearance behaviour in vivo. *Adv. Drug. Deliv. Rev.*, **1998**, *32*, 3-17.
- [62] Chonn, A.; Semple, S. C.; Cullis, P. R. Association of blood proteins with large unilamellar liposomes in vivo. *J. Biol. Chem.*, **1992**, *267* (26), 18759-18765.
- [63] Lasic, D.D. *Liposomes: from Physics to Applications*, Elsevier Science Publishers, Amsterdam, **1993**.
- [64] Litzinger D.C.; Buiting, A.M.J.; van Rooijen, N.; Huang, L. Effect of liposome size on the circulation time and intraorgan distribution of amphipathic poly(ethylene glycol)-containing liposomes. *Biochim. Biophys. Acta.*, **1994**, *1190*, 99-107.
- [65] Dadashzadeh, S.; Mirahmadi, N.; Babaei, M. H.; Vali, A. M. Peritoneal retention of liposomes: Effects of lipid composition, PEG coating and liposome charge. *J. Controlled Release*, **2010**, *148*, 177-186.
- [66] Hirano, K.; Hunt, C.A. Lymphatic transport of liposome-encapsulated agents: effects of liposome size following intraperitoneal administration. *J. Pharm. Sci.*, **1985**, *74*, 915-921.
- [67] Ishida, O.; Maruyama, K.; Sasaki, K.; Iwatsuru, M. Size-dependent extravasation and interstitial localization of polyethyleneglycol liposomes in solid tumor-bearing mice. *Int J Pharm.*, **1999**, *190* (1), 49-56.
- [68] Sadzuka, Y.; Hirota, S.; Sonobe, T. Intraperitoneal administration of doxorubicin encapsulating liposomes against peritoneal dissemination. *Toxicol. Lett.*, **2000**, *116*(1-2), 51-9.
- [69] Oussoren, C.; Storm, G.; Liposomes to target the lymphatics by subcutaneous administration. *Adv. Drug Deliv. Rev.*, **2001**, *50*, 143-156.
- [70] Schettini, D.A.; Ribeiro, R.R.; Demicheli, C.; Rocha, O.G.F.; Melo, M.N.; Michalic, M.S.M.; Frézar, F. Improved targeting of antimony to the bone marrow of dogs using liposomes of reduced size. *Int. J. Phar.*, **2006**, *315*, 140-147.
- [71] Niu, M.; Lu, Y.; Hovgaard, L.; Guan, P.; Tan Y.; Lian, R.; Wu, W.; Qi, J. Hypoglycemic activity and oral bioavailability of insulin-loaded liposomes containing bile salts in rats: The effect of cholate type, particle size and administered dose. *Eur. J. Pharm. Biopharm.*, **2012**, *81*, 265-272.
- [72] Kibria, G.; Hatakeyama, H.; Ohga, N.; Hida, K.; Harashima, H. The effect of liposomal size on the targeted delivery of doxorubicin to Integrin  $\alpha\beta 3$ -expressing tumor endothelial cells. *Biomaterials*, **2013**, *34*, 5617-5627.
- [73] Kaur, I. P.; Garg, A.; Singla, A. K.; Aggarwal, D. Vesicular systems in ocular drug delivery: an overview. *Int. J. Pharm.*, **2004**, *269*, 1-14.
- [74] Inokuchi Y, Hironaka K, Fujisawa T, et al. Physicochemical properties affecting retinal drug/coumarin-6 delivery from nanocarrier systems via eyedrop administration. *Invest. Ophthalmol. Vis. Sci.*, **2010**, *51*(6), 3162-70.
- [75] Tsukamoto, T.; Hironaka, K.; Fujisawa, T.; Yamaguchi, D.; Tahara, K.; Tozuka, Y.; Takeuchi, H. Preparation of bromfenac-loaded liposomes modified with chitosan for ophthalmic drug delivery and evaluation of physicochemical properties and drug release profile. *Asian J Pharm.*, **2013**, *8*, 104-109
- [76] Hironaka, K.; Inokuchi, Y.; Tozuka, Y. Design and evaluation of a liposomal delivery system targeting the posterior segment of the eye. *J. Controlled. Release*, **2009**, *136* (3), 247-253.
- [77] Krieger, J., Childs, S., Klimberg, I., 1999. UTI treatment using liposomal amikacin (MiKasome®). In: Program and Abstract of the Ninth European Congress of Clinical Microbiology and Infectious Diseases. *Clin. Microbiol. Inf.*, **1999**, 136.
- [78] Alhajlan, M.; Alhariri, M.; Omri, A. Efficacy and Safety of Liposomal Clarithromycin and Its Effect on *Pseudomonas aerugi-*

- nosa* Virulence Factors. *Antimicrob. Agents Chemother.* **2013**, *57*(6), 2694-2904.
- [79] Bakker-Woudenberg, I.A.J.M.; Storm, G.; Woodle, M.C. Liposomes in the treatment of infections. *J. Drug Target*, **1994**, *2*, 363-371.
- [80] Carstens, M.G.; Camps, M.G.; Henriksen-Lacey, M.; Franken, K.; Ottenhoff, T. H.; Perrie, Y.; Bouwstra, J.A.; Ossendorp, F.; Jiskoot, W. Effect of vesicle size on tissue localization and immunogenicity of liposomal DNA vaccines. *Vaccine*, **2011**, *29*, 4761- 4770.
- [81] Milicic, A.; Kaur, R.; Reyes-Sandoval, A.; Tang, C. K.; Honeycutt, J.; Perrie, Y.; Hill, A. V. S. Small cationic DDA:TBD liposomes as protein vaccine adjuvants obviate the need for TLR agonists in inducing cellular and humoral responses. *PLoS ONE*, **2012**, *7*(3), e34255
- [82] du Plessis, J.; Ramachandran, C.; Weiner, N.; Muller, D. G. The influence of particle size of drug of liposomes on the deposition into skin. *Int. J. Pharm*, **1994**, *103*, 277-282.
- [83] Verma, D.D.; Verma, S.; Blume, G.; Fahr, A. Particle size of liposomes influences dermal delivery of substances into skin. *Int. J. Pharm*, **2003**, *258*, 141-151.
- [84] Chougule, M.; Padhi, B.; Misra, A. Development of Spray Dried Liposomal Dry Powder Inhaler of Dapsone. *AAPS. Pharm. Sci. Tech*, **2008**, *9*(1), 47-53.
- [85] Huang, Y. Y.; Wang, C. H. Pulmonary delivery of insulin by liposomal carriers. *J. Controlled Release*, **2006**, *113*, 9-14.



(1)

Search for...

Search

Search in:  All  Article  Chapter  eBook[Purchase PDF](#)

## Peptides, Proteins and Peptide/Protein-Polymer Conjugates as Drug Delivery System

**Author(s):** Biswajit Mukherjee, Swapna D. Karmakar, Chowdhury M. Hossain, Sanchari Bhattacharya.

**Journal Name:** Protein & Peptide Letters

**Volume 21 , Issue 11 , 2014**

**DOI :** 10.2174/0929866521666140804160907 (<https://doi.org/10.2174/0929866521666140804160907>)

[Journal Home \(/node/628\)](#)

8th INTERNATIONAL CONFERENCE ON  
DRUG DISCOVERY & THERAPY 2019  
February 13 - 15, 2019, BANGKOK, THAILAND [Register Now](#)  
**Call for Abstracts**

(<https://bit.ly/2MrrXwV>)

### Abstract:

In the last few decades, novel drug delivery strategies have been a big priority to the formulation scientists. Peptides and proteins have drawn a special attention for their wide scope in the area. Serum albumin, transferrin, recombinant proteins, virus capsids etc. are used as carrier for drug and biomolecules. Conjugates of polymers with proteins have also shown strong potency in the field of drug delivery. Polyethylene glycol is one of the most successful polymers that has been used extensively to develop protein conjugated formulations. Besides, polyvinyl pyrrolidone, polylactic-co-glycolic acid, N-(2-hydroxypropyl) methacrylamide copolymer, polyglutamic acid have also been investigated. In this re-

we will highlight on the most recent overview of various advantages, limitations and marketed products of proteins, peptides and protein/peptide-polymer conjugates as drug carriers, such products in clinical trials and their various uses in the field of modern drug delivery. Understanding the key features of these materials and the vigorous research in this field will develop new drug formulations that will combat various types of life-threatening diseases.

**Keywords:** Conjugates, drug delivery, peptides, proteins, virus nanoparticles.

[Mark Item](#)
[Purchase PDF](#)
[Rights & Permissions](#)
[Print](#)
[Export](#)
[Cite as](#)

Other

### Article Details

VOLUME: 21

ISSUE: 11

Year: 2014

Page: [1121 - 1128]

Pages: 8

DOI: 10.2174/0929866521666140804160907

(<https://doi.org/10.2174/0929866521666140804160907>)

Price: \$58

### Article Metrics

PDF: 47

### We recommend

Polymer based protein therapeutics

Showkat Ahmad Bhawani et. al., *Curr Protein Pept Sci*

Multifunctional delivery systems for advanced oral uptake of peptide/protein drugs.

Jin Woo Park et al., *Curr Pharm Des*

Progress in nanoparticulate systems for peptide, proteins and nucleic acid drug delivery.

Stanislaw Slomkowski et al., *Curr Pharm Biotechnol*

Biodegradable Polymer Based Particulate Carrier(s) for the Delivery of Proteins and Peptides  
Antiinflamm Antiallergy Agents *Med Chem*

Recent advances on patents in poly(ethylene glycol)-based drug delivery.

Conjugation of cell-penetrating peptides with poly(lactic-co-glycolic acid)-polyethylene glycol nanoparticles improves ocular drug delivery

Aimee Vasconcelos et al., *International Journal of Nanomedicine*

Polyethylene glycol in spinal cord injury repair: a critical review

Xi Lu et al., *Journal of Experimental Pharmacology*

Poly(organo)phosphazenes: recent progress in the synthesis and applications in tissue engineering and drug delivery

Rizwan Ullah Khan et al., *Russian Chemical Reviews*

Recent Innovations in Peptide Based Targeted Drug Delivery to Cancer Cells



Gian M Bonora et al., Recent Pat Drug Deliv  
Formul

Yosi Gilad, Biomedicines

Design, Synthesis and Characterization of Novel  
Co-Polymers Decorated with Peptides for the  
Selective Nanoparticle Transport across the  
Cerebral Endothelium

Falanga et. al.; Melone, Pietro ; Cagliani,  
Roberta ; Borbone, Nicola ; D'Errico, Stefano ;  
Piccialli, Gennaro ; Netti, Paolo A.; Guarnieri,  
Daniela et al., Molecules

Powered by **TREND MD**

(/terms/termandcondition.html?1)

© 2018 Bentham Science Publishers (<http://www.eurekaselect.com/136826/page/terms-and-conditions>)



[Get Access](#)[Export](#)

## Nano- and Microscale Drug Delivery Systems

Design and Fabrication

2017, Pages 357-375

### Chapter 19 - Pharmacokinetic and Pharmacodynamic Modulations of Therapeutically Active Constituents From Orally Administered Nanocarriers Along With a Glimpse of Their Advantages and Limitations

Biswajit Mukherjee, Bhabani S. Satapathy, Sanchari Bhattacharya, Rhitabrita Chakraborty, Vimal P. Mishra

[Show more](#)

<https://doi.org/10.1016/B978-0-323-52727-9.00019-4>

[Get rights and content](#)

#### Abstract

Oral delivery is the most accepted route for administration of drugs due to higher patient compliance. However, delivery of molecules, such as proteins, **peptides**, and **antibodies**, is extremely challenging through this route. Poor stability, enzymatic degradation in **gastrointestinal tract** (GIT), low **bioavailability** along with rapid **mucosal** clearance are the major limitations in oral delivery. To overcome these problems, nanocarrier-based drug delivery technology has emerged as an attractive alternative in recent times. The main advantages of the drug **nanocarriers** involve protection of the loaded cargo in external GI environment, overcome the mucosal barrier due to nanosize, increased solubility, and bioavailability due to higher surface area, as well as **controlled release**. These systems are now being investigated to improve the efficacy, safety, **pharmacokinetic**, and **pharmacodynamic** parameters of orally delivered **therapeutic agents**. Selective targeting can also be achieved through active functionalized groups attached on the surface of nanocarriers. The modified nanocarriers are thus intended to provide enhanced pharmacological effects with less side effects leading to better therapeutic index and clinical outcomes. The pharmacokinetic and pharmacodynamic properties of orally delivered nanocarriers depend on several factors, including size, **surface modification**, **surface charge**, mucoadhesive property. The chapter focuses on the advancement in the oral delivery of drug nanocarriers,

highlighting on the pharmacokinetic and pharmacodynamics modulations, their advantages along with the fundamental limitations and the future perspective based on the recent findings in the field.

[< Previous](#)

[Next >](#)

## Keywords

oral nanocarriers; drug delivery; pharmacokinetics; nanoparticles; GI barriers; transcellular transport; pharmacodynamics

---

[Recommended articles](#)

[Citing articles \(0\)](#)

Copyright © 2017 Elsevier Inc. All rights reserved.

---

**ELSEVIER**

[About ScienceDirect](#) [Remote access](#) [Shopping cart](#) [Contact and support](#) [Terms and conditions](#)  
[Privacy policy](#)

We use cookies to help provide and enhance our service and tailor content and ads. By continuing you agree to the [use of cookies](#).

Copyright © 2018 Elsevier B.V. or its licensors or contributors. ScienceDirect® is a registered trademark of Elsevier B.V.

 **RELX Group™**

---

# Targets and Approaches to Control Hepatocellular Carcinoma in Future

---

Mukherjee Biswajit,  
Hossain Chowdhury Mobaswar ,  
Bhattacharya Sanchari and Shampa Ghosh

Additional information is available at the end of the chapter

<http://dx.doi.org/10.5772/56867>

---

## 1. Introduction

Cancer is uncontrolled proliferation of cells, which results from the loss of proper balance between cell death and cell growth. The transformed phenotypes of cancer cells are caused by the accumulation of mutations in a variety of genes, products of which normally play a role in the biochemical pathways that regulate cell death and cell proliferation. Cancer is a broad term used to define a group of more than 250 different diseases (Roncalli et al. 2010). It is a slow multi-stage, multi-step process (Cammà et al. 2008; Calvisi et al. 2009; Sherman 2011). In the first instance, these cells, derived initially from a normal cell, form a primary tumor which comprises a growth-transformed population of cells. The cells acquire a set of mutations to a set of genes which allow them to divide repeatedly in a way that normal cells cannot (Besaratina et al. 2009; Calvisi et al. 2009). Histologically, cancer is characterized by several morphological alterations, including changes in tissue architecture, cytological abnormalities of both the nucleus and cytoplasm and the presence of abnormal mitoses. A stepwise several biochemical, genetic and biological alterations eventually result in a cancer.

Primary liver cancer or hepatocellular carcinoma (HCC) is a very common malignant hepatobiliary disease and it represents the fifth most frequent neoplastic disease which causes approximately 1 million deaths per year (Yang and Roberts, 2010, Cha et al. 2010). HCC is the third leading cause of cancer related death worldwide (Raphael 2012). Viruses and chemicals have been identified as the most important etiological factor associated with the development of human liver cancer (Carr et al. 2010). The most common cause of HCC is hepatitis B and C (Woo et al. 2008; Masuzaki et al. 2008, Gouas et al. 2010; Iavarone and Colombo 2011) and a

number of risk factors that have been identified (Shariff et al. 2009; Sherman 2010; Gomaa et al. 2008 and 2009). Most of HCC cases develop from a cirrhotic liver (Bartolomeo et al. 2011; Chagas et al. 2009; Orlando et al. 2009; Cammà et al. 2008) with an annual incidence of 2-6% for hepatitis B virus carriers (Kew 2010; Lim et al. 2009; Hadziyannis 2011) and 3-5% for hepatitis C virus-infected patients (Masuzaki et al. 2008; Rosen 2011). Males are more susceptible to HCC.

Despite the advances in cancer treatments there is no effective chemotherapeutic protocol to treat HCC (Andreana et al. 2009; Arii et al. 2010). Advanced HCC has a poor prognosis (Simile et al. 2011; Sonja et al. 2010). Historically, no effective systemic chemotherapy treatment options have been available for patients with advanced HCC (Bruix and Sherman 2011). Thus, proper understanding of the molecular basis of pathogenesis of HCC can lead us to plan for proper therapeutic strategies to combat the notorious disease.

Accumulating epidemiological evidence suggests that a pronounced predisposition to develop cancer as a consequence of a mutation in a single gene is rare (approximately 1-5%) (Frau et al. 2010). One possible explanation for this finding is that carcinogenesis is a multi-stage process involving a number of different genes and environmental factors (Chung et al. 2008; Forner et al. 2010; Frau et al. 2010). In connection with many distinct subtypes of cancer, some functional alterations are required for malignant transformation. They are, namely, sufficiency with respect to growth signals, insensitivity to growth-inhibitory signals, evasion of programmed cell death (apoptosis), the potential for unlimited replication, sustained angiogenesis, tissue invasion and metastasis (Bergers and Hanahan 2008; Bartolomeo et al. 2011; Cao et al. 2010; Frau et al. 2010; Gouas et al. 2010). The exact number of distinct stages involved may vary from tumor to tumor, since some of these acquired characteristics probably interact with other processes (Roncalli 2010). Indeed, the heterogeneity of tumors, both with regards to morphology and pattern of gene expression, may even indicate the participation of many more sequential steps.

A highly regulatory network controls cellular proliferation in multicellular organisms. Normally cells in many tissues and organs remain in a non-proliferative state. In response to external stimuli such as growth factors, hormones or antigens, cells are stimulated to begin DNA synthesis and cellular proliferation according to the need of the living system. As soon as the need is fulfilled, the cell division stops. However, cancerous cells are characterized by the unrestrained cellular proliferation due to the alteration of normal cellular signalling process and they acquire complete or partial independence of mitogenic signals through production of growth factors (Garrett et al. 2008; Hironaka et al. 2009) and /or alteration in number or structure of cellular receptors (Lachenmayer et al. 2010) and/ or modulation in the activity of post receptor signalling pathway (Cavard et al. 2008; Chen et al. 2009). The communication of extracellular signals to the cells, then to the nucleus to modulate gene expression is governed by phosphorylation regulated signal transduction cascades which act to amplify the events generated at the cellular membrane by ligand-receptor interaction or cell stress. Therefore, identification of the extracellular factors that modulate cell proliferation and elucidation of the cellular molecular mechanism during the development of cancer can answer many fundamental questions in cancer cell biology. It is important to understand in details the

receptors and the signal transduction pathways involved in the pathogenesis of cancer to provide potential target for therapeutic intervention. Many studies have focused to identify molecular pathways to elicit cancer cell proliferation, including HCC. Here many of them have been highlighted to identify fundamental targets of hepatocellular oncogenesis. Thus, the present chapter has been projected to the molecular targets and approaches to intervene the targets for the management of HCC in humans in coming years.

## 2. Therapeutic targets for HCC

Three generally considered fundamental but interrelated targets of controlling oncogenesis are regulation of deregulated energy metabolism and ion homeostasis; signal transduction, oncogenes and growth factors; and immunomodulation. One of the most characteristic phenotypes of rapidly growing cancer cells is their propensity to catabolise glucose at high rates. Rapidly growing activity to cancer cells has a reduced number of mitochondria and increased glycolytic activity with a shift from respiratory to fermentative ATP supply to cover most of their energy requirement. The stimulation of the  $K^+$ ,  $H^+$  and  $Na^+$  fluxes is a general early response in most of the quiescent cells stimulated to proliferate by multiple combinations of growth promoting factors. Growth factors, cytokines exert their action on cell proliferation by modulation of cell signalling process. There is a strong relationship between the immune system and cell proliferation. Immune suppressive agents have a powerful effect on hepatocyte growth regulation in HCC.

Reviewing current literature, a selection of therapeutic targets of HCC has been described below.

Like most other cancers, growth factors, their receptors, and downstream signalling proteins play a pivotal role in the development and maintenance of HCC and are of significant interest for future therapeutic approaches. In foetal liver, a large number of growth factors such as epidermal growth factor (EGF), fibroblast growth factor (FGF), hepatocyte growth factor (HGF), insulin-like growth factors (IGFs), platelet-derived growth factor (PDGF), transforming growth factors- $\alpha$  and - $\beta$  (TGF- $\alpha$ , TGF- $\beta$ ), and vascular endothelial growth factor (VEGF) (Höpfner et al. 2008; Hoshida et al. 2008 and 2009) are produced. Their secretion either declines or shuts down in adult liver. However, during hepatic regeneration due to the cause of hepatic injury or damage many such growth factors (Böhm et al. 2010), namely, EGF, TGF- $\alpha$ , IGFs, and VEGF are upregulated in normal hepatocytes. The transient upregulation of those factors is dysregulated in the chronic injured liver leading to sustained mitogenic/ oncogenic signalling, during the development of HCC. FGF and PDGF released from non-hepatocyte sources such as activated hepatic stellate cells, myofibroblasts, endothelial cells, Kupffer cells, and bile duct epithelia have been shown to play important roles in promoting hepatic fibrosis and HCC growth (Friedman 2008). The ubiquitin-proteasome pathway has emerged as a key player in the regulation of several diverse cellular processes. Inhibition of poly-ubiquitination using proteasome inhibitors has shown some light in HCC treatment. Besides, immunomodulation has been found to be

effective in stabilizing HCC growth in patients. Number of immunomodulators has been investigated and few of them have been found to be effective. They have been discussed below under immunomodulation agents. Signal transduction, and growth factors; inhibitors of proteasome pathway, immunomodulation and antisense oligomer-mediated inhibition of targeted oncogenes have been projected as future targets and approaches of HCC (Table 1).

Molecular targets in HCC	Inhibitors / Modulators / Antisense oligonucleotides
Growth factors, e.g., EGFR, EGF, TGF- $\alpha$ , TGF- $\beta$ , VEGF	Cetuximab, Gefitinib, Erlotinib, Vandetanib.
mTOR	Rapamycin, Temsirolimus, Salirasib, RAD001
Multikinase	Sorafenib, Everolimus, AP23573, RAD001.
Proteasome	Bortezomeb
Immunomodulators used in HCC	Thymostimulin, Retinoids, Everolimus, Azathioprine, 6-mercaptopurine.
Antisense oligonucleotides used in HCC	ISIS5132. ISIS2513

**Table 1.** Growth factors, proteasome-inhibitors, immunomodulators and antisense oligomers in HCC

### 3. Approaches

A selection of agents currently in the development and/or testing stages for the clinical application in targeted HCC treatment is summarized in the following section.

#### 3.1. Therapies against EGFR

There are two classes of anti-EGFR agents found to have antitumor activity against HCC. One of them belongs to monoclonal antibodies (as an example cetuximab) which competitively inhibit extracellular endogenous ligand binding. The other class belongs to chemicals such as gefitinib, erlotinib which inhibit the intracellular tyrosine kinase domain. EGF, TGF- $\alpha$ , heparin binding-EGF and EGFR have been shown to involve in the pathogenesis of HCC. Thus, EGFR signalling pathways have become a potential investigating area of research to identify the target (s) to inhibit proliferation of HCC and metastasis. Gefitinib, erlotinib, cetuximab were tested in patients with advanced HCC (Thomas et al. 2007; Philip et al. 2005; Asnacios et al. 2008; Wu et al. 2011, Levêque 2011) and were reported to possess signals of activity in controlling the progress of HCC in a variable extent.

#### 3.2. Targeting approaches towards VEGF and VEGFR

HCCs rely on the formation of new blood vessels for growth, and VEGF is critical in this process (Zhu et al. 2011). HCCs are with high vascular architecture and VEGF is a key factor in tumor angiogenesis (Bergers and Hanahan, 2008; Garrett et al. 2008; Hironaka et al. 2009). Therefore,

the inhibition of angiogenesis is a potential and promising therapeutic approach in HCC. Anti-VEGF therapy with sorafenib was the first systemic therapy against VEGF to demonstrate improved survival in patients with advanced-stage HCC (Cheng et al. 2009; Zhu et al. 2011, Miller et al. 2009; Zhu 2008, Llovet et al. 2008a). Sorafenib was also tested in advanced stage liver cirrhosis patients with unresectable HCC (Pinter et al. 2009). Bevacizumab alone or in combination with other agents showed promise in patients with advanced HCC (Siegel et al. 2008; Thomas et al. 2009; Thomas et al. 2008; Kaseb et al. 2012). However, the common bevacizumab-related side effects were hypertension, bleeding, and proteinuria (Thomas et al. 2009; Siegel et al. 2008a; Kopetz et al. 2009). Besides, inhibition of the tyrosine kinase activity of VEGFR has been tried as an effective measure to inhibit angiogenesis in HCC (Bhide et al. 2010). PTK787/ ZK222584 (vatalanib) is an oral angiogenesis inhibitor that targets tyrosine kinase activity of VEGFR (Gauler et al. 2012). Pan-VEGFR tyrosine kinase activity inhibitor with activity against PDGFRs also carries a new hope.

### 3.3. Multi-kinase inhibitor

Like all other cancers diverse signaling pathways in HCC are very complex. One of the key pathways regulating cellular proliferation is the mitogen activated protein Kinase (MAPK) pathway. Other pathways involved in the development of HCC include the PI3K/Akt/mTOR, hepatocyte growth factor (HGF)/c-MET, insulin-like growth factor (IGF) and its receptor (IGFR) pathways, and the Wnt- $\beta$  catenin pathway (Cavard et al. 2008; Chen et al. 2009; Desbois-Mouthon et al. 2009; Takigawa and Nouse 2008; Zhang et al. 2008). The Raf family of kinases are central to this pathway where the transduction of extracellular growth signals from the cell surface to the nucleus occurs via the ras-raf-MEK-ERK signaling cascade. The several experiments have shown that Raf, MEK, MAP Kinase are downstream effector molecules of Ras and their sequential order in the pathway. The Raf serine/threonine kinases are the principal effectors of Ras in this mitogen activated protein Kinase (MAPK) signaling pathway. As serine/threonine kinases, Raf proteins phosphorylate and activate serine and threonine residues on subsequent downstream effector proteins of Ras. Therefore, molecularly targeted agents that interact with multiple signaling pathways/ effectors appear to be very promising in the treatment of patients with HCC (Cervello et al. 2012; Cheng et al. 2009). The novel bi-aryl urea sorafenib, an orally available multi-kinase inhibitor, targets kinases of wild-type B-Raf, mutant V559EB-Raf and cRaf, thereby blocking tumor growth (Spangenberg et al. 2008). There are three ras protooncogenes that encode 21 Kd proteins – H-Ras (Harvey murine sarcoma virus), N-Ras (neuroblastoma cell line) and two alternatively spliced K-Ras, K-Ras 4A, and K-Ras 4B; These isoforms are capable of differentially activating various critical effectors, thereby exerting distinct biologic effects. Sorafenib, an inhibitor of receptor tyrosine kinases was found to stabilize the advanced unresectable HCC patients by regulating angiogenesis, and was approved by regulatory agencies in 2007. It has a role on human VEGF receptors-2 and -3 (VEGFR-2/-3) and PDGF- $\beta$ R. However, sorafenib has been also suggested to provide antitumor action in HCC by inhibition of the Raf/MEK/ERK pathway (Llovet and Bruix, 2008 and 2009). Multikinase inhibitor sunitinib is a small molecule that inhibits members of the split-kinase domain family of receptor tyrosine kinase including VEGFR types 1 and 2 (Llovet et al. 2008a). Antiangiogenic effects of sunitinib have been suggested through VEGFR and PDGFR.



However, a randomized phase 3 study in HCC failed to show a significant survival benefit as compared to sorafenib and study stopped in 2011.

### **3.4. mTOR inhibitors**

mTOR inhibitors are potential anti-HCC agents for future (Zhou et al. 2009). Promising mTOR inhibitors are rapamycin and its analogues such as sirolimus, temsirolimus (CCI-779), everolimus (RAD001) and AP23573 (Nocera et al 2008; Rizell et al. 2008). Rapamycin and its analogues such as temsirolimus ( the cell cycle inhibitor) and everolimus and AP23573 (an orally bioavailable derivative of rapamycin) modulate angiogenesis to improve survival of patients in advanced HCC (Heuer 2009, Huynh et al. 2008 ). RAD001, an orally-administered, novel mTOR inhibitor was evaluated in a phase I study (Huynh et al. 2008 and 2008a; Chen et al 2009). Treatment of patients with the combination of rapamycin/ rapamycin-analogue(s) with conventional anticancer drug(s) such as doxorubicin, vinblastine has been found to improve survival in advanced HCC patients (Spangenberg et al. 2008).

### **3.5. Proteasome inhibition**

HCC is highly ubiquitinated. The ubiquitination is important to the development and progression of HCC. Proteasome inhibitor such as bortezomib blocks multi-ubiquitinated protein degradation by reversible and competitive inhibition of the active site threonine residue of the 26S proteasome (Cao and Mao, 2011; Boozari et al. 2009). Antineoplastic activity of bortezomib approved for the treatment of mantle cell lymphoma has already been shown to stabilize advanced HCC in patients (Höpfner et al 2008).

### **3.6. Immunomodulatory agents**

An immunomodulator is a substance which has an effect on the immune system. An immunomodulator may be at the same time an immunosuppressant or an immunostimulant and can act on different targets within the immune system. Cell signalling process regulates immune system consisting of immunomodulatory endogenous chemicals and cells. Immunomodulators interfere with the signalling process by shifting the homeostasis of the immune system to reduce or eliminate disease symptoms. Thus these compounds are the obvious choice for therapeutic intervention of HCC. Thymostimulin (a standardized low molecular protein fraction containing thymosin alpha 1 and thymic humoral factor) has been shown to produce cytotoxic immune reaction against HCC. Phase II trials using thymostimulin in patients with advanced and metastasised HCC have shown to control metastatic HCC without predominant side-effects (Dollinger et al. 2010). However, thymostimulin administration in some patients was found to accumulate ascites and cause renal failure (Dollinger et al. 2010).

### **3.7. Antisense therapy**

Antisense oligonucleotides offer one approach to target genes involved in cancer progression. They are typically less than 50 nucleotides long and are specifically designed to hybridize to corresponding gene/ mRNA by Watson-Crick binding. They inhibit mRNA function in several

ways, including modulation of splicing and inhibition of protein translation by disruption of ribosome assembly. Single stranded synthetic nucleic acid (oligonucleotide) when hybridize with DNA or RNA alters transcription or prevents translation thus, preventing or modifying protein production. Because of the volume of information nowadays available on gene sequencing, there has been burst of exploration of capacity for oligomers to inhibit gene/protein expression. Thus, antisense therapies focus on controlling the production of the proteins on a genetic level. A strand of mRNA is transcribed from DNA, and is a copy of the "coding" or "sense" strand of the gene. The main form of therapy uses the complementary or antisense strand to hybridize the sense strand or mRNA and thus it prevents production of the protein by blocking or altering transcription or translation (Figure 1). With the backbone chemical modifications (in phosphate linkage), antisense oligonucleotides increase resistance to nuclease digestion, prolong their biological half-lives and significantly suppress target-gene expression. Antisense oligonucleotides have been studied for several years as treatments for many diseases and genetic disorders. The therapy is based on the principles of genetic expression. The most widely used modified oligomers in antisense therapies is phosphorothioate oligonucleotides, which have much greater resistance to digestion by nucleases. Phosphorothioate oligonucleotides are rapidly and extensively absorbed and distributed from blood.

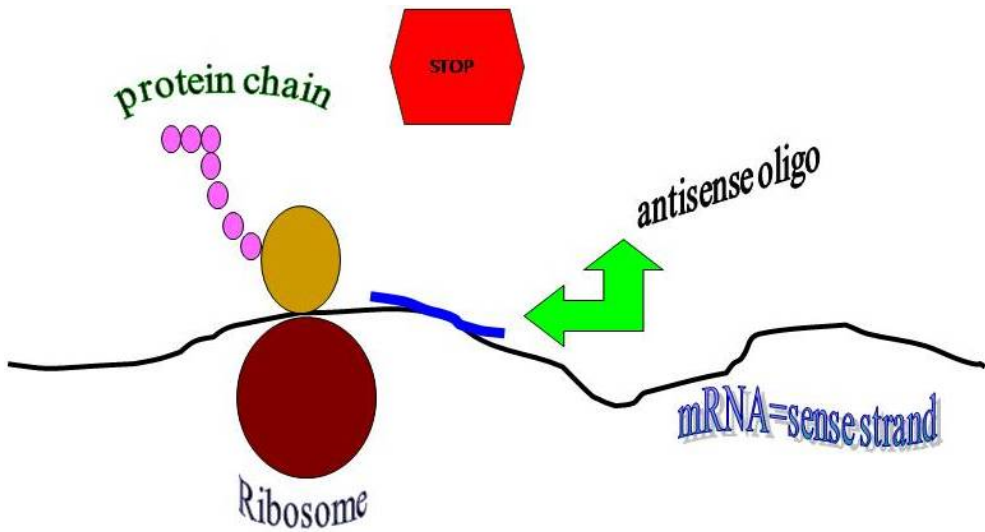


**Figure 1.** Antisense oligomer-mRNA duplex inhibiting to synthesize peptide chain

The first antisense treatment to get FDA approval to date has been Formivirsen (Vitravene), which is a treatment for cytomegalovirus (CMV) retinitis in people with acquired immunodeficiency disease (AIDS) (Rahman et al. 2008). Several antisense oligonucleotides were shown to target various oncogenes, to overcome tumour escape and to improve therapeutic activity.

Several studies have shown the anticancer potential of antisense oligonucleotides (Das et al. 2010; Rayburn and Zhang, 2008) and many of them are in clinical trial. They have less cytotoxic side-effects than conventional chemotherapy agents. Systemic treatment with fomivirsen is a milestone in the field of antisense treatment with antisense oligonucleotides. This has led the way for development of antisense oligonucleotides for various new potential targets for the treatment of cancer, including HCC.

#### 4. Conclusion

Several experimental evidences have established that targeted inhibition of genes/ proteins involved in controlling HCC growth combined with cytostatic anticancer treatments is a promising approach for HCC therapy. Blocking of single gene/ protein has been found to control neoplastic cellular proliferation *in vitro* effectively. However, considering the multitude of molecular entities and signalling pathways that regulate the proliferation and the life/death decision in cancer cells, inhibition of a single target gene may not be sufficient to suppress tumor growth. The preclinical/ clinical trials of several potential compounds targeting liver cancer-relevant genes/ proteins may address more specific and adequate future therapies for HCC.

#### Acknowledgements

Authors are indebted to the grants from Department of Science Technology (Govt. of India) (DST/Inspire Fellowship/ 2010/ 87) and Indian Council of Medical Research (58/7/2009-BMS) for funding the related projects and findings of which have helped us partially to write this work.

#### Author details

Mukherjee Biswajit\*, Hossain Chowdhury Mobaswar , Bhattacharya Sanchari and Shampa Ghosh

\*Address all correspondence to: biswajit55@yahoo.com

Department of Pharmaceutical Technology, Jadavpur University, Kolkata, India

#### References

- [1] Andreana L, Isgr Ó G, Pleguezuelo M. Surveillance and diagnosis of hepatocellular carcinoma in patients with cirrhosis. *World J Hepatol* 2009; 1 (1) 48–61.

- [2] Arii S, Sata M, Sakamoto M, Shimada M, Kumada T, Shiina S. Management of hepatocellular carcinoma Report of Consensus Meeting in the 45th Annual Meeting of the Japan Society of Hepatology. *Hepatol Res* 2010; 40 (7) 667–685.
- [3] Asnacios A, Fartoux L, Romano O, Tesmoingt C, Louafi SS, Mansoubakht T. Gemcitabine plus oxaliplatin Gemox combined with cetuximab in patients with progressive advanced stage hepatocellular carcinoma: results of a multicenter phase 2 studies. *Cancer* 2008; 112 (12) 2733–2739.
- [4] Bartolomeo N, Trerotoli P, Serio G. Progression of liver cirrhosis to HCC: an application of hidden Markov model. *BMC Med Res Methodol* 2011; 11 (38) 1–8.
- [5] Bergers G, Hanahan D. Modes of resistance to anti-angiogenic therapy. *Nat Rev Cancer* 2008; 8 (8) 592–603.
- [6] Besaratinia A, Kim SI, Hainaut P, Pfeifer GP. In vitro recapitulating of TP53 mutagenesis in hepatocellular carcinoma associated with dietary aflatoxin B1 exposure. *Gastroenterology* 2009; 137 (3) 1127–1137.
- [7] Bhide RS, Lombardo LJ, Hunt JT. The antiangiogenic activity in xenograft models of brivanib alaninate a dual inhibitor of VEGFR-2 and FGFR-1 kinases. *Mol Cancer Ther* 2010; 9 (2) 369–378.
- [8] Böhm F, Köhler UA, Speicher T, Werner S. Regulation of liver regeneration by growth factors and cytokines. *EMBO Mol Med* 2010; 2 (8) 294–305.
- [9] Boozari B, Wirth T, Woller N, Manns MP, Kubicka S, Kühnel F. Efficacy of HCC treatment with proteasome inhibitor Bortezomib is increased by oncolytic virotherapy mediated downregulation of Mcl-1 and Bip. *Z Gastroenterol* 2009; 47 3–4.
- [10] Bruix J, Sherman M. Management of hepatocellular carcinoma: an update. *Hepatology* 2011; 53 (3) 1020–1022.
- [11] Calvisi DF, Pinna F, Ladu S, Pellegrino R, Simile MM, Frau M. Forkhead box M1B is a determinant of rat susceptibility to hepatocarcinogenesis and sustains ERK activity in human HCC. *Gut* 2009; 58 (5) 679–87.
- [12] Cammà C, Di Marco V, Cabibbo G. Survival of patients with hepatocellular carcinoma in cirrhosis: a comparison of BCLC CLIP and GRETCH staging systems. *Aliment Pharmacol Ther* 2008; 28 (1) 62–75.
- [13] Cao B, Mao X. The ubiquitin-proteasomal system is critical for multiple myeloma: implications in drug discovery. *Am J Blood Res* 2011; 1 (1) 46–56.
- [14] Cao CQ, Yan TD, Bester L, Liauw W, Morris DL. Radioembolization with yttrium microspheres for neuroendocrine tumour liver metastases. *Brit J Surg* 2010; 97 (4) 537–543.
- [15] Carr BI, Kondragunta V, Buch SC, Branch RA. Therapeutic equivalence in survival for hepatic arterial chemoembolization and yttrium 90 microsphere treatments in un-

- resectable hepatocellular carcinoma: a two-cohort study. *Cancer* 2010; 116 (5) 1305–1314.
- [16] Cavard C, Colnot S, Audard V. Wnt/ $\beta$ -catenin pathway in hepatocellular carcinoma pathogenesis and liver physiology. *Future Oncol* 2008; 4 (5) 647–660.
- [17] Cervello M, McCubrey JA, Cusimano A, Lampiasi N, Azzolina A, Montalto G. Targeted therapy for hepatocellular carcinoma: novel agents on the horizon. *Oncotarget* 2012; 3 (3) 236–260.
- [18] Cha CH, Saif MW, Yamane BH, Weber SM. Hepatocellular carcinoma: current management. *Curr Prob Surg* 2010; 47 (1) 10–67.
- [19] Chagas AL, Kikuchi LOO, Oliveira CPMS. Does hepatocellular carcinoma in non-alcoholic steatohepatitis exist in cirrhotic and non-cirrhotic patients? *Braz J Med Biol Res* 2009; 42 (10) 958–962.
- [20] Chen JS, Wang Q, Fu XH. Involvement of PI3K/PTEN/AKT/mTOR pathway in invasion and metastasis in hepatocellular carcinoma: association with MMP-9. *Hepatol Res* 2009; 39 (2) 177–186.
- [21] Cheng AL, Kang YK, Chen Z, Tsao CJ, Queen S, King JS. Efficacy and safety of sorafenib in patients in the Asia-Pacific region with advanced hepatocellular carcinoma: a phase III randomised double-blind placebo-controlled trial. *Lancet Oncol* 2009; 10 (1) 25–34.
- [22] Chung H, Kudo M, Takahashi S. Comparison of three current staging systems for hepatocellular carcinoma: Japan integrated staging score new Barcelona Clinic Liver Cancer staging classification and Tokyo score. *J Gastroen Hepatol* 2008; 23 (3) 445–452.
- [23] Das T, Patra F, Mukherjee B. Effect of antisense oligomer in controlling c-raf1 overexpression during diethylnitrosamine-induced hepatocarcinogenesis in rats. *Cancer Chemother Pharmacol* 2010; 65 (2) 309–318.
- [24] Desbois-Mouthon C, Baron A, Blivet-Van Eggelpoël MJ. Insulin-like growth factor-1 receptor inhibition induces a resistance mechanism via the epidermal growth factor receptor/HER3/AKT signaling pathway: rational basis for cotargeting insulin-like growth factor-1 receptor and epidermal growth factor receptor in hepatocellular carcinoma. *Clin Cancer Res* 2009; 15 (17) 5445–5456.
- [25] Dollinger MM, Lautenschlaeger C, Lesske J, Tannapfel A, Wagner AD, Schoppmeyer K. Thymostimulin versus placebo for palliative treatment of locally advanced or metastasised hepatocellular carcinoma: a phase III clinical trial. AIO Hepatobiliary Study Group *BMC Cancer* 2010; 24 (10) 457–467.
- [26] Forner A, Reig ME, de Lope CR, Bruix J. Current strategy for staging and treatment: the BCLC update and future prospects. *Semin Liv Dis* 2010; 30 (1) 61–74.

- [27] Frau M, Biasi F, Feo F, Pascale RM. Prognostic markers and putative therapeutic targets for hepatocellular carcinoma. *Mol Aspects Med* 2010; 31 (2) 179–193.
- [28] Friedman SL. Hepatic stellate cells: protean multifunctional and enigmatic cells of the liver. *Physiol Rev* 2008; 88 (1) 125–172.
- [29] Garrett C, Siu L, El-Khoueiry A. A phase I study of brivanib alaninate BMS-582664 an oral dual inhibitor of VEGFR and FGFR tyrosine kinases in combination with full-dose cetuximab in patients with advanced gastrointestinal malignancies who failed prior therapy. *J Clin Oncol* 2008; 26 suppl:abstr 4111.
- [30] Gauler TC, Besse B, Mauguen A, Meric JB, Gounant V. Phase II trial of PTK787/ZK 222584 vatalanib administered orally once-daily or in two divided daily doses as second-line monotherapy in relapsed or progressing patients with stage IIIB/IV non-small-cell lung cancer NSCLC. *Ann Oncol* 2012; 23 (3) 678–687.
- [31] Gomaa AI, Khan SA, Toledano MB, Waked I, Taylor-Robinson SD. Hepatocellular carcinoma: epidemiology risk factors and pathogenesis. *World J Gastroenterol* 2008; 14 (27) 4300–4308.
- [32] Gomaa AI, Khan SA, Leen ELS, Waked I, Taylor-Robinson SD. Diagnosis of hepatocellular carcinoma. *World J Gastroenterol* 2009; 15 (11) 1301–1314.
- [33] Gouas DA, Shi H, Hautefeuille AH. Effects of the TP53 pR249S mutant on proliferation and clonogenic properties in human hepatocellular carcinoma cell lines: Interaction with hepatitis B virus X protein. *Carcinogenesis* 2010; 31 (8) 1475–1482.
- [34] Hadziyannis SJ. Natural history of chronic hepatitis B in Euro-Mediterranean and African countries. *J Hepatol* 2011; 55 (1) 183–191.
- [35] Heuer M, Benko T, Cicinnati VR, Kaiser GM, Sotiropoulos GC, Baba HA. Effect of low-dose rapamycin on tumor growth in two human hepatocellular cancer cell lines. *Transplant Proc* 2009; 41 (1) 359–365.
- [36] Hironaka S, Onozawa Y, Aramaki T. Phase 1 study of brivanib alaninate a novel FGF and VEGF receptor inhibitor. Japanese Society for Clinical Oncology JSCO Annual Conference Yokohama October 2009; 22– 24 abstr OS036-3.
- [37] Höpfner M, Schuppan D, Scherübl H. Growth factor receptors and related signalling pathways as targets for novel treatment strategies of hepatocellular cancer. *World J Gastroenterol* 2008; 14 (1) 1–14.
- [38] Hoshida Y, Villanueva A, Kobayashi M, Peix J, Chiang DY, Camargo A. Gene expression in fixed tissues and outcome in hepatocellular carcinoma. *N Engl J Med* 2008; 359 (19) 1995–2004.
- [39] Hoshida Y, Villanueva A, Llovet JM. Molecular profiling to predict hepatocellular carcinoma outcome. *Expert Rev Gastroenterol Hepatol* 2009; 3 (2) 101–103.

- [40] Huynh H, Chow KP, Soo KC, Toh HC, Choo SP, Foo KF. Rad001 (Everolimus) inhibits tumor growth in xenograft models of human hepatocellular carcinoma. *J Cell Mol Med* 2009; 13 (7) 1371–1380.
- [41] Huynh H, Ngo VC, Fargnoli J. Brivanib alaninate a dual inhibitor of vascular endothelial growth factor receptor and fibroblast growth factor receptor tyrosine kinases induces growth inhibition in mouse models of human hepatocellular carcinoma. *Clin Cancer Res* 2008a; 14 (19) 6146–6153.
- [42] Iavarone M, Colombo M. HBV-related HCC clinical issues and therapy. *Digest Liver Dis* 2011; 43 supplement 1 S32–S39.
- [43] Kaseb AO, Garrett-Mayer E, Morris JS, Xiao L, Lin E, Onicescu G. Efficacy of Bevacizumab plus Erlotinib for advanced hepatocellular carcinoma and predictors of outcome: final results of a phase II trial. *Oncology* 2012; 82 (2) 67–74.
- [44] Kew MC. Epidemiology of chronic hepatitis B virus infection hepatocellular carcinoma and hepatitis B virus-induced hepatocellular carcinoma. *Pathol Biol* 2010; 58 (4) 273–277.
- [45] Kopetz S, Hoff PM, Eng MJ. Angiogenic cytokines are increased prior to disease progression in metastatic colorectal cancer patients treated with bevacizumab. *ASCO Gastrointestinal Cancers Symposium San Francisco January 15–17 2009*; abstr 292.
- [46] Lachenmayer A, Alsinet C, Chang CY, Llovet JM. Molecular approaches to treatment of hepatocellular carcinoma. *Digest Liver Dis* 2010; 42(3) 264–272.
- [47] Levêque D. Pharmacokinetics of gefitinib and erlotinib. *Lancet Oncol* 2011; 12 (12) 1093.
- [48] Lim SG, Mohammed R, Yuen MF, Kao JH. Prevention of hepatocellular carcinoma in hepatitis B virus infection. *J Gastroenterol Hepatol* 2009; 24 (8) 1352–1357.
- [49] Llovet JM, Bruix J. Molecular targeted therapies in hepatocellular carcinoma. *Hepatology* 2008; 48 (4) 1312–1327.
- [50] Llovet JM, Bruix J. Testing molecular therapies in hepatocellular carcinoma: the need for randomized phase II trials. *J Clin Oncol* 2009; 27 833–835.
- [51] Llovet JM, Ricci S, Mazzaferro V, Hilgard P, Gane E, Blanc JF. Sorafenib in advanced hepatocellular carcinoma. *N Engl J Med* 2008a; 359 (4) 378–390.
- [52] Masuzaki R, Yoshida H, Tateishi R, Shiina S, Omata M. Hepatocellular carcinoma in viral hepatitis: improving standard therapy. *Best Pract Res* 2008; 22 (6) 1137–1151.
- [53] Miller AA, Murry DJ, Owzar K, Hollis DR, Kennedy EB, Abou-Alfa G. Phase I and pharmacokinetic study of sorafenib in patients with hepatic or renal dysfunction: CALGB 60301. *J Clin Oncol* 2009; 27 (11) 1800–1805.

- [54] Nocera A, Andorno E, Tagliamacco A, Morelli N, Bottino G, Ravazzoni F. Sirolimus therapy in liver transplant patients: an initial experience at a single center. *Transplant Proc* 2008; 40 (6) 1950–1952.
- [55] Orlando A, Leandro G, Olivo M, Andriulli A, Cottone M. Radiofrequency thermal ablation vs percutaneous ethanol injection for small hepatocellular carcinoma in cirrhosis: meta-analysis of randomized controlled trials. *Am J Gastroenterol* 2009; 104 (2) 514–524.
- [56] Philip P, Mahoney M, Allmer C, Thomas J, Pitot H, Kim G. Phase II study of Erlotinib (OSI-774) in patients with advanced hepatocellular cancer. *J Clin Oncol* 2005; 23 (27) 6657–6663.
- [57] Pinter M, Sieghart W, Graziadei I, Vogel W, Maieron A, Konigsberg R. Sorafenib in unresectable hepatocellular carcinoma from mild to advanced stage liver cirrhosis. *Oncologist* 2009 ; 14 (1) 70–76.
- [58] Rahman SMA, Seki S, Obika S, Yoshikawa H, Miyashita K, Imanishi T. Design synthesis and Properties of 2', 4'-BNA<sup>NC</sup>: a bridged nucleic acid analogue. *J Am Chem Sc* 2008; 130 (14) 4886–4896.
- [59] Raphael SW, Yangde Z, Xiang CY. Hepatocellular carcinoma: focus on different aspects of management. *ISRN Oncology* 2012; 2012 1–12.
- [60] Rayburn ER, Zhang R. Antisense RNAi and gene silencing strategies for therapy: mission possible or impossible? *Drug Discov Today* 2008; 13 (11-12) 513–521.
- [61] Rizell M, Andersson M, Cahlin C, Hafstrom L, Olausson M, Lindner P. Effects of the mTOR inhibitor sirolimus in patients with hepatocellular and cholangiocellular cancer. *Int J Clin Oncol* 2008; 13 (1) 66–70.
- [62] Roncalli M, Park YN, di Tommaso L. Histopathological classification of hepatocellular carcinoma. *Digest Liver Dis* 2010; 42 (3) 228–234.
- [63] Rosen HR. Clinical practice chronic hepatitis C infection. *N Engl J of Med* 2011; 364 (25) 2429–2438.
- [64] Shariff MIF, Cox IJ, Goma AI, Khan SA, Gedroyc W, Taylor-Robinson SD. Hepatocellular carcinoma: current trends in worldwide epidemiology risk factors diagnosis and therapeutics. *Expert Rev Gastroenterol Hepatol* 2009; 3 (4) 353–367.
- [65] Sherman M. Epidemiology of hepatocellular carcinoma. *Oncology* 2010; 78 (1) 7–10.
- [66] Sherman M. Hepatocellular carcinoma: screening and staging. *Clin Liver Dis* 2011; 15 (2) 323–334.
- [67] Siegel AB, Cohen EI, Ocean A, Lehrer D, Goldenberg A, Knox JJ. Phase II trial evaluating the clinical and biologic effects of bevacizumab in unresectable hepatocellular carcinoma. *J Clin Oncol* 2008; 24 (26) 2992–2998.

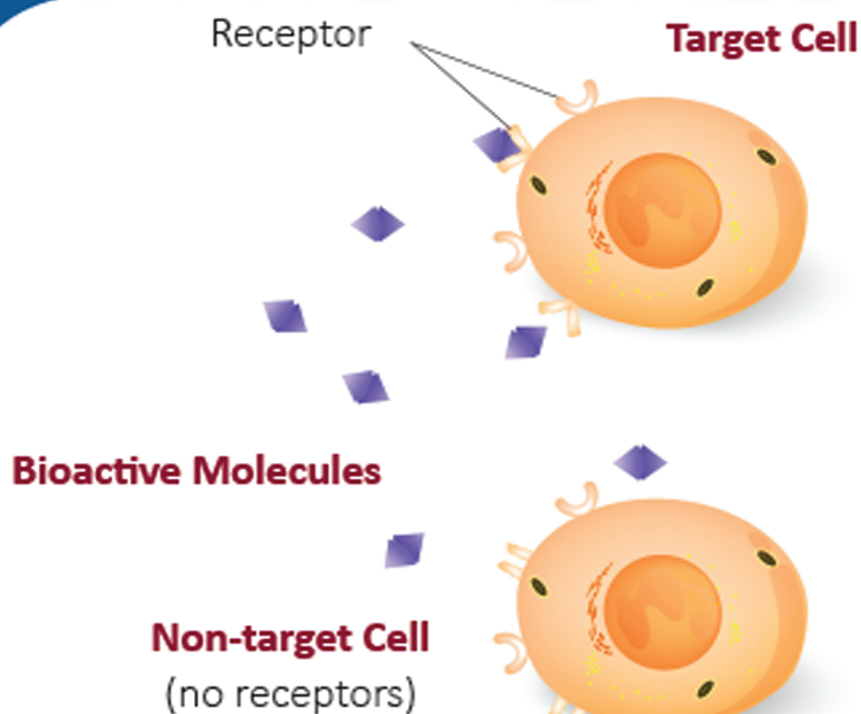


- [68] Siegel AB, McBride RB, El-Serag HB, Hershman DL, Brown Jr RS, Renz JF. Racial disparities in utilization of liver transplantation for hepatocellular carcinoma in the United States 1998-2002. *Am J Gastroenterol* 2008a; 103 (7) 120-127.
- [69] Simile MM, Frau M, Pascale RM, Feo F. New putative prognostic markers and therapeutic targets for the molecular approach to treatment of hepatocellular carcinoma. *J Exp Integr Med* 2011; 1 85-97.
- [70] Sonja K, Olsen RS, Brown JR, Siegel AB. Review: Hepatocellular carcinoma: review of current treatment with a focus on targeted molecular therapies. *Therap Adv Gastroenterol* 2010; 3 (1) 55-56.
- [71] Spangenberg HC, Thimme R, Blum HE. Evolving therapies in the treatment of hepatocellular carcinoma. *Biologics* 2008; 2 (3) 453-462.
- [72] Takigawa Y, Brown AM. Wnt signaling in liver cancer. *Curr Drug Targets* 2008; 9 (11) 1013-1024.
- [73] Thomas MB, Chadha R, Glover K, Wang X, Morris J, Brown T. Phase 2 study of erlotinib in patients with unresectable hepatocellular carcinoma. *Cancer* 2007; 110 (5) 1059-1067.
- [74] Thomas MB, O'Beirne JP, Furuse J, Chan ATC, Abou-Alfa G Johnson P. Systemic therapy for hepatocellular carcinoma: cytotoxic chemotherapy targeted therapy and immunotherapy. *Ann Surg Oncol* 2008; 15 (4) 1008-1014.
- [75] Thomas MB, Morris JS, Chadha R, Iwasaki M, Kaur H, Lin E. Phase II trial of the combination of bevacizumab and erlotinib in patients who have advanced hepatocellular carcinoma. *J Clin Oncol* 2009; 27 (6) 843-850.
- [76] Woo HG, Park ES, Cheon JH, Kim JH, Lee JS, Park BJ. Gene Expression-based recurrence prediction of hepatitis B virus-related human hepatocellular carcinoma. *Clin Cancer Res* 2008; 14 (7) 2056-2064.
- [77] Wu JY, Wu SG, Yang CH, Chang YL, Chang YC, Hsu YC, Shih JY, Yang PC. Comparison of gefitinib and erlotinib in advanced NSCLC and the effect of EGFR mutations. *Lung cancer* 2011; 72 (2) 205-212.
- [78] Yang JD, Roberts LR. Epidemiology and management of hepatocellular carcinoma infectious disease. *Clin N Am* 2010; 24 (4) 899-919.
- [79] Zhang XF, Yu L, Lu Y. Wnt/ $\beta$ -catenin signaling pathway and its role in hepatocellular carcinoma. *Front Med China* 2008; 2 (3) 216-228.
- [80] Zhou L, Huang Y, Li J, Wang Z. The mTOR pathway is associated with the poor prognosis of human hepatocellular carcinoma. *Med Oncol* 2009; 27(2) 255-261.
- [81] Zhu AX, Duda DG, Sahani DV, Jain RK. HCC and angiogenesis: possible targets and future directions. *Nat Rev Clin Oncol* 2011; 8 (5) 292-302.

- [82] Zhu AX. Development of sorafenib and other molecularly targeted agents in hepatocellular carcinoma. *Cancer* 2007; 112 (2) 250–259.



# BIO-TARGETS AND DRUG DELIVERY APPROACHES



EDITED BY

Sabyasachi Maiti  
Kalyan Kumar Sen



CRC Press  
Taylor & Francis Group

BIO-TARGETS  
AND DRUG  
DELIVERY  
APPROACHES



**Taylor & Francis**

Taylor & Francis Group

<http://taylorandfrancis.com>

# BIO-TARGETS AND DRUG DELIVERY APPROACHES

EDITED BY

Sabyasachi Maiti  
Kalyan Kumar Sen



CRC Press

Taylor & Francis Group

Boca Raton London New York

---

CRC Press is an imprint of the  
Taylor & Francis Group, an **informa** business

CRC Press  
Taylor & Francis Group  
6000 Broken Sound Parkway NW, Suite 300  
Boca Raton, FL 33487-2742

© 2017 by Taylor & Francis Group, LLC  
CRC Press is an imprint of Taylor & Francis Group, an Informa business

No claim to original U.S. Government works

Printed on acid-free paper  
Version Date: 20160314

International Standard Book Number-13: 978-1-4987-2999-4 (Hardback)

This book contains information obtained from authentic and highly regarded sources. Reasonable efforts have been made to publish reliable data and information, but the author and publisher cannot assume responsibility for the validity of all materials or the consequences of their use. The authors and publishers have attempted to trace the copyright holders of all material reproduced in this publication and apologize to copyright holders if permission to publish in this form has not been obtained. If any copyright material has not been acknowledged please write and let us know so we may rectify in any future reprint.

Except as permitted under U.S. Copyright Law, no part of this book may be reprinted, reproduced, transmitted, or utilized in any form by any electronic, mechanical, or other means, now known or hereafter invented, including photocopying, microfilming, and recording, or in any information storage or retrieval system, without written permission from the publishers.

For permission to photocopy or use material electronically from this work, please access [www.copyright.com](http://www.copyright.com) (<http://www.copyright.com/>) or contact the Copyright Clearance Center, Inc. (CCC), 222 Rosewood Drive, Danvers, MA 01923, 978-750-8400. CCC is a not-for-profit organization that provides licenses and registration for a variety of users. For organizations that have been granted a photocopy license by the CCC, a separate system of payment has been arranged.

**Trademark Notice:** Product or corporate names may be trademarks or registered trademarks, and are used only for identification and explanation without intent to infringe.

---

#### Library of Congress Cataloging-in-Publication Data

---

Names: Maiti, Sabyasachi, editor. | Sen, Kalyan Kumar, editor.  
Title: Bio-targets and drug delivery approaches / editors, Sabyasachi Maiti and Kalyan Kumar Sen.  
Other titles: Biotargets and drug delivery approaches  
Description: Boca Raton : Taylor & Francis, 2017. | Includes bibliographical references and index.  
Identifiers: LCCN 2016012233 | ISBN 9781498729994 (alk. paper)  
Subjects: | MESH: Drug Delivery Systems  
Classification: LCC RS199.5 | NLM QV 785 | DDC 615/.6--dc23  
LC record available at <http://lccn.loc.gov/2016012233>

---

Visit the Taylor & Francis Web site at  
<http://www.taylorandfrancis.com>

and the CRC Press Web site at  
<http://www.crcpress.com>



---

# Contents

Preface.....	ix
Contributors .....	xi
<b>Chapter 1</b> Basic Concepts in Drug Targeting .....	1
<i>Kalyan Kumar Sen and Sabyasachi Maiti</i>	
<b>Chapter 2</b> Biological Targets: Identification, Selection, and Validation .....	33
<i>Rana Datta and Sugata Banerjee</i>	
<b>Chapter 3</b> Emerging Therapeutic Targets for Diabetes .....	53
<i>Sudipta Saha, Ashok K. Singh, Amit K. Keshari, Priya Singh Kushwaha, and Siddhartha Maity</i>	
<b>Chapter 4</b> Prodrug Strategy: An Effective Tool in Drug Delivery and Targeting.....	77
<i>Buddhadev Layek, Shubhajit Paul, and Jagdish Singh</i>	
<b>Chapter 5</b> Drug-Targeting Strategies to CNS Disorders .....	113
<i>Somasree Ray</i>	
<b>Chapter 6</b> Natural Polymers in Colon Targeting: Approaches and Future Perspectives.....	133
<i>Sougata Jana, Arijit Gandhi, and Subrata Jana</i>	
<b>Chapter 7</b> Lymphatic Drug Targeting .....	161
<i>Raghavendra V. Kulkarni and Biswanath Sa</i>	
<b>Chapter 8</b> New Drug Targets and Drug Delivery Strategies for Various Ocular Disorders .....	181
<i>Subramanian Natesan, Venkateshwaran Krishnaswami, Saranya Radhakrishnan, Vaishnavi Suresh Kumar, Nirmal Sonali, Jayabalan Nirmal, and Shovanlal Gayen</i>	

- Chapter 9** Bone-Targeted Drug Delivery Systems.....207  
*Amit Kumar Nayak and Kalyan Kumar Sen*
- Chapter 10** Targeted Drug Delivery in Solid Tumors: An Overview  
and Novel Approaches for Therapy.....233  
*Mintu Pal and Lay Poh Tan*
- Chapter 11** Mitochondria as an Emerging Target for the Delivery of Small  
Therapeutic Molecules .....259  
*Avik Das, Sabyasachi Maiti, and Kalyan Kumar Sen*
- Chapter 12** Antisense Oligonucleotide-Mediated Target-Specific Gene  
Silencing: Design, Delivery Strategies, and Therapeutic  
Applications.....297  
*Biswajit Mukherjee, Samrat Chakraborty, Laboni Mondal,  
Ankan Choudhury, Bhabani Sankar Satapathy,  
and Sanchari Bhattacharya*
- Chapter 13** Biodegradable Polymeric Carriers for Delivery of siRNA .....347  
*Sanika A. Rege, Sudip K. Das, and Nandita G. Das*
- Chapter 14** Organic–Inorganic Nanocomposites for Biomedical  
Applications.....375  
*Subham Banerjee and Animesh Ghosh*
- Chapter 15** Carbon Nanotube-Induced Targeted Drug Delivery.....403  
*Anish Bhattacharya and Amit K. Chakraborty*
- Chapter 16** Functionalized Cyclodextrin: A Versatile Supramolecular  
System for Drug Delivery .....437  
*Subrata Jana and Sougata Jana*
- Chapter 17** Nanopolymer Scaffolds as Novel Carriers for Cells and Drugs .....465  
*Aum Solanki, Bhargav Hirapara, Emily Johnson,  
and Yashwant Pathak*

<b>Chapter 18</b> Bio-Targets for Polyionic Glucan Derivatives and Their Nano-Therapeutic Systems .....	487
<i>Manabendra Dhua, Kalyan Kumar Sen, and Sabyasachi Maiti</i>	
<b>Chapter 19</b> Novel Carriers for Targeted Delivery of Herbal Medicines.....	523
<i>Sankhadip Bose</i>	
<b>Chapter 20</b> Toxicological Concerns Related to Nanoscale Drug Delivery Systems .....	541
<i>Sabyasachi Maiti, Sanmoy Karmakar, and Kumar Anand</i>	
<b>Index</b> .....	569



**Taylor & Francis**

Taylor & Francis Group

<http://taylorandfrancis.com>

---

# Preface

In recent years, the search for biological targets and the consequent development of targeted delivery systems have been an intensive area of pharmaceutical research. Drugs cannot exert their therapeutic effects if they do not reach their target sites in the body at the appropriate concentration and persist for a sufficient length of time. To maximize drug utilization, it is necessary to deliver drugs at the target tissue. Therefore, the design of controlled release or bioresponsive formulation, which can liberate the active constituents over a long period of time, has been proven beneficial in terms of better pharmacological performance at low doses with reduced side effects. New modes of drug administration are also under investigation to overcome the obstacles associated with biodegradation and pharmacokinetics. Most general pharmacy textbooks focus on conventional pharmaceutical formulations such as tablets, capsules, ointments, suppositories, etc.

Although the targeting of therapeutics is an expanding field of research, there is currently a scarcity of books that covers all aspects of novel drug targeting strategies. There are excellent reviews and book chapters that deal with one or more topics, but a book containing comprehensive coverage and up-to-date progress in the area of drug targeting is not available. Our attempt is to bridge this gap by providing a chapter-wise discussion on various aspects of drug delivery and targeting in a single comprehensive text. This book emphasizes ongoing worldwide research on biological target identification for a particular disease or disorder and the delivery of bioactive molecules at the molecular, cellular, and higher levels. This book captures current topics of interest and the latest research updates in this field.

The book is divided into 20 chapters to provide a clear overview of each topic. The book starts with a basic understanding of drug targeting ([Chapter 1](#)) followed by bio-target identification ([Chapter 2](#)). This is subsequently illustrated with an example of therapeutic targets for diabetes in [Chapter 3](#). The prodrug strategy that may augment target specificity and drug development is discussed in [Chapter 4](#). Later on, cell/organ-based approaches such as those for targeting central nervous systems (CNS), colon, lymphatic systems, ocular regions, bone, solid tumors, and mitochondria are covered in [Chapters 5](#) through [11](#). In addition, different drug targeting devices are included in [Chapters 12](#) through [18](#) emphasizing antisense oligonucleotide-based targeting strategies, biodegradable polymeric carriers, organic–inorganic composites, carbon nanotubes, functionalized cyclodextrin, nanopolymer scaffolds, and nano-therapeutic systems of polyionic glucan derivatives. Herbal medicines are currently receiving increasing attention due to their near-zero side effects. Therefore, [Chapter 19](#) is devoted to a discussion of different novel carriers for herbal medicines of clinical significance. The toxicity of nanomaterials has been a great concern before their clinical application. Keeping this in mind, [Chapter 20](#) takes into account the toxicity of nanomaterials that may cause harm to various organs of our body.

In this book we have tried our best to cover recent developments in targeted delivery approaches for therapeutic molecules. To make this book reader-friendly and useful, we have provided in-depth literature reports and suitable illustrations. Important

references have been included in each chapter for the benefit of readers who wish to pursue any of these topics in greater depth. We hope that this book will meet the demand of a reference book for concerned professionals and researchers who intend to conceptualize, develop, and optimize targeted drug delivery approaches.

This book is primarily intended for undergraduate and postgraduate students undertaking programs in pharmaceutical sciences, medicine, biotechnology, biomedical engineering, and other related subjects. It will also be helpful as a reference for research workers seeking information concerning the design and development of drug targeting systems. We strongly believe that this book will also provide assistance to research workers in developing innovations for humankind. We are most grateful to the authors for their contribution and kind cooperation for the successful completion of this book. Without the skillful sharing of knowledge from a diverse class of expertise, the completion of this book would not have been possible. The contributions of all authors are acknowledged overleaf. We are proud of our family members for their continuous moral support and inspiration during the preparation of this book. We are thankful to CRC Press for their keen interest in and expert assistance with the design of an impressive book cover, and preparation and publication of this book. Constructive comments and suggestions from readers in improving the quality of this book are welcome.

Together with our contributing authors, we will be extremely pleased if our efforts fulfill the needs of pharmaceutical and biomedical students and researchers.

**Dr. Sabyasachi Maiti**  
**Dr. Kalyan Kumar Sen**

---

# Contributors

**Kumar Anand**

Division of Pharmacology  
Department of Pharmaceutical  
Technology  
Jadavpur University  
Kolkata, India

**Subham Banerjee**

Centre for Biodesign and Diagnostics  
Translational Health Science and  
Technology Institute  
Faridabad, India

**Sugata Banerjee**

Department of Pharmaceutical Sciences  
and Technology  
Birla Institute of Technology  
Ranchi, India

**Anish Bhattacharya**

Carbon Nanotechnology Laboratory  
National Institute of Technology  
Durgapur, India

**Sanchari Bhattacharya**

Department of Pharmaceutical  
Technology  
Jadavpur University  
Kolkata, India

**Sankhadip Bose**

Department of Phytochemistry  
Gupta College of Technological  
Sciences  
Asansol, India

**Amit K. Chakraborty**

Carbon Nanotechnology Laboratory  
National Institute of Technology  
Durgapur, India

**Samrat Chakraborty**

Department of Pharmaceutical  
Technology  
Jadavpur University  
Kolkata, India

**Ankan Choudhury**

Department of Pharmaceutical  
Technology  
Jadavpur University  
Kolkata, India

**Avik Das**

Department of Pharmacology and  
Toxicology  
Gupta College of Technological  
Sciences  
Asansol, India

**Nandita G. Das**

College of Pharmacy and Health  
Sciences  
Department of Pharmaceutical Sciences  
Butler University  
Indianapolis, Indiana

**Sudip K. Das**

College of Pharmacy and Health  
Sciences  
Department of Pharmaceutical Sciences  
Butler University  
Indianapolis, Indiana

**Rana Datta**

Department of Pharmacology and  
Toxicology  
Gupta College of Technological  
Sciences  
Asansol, India

**Manabendra Dhua**

Department of Pharmaceutical  
Chemistry  
Gupta College of Technological  
Sciences  
Asansol, India

**Arijit Gandhi**

Department of Quality Assurance  
Albert David Ltd.  
Kolkata, India

**Shovanlal Gayen**

Department of Pharmaceutical Sciences  
Dr. Harisingh Gour Central University  
Madhya Pradesh, India

**Animesh Ghosh**

Department of Pharmaceutical Sciences  
and Technology  
Birla Institute of Technology  
Ranchi, India

**Bhargav Hirapara**

College of Pharmacy  
University of South Florida Health  
Tampa, Florida

**Sougata Jana**

Department of Pharmaceutics  
Gupta College of Technological  
Sciences  
Asansol, India

**Subrata Jana**

Department of Chemistry  
Indira Gandhi National Tribal  
University  
Madhya Pradesh, India

**Emily Johnson**

College of Pharmacy  
University of South Florida Health  
Tampa, Florida

**Sanmoy Karmakar**

Department of Pharmaceutical  
Technology  
Jadavpur University  
Kolkata, India

**Amit K. Keshari**

Department of Pharmaceutical Sciences  
Babasaheb Bhimrao Ambedkar  
University  
Lucknow, India

**Venkateshwaran Krishnaswami**

Department of Pharmaceutical  
Technology  
Bharathidasan Institute of Technology  
Anna University  
Tamil Nadu, India

**Raghavendra V. Kulkarni**

Department of Pharmaceutical  
Technology  
BLDEA's College of Pharmacy  
BLDE University Campus  
Karnataka, India

**Vaishnavi Suresh Kumar**

Department of Pharmaceutical  
Technology  
Bharathidasan Institute of Technology  
Anna University  
Tamil Nadu, India

**Priya Singh Kushwaha**

Department of Pharmaceutical Sciences  
Babasaheb Bhimrao Ambedkar  
University  
Lucknow, India

**Buddhadev Layek**

Department of Pharmaceutics  
University of Minnesota  
Minneapolis, Minnesota



**Sabyasachi Maiti**

Department of Pharmaceutics  
Gupta College of Technological Sciences  
Asansol, India

**Siddhartha Maity**

Council of Scientific and Industrial  
Research  
Department of Pharmaceutical  
Technology  
Jadavpur University  
Kolkata, India

**Laboni Mondal**

Department of Pharmaceutical  
Technology  
Jadavpur University  
Kolkata, India

**Biswajit Mukherjee**

Department of Pharmaceutical  
Technology  
Jadavpur University  
Kolkata, India

**Subramanian Natesan**

Department of Pharmaceutical  
Technology  
Bharathidasan Institute of Technology  
Anna University  
Tamil Nadu, India

**Amit Kumar Nayak**

Department of Pharmaceutics  
Seemanta Institute of Pharmaceutical  
Sciences  
Odisha, India

**Jayabalan Nirmal**

School of Materials Science and  
Engineering  
Nanyang Technological University  
Singapore

**Mintu Pal**

Biotechnology Division  
CSIR-North East Institute of Science  
and Technology  
Assam, India

**Yashwant Pathak**

College of Pharmacy  
University of South Florida Health  
Tampa, Florida

**Shubhajit Paul**

Department of Pharmaceutics  
University of Minnesota  
Minneapolis, Minnesota

**Saranya Radhakrishnan**

Department of Pharmaceutical  
Technology  
Bharathidasan Institute of Technology  
Anna University  
Tamil Nadu, India

**Somasree Ray**

Department of Pharmaceutics  
Gupta College of Technological  
Sciences  
Asansol, India

**Sanika A. Rege**

College of Pharmacy and Health  
Sciences  
Department of Pharmaceutical Sciences  
Butler University  
Indianapolis, Indiana

**Biswanath Sa**

Department of Pharmaceutical  
Technology  
Jadavpur University  
Kolkata, India

**Sudipta Saha**

Department of Pharmaceutical Sciences  
Babasaheb Bhimrao Ambedkar  
University  
Lucknow, India

**Bhabani Sankar Satapathy**

Department of Pharmaceutical  
Technology  
Jadavpur University  
Kolkata, India

**Kalyan Kumar Sen**

Department of Pharmaceutics  
Gupta College of Technological  
Sciences  
Asansol, India

**Ashok K. Singh**

Department of Pharmaceutical Sciences  
Babasaheb Bhimrao Ambedkar  
University  
Lucknow, India

**Jagdish Singh**

Department of Pharmaceutical Sciences  
College of Health Professions  
North Dakota State University  
Fargo, North Dakota

**Aum Solanki**

College of Pharmacy  
University of South Florida Health  
Tampa, Florida

**Nirmal Sonali**

School of Materials Science and  
Engineering  
Nanyang Technological University  
Singapore

**Lay Poh Tan**

Division of Materials Technology  
School of Materials Science and  
Engineering  
Nanyang Technological University  
Singapore